

NUREG/CR-4599
BMI-2173
Vol. 3, No. 1

Short Cracks in Piping and Piping Welds

Semiannual Report
April 1992 - September 1992

Prepared by
G. M. Wilkowski, F. Brust, R. Francini,
N. Ghadiali, T. Kilinski, P. Krishnaswamy, M. Landow,
C. W. Marschall, S. Rahman, P. Scott

Battelle

Prepared for
U.S. Nuclear Regulatory Commission

9311080268 931031
PDR NUREG
CR-4599 R PDR

AVAILABILITY NOTICE

Availability of Reference Materials Cited in NRC Publications

Most documents cited in NRC publications will be available from one of the following sources:

1. The NRC Public Document Room, 2120 L Street, NW, Lower Level, Washington, DC 20555-0001
2. The Superintendent of Documents, U.S. Government Printing Office, Mail Stop SSOP, Washington, DC 20402-9328
3. The National Technical Information Service, Springfield, VA 22161

Although the listing that follows represents the majority of documents cited in NRC publications, it is not intended to be exhaustive.

Referenced documents available for inspection and copying for a fee from the NRC Public Document Room include NRC correspondence and internal NRC memoranda; NRC Office of Inspection and Enforcement bulletins, circulars, information notices, inspection and investigation notices; Licensee Event Reports; vendor reports and correspondence; Commission papers; and applicant and licensee documents and correspondence.

The following documents in the NUREG series are available for purchase from the GPO Sales Program: formal NRC staff and contractor reports, NRC-sponsored conference proceedings, and NRC booklets and brochures. Also available are Regulatory Guides, NRC regulations in the *Code of Federal Regulations*, and *Nuclear Regulatory Commission Issuances*.

Documents available from the National Technical Information Service include NUREG series reports and technical reports prepared by other federal agencies and reports prepared by the Atomic Energy Commission, forerunner agency to the Nuclear Regulatory Commission.

Documents available from public and special technical libraries include all open literature items, such as books, journal and periodical articles, and transactions. *Federal Register* notices, federal and state legislation, and congressional reports can usually be obtained from these libraries.

Documents such as theses, dissertations, foreign reports and translations, and non-NRC conference proceedings are available for purchase from the organization sponsoring the publication cited.

Single copies of NRC draft reports are available free, to the extent of supply, upon written request to the Office of Information Resources Management, Distribution Section, U.S. Nuclear Regulatory Commission, Washington, DC 20555-0001.

Copies of industry codes and standards used in a substantive manner in the NRC regulatory process are maintained at the NRC Library, 7920 Norfolk Avenue, Bethesda, Maryland, and are available there for reference use by the public. Codes and standards are usually copyrighted and may be purchased from the originating organization or, if they are American National Standards, from the American National Standards Institute, 1430 Broadway, New York, NY 10018.

DISCLAIMER NOTICE

This report was prepared as an account of work sponsored by an agency of the United States Government. Neither the United States Government nor any agency thereof, or any of their employees, makes any warranty, expressed or implied, or assumes any legal liability of responsibility for any third party's use, or the results of such use, of any information, apparatus, product or process disclosed in this report, or represents that its use by such third party would not infringe privately owned rights.

NUREG/CR-4599
BMI-2173
Vol. 3, No. 1

Short Cracks in Piping and Piping Welds

Semiannual Report
April 1992 - September 1992

Manuscript Completed: September 1993
Date Published: October 1993

Prepared by
G. M. Wilkowski, F. Brust, R. Francini,
N. Ghadiali, T. Kilinski, P. Krishnaswamy, M. Landow,
C. W. Marschall, S. Rahman, P. Scott

Battelle
505 King Avenue
Columbus, OH 43201

Prepared for
Division of Engineering
Office of Nuclear Regulatory Research
U.S. Nuclear Regulatory Commission
Washington, DC 20555
NRC FIN B5702

ABSTRACT

This is the fifth semiannual report of the U.S. Nuclear Regulatory Commission's research program entitled "Short Cracks in Piping and Piping Welds." This 4-year program began in March 1990. The program objective is to verify and improve fracture analyses for circumferentially cracked large-diameter nuclear piping with crack sizes typically used in leak-before-break analyses or in-service flaw evaluations.

During this reporting period, the overall program as well as the results to date were reviewed very critically. It was found that several changes to the current program were needed to meet the final objectives at the end of the 4 years. Hence, the program was restructured. As a result, several activities were put on hold during this reporting period until restructuring was finalized. The changes to the existing program as well as the deliverables from the additional activities are detailed in this report.

In the surface-cracked pipe evaluations, work progress involved: (1) evaluating the tensile and Charpy V-notch data for a carbon-manganese submerged arc weld metal (Plate DP2-F49W), and (2) conducting 3D finite-element (FE) analyses of uncracked stainless steel pipe experiments conducted in Japan to resolve the discrepancies between experimental data and FE predictions.

Significant efforts during this period involved quantifying the leak rate from cracked pipe using advanced probabilistic analysis. This work was conducted to provide a technical basis for changes to NRC Reg. Guide 1.45. A special topical report that describes our methodology and our results was written and submitted to NRC for review. The details of this progress are given in Section 7 of this report.

A new PC-based version of the code to evaluate circumferential surface-cracked pipe, NRCPIPES Version 1.0, was completed and sent to the NRC for testing along with a user's manual.

Most of the analysis of the influence of the residual stress field on cracks in welds, being conducted under a subcontract to the University of Michigan, was completed during this reporting period and is included here. Also, under a separate subcontract to Brown University, a program entitled "Validity Limits on J-R Curve Determination" is being continued.

As part of the program, the results from this program were presented to the Flaw Evaluation Group of ASME Section XI. Technical efforts related to that activity during this reporting period are summarized.

CONTENTS

	<u>Page</u>
LIST OF FIGURES	ix
LIST OF TABLES	xiv
PREVIOUS REPORTS IN SERIES	xv
EXECUTIVE SUMMARY	xvii
ACKNOWLEDGMENTS	xxi
NOMENCLATURE	xxiii
1. INTRODUCTION	1-1
2. TASK 1 SHORT TWC PIPE EVALUATIONS	2-1
2.1 Task Objective	2-1
2.2 Task Rationale	2-1
2.3 Task Approach	2-1
2.3.1 Subtask 1.4 Analyses for Short Through-Wall Cracks in Pipes	2-1
2.4 Plans for Next Year of the Program	2-3
2.4.1 Subtask 1.1 Material Characterization for Short TWC Pipe Experiments	2-3
2.4.2 Subtask 1.3 Large-Diameter Pipe Fracture Experiments	2-3
2.4.3 Subtask 1.4 Analyses for Short Through-Wall Cracks in Pipes	2-4
2.5 References	2-4
3. TASK 2 SHORT SC PIPE EVALUATIONS	3-1
3.1 Task Objective	3-1
3.2 Task Rationale	3-1
3.3 Task Approach	3-1
3.3.1 Subtask 2.1 Material Characterization for Surface-Cracked Pipe Experiments	3-1
3.3.2 Subtask 2.4 Analysis of Short Surface Cracks in Pipes	3-6
3.4 Plans for Next Year of the Program	3-15

CONTENTS

	<u>Page</u>
3.4.1 Subtask 2.1 Material Characterization for Surface-Cracked Pipe Experiments	3-15
3.4.2 Subtask 2.2 Small-Diameter Pipe Fracture Experiments in Pure Bending for Limit-Load Ovalization Correction	3-15
3.4.3 Subtask 2.3 Large-Diameter Surface-Cracked Pipe Fracture Experiments Under Combined Bending and Tension (Pressure)	3-15
3.4.4 Subtask 2.4 Analysis of Short Surface Cracks in Pipes	3-17
3.5 References	3-17
4. TASK 3 BIMETALLIC WELD CRACK EVALUATIONS	4-1
5. TASK 4 DYNAMIC STRAIN AGING	5-1
5.1 Task Objective	5-1
5.2 Task Rationale	5-1
5.3 Task Approach	5-1
5.4 Plans for Next Year of the Program	5-2
5.4.1 Subtask 4.1 Establish a Screening Criterion to Predict Unstable Crack Jumps in Ferritic Steels	5-2
5.4.2 Subtask 4.2 Evaluate Procedures for Assessing Fracture Resistance During Crack Jumps in Laboratory Specimens	5-2
6. TASK 5 FRACTURE EVALUATIONS OF PIPE ANISOTROPY	6-1
6.1 Task Objective	6-1
6.2 Task Rationale	6-1
6.3 Task Approach	6-1
6.4 Plans for Next Year of the Program	6-1
7. TASK 6 CRACK-OPENING AREA EVALUATIONS	7-1
7.1 Task Objective	7-1
7.2 Task Rationale	7-1
7.3 Task Approach	7-1
7.3.1 Subtask 6.6 Leak Rate Quantification	7-1
7.4 Plans for Next Year of the Program	7-42
7.4.1 Subtask 6.1 Create Combined Loading Improvements	7-43
7.4.2 Subtask 6.2 Implement Short TWC Crack-Opening Improvements	7-43
7.4.3 Subtask 6.3 Improve Weld Crack Evaluations	7-43
7.4.4 Subtask 6.4 Modify SQUIRT Code	7-43

CONTENTS

	<u>Page</u>
7.4.5 Subtask 6.5 Prepare Topical Report on Crack-Opening-Area Improvements	7-47
7.4.6 Subtask 6.6 Leak Rate Quantification	7-47
7.5 References	7-47
8. TASK 7 NRCPIPE IMPROVEMENTS	8-1
8.1 Task Objective	8-1
8.2 Task Rationale	8-1
8.3 Task Approach	8-1
8.3.1 Subtask 7.1 Improve Efficiency of Current Version of NRCPIPE	8-1
8.3.2 Subtask 7.2 Incorporate TWC Improvements in NRCPIPE	8-1
8.3.3 Subtask 7.3 Make Surface Crack Version of NRCPIPE	8-2
8.3.4 Subtask 7.4 Provide New User's Manual	8-2
8.4 Plans for Next Year of the Program	8-2
8.4.1 Subtask 7.1 Improve Efficiency of Current Version	8-2
8.4.2 Subtask 7.2 Incorporate TWC Improvements in NRCPIPE	8-3
8.4.3 Subtask 7.3 Make Surface Crack Version of NRCPIPE	8-3
8.4.4 Subtask 7.4 Provide New User's Manual	8-3
9. TASK 8 ADDITIONAL EFFORTS	9-1
9.1 Task Objective	9-1
9.2 Task Rationale	9-1
9.2.1 Subtask 8.1 Validity Limits on J-R Curve Determination	9-1
9.2.2 Subtask 8.2 Stainless Steel SAW Fusion-Line Toughness	9-2
9.2.3 Subtask 8.3 Update PIFRAC Data Files	9-9
9.2.4 Subtask 8.4 Develop Data Base for Circumferential Pipe Fracture Experiments	9-10
9.2.5 Subtask 8.5 Data File Conversion from HP to IBM Format	9-13
9.3 Plans for Next Year of the Program	9-14
9.3.1 Subtask 8.1 Validity Limits on J-R Curve Determination	9-14
9.3.2 Subtask 8.2 Stainless Steel SAW Fusion-Line Toughness	9-15
9.3.3 Subtask 8.3 Update PIFRAC Data Files	9-15
9.3.4 Subtask 8.4 Develop Data Base for Circumferential Pipe Fracture Experiments	9-15
9.3.5 Subtask 8.5 Data File Conversion from HP to IBM Format	9-15

CONTENTS

	<u>Page</u>
9.4 References	9-15
10. TASK 9 INTERPROGRAM COOPERATION AND PROGRAM MANAGEMENT	10-1
10.1 Task Objective	10-1
10.2 Task Rationale	10-1
10.3 Task Approach	10-1
10.3.1 Subtask 9.1 Technical Exchange and Information Meetings	10-1
10.4 Plans for Next Year of the Program	10-36
10.4.1 Subtask 9.1 Technical Exchange and Information Meetings	10-36
10.5 References	10-37
APPENDIX A MEAN AND COVARIANCE OF RANDOM MATERIAL PROPERTIES	A-1

LIST OF FIGURES

<u>Figure</u>	<u>Page</u>
3.1 Transverse tensile properties of weld DP2-F49W: (a) engineering stress-strain curves and (b) true stress-strain curves	3-4
3.2 Comparison between analytical predictions and experimental data from an uncracked four-point bend bar specimen	3-11
3.3 Longitudinal strains versus beam depth showing that plane sections do remain plane during plastic deformation	3-12
3.4 Finite-element mesh of JAERI Uncracked Pipe Experiment S-17 using 3-D solid elements. One element through thickness	3-13
3.5 Finite-element mesh of JAERI Uncracked Pipe Experiment S-17 using 3-D solid elements. Four elements through thickness	3-13
3.6 Load-line displacement versus load for Uncracked Pipe Experiment S-17	3-14
3.7 Axial strain distribution around the pipe circumference at the center section of Pipe S-17 under pure bending	3-16
3.8 Outer surface for midsection of pipe for Uncracked Pipe Experiment S-17	3-16
7.1 Comparison of SQUIRT thermal-hydraulic model predictions with the experimental data of Collier et al. (Reference 7.7) for cracks with a COD of 108 μm	7-5
7.2 Crack-opening displacement in Experiment 4111-1 up to load at crack initiation	7-6
7.3 Comparisons of load-displacement of through-wall-cracked pipe under combined bending and tension (Experiment 4131-3)	7-8
7.4 Through-wall-cracked pipe under combined bending and tension	7-10
7.5 Comparisons of actual N+SSE stresses with various service limits	7-18
7.6 Plasticity correction for elastically calculated stresses	7-19
7.7 Histogram of LBB detectable flaw size for BWR-1	7-20
7.8 Conditional probability of failure by various methods (BWR-1)	7-22
7.9 Computational efficiency of FORM/SORM (BWR-1)	7-23

LIST OF FIGURES

<u>Figure</u>	<u>Page</u>
7.10 (a) Conditional failure probability by SORM for BWR-1 (base metal) (b) Conditional failure probability by SORM for BWR-1 (weld metal)	7-24
7.11 (a) Conditional failure probability by SORM for BWR-2 (base metal) (b) Conditional failure probability by SORM for BWR-2 (weld metal)	7-25
7.12 Conditional failure probability by SORM for BWR-1 (random crack location)	7-26
7.13 Conditional failure probability by SORM for BWR-2 (random crack location)	7-26
7.14 Conditional failure probability by SORM for BWR-3 (random crack location)	7-27
7.15 Conditional failure probability by SORM for BWR-4 (random crack location)	7-27
7.16 Conditional failure probability by SORM for BWR-5 (random crack location)	7-28
7.17 Conditional failure probability by SORM for BWR-6 (random crack location)	7-28
7.18 Conditional failure probability as a function of diameter in BWR pipes	7-30
7.19 (a) Conditional failure probability by SORM for PWR-1 (base metal) (b) Conditional failure probability by SORM for PWR-1 (weld metal)	7-31
7.20 (a) Conditional failure probability by SORM for PWR-2 (base metal) (b) Conditional failure probability by SORM for PWR-2 (weld metal)	7-32
7.21 Conditional failure probability by SORM for PWR-1 (random crack location)	7-33
7.22 Conditional failure probability by SORM for PWR-2 (random crack location)	7-33
7.23 Conditional failure probability by SORM for PWR-3 (random crack location)	7-34
7.24 Conditional failure probability by SORM for PWR-4 (random crack location)	7-34
7.25 Conditional failure probability by SORM for PWR-5 (random crack location)	7-35
7.26 Conditional failure probability by SORM for PWR-6 (random crack location)	7-35
7.27 Conditional failure probability as a function of diameter in PWR pipes	7-36
7.28 (a) Histogram of leak rate under 50 percent of Service Level-A limit for BWR-1 (b) Histogram of leak rate under 100 percent of Service Level-A limit for BWR-1	7-38 7-39

LIST OF FIGURES

<u>Figure</u>	<u>Page</u>
7.29 (a) Histogram of leak rate under 50 percent of Service Level-A limit for BWR-2	7-40
(b) Histogram of leak rate under 100 percent of Service Level-A limit for BWR-2	7-41
7.30 Conditional failure probability by SORM for BWR-7 (random crack location)	7-44
7.31 Conditional failure probability by SORM for BWR-8 (random crack location)	7-44
7.32 Conditional failure probability by SORM for BWR-9 (random crack location)	7-45
7.33 Conditional failure probability by SORM for BWR-10 (random crack location)	7-45
7.34 Conditional failure probability as a function of d/t in complex-cracked BWR pipes	7-46
9.1 Schematic of straight and slant-notch oriented C(T) specimens	9-4
9.2 Schematic illustration of slant-vee weld	9-4
9.3 Examples of K-weld preparation with out-of-plane bulging of the fusion line at the root passes	9-5
9.4 Comparison of slant-notch and standard-notch orientation effect on toughness of base metals	9-7
9.5 Schematic illustration of fusion-line C(T) specimen machined from a slant-vee weld	9-8
9.6 Schematic illustration of slant-notch C(T) specimen	9-8
10.1 Comparison of quasi-static pipe test loads at failure to IPIRG-1 pipe system test failure loads on identical pipes with same crack size	10-5
10.2 Comparison of Maxey with Chell local limit load axial surface-cracked pipe failure pressures for $R_1/t = 10$	10-7
10.3 Comparison of Maxey with Chell local limit load axial surface-cracked pipe failure pressures for $R_1/t = 15$	10-7
10.4 Comparison of Maxey with Chell local limit load axial surface-cracked pipe failure pressures for $R_1/t = 20$	10-8
10.5 Comparison of Maxey and Chell local limit load predicted failure pressures with experimental data from Battelle	10-9

LIST OF FIGURES

<u>Figure</u>	<u>Page</u>
10.6 A schematic plot of the geometry of the welded plate and the coordinate system for modeling the welding process	10-13
10.7 (a) Finite-element mesh for 8.64-mm (0.34-inch) thick plate and 127-mm (5-inch) width plate for straight and V-groove geometry, (b) the welding passes with the V-groove geometry, (c) J-integral paths and the straight groove geometry, and (d) actual weld sequence of an 8.64-mm (0.34-inch) thick plate	10-14
10.8 (a) Finite-element mesh for 33-mm (1.3-inch) thick plate and 254-mm (10-inch) wide plate for straight and V-groove geometry, (b) the welding passes with the V-groove geometry, and (c) J-integral paths and the straight groove geometry	10-16
10.9 Temperature-dependent material properties for 304 stainless steel	10-17
10.10 Residual stress distributions along the crack line for 8.6-mm (0.34-inch) thick plate, (a) straight groove, (b) V-groove	10-21
10.11 Residual stress distributions along the crack line for 33-mm (1.3-inch) thick plate, (a) straight groove, (b) V-groove	10-22
10.12 Residual σ_z stress distributions in weldment and HAZ for 8.6-mm (0.34-inch) thick plate with (a) straight groove, (b) single-V groove for 33-mm (1.3-inch) thick plate with (c) straight groove (d) V-groove	10-24
10.13 σ_z distributions along the crack line before and after releasing 10 nodal points for the refined mesh of 33-mm (1.3-inch) thick plate, (a) straight groove, (b) single-V groove	10-25
10.14 J-integral versus applied load (without thermal residual stresses), (a) 8.64 mm (0.34-inch) thick plate, (b) 33-mm (1.3 inch) thick plate	10-26
10.15 J-integral values for different contours for 8.64-mm (0.34-inch) thick plate with the thermal residual stresses, (a) straight groove, (b) single-V groove	10-27
10.16 J-integral values for different contours for 33-mm (1.3-inch) thick plate with the thermal residual stresses, (a) straight groove, (b) single-V groove	10-28
10.17 J-integral values for different contours for 8.6-mm (0.34-inch) thick plate with the thermal residual stresses, (a) straight groove, (b) single-V groove	10-30

LIST OF FIGURES

<u>Figure</u>	<u>Page</u>
10.18 J-integral values for different contours for 33-mm (1.3-inch) thick plate with the thermal residual stresses, (a) straight groove, (b) single-V groove	10-31
10.19 CTOA versus applied load for 8.64-mm (0.34-inch) thick plate, (a) straight groove, (b) single-V groove	10-33
10.20 CTOA versus applied load for 33-mm (1.3-inch) thick plate, (a) straight groove, (b) single-V groove	10-35

LIST OF TABLES

<u>Table</u>	<u>Page</u>
1.1 Changes in the program due to restructuring	1-2
1.2 Restructured test matrix of pipe experiments	1-5
3.1 Tensile properties of the carbon-manganese-molybdenum submerged-arc weld metal (DP2-F49W) in 31.8-mm thick (1.25-inch) A516 Grade 70 plate	3-3
3.2 Charpy V-notch results for submerged-arc weld metal (DP2-F49W) in 31.8-mm thick (1.25-inch) A516 Grade 70 plate	3-5
3.3 JAERI uncracked stainless steel pipe experiments to be analyzed	3-7
3.4 Summary of surface-cracked pipe FE analyses	3-8
7.1 Through-wall-cracked BWR and PWR piping systems for probabilistic fracture evaluations	7-16
7.2 Complex-cracked BWR piping systems for probabilistic fracture evaluations	7-43
9.1 Typical self-shielded flux-cored arc-welding procedures for stainless steels using stainless steel electrodes	9-6
9.2 List of programs for which circumferential pipe fracture data will be included	9-11
9.3 List of test parameters, results, and material property data included in database	9-12
10.1 Welding parameters used in computations	10-19

PREVIOUS REPORTS IN SERIES

Previous Reports from this Program

"Short Cracks in Piping and Piping Welds," First Semiannual Report, NUREG/CR-4599, Vol. 1, No. 1, March 1991.

"Short Cracks in Piping and Piping Welds," Second Semiannual Report, NUREG/CR-4599, Vol. 1, No. 2, April 1992.

"Short Cracks in Piping and Piping Welds," Third Semiannual Report, NUREG/CR-4599, Vol. 2, No. 1, September 1992.

"Short Cracks in Piping and Piping Welds," Fourth Semiannual Report, NUREG/CR-4599, Vol. 2, No. 2, February 1993.

Previous Related Documents from NRC's Degraded Piping Program

"Degraded Piping Program - Phase II," Semiannual Report, NUREG/CR-4082, Vol. 1, October 1984.

"Degraded Piping Program - Phase II," Semiannual Report, NUREG/CR-4082, Vol. 2, June 1985.

"Degraded Piping Program - Phase II," Semiannual Report, NUREG/CR-4082, Vol. 3, March 1986.

"Degraded Piping Program - Phase II," Semiannual Report, NUREG/CR-4082, Vol. 4, July 1986.

"Degraded Piping Program - Phase II," Semiannual Report, NUREG/CR-4082, Vol. 5, December 1986.

"Degraded Piping Program - Phase II," Semiannual Report, NUREG/CR-4082, Vol. 6, April 1988.

"Degraded Piping Program - Phase II," Semiannual Report, NUREG/CR-4082, Vol. 7, March 1989.

"Degraded Piping Program - Phase II," Semiannual Report, NUREG/CR-4082, Vol. 8, March 1989.

"NRC Leak-Before-Break (LBB/NRC) Analysis Method for Circumferentially Through-Wall Cracked Pipes Under Axial Plus Bending Loads," Topical Report, NUREG/CR-4572, March 1986.

"Elastic-Plastic Finite Element Analysis of Crack Growth in Large Compact Tension and Circumferentially Through-Wall-Cracked Pipe Specimen--Results of the First Battelle/NRC Analysis Round Robin," Topical Report, NUREG/CR-4573 September 1986.

Previous Reports in Series

"An Experimental and Analytical Assessment of Circumferential Through-Wall Cracked Pipes Under Pure Bending," Topical Report, NUREG/CR-4574, June 1986.

"Predictions of J-R Curves With Large Crack Growth From Small Specimen Data," Topical Report, NUREG/CR-4575, August 1986.

"An Assessment of Circumferentially Complex-Cracked Pipe Subjected to Bending," Topical Report, NUREG/CR-4687, September 1986.

"Analysis of Cracks in Stainless Steel TIG Welds," Topical Report, NUREG/CR4806, November 1986.

"Approximate Methods for Fracture Analyses of Through-Wall Cracked Pipes," Topical Report, NUREG/CR-4853, January 1987.

"Assessment of Design Basis for Load-Carrying Capacity of Weld-Overlay Repair," Topical Report, NUREG/CR-4877, February 1987.

"Analysis of Experiments on Stainless Steel Flux Welds," Topical Report, NUREG/CR-4878, February 1987.

"Experimental and Analytical Assessment of Circumferentially Surface-Cracked Pipes Under Bending," Topical Report, NUREG/CR-4872, April 1987.

Previous Related Documents from NRC's International Piping Integrity Research Group (IPIRG) Program

"Evaluation and Refinement of Leak-Rate Estimation Models," NUREG/CR-5128, April 1991.

EXECUTIVE SUMMARY

The U.S. Nuclear Regulatory Commission's (NRC) program "Short Cracks in Piping and Piping Welds Research", began in March of 1990 and will extend for four years. The program objective is to verify and improve fracture analyses for circumferentially cracked large-diameter nuclear piping using integrated results from analytical, material characterization, and full-scale pipe fracture efforts. Only quasi-static loading rates are evaluated, since the NRC's International Piping Integrity Research Group (IPIRG) Program is evaluating the effects of seismic loading rates on cracked piping systems.

The term "short cracks" encompasses crack sizes typically considered in leak-before-break (LBB) or pragmatic in-service flaw evaluations. The size of a typical leak-before-break (LBB) crack for a large diameter pipe is 6 percent of the circumference, which is much less than the 20 to 40 percent ratios investigated in many past pipe fracture programs. Some key results from this reporting period are summarized below.

During this period, the program was restructured to initiate several new activities in this program. These activities were found to be essential after reviewing the results to date in this program. Some key results in the various tasks during this reporting period are given below.

Short-Through-Wall Cracked Pipe

This task was virtually inactive. The progress during April 1992 was reported in the previous semiannual for the sake of completeness. One new subtask to evaluate additional GE/EPRI functions for through-wall-cracked pipe was identified in the restructuring of the program.

Short-Surface-Cracked Pipe

The material properties for DP2-F49W were evaluated during this time. Also, the finite-element (FE) analysis of uncracked stainless steel pipe showed that 3-D analysis rather than mesh refinement can resolve the discrepancy found between experimental data and FE analysis. A two-dimensional analysis using thick shell or elbow elements is inadequate in modelling the plastic behavior of uncracked pipe. Three new activities involving mesh refinement and J-estimation scheme were identified as being critical to the final results of the 4-year program and were included in the restructuring of the program.

Dynamic Strain Aging

A screening criterion to predict dynamic strain aging and unstable crack jumps in ferritic steels was developed. Also, a few confirmatory dynamic strain aging tests are included in the restructuring of the program.

Crack Opening Area Evaluations

Most of the efforts in this task involved completing a report to provide a technical basis for potential changes to NRC Reg. Guide 1.45. Advanced probabilistic methods (FORM/SORM) that are computationally far more efficient as compared with conventional Monte Carlo Simulations were

Executive Summary

developed and used in this effort. The results involve a methodology to predict the probability of unstable failure of cracked pipes under normal plus safe shutdown earthquake loads based on the variability of crack morphology (surface roughness, actual length of leakage path, etc.). As part of this effort an improved leak rate model was developed with statistics of crack morphology parameters for cracks removed from service; many of these parameters have not been considered in the past. The failure probabilities for numerous typical PWR and BWR piping systems were determined as a function of the leak rate.

NRCPIPE Improvements

A PC version of a computer code to conduct fracture analyses of circumferential surface-cracked pipe based on the J-estimation scheme was developed and sent to the NRC for evaluation. This code used the SC.TNP and SC.TKP J-estimation scheme methods developed in the Degraded Piping Program and is called NRCPIPES.

Additional Efforts

Several additional efforts were initiated in this task as part of the restructuring of the program. These include: (1) updating the PIFRAC data base, (2) converting old data files from the HP to IBM format, (3) compiling a data base of all circumferential cracked pipe experiments that have been conducted, and (4) evaluating the fusion-line toughness of stainless steel submerged arc welds.

Interprogram Cooperation and Program Management

As part of the interprogram cooperative efforts, working with the ASME Section XI Pipe Flaw Evaluation Task Group is a key aspect of the technology transfer of results of this program to practical application. During this time period, three technical activities were conducted for the ASME Section XI Pipe Flaw Evaluation Task Group: (1) a Charpy energy based elastic-plastic fracture mechanics axial surface crack analysis was developed, (2) an IPIRG-1 program pipe system data base was developed, and (3) an evaluation was made of axial surface crack limit-load analyses.

A second effort was undertaken as a cooperative effort with the Japanese Elastic-Plastic Fracture in Inhomogeneous Materials (EPI) Program. Here an analysis effort was conducted to determine numerically the effect of residual stresses on elastic-plastic fracture for a crack in a weld. This effort was conducted at the University of Michigan under the direction of Professor Jwo Pan. The first phase of the work examined the effect of residual stresses for a crack in a flat plate. For this case, the residual stresses were smaller than those for a pipe weld. The numerical results showed that for the position of the surface crack studied (the center of the weld), the residual stresses had significant effect only on the elastic response. At this location, the J applied was actually less than that for the case without the residual stresses at this same load. Future efforts will involve axisymmetric weld calculations where the residual stresses will be much higher.

Major Conclusions

During this reporting period, work proceeded on contributing efforts to major conclusions which should be described in the next semiannual report. One major effort was the completion of the

probabalistic leak-rate quantification report. In this work, we showed where material property data were lacking, reported a new leak-rate model, developed the first statistical database on crack morphology variables, and incorporated elastic-plastic fracture mechanics analyses into more advanced analytical probabalistic analyses (FORM/SORM).

Major conclusions to date are:

- Short circumferential through-wall flaws fail closer to limit-load (net-section-collapse) predictions than the longer flaws tested in past programs. The significance of this is that for LBB analyses, typically the circumferential flaw lengths in large diameter pipe (28 inches or larger) are quite short, approximately 6 percent of the circumference. This short length means that: (1) the failure loads are not as sensitive to toughness variations, and (2) if using a criterion such as the ASME Z-factor approach, which is based on long circumferential flaws, then there is an extra degree of conservatism. However, for small diameter pipe (i.e., 4 to 6 inches), the LBB through-wall-crack size may be up to 30-percent of the circumference. Hence these pipes would be more sensitive to toughness variations, and the ASME Section XI Z-factor based criterion would be more appropriate. It is possible to develop engineering corrections to the Z-factor approach that would account for crack length, as well as diameter, to have a more consistent fracture analysis for LBB of any size pipe.
- From the surface-cracked pipe results, it was found that the effect of R/t ratio on the Net-Section-Collapse analysis predicted loads were consistent for large cracks ($d/t = .66$ and $\Theta/\pi = 0.5$) experiments from the Degraded Piping Program and short cracked ($d/t = .50$ and $\Theta/\pi = 0.25$) pipe experiments from this program. The trend is that as R/t increases, the failure load decreases relative to the Net-Section-Collapse predicted failure load.

ACKNOWLEDGMENTS

This work is supported by the U.S. Nuclear Regulatory Commission through the Materials Engineering Branch of the Office of Nuclear Regulatory Research under Contract No. NRC-04-90-069. Mr. A. Hiser is the NRC program manager.

We would also like to thank others at Battelle who have helped in these efforts. Technicians who have contributed to the initial efforts are: Mr. R. Gertler, Mr. P. Held, Mr. J. Kramer, Mr. P. Mincer, Mr. D. Rider, Mr. J. Ryan, Mr. D. Shoemaker, and Mr. J. Woods. We thank Mrs. G. Walter and Mrs. V. Kreachbaum for typing this report, Dr. A. Hopper and Mr. M. Steve for editorial review comments, and Mr. D. Hayes for drafting assistance.

NOMENCLATURE

1. SYMBOLS

a	Half the crack length
a^*	Semi-elliptical crack depth
A_c	Area of Charpy specimen
B_1, B_2	Primary stress indices from ASME Section III, Article NG-3652
c	Half the mean circumferential crack length
C	Coefficient used to fit J-resistance curve
c_h	Heat capacity
CVP	Charpy upper-shelf energy
d	Flaw depth
D	Nominal pipe diameter
D_i	Inside diameter
D_m	Mean pipe diameter
D_o	Outside diameter
E	Young's modulus
F	Function relating elastic stress intensity factor to stress in GE/EPRI estimation scheme
$F_X(x)$	Joint distribution function of the random vector X
f_1, f_2	Elastic functions tabulated for use in various estimation schemes
$f_{2a}(x)$	Probability of detecting the LBB detectable flaw of size $2a$
$f_X(x)$	Joint probability density function of the random vector X
$g^{(i)}$	Value of g evaluated at $x^{(i)}$
$g(X)$	Performance function or limit state function

Nomenclature

$g_L(u)$	First-order approximation to tangent surface to the limit state at the design point
$g_q(u)$	Second-order approximation to the tangent surface to the limit state at the design point
$g_U(u)$	Performance function in u-space of independent standard Gaussian variables
h_1, h_2, h_3, h_4	Functions tabulated in GE/EPRI method
h_e	Dimension of element in crack line and behind crack tip
J	J-integral fracture parameter
J_D	Deformation J
J_e	Elastic component of J
J_i	J-integral at crack initiation but not necessarily a valid J_{Ic} by ASTM E813-81
J_{Ic}	J at crack initiation under Mode I loading
J_{IIIc}	J at crack initiation under Mode III loading
J_M	Modified value of J integral
J_P	Plastic component of J-integral
J-R	J-integral resistance (curve)
J_{tot}	Total value of J integral
k	Thermal conductivity
K_I	Mode I stress intensity factor
L	Total number of analyses in deterministic probabilistic analysis
L_f	Number of analyses associated with failure condition
ℓ	Total axial flaw length
m	Exponent used to fit J-resistance curve
M	Moment
MBL	Modified boundary layer

M_{max}	Maximum moment
M_T	Folias through-wall-crack bulging factor
n	Ramberg-Osgood strain-hardening exponent
n_1	x_1 component of outward normal to Γ
P	Tension due to internal pressure
P_F	Probability of failure
$P_{F,1}$	Probability of failure from first-order theory
$P_{F,2}$	Probability of failure from second-order theory
$P_{F,MCS}$	Probability of failure from Monte Carlo simulation
P_o	Failure pressure
P_s	Reliability; Probability of survival
q	Rate of heat input
Q	Nonlinear constraint parameter; heat flux
r_h	Distance from heat source
R_i	Inside radius
R_m	Mean pipe radius
S_m	ASME design stress
S_u	ASME ultimate stress
S_y	ASME yield strength
t	Thickness of pipe wall
T	Temperature
t_i	Components of traction
T_o	Ambient temperature

Nomenclature

T_w	Temperature of weldment
u	Space of independent standard Gaussian variables
u_i	Components of displacement
V	Heat source velocity
V_1, V_2, V_3	Displacement functions in GE/EPRI analysis
W	Strain energy density
X	Complete vector of input random parameters
x	Sample of input random vector X
$x^{(i)}$	Specific input random vector
Y	Vector
α	Ramberg-Osgood parameter
β -point	Design point
β_{HL}	Distance from β -point to origin in u space
Γ	Contour around crack tip
Δa	Increment of crack growth
δ_e	Displacement at node behind crack tip
η	Geometric factor used in J-integral analysis
θ	Crack angle
κ_i	Principal curvatures of the limit-state surface at the design point
ξ	Distance from heat source along a line parallel to the direction of its movement
ρ	Random correction factor
σ_e	Equivalent stress
σ_f	Flow stress

σ_h	Hoop stress
$\hat{\sigma}_{ij}$	Deviatoric stresses
σ_o	Flow stress
σ_R	Stress in R-direction
σ_{RZ}	Shear stress
$\sigma_{service}$	Service stress
σ_T	Out-of-plane stress components
σ_Z	Stress in Z-direction
$\Phi(u)$	Cumulative distribution fraction of a standard Gaussian (normal) random variable
σ_u	Ultimate stress
σ_y	Yield stress

2. ACRONYMS AND INITIALISMS

ABACRACK	Computer code to generate finite element meshes for surface cracks
AEC	Atomic Energy Commission
ASME	American Society of Mechanical Engineers
ASTM	American Society for Testing and Materials
BWR	Boiling Water Reactor
COD	Crack-opening displacement
CS	Carbon steel
CTOA	Crack-tip-opening angle
C(T)	Compact (tension) specimen
CPU	Central processing unit
DEGB	Double-ended guillotine break

Nomenclature

DOS	Disk Operating System
DP ³ II	Degraded Piping program - Phase II
DSA	Dynamic strain aging
EA3	Weld rod designation
EPFM	Elastic-plastic fracture mechanics
EPI	Japanese Elastic-Plastic Fracture of Inhomogeneous Materials program
EPRI	Electric Power Research Institute
FE	Finite element
FORM	First-Order Reliability Method
GE	General Electric
GMAW	Gas metal arc welding
HAZ	Heat affected zone
HP	Hewlett Packard (computer)
IBM	International Business Machine (computer)
IGSCC	Intergranular stress-corrosion cracking
IPIRG	International Piping Integrity Research Group
JAERI	Japanese Atomic Energy Research Institute
LBB	Leak-before-break
L-C	Longitudinal-circumferential orientation (direction of through-wall crack growth around pipe circumference)
LBB.ENG	Original TWC analysis method developed at Battelle
LBB.ENG2	TWC analysis method developed at Battelle
LBB.NRC	TWC analysis method used at NRC
MCS	Monte Carlo simulation

N	Normal operating stresses
NED	Nuclear Engineering and Design Journal
N+SSE	Normal operating plus safe shutdown earthquake
NRC	Nuclear Regulatory Commission
NRC-NRR	Nuclear Regulatory Commission - Office of Nuclear Reactor Regulation
NRC-RES	Nuclear Regulatory Commission - Office of Nuclear Regulatory Research
NRCPIPE	PC computer program for TWC LBB analysis
NUREG/CR	Nuclear Regulatory Commission Contractor Report
PC	Personal computer
PICEP	Pipe Crack Evaluation Program
PRAISE	Piping Reliability Analysis; Including Seismic Events
PROLBB	Computer code to evaluate the failure probability of flawed nuclear piping subject to combined tension and bending
PSQUIRT	Computer code to estimate the probability density of the LBB detectable flaw
PIFRAC	NRC's Piping Fracture Mechanics Database
PNL	Pacific Northwest Laboratories
PVP	Pressure Vessel and Piping
PWR	Pressurized water reactor
QS-CIRC.WK1	LOTUS database of circumferentially cracked pipe experimental results
RT	Room temperature
RIL	Research Information Letter
R,Z,T	Coordinate system used in welding finite element models
SAW	Submerged-arc weld
SC	Surface crack

Nomenclature

SC	Surface crack
SC.TKP	Surface crack analysis using thick pipe approximations
SC.TNP	Surface crack analysis using thin pipe approximations
SF	Safety factor
SFA 5.23	Weld rod designation
SMAW	Submerged arc weld
SORM	Second-Order Reliability Method
SQUIRT	Seepage Quantification of Upsets in Reactor Tubes, a leak rate computer program
SSE	Safe shut-down earthquake
TIG	Tungsten inert gas
TWC	Through-wall crack, through-wall-cracked
VAX	Mainframe computer

1. INTRODUCTION

The "Short Cracks in Piping and Piping Welds" program was initiated to address Nuclear Regulatory Commission (NRC) licensing needs and to resolve some critical findings from the NRC's Degraded Piping Program. The term "short cracks" refers to the type of cracks assessed in leak-before-break (LBB) or pragmatic in-service flaw evaluations. A typical LBB-size crack for a large-diameter pipe is 6 percent of the circumference, which is much less than the circumferential lengths of 20 to 40 percent investigated in other pipe fracture programs conducted in the past. Hence, the term "short cracks" in this project does not refer to microscopic cracks in the sense of the technical interests of the aerospace industry.

The 4-year program started on March 23, 1990. This fifth semiannual report describes progress in all the tasks during the period April through September 1992, and provides information on plans for the next 12 months.

The nine tasks addressed in this program are:

- (1) Short through-wall-cracked (TWC) pipe evaluations
- (2) Short surface-cracked (SC) pipe evaluations
- (3) Bi-metallic weld crack evaluations
- (4) Dynamic strain aging and crack instabilities evaluations
- (5) Fracture evaluations of anisotropic pipe
- (6) Crack-opening-area evaluations
- (7) NRCPIPE Code improvements
- (8) Additional tasks, if needed
- (9) Interprogram cooperation and program management.

Of these, significant work was conducted in Tasks 2, 4, 6, and 7 during this period. In addition, several tasks were initiated in the program as part of the program restructuring. This report describes the objective, rationale, approach, and deliverables of these new activities. Table 1.1 lists the changes to the existing program.

Table 1.2 gives an updated summary of the pipe experiments conducted under the Short Cracks in Piping and Piping Welds program. Most of the tasks involve integrated analytical, material characterization, and full-scale pipe fracture experimental efforts. This program addresses only circumferential cracks in straight pipe under quasi-static loading rates. Seismic loading rate behavior of cracked pipe is being investigated in the NRC's Second International Piping Integrity Research Program (IPIRG-2).

Table 1.1 Changes in the program due to restructuring

Task 1 Short TWC Evaluations

Additions

Activity 1.4.4 Develop New GE/EPRI Functions

Deletions

Subtask 1.2 Upgrading of the Large-Pipe Testing System
 Subtask 1.3 Experiment 1.1.1.22 on Cold-leg Short TWC Base Metal Pipe

Task 2 Short SC Evaluations

Additions

Activity 2.1.4 Characterization of Westinghouse Savannah River Stainless Steel
 Pipe Material
 Activity 2.1.5 Tensile Tests on DP2-F4 (A106 Gr B Material)
 Activity 2.4.6 Uncracked Stainless Steel Pipe Mesh Refinement Study
 Activity 2.4.7 Effect of Mesh Refinement on Surface Crack Analyses
 Activity 2.4.8 Verification of J-Estimation Schemes for Surface Cracks

Revisions

Subtask 2.3 Experiment 1.2.3.17 on Cold-leg Short SC Pipe (24-inch
 A106 GrB)

Deletions

Subtask 2.3 Experiment 1.2.3.17 on Cold-leg Short SC SAW Pipe (36-inch
 Schedule 40 A516)

Task 3 Bi-metallic Weld Crack Evaluations

Deletions

Activity 3.2.1 Experiment 1.1.3.8 on Short TWC Bi-metallic Weld Pipe
 Activity 3.2.2 Experiment 1.2.3.21 on Short SC Bi-metallic Weld Pipe
 Activity 3.3.3 Analysis of SC Pipe Bi-metallic Weld Data

Table 1.1 (Continued)

Revisions

Activity 3.2.1 Experiment 1.1.3.8 on Long TWC Bi-metallic Weld Pipe

Task 4 Dynamic Strain Aging

Additions

Activity 4.1.7 Confirmatory Dynamic Strain Aging Tests

Task 5 Fracture Evaluations of Pipe Anisotropy

No Changes

Task 6 Crack Opening Area Evaluations

Additions

Activity 6.6.2 Revisions to SQUIRT Code

Task 7 NRCPIPE Improvements

No Changes

Table 1.1 (Continued)

Task 8 Additional Efforts

Additions

Subtask 8.2	Stainless Steel SAW Fusion-line Toughness
Subtask 8.3	Update of PIFRAC Data Files
Subtask 8.4	Circumferential Pipe Fracture Data Base
Subtask 8.5	Data File Conversion

Task 9 Interprogram Cooperation and Program Management

Deletions

Activity 9.1.3	Participation in ASME PVP Round Robin Efforts
----------------	---

Table 1.2 Restructured test matrix of pipe experiments

Expt. No.	Diameter, in.	Schedule	Material	Temperature	Test Date
<u>Unpressurized through-wall-cracked pipe experiments</u>					
1.1.1.21	28	60	A515 Gr60	288C (550F)	10/25/90
1.1.1.23	28	80	TP316L SAW	288C (550F)	5/23/91
1.1.1.24	24	80	A333 Gr6 SAW	288C (550F)	3/13/92
1.1.1.26	4	80	TP316LN	22C (72F)	2/27/91
<u>Unpressurized uncracked pipe experiment</u>					
1.1.1.25	28	60	A515 Gr60	288C (550F)	2/07/92
<u>Bi-metallic weld fusion line experiments - TWC</u>					
1.1.3.8	36	160	A516/SS-SAW	288C (550F)	9/93
<u>Unpressurized surface-cracked pipe experiments</u>					
1.2.1.20	16	30	TP316	99C (210F)	1/15/92
1.2.1.21	6	XXS	TP304	288C (550F)	4/16/91
1.2.1.22	6	40	TP304	288C (550F)	3/15/91
<u>Pressurized surface-cracked pipe experiments</u>					
1.2.3.15	28	60	A515 Gr60	288C (550F)	11/08/91
1.2.3.16	28	80	TP316L SAW	288C (550F)	9/05/91
1.2.3.17	24	100	A106B SAW	288C (550F)	6/93

2. TASK 1 SHORT TWC PIPE EVALUATIONS

2.1 Task Objective

The objective of this task is to modify and verify analyses for short through-wall-cracked (TWC) pipe using existing and new data on large-diameter pipe.

2.2 Task Rationale

The results of this task will help to refine the fracture analyses in leak-before-break (LBB) procedures used to evaluate through-wall cracks in large-diameter pipes.

2.3 Task Approach

The five subtasks in this task are:

- Subtask 1.1 Material characterization for short TWC pipe experiments
- Subtask 1.2 Upgrading of the large-pipe testing system
- Subtask 1.3 Large-diameter pipe fracture experiments
- Subtask 1.4 Analysis for short through-wall cracks in pipes
- Subtask 1.5 Topical report.

During this reporting period, no work was planned in Subtask 1.1, 1.2, 1.4, and 1.5. Progress in Subtask 1.3 involved reducing the data from the 24-inch-diameter TWC Experiment No. 1.1.1.24 conducted in March 1992. For completeness, this was discussed in the previous semiannual report (Ref. 2.1).

Several changes to the current program are necessary as a result of recent restructuring. In Task 1, these changes involve Subtasks 1.2 and 1.4. Subtask 1.2 will be eliminated from the program. Subtask 1.4 is changed as described below.

2.3.1 Subtask 1.4 Analyses for Short Through-Wall Cracks in Pipes

2.3.1.1 Objective

The objective of this subtask is to develop, improve, and verify the engineering analyses for short circumferential through-wall-cracked pipe.

2.3.1.2 Rationale

The short through-wall-cracked pipe analysis improvements are aimed at LBB fracture evaluations for larger-diameter pipe.

2.3.1.3 Approach

The four activities in this subtask are:

Activity 1.4.1	Improve short through-wall-cracked pipe analysis and compare predictions with existing data
Activity 1.4.2	Analyze large-diameter pipe TWC test results
Activity 1.4.3	Analyze through-wall cracks in welds.
Activity 1.4.4	Develop new GE/EPRI functions.

Activity 1.4.4 Develop New GE/EPRI Functions

Activity 1.4.4 has been included as part of the recent program restructuring and is, therefore, described in detail.

Objective The objective of this activity is to compute additional F, V, and h functions for circumferentially cracked pipes under bending, tension, and combined bending and tension.

Rationale The computations of the functions above using 3-D analysis for short-crack lengths for TWC pipe in bending has shown that the GE-EPRI functions are in error as they were developed using shell elements, possibly because they can be stiffer than 3-D brick elements. Therefore, it is necessary to compute these functions for various crack lengths and other loading configurations, that is, under tension and under combined bending and tension. Since the mesh generation and computational procedure has already been established, conducting additional runs to calculate these functions is quite straightforward.

Approach The functions listed above will be calculated for the following cases (i) through (iv) where d/t = flaw depth/wall thickness, R_m/t = mean radius/wall thickness, n = Ramberg-Osgood exponent for stress-strain curve, and $2a/\pi D_m$ = mean flaw length/mean pipe circumference.

(i) Elastic-plastic run for 360-degree, deep surface-cracked pipe ($d/t = 7/8$; $R_m/t = 5, 10, \text{ and } 20$; $n = 1, 3, 5, 7, \text{ and } 10$) under tension. Since this is an axis-symmetric problem, a 2-D analysis will be sufficient to yield h functions for deep surface cracks not provided in the GE/EPRI Handbook (Ref. 2.2). This is necessary for the SC.TNP and SC.TKP analyses in the surface crack J-estimation schemes.

(ii) Elastic-plastic runs for tension loading of short through-wall-crack lengths; $2a/\pi D_m = 1/8$ and $1/16$; $n = 3, 5, 7, \text{ and } 10$; $R_m/t = 5, 10, \text{ and } 20$.

(iii) Elastic-plastic runs for combined bending and tension loads and short through-wall-crack lengths using the same meshes generated for Case (ii). For Case (iii), the recent GE/EPRI report, Ref. 2.3, on combined bending and tension loads will be carefully reviewed before proceeding with these analyses.

(iv) Elastic-plastic FE runs for bending loads and longer through-wall-crack lengths; $2a/\pi D = 1/4$ and $1/2$; $n = 3, 5, 7,$ and 10 ; $R/t = 5, 10,$ and 20 . The efforts to date have been on $2a/\pi D = 1/16$ and $1/8$.

Deliverables The results of this item along with those already obtained in Subtask 1.4 will provide a complete set of improved and more accurate GE/EPRI functions for the analysis of through-wall-cracked pipe subjected to bending, tension, and combined bending and tension loads. The TWC results will be reported in the currently planned topical report in Task 1 (Short TWC's); the SC results will be given in the topical report for Task 2 (Short SC's). The results will also be summarized in semiannual and program final reports as appropriate.

2.3.3.4 Progress

The GE/EPRI finite element analysis to develop the F , V_3 , and h_4 functions for short circumferentially cracked pipes in Activity 1.4.1c was completed. Most of this progress occurred in the early part of this reporting period and was presented in a previous semiannual report (Ref. 2.1); hence, it will not be repeated here.

2.4 Plans for Next Year of the Program

Work expected to be completed during the next 12 months is described below.

2.4.1 Subtask 1.1 Material Characterization for Short TWC Pipe Experiments

Fabrication and characterization of a weld in a carbon-steel plate, nominally identical to a weld in a carbon steel pipe, which was tested in Task 1, will be carried out within Task 2. Tensile and Charpy V-notch testing of specimens machined from the welded plate was accomplished during the current reporting period and is reported in Section 3.3.1.4; J-R curve tests at room temperature and at 288 C (550 F) are expected to be completed during the next reporting period.

Determination of the tensile properties at 288 C (550 F) of Pipe DP2-F4 (24-inch-diameter A106 Grade B) base metal, which was used in a submerged-arc weld pipe experiment, will be completed during the next year.

2.4.2 Subtask 1.3 Large-Diameter Pipe Fracture Experiments

During the next year, the data record book for Experiment 1.1.1.24 (24-inch-diameter carbon steel weld through-wall-cracked pipe experiment) will be completed. This effort will complete this subtask.

2.4.3 Subtask 1.4 Analyses for Short Through-Wall Cracks in Pipes

The following activities will continue in the next year.

Activity 1.4.1(a). During the next reporting period, we shall complete the finite element analysis of the 28-inch-diameter Experiment 1.1.1.21. Analysis of this experiment up to crack initiation had already been completed and was put on hold until issues involving the effect of mesh refinement were resolved (in Task 2).

Activity 1.4.1(b). The GE/EPRI functions developed in this program and reported in Semiannual Report Vol. 2, No. 1 will be incorporated into the NRCPIPE program.

Activity 1.4.4. Since the original functions were found to be in error, additional F, V, and h functions for circumferentially cracked pipes under bending, tension, and combined bending and tension will be computed in conformance with recent program restructuring.

2.5 References

- 2.1 Wilkowski, G. M., et al., "Short Cracks in Piping and Piping Welds," Semiannual Report, October 1991 - March 1992, NUREG/CR-4599, Vol. 2, No. 2, February 1993.
- 2.2 Kumar, V., et al., "An Engineering Approach for Elastic-Plastic Fracture Analysis," EPRI Report NP-1931, July 1981.
- 2.3 Kumar, V. and others, "Advances in Elastic-Plastic Fracture Analysis", EPRI Final Report NP-3607, August, 1984.

3. TASK 2 SHORT SC PIPE EVALUATIONS

3.1 Task Objective

The objective of this task is to modify and verify analyses for short surface-cracked (SC) pipe using existing and new data on large-diameter pipe.

3.2 Task Rationale

These results will verify and may refine analyses that have been used for pragmatic in-service flaw evaluations such as those in ASME Section XI.

3.3 Task Approach

The five subtasks in this task are:

- Subtask 2.1 Material characterization for surface-cracked pipe experiments
- Subtask 2.2 Small-diameter pipe fracture experiments in pure bending for limit-load ovalization correction
- Subtask 2.3 Large-diameter surface-cracked pipe fracture experiments under combined bending and tension (pressure)
- Subtask 2.4 Analysis of short surface cracks in pipes
- Subtask 2.5 Topical report.

During the last reporting period, only Subtasks 2.1 and 2.4 were active as detailed below. In Subtask 2.2, the data record book for Experiment 1.2.1.20, conducted previously, was prepared during this period.

3.3.1 Subtask 2.1 Material Characterization for Surface-Cracked Pipe Experiments

3.3.1.1 Objective

The objective of this activity is to generate the data necessary to document the material strength and toughness for analysis in Subtask 2.4.

3.3.1.2 Rationale

The material property data needed for the analysis procedures in Subtask 2.4 will be determined for each pipe and weld to be subjected to a pipe fracture experiment. These data are also to be included in the NRC PIFRAC database (Ref. 3.1).

3.3.1.3 Approach

Material property data for pipes to be tested within Task 2, i.e., Charpy, chemical analyses, tensile, and J-R curves, are already available from the Degraded Piping Program (Ref. 3.2). One exception is a 16-inch-diameter Schedule 30 stainless steel pipe that replaces the pipe damaged in the accident associated with the IPIRG-1 Experiment 1.3-7. The pipe that was damaged had previously been characterized in the Degraded Piping Program. Since that pipe is not available for testing in Task 2, a replacement pipe was procured and characterized.

The data will be recorded digitally and reduced to a format identical to that used in past Degraded Piping Program data record book entries. These data will also be available for input into the NRC PIFRAC database.

3.3.1.4 Progress

Material characterization work was initiated on one of the two submerged-arc, carbon-manganese-molybdenum weldments prepared from A516 Grade 70 carbon steel plate material, described in Ref. 3.3. Specifically, testing was initiated on specimens machined from the weld metal in a weldment identified as Plate DP2-F49W. That welded plate was 0.9 m (36 inches) in length and 31.8 mm (1.25 inches) thick and simulated the girth weld in a 24-inch-diameter carbon steel pipe of approximately the same thickness, to be tested in Subtask 2.3. The plate weldments were prepared at the United McGill Corporation in Columbus, Ohio, at the same time as a girth weld was prepared in the 24-inch-diameter carbon steel pipe. Both the plate welds and the pipe weld followed the recommendations of Babcock & Wilcox for bevel, gap, and backing strip. The welding wire was a high manganese, high molybdenum material carrying the designations EA3 and SFA 5.23; the flux was Linde 80. It was expected that the welds produced following Babcock & Wilcox's recommendation would typify 90 percent of those used in B&W plants.

The tensile properties of the weld metal in Plate DP2-F49W are shown in Table 3.1 and the stress-strain curves are shown in Figure 3.1. Note that raising the test temperature from room temperature to 288 C (550 F) slightly increased the ultimate strength while slightly decreasing both the yield strength and the tensile ductility. The increase in the ultimate tensile strength as the temperature is raised probably indicates that the weld metal is susceptible to dynamic strain aging, a phenomenon commonly observed in carbon steels.

Charpy V-notch data for the weld metal in Plate DP2-F49W are shown in Table 3.2. Note that both the absorbed energy and the percentage of shear area on the fracture surface are increased as the temperature is raised from room temperature to 288 C (550 F).

3.3.2 Subtask 2.4 Analysis of Short Surface Cracks in Pipes

3.3.2.1 Objective

The objective of this subtask is to develop, improve, and verify the engineering analyses for short circumferential surface-cracked large-diameter pipe where elastic-plastic fracture is expected.

Table 3.1 Tensile properties of the carbon-manganese-molybdenum submerged-arc weld metal (DP2-F49W) in 31.8-mm-thick (1.25-inch) A516 Grade 70 plate

Specimen I.D.	Test Temperatures		Strain Rate, s ⁻¹	0.2 Percent Offset Yield Strength		Ultimate Tensile Strength		Elongation, percent in 25.4 mm: (1 inch)	Area Reduction, percent
	C	F		MPa	ksi	MPa	ksi		
F49W-1	22	72	4.2x10 ⁻⁴	447	64.8	554	80.4	20.8	62.1
F49W-2	22	72	4.2x10 ⁻⁴	<u>445</u>	<u>64.5</u>	<u>554</u>	<u>80.3</u>	<u>21.2</u>	<u>62.6</u>
			Average	446	64.7	554	80.4	21.0	62.5
F49W-3	288	550	4.0x10 ⁻⁴	412	59.8	574	83.3	19.9	54.1
F49W-4	288	550	3.9x10 ⁻⁴	<u>417</u>	<u>60.5</u>	<u>576</u>	<u>83.5</u>	<u>17.1</u>	<u>48.8</u>
			Average	415	60.2	575	83.4	18.5	51.5

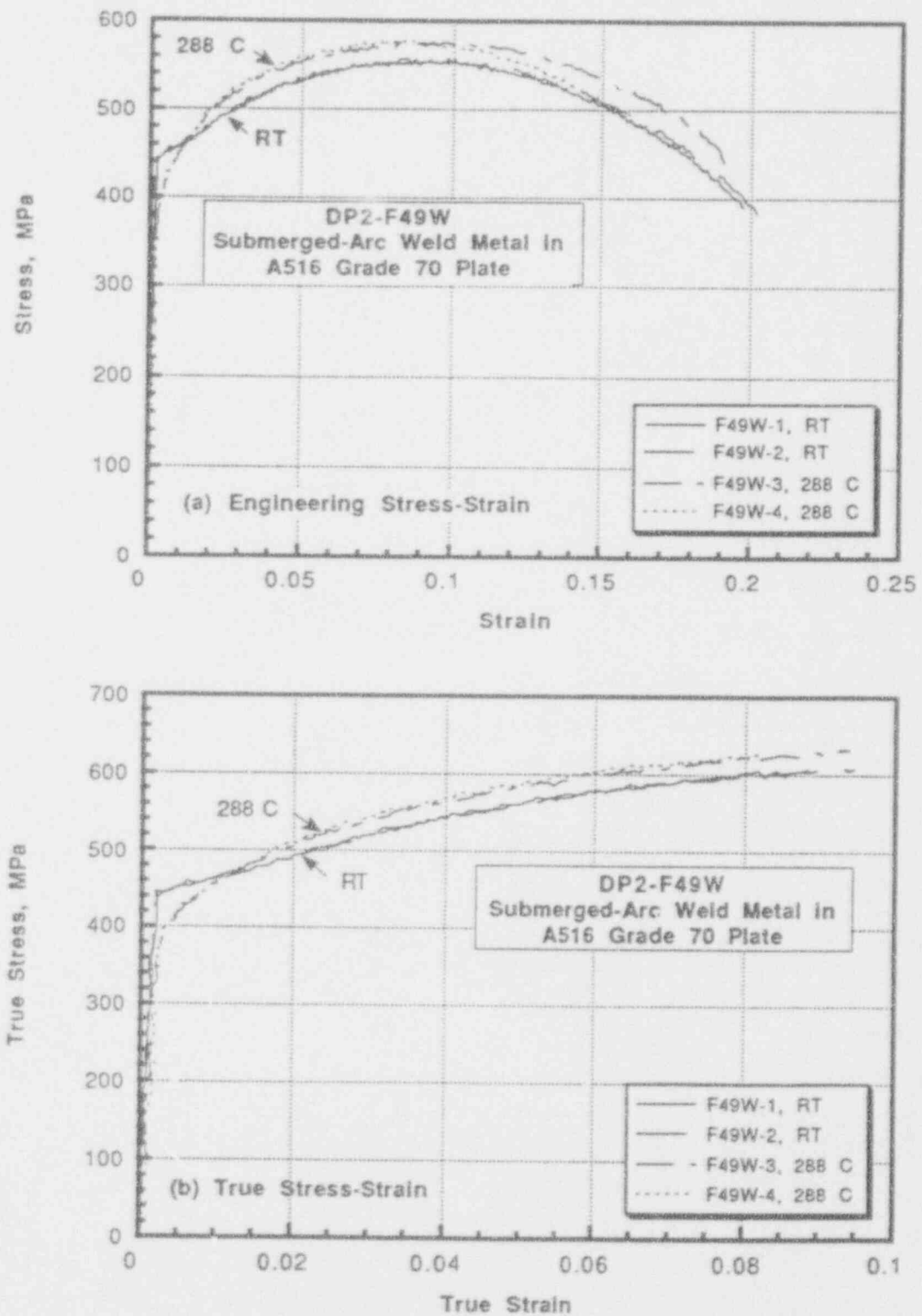


Figure 3.1 Transverse tensile properties of weld DP2-F49W: (a) engineering stress-strain curves and (b) true stress-strain curves

Table 3.2 Charpy V-notch results for submerged-arc weld metal (DP2-F49W) in 31.8-mm-thick (1.25-inch) A516 Grade 70 plate

Test Temperature, C	Absorbed Energy, J (ft-lb)	Percent Shear
21	76.6 (56.5)	75
21	84.1 (62.0)	80
21	<u>70.5 (52.0)</u>	<u>75</u>
Average	77.1 (56.8)	77
288	103.7 (76.5)	100
288	109.9 (81.0)	100
288	<u>103.1 (76.0)</u>	<u>100</u>
Average	105.6 (77.8)	100

3.3.2.2 Rationale

The short surface-cracked (SC) pipe analysis improvements are aimed at assessing and improving the ASME Section XI flaw evaluation criteria (Refs. 3.4 and 3.5).

3.3.2.3 Approach

The nine activities in this subtask are:

- Activity 2.4.1 Uncracked pipe analysis
- Activity 2.4.2 Improve SC.TNP and SC.TKP analyses
- Activity 2.4.3 Compare improved limit-load solutions with short surface-cracked small-diameter pipe data
- Activity 2.4.4 Analyze large-diameter surface-cracked pipe test data
- Activity 2.4.5 Evaluate procedures in J-estimation schemes for surface cracks in welds.
- Activity 2.4.6 Extend SC.TNP and SC.TKP for external surface-crack geometries under combined loading
- Activity 2.4.7 Uncracked SS Pipe Mesh Refinement
- Activity 2.4.8 Surface-Cracked Mesh Refinement Study
- Activity 2.4.9 SC J-estimation Verification.

Activities 2.4.7, 2.4.8, and 2.4.9 are new efforts as a result of the recent program restructuring. The objective, scope, and deliverables of these activities are described below.

Activity 2.4.7 Uncracked SS Pipe Mesh Refinement

Objective The objective of this work is to conduct finite-element (FE) analysis of uncracked stainless steel pipe and bend bars using different mesh sizes and improved constitutive relations in order to evaluate the accuracy of simplified analyses to predict load and displacement prediction for short-cracked pipe.

Rationale The overall objective of this activity is to resolve the discrepancy observed between the experimental data and FE analysis of cracked stainless steel pipe test. As a first step, therefore, this discrepancy for uncracked pipes and bend bars will be resolved.

Approach Results to date in Subtask 2.4 have shown that FE analyses underpredict the maximum load for an uncracked stainless steel pipe by as much as 20 percent. This was further confirmed by analysis of stainless steel bend-bar specimens conducted in Sweden, the data being provided by Dr. B. Brickstad. One potential source of this discrepancy is the size of the mesh used in modelling the experiments. Specifically, if a finer mesh is used to model the compressive side of an uncracked pipe under bending loads, then we would expect that the through-thickness strains will be modelled more accurately. The incorrect modelling of these strains could have led to the lower FE predictions in the past.

The first step in this effort will involve analyzing the data provided by Dr. B. Brickstad on the uncracked bend-bar specimens using 3-D FE analysis. Several elements (2, 3, and 5 if needed) in the thickness directions will be used in the analysis and compared with the experimental data as well as the plane stress and plane strain solutions obtained in the past. If the FE predictions match the data accurately, such a match would confirm the hypothesis that mesh refinement rather than incorrect constitutive modelling was the source of error in earlier analyses. Once this is resolved, the experiments from JAERI (Ref. 3.6) on uncracked stainless steel pipe will be reanalyzed using finer mesh sizes and compared with data. Table 3.3 shows the matrix of experiments to be analyzed.

Table 3.3 JAERI uncracked stainless steel pipe experiments to be analyzed

Experiment No.	Diameter, inches	Schedule	Material
S-17	3	80	TP304
S-1	3	40	TP304
TT-00	6	80	TP304

Experiment S-17 in Table 3.3 will be used to first evaluate the effect of mesh refinement using three different mesh sizes. Experiments S-1 and TT-00 will then be used to verify results using only two different sizes.

Deliverables The uncracked pipe analysis results will yield the ovalization correction factor for short through-wall and surface-cracked pipe J -estimation schemes as well as for modifications to the Net-Section-Collapse analysis. These values can also be used to make corrections for the η (eta) factor J analysis of the pipe experiments so that the plastic displacements or rotations from the uncracked pipe can be accounted for.

Progress in this activity will be reported in semiannual reports. In addition, the topical report on Short Surface Cracks (Task 2) will include all the results obtained in this activity.

Activity 2.4.8 Surface-Cracked Mesh Refinement Study

Objective The objective of this task is to investigate the effect of mesh size on numerical results for 3-D FE analyses of circumferential surface-cracked pipe.

Rationale In recent numerical analyses, a question that has arisen frequently is what effect mesh refinement has on the results obtained. Specifically, in elastic-plastic fracture mechanics (EPFM) analyses of surface-cracked pipe, the size of elements in the vicinity of the crack tip region as well as the number of elements used through the thickness influence the convergence of the solution in nonlinear problems. Two aspects of this problem will be addressed in this task: (1) the influence of mesh refinement on high and low toughness pipe materials and different crack sizes, and (2) a comparison between the results using refined three-dimensional meshes and line-spring models.

Approach The approach for this activity involves detailed FE investigations of past carbon steel and stainless steel surface-cracked pipe tests with long and short cracks (see Table 3.4). As part of the

plan, an investigation on a long surface-cracked carbon steel pipe experiment will be conducted at Battelle. In addition, as part of our existing contract, we will work with Westinghouse Savannah River staff on their FE analysis of a short surface-cracked stainless steel pipe experiment.

Table 3.4 Summary of surface-cracked pipe FE analyses

Experiment Number	Material Diameter, Schedule	Crack Size Parameters	Organization Conducting Analysis
4112-8 (Degraded Piping Program)	A106 Gr B (16-inch diameter, Schedule 100)	Large $d/t = 0.66$ $2a/\pi D_m = 0.5$	Battelle
1.2.1.20 (Short Cracks Program)	TP304LN (16-inch diameter, Schedule 30)	Short $d/t = 0.5$ $2a/\pi D_m = 0.25$	Westinghouse Savannah River Staff

New Efforts in Activity 2.4.8 The first step in this plan involves conducting a FE analysis of a long surface-cracked carbon steel pipe experiment (Number 4112-8) completed during the Degraded Piping Program Phase II (Ref. 3.7) and analyzed in a past FE round-robin. Three sets of FE meshes with various levels of refinement will be prepared first using ABACRACK, a special purpose software that is available specifically for this purpose. The results from this analysis will indicate the level of refinement necessary to obtain sufficiently accurate results.

The next step involves conducting an analysis for the same geometry using line-spring models as is frequently done for surface cracks. A line-spring representation of the surface crack is computationally more efficient and less expensive. However, the numerical accuracy of this model has to be validated. This will be done by comparing the 3-D solutions using EPFM analysis with those of this model. A recommendation can then be made regarding conditions under which the line-spring model is adequate and can, therefore, be used to represent surface cracks in piping or pressure vessels. Note that the Battelle *J*-estimation scheme for surface-cracked pipe is actually a form of the line-spring model.

Westinghouse Savannah River FE Analysis As part of our current work scope, we are cooperating with Westinghouse Savannah River staff in conducting a FE analysis of a pipe fracture experiment conducted in this program on pipe material they donated to us. The experiment is complete except for the material characterization efforts.

Deliverables The two deliverables for this activity will be

- (1) The size of mesh refinement required to obtain sufficiently accurate results for circumferentially surface-cracked pipe
- (2) The accuracy and adequacy of line-spring models in surface-cracked pipe analysis.

These will be included in the topical report on surface-cracked pipe that is currently planned as well as semiannual reports and the program final report.

Activity 2.4.9 SC J-Estimation Scheme Verification

Objective The objective of this activity is to conduct FE analyses for internal and external surface-cracked pipe for comparison with the results of the estimation schemes that have been developed in this program.

Rationale The J-estimation scheme developed by Battelle for Brookhaven in Activity 2.4.6 is applicable to both internal and external surface cracks as well as to combined bending and pressure loads. Also, various types of surface crack shapes (constant depth, elliptical, circular) have been considered in this analysis. The only verification of this method that we are aware of involves one FE analysis performed by Professor Kikuchi in Japan of Experiment No. 4131-4 (Degraded Piping Program - Phase II), this involves an internal flaw in an A106 Grade B pipe subjected to bending and pressure. This J-estimation analysis is now being incorporated into a surface-cracked version of the SC.TNP and SC.TKP J-estimation schemes in the NRCPIPES computer code. Before this code is put in the public domain, it is necessary to check the results of the estimation scheme against some FE results or other methods such as the line-spring model.

Approach The following FE analyses are planned for constant depth flaws, since these represent the most common assumptions used for surface flaws.

Flaw type:	Internal and external
Flaw length:	1/16, 1/8, and 1/2 of mean circumference
Flaw depth/thickness:	1/2, 2/3
Load type:	Bending, tension, bending plus tension
Analysis type:	EPFM theory or line-spring model.

As part of the mesh refinement study (Activity 2.4.8), a comparison between the results of the detailed 3-D FE analyses and line-spring models for the same geometries will be made. If the two are in agreement, then all further FE analysis will proceed with the line-spring model, because it is computationally less expensive. Only specific cases involving combinations of the parameters given above will be studied in order to verify the estimation procedure for a variety of problems.

Based on the discrepancy between the FE results and SC.TNP or SC.TKP analyses, the limitations of the J-estimation schemes and the error involved will be identified. Some simple corrections to the J-estimation schemes to account for potential discrepancies will also be attempted for incorporation into NRCPIPES.

Deliverables A comparison between detailed FE analysis and the J-estimation schemes will be available. Hence, the accuracy of simpler J-estimation schemes for surface cracks in piping can be established. These results will be reported in the currently planned topical report on surface-cracked pipe as well as the semiannual and final reports, as appropriate.

3.3.2.4 Progress

Only Activities 2.4.1 and 2.4.7 were active during this reporting period. Since these are related, the progress in these two activities are discussed together.

Activity 2.4.1 Uncracked Pipe Analysis

Efforts during this reporting period involved trying to resolve the discrepancy between the experimental data and FE prediction on uncracked stainless-steel pipe. To this end, first the uncracked four-point bend-bar experiment conducted at the Royal Institute of Stockholm, Sweden was analyzed. Then, a JAERI experiment (Ref. 3.6) on an uncracked stainless-steel pipe was analyzed.

The finite-element analysis of the four-point, stainless-steel, bend-bar experiment conducted in Sweden continued in this reporting period. Two 3-D meshes with different levels of mesh refinement were used to perform the analysis. In addition, the closed-form solution using inelastic beam theory was also obtained for the specimen. The two FE solutions using the two meshes were identical, indicating that the solution had converged in each case. While there is excellent agreement between moments from the closed-form solution and the FE results, as seen in Figure 3.2, both analyses underpredict the experimental normalized moment versus outer fiber strain curve. At a strain value of 0.5 percent, the discrepancy between the analysis and experiment is almost 9 percent. The 2-D plane strain solution for this problem gives higher moments, as would be expected. Contrary to expectations, mesh refinement in the FE analysis does not resolve the problems involved in predicting the experimental results for the stainless-steel bar.

Figure 3.3 shows a plot of the FE predictions of the longitudinal strain in the beam as it varies with the beam depth at two load levels: (i) at the onset of inelastic behavior (0.2 percent strain), and (ii) at 0.5 percent outer fiber strain. As seen, the strain distribution across the depth is linear, indicating that plane sections do remain plane as assumed in the beam theory analysis of the problem.

Even though this discrepancy has not been resolved, we decided to continue the effort involving FE analysis of the uncracked stainless steel pipe experiment conducted at JAERI. A discrepancy of 9 percent observed in the bend bar could possibly be attributed to statistical variation in material properties and is not highly significant. However, the discrepancy between analysis and experiment for the uncracked pipe was found to be as much as 20 percent in our earlier work, which is greater than the statistical variation of material properties. Therefore, the influence of mesh refinement on the uncracked pipe analysis was investigated next.

Figures 3.4 and 3.5 show the 3-D meshes with one and four elements through the pipe thickness used in the analysis of JAERI Experiment No. S-17. Figure 3.6 shows the experimental load-displacement curve along with the FE predictions. Predictions using both meshes agreed closely with the experiment and hence the analysis using four elements was stopped at a load-line displacement of 10 mm since the computational costs for this case are significantly higher. This indicates that 3-D analysis rather than mesh refinement can resolve the discrepancy observed earlier between FE results (using the elbow element and shell elements with three nodes through the thickness) and the experimental observations.

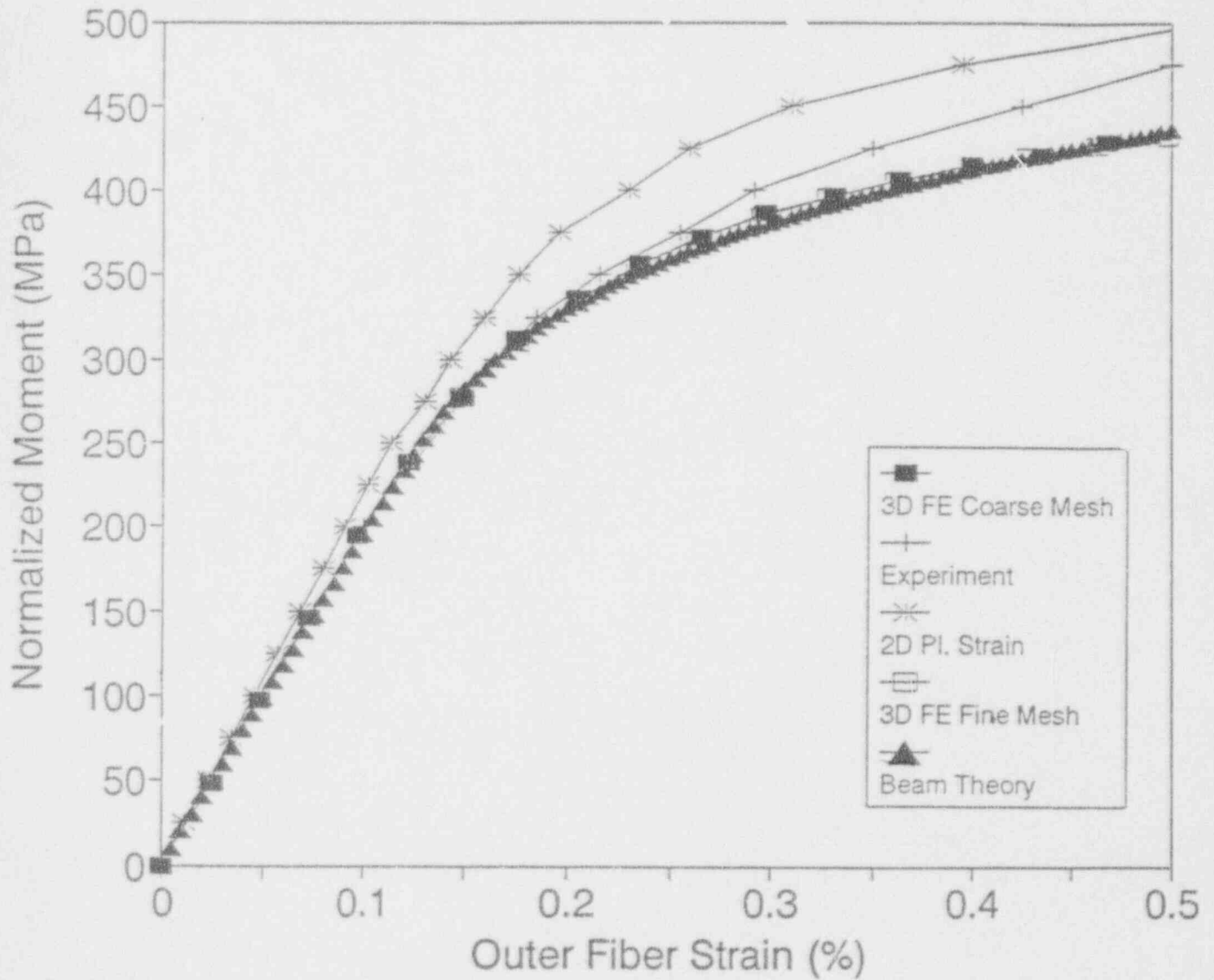


Figure 3.2 Comparison between analytical predictions and experimental data from an uncracked four-point bend bar specimen

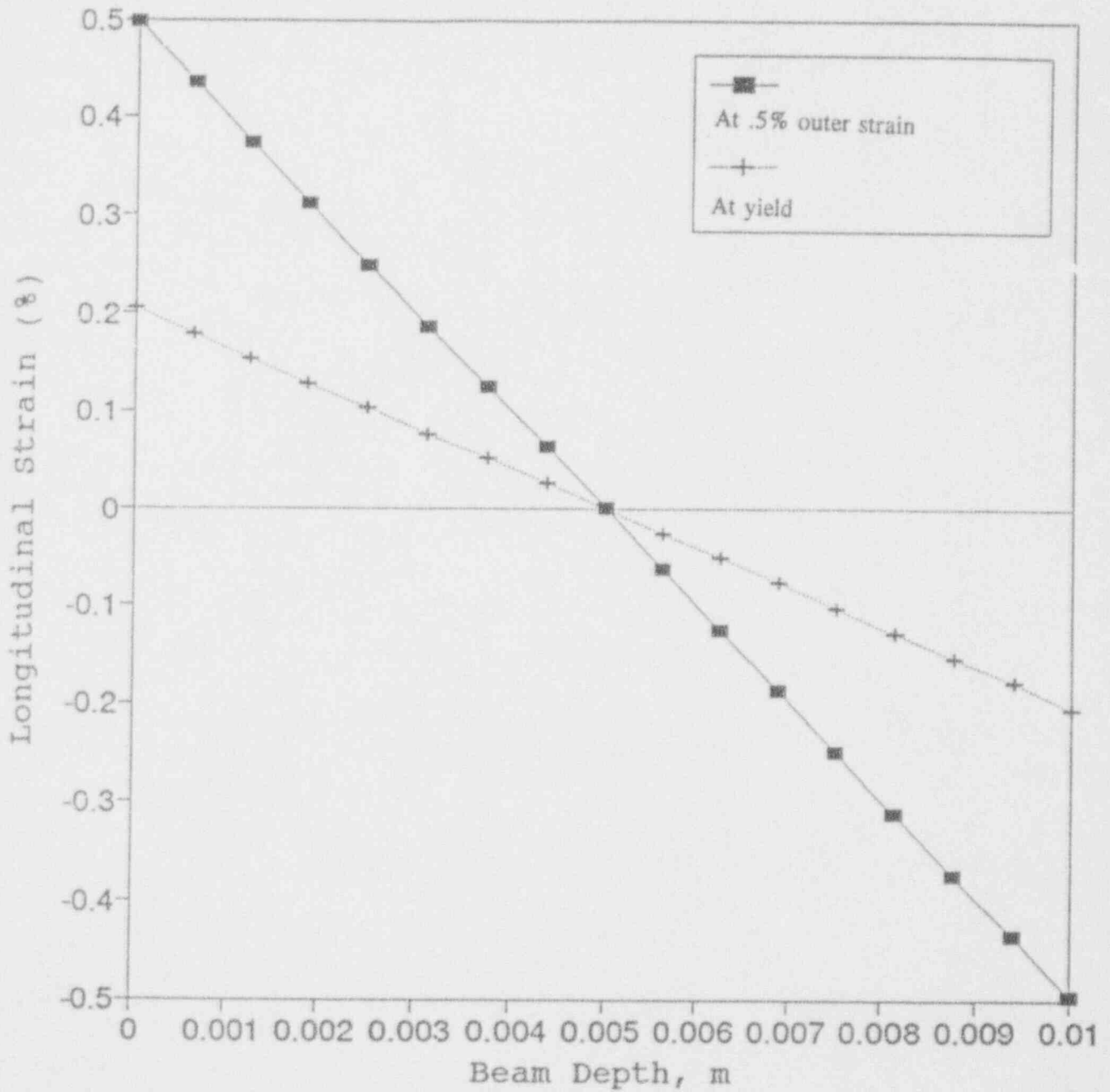


Figure 3.3 Longitudinal strains versus beam depth showing that plane sections do remain plane during plastic deformation

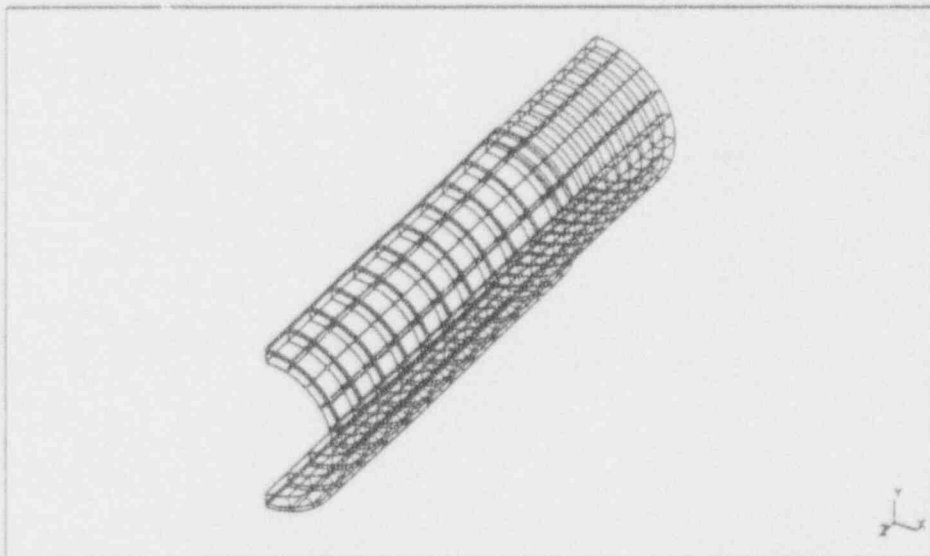


Figure 3.4 Finite-element mesh of JAERI Uncracked Pipe Experiment S-17 using 3-D solid elements. One element through thickness.

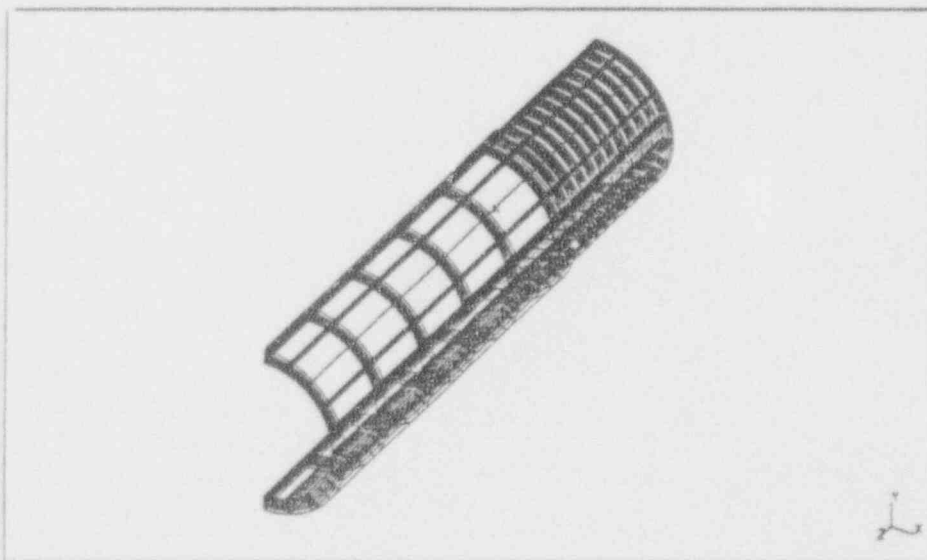


Figure 3.5 Finite-element mesh of JAERI Uncracked Pipe Experiment S-17 using 3-D solid elements. Four elements through thickness.

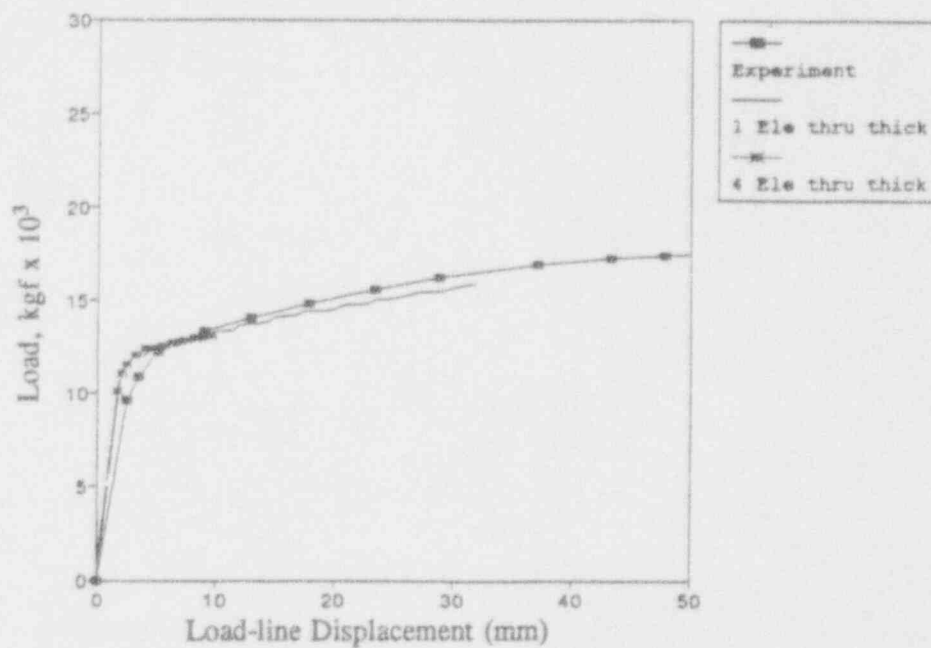


Figure 3.6 Load-line displacement versus load for Un-cracked Pipe Experiment S-17. Experiment and finite-element results.

A point of interest in the experimental data is that the axial strains reported in Ref. 3.6 in the compressive region on the pipe center section are much lower than those in the tension region, see Figure 3.7. Since the shift in neutral axis is negligibly small, it would indicate that the compressive stress-strain properties are significantly different from tensile material behavior; this, however, seems unlikely from past data on stainless steel. The FE predictions of strain in this region are shown in Figure 3.8. As seen, the strains do not remain linear through the thickness at the various load levels indicating that plane sections may not remain plane. Upon further investigation, we found that the inner span used in the 4-point bending tests was two and one-half times the outer pipe diameter. In our experience, this span has to be at least four times the pipe diameter to create a pure bending moment at the pipe center section. This could explain the observed discrepancy between the observed tensile and compressive strains.

3.4 Plans for Next Year

The efforts described below will be undertaken during the 12-month period.

3.4.1 Subtask 2.1 Material Characterization for Surface-Cracked Pipe Experiments

During the next year, it is expected that characterization of the replacement 16-inch-diameter austenitic stainless steel pipe from Savannah River will be completed. In addition, J-R curve tests at both room temperature and at 288 C (550 F) for the carbon-steel submerged-arc weld in 25.4-mm (1-inch) thick A516 Grade 70 plate (Plate DP2-F49W) will be completed.

3.4.2 Subtask 2.2 Small-Diameter Pipe Fracture Experiments in Pure Bending for Limit-Load Ovalization Correction

During the next year, the data record book for Experiment 1.2.1.20 (16-inch-diameter Schedule 30 stainless steel surface-cracked pipe experiment) will be completed. This effort will complete this subtask.

3.4.3 Subtask 2.3 Large-Diameter Surface-Cracked Pipe Fracture Experiments Under Combined Bending and Tension (Pressure)

During the next year, Experiment 1.2.3.17 (24-inch-diameter carbon steel short surface-cracked pipe experiment) will be conducted. The pipe sample for this experiment is a section of A106 Grade B pipe left over from a previous Atomic Energy Commission (AEC) program conducted at Battelle. The crack will be located in a submerged-arc weld (SAW) and loaded under combined pressure and four-point bending.

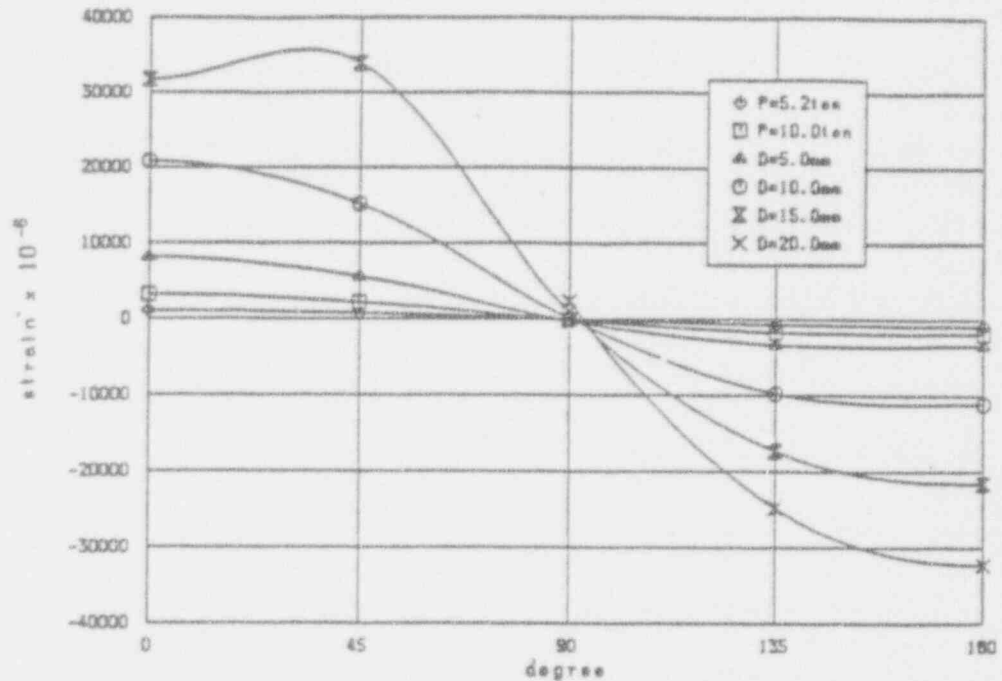


Figure 3.7 Axial strain distribution around the pipe circumference at the center section of Pipe S-17 under pure bending. Note the difference in tensile and compressive strains at various load levels (from JAERI-M87-068)

SCM-10/92-F1

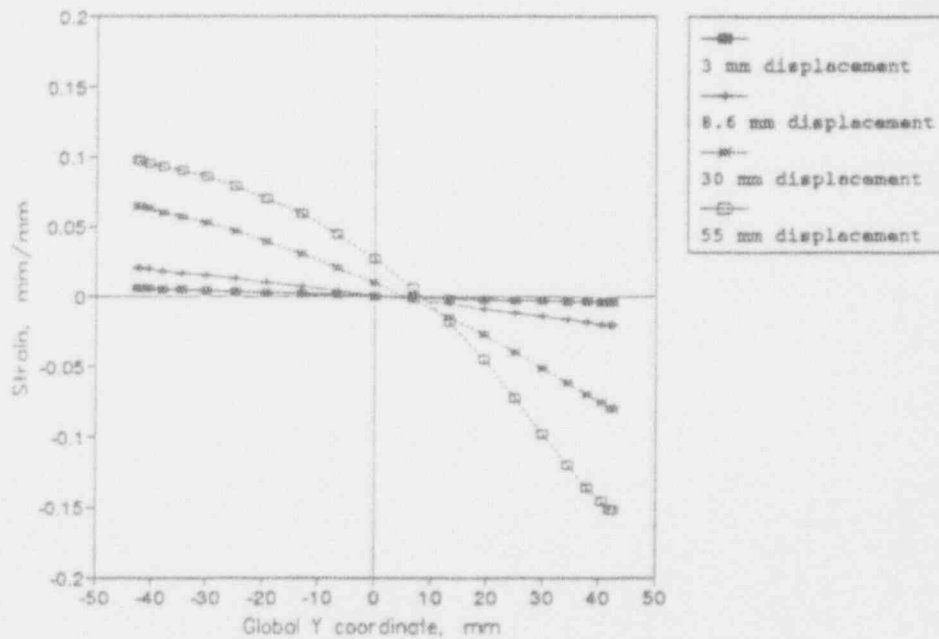


Figure 3.8 Outer surface for midsection of pipe for Uncracked Pipe Experiment S-17. Finite-element result for one element through thickness.

3.4.4 Subtask 2.4 Analysis of Short Surface Cracks in Pipes

The work on the uncracked pipe study, Activities 2.4.1 and 2.4.7, shall be completed in the next reporting period. In Activity 2.4.2, the PC version of SC.TNP will be tested and improvements made whenever necessary. Activity 1.4.8, SC Mesh Refinement Study, shall be started next year.

3.5 References

- 3.1 Hiser, A. L. and Callahan, G. M., "A User's Guide to the NRC's Piping Fracture Mechanics Database (PIFRAC)," NUREG/CR-4894, May 1987.
- 3.2 Wilkowski, G. M. and others, "Degraded Piping Program - Phase II," Summary of Technical Results and Their Significance to Leak-Before-Break and In-Service Flaw Acceptance Criteria, March 1984-January 1989, by Battelle Columbus Division, NUREG/CR-4082, Vol. 8, March 1989.
- 3.3 Wilkowski, G. M. and others, "Short Cracks in Piping and Piping Weld," NUREG/CR-4599, Vol. 2, No. 1, September 1992.
- 3.4 "Evaluation of Flaws in Austenitic Steel Piping" (Technical basis document for ASME IWB-3640 analysis procedure), prepared by Section XI Task Group for Piping Flaw Evaluation, EPRI Report NP-4690-SR, April 1986.
- 3.5 American Society of Mechanical Engineers Boiler and Pressure Vessel Code, Section XI, Article IWB-3650, 1992 Edition, July 1, 1992. Published by American Society of Mechanical Engineers, New York, N.Y. 10017.
- 3.6 Yasuda, Y., et al., "Investigations on Ductile Fracture Behavior of 3-Inch Diameter Type 304 Stainless Steel Pipe with a Circumferential Through-Wall Crack," JAERI-87-068, 1987.
- 3.7 Scott, P. M., and Ahmad, J., "Experimental and Analytical Assessment of Circumferentially Surface-Cracked Pipes Under Bending," by Battelle, NUREG/CR-4872, April 1987.

4. TASK 3 BIMETALLIC WELD CRACK EVALUATIONS

This task was not active this reporting period; hence there is no progress to report. The task will start in the next reporting period and will be discussed in future semiannual reports.

5. TASK 4 DYNAMIC STRAIN AGING

5.1 Task Objective

The objective of this task is to evaluate and predict the effects of crack instabilities, believed to be due to dynamic strain aging (DSA), on the fracture behavior of pipe. Specific objectives are (1) to establish a simple screening criterion to predict which ferritic steels may be susceptible to unstable crack jumps, and (2) to evaluate the ability of current J-based analysis methodologies to assess the effect of unstable crack jumps on the fracture behavior of ferritic steel pipe. If necessary, alternative procedures for predicting pipe behavior in the presence of crack jumps will be derived.

5.2 Task Rationale

The methodology developed here will be applicable to both LBB and in-service flaw evaluations. It will also be valuable for selection of materials for future advanced reactor designs.

5.3 Task Approach

The four subtasks and two optional subtasks in this task are:

- | | |
|-------------|---|
| Subtask 4.1 | Establish a screening criterion to predict unstable crack jumps in ferritic steels |
| Subtask 4.2 | Evaluate procedures for characterizing fracture resistance during crack jumps in laboratory specimens |
| Subtask 4.3 | Assess current procedures for predicting crack jump magnitudes in pipes |
| Subtask 4.4 | Prepare interim and topical reports on dynamic strain aging induced crack instabilities in ferritic nuclear piping steels at LWR temperatures |
| Subtask 4.5 | (Optional Subtask) Refine procedures for characterizing fracture resistance during crack jumps in laboratory specimens |
| Subtask 4.6 | (Optional Subtask) Refine procedures for predicting crack jump magnitudes in pipes |

In the recent restructuring of the program, Activity 4.1.7 was added to Subtask 4.1. This activity involves conducting additional fracture tests on a carbon steel weld where the DSA high-temperature hardness screening criterion indicated DSA should occur at a higher temperature than typical of other ferritic steels. This activity is discussed below.

Activity 4.1.7 Confirming Dynamic Strain Aging Tests

Objective The objective of this effort is to conduct four additional fracture toughness tests on a carbon steel weld (DP2-F29W) at temperatures between 315 and 400 C (600 and 750 F) to determine the presence or lack of dynamic strain aging (DSA) indications (crack jumps) within this temperature range for this weld.

Rationale This task addresses dynamic strain aging; in particular, methods for evaluating crack jumps and predicting which materials are susceptible to DSA. An hypothesis has been developed which relates hardness and strength differences from ambient and elevated temperature tests as a key indicator of DSA susceptibility. The carbon steel weld being studied in the task (DP2-F29W) was found, on the basis of tensile and hardness tests, to be susceptible to DSA but at a significantly higher temperature than were the carbon steel base metals. Compact specimen tests of the weld at 288 C (550 F), a temperature which usually produced crack jumps in carbon steel base metals susceptible to DSA, revealed no crack jumps. However, if, as presently believed, crack jumps are related to DSA susceptibility, it is likely that additional compact specimen tests at temperatures somewhat higher than 288 C (550 F) will produce crack jumps. Thus, these additional tests are important to the hypothesis that DSA is, in fact, responsible for crack jumps.

Approach Four additional compact specimen tests will be conducted on a carbon steel weld (DP2-F29W) at temperatures between approximately 315 and 400 C (600 and 750 F) to determine the presence or absence of crack jumps. The specific test temperatures will be determined by Battelle. Since specimens from this weld remain from previous work, this effort simply involves testing the specimens, and analyzing and reporting the results.

Deliverables The results of this effort will be combined with other results from this task and will be included in the topical report for this task. They will also be described in monthly, semiannual, and program final reports. The digital data files of the test results will be incorporated into the PIFRAC data base and also sent to NRC.

5.4 Plans for Next Year of the Program

The efforts described below will be undertaken during the next year.

5.4.1 Subtask 4.1 Establish a Screening Criterion to Predict Unstable Crack Jumps in Ferritic Steels

The confirmatory dynamic strain aging fracture tests in Activity 4.1.7 will be completed next year.

5.4.2 Subtask 4.2 Evaluate Procedures for Assessing Fracture Resistance During Crack Jumps in Laboratory Specimens

One finite-element analysis of a C(T) specimen experiment showing crack jumps will be undertaken in the next year. The experimental load-displacement and crack-growth load-line displacement curves will be used in the FE analysis. The behavior of the J-integral as well as other fracture parameters such as the Crack Tip Opening Angle (CTOA) shall be investigated during the crack-jump phenomenon.

6. TASK 5 FRACTURE EVALUATIONS OF PIPE ANISOTROPY

6.1 Task Objective

The objective of this subtask is to assess if anisotropic fracture properties (where the toughness is typically lower in a helical direction or the axial direction for ferritic seamless pipe) together with the occurrence of high principal stresses in a helical direction can cause a lower failure stress than calculated using the toughness in the L-C orientation and using only the longitudinal stresses.

6.2 Task Rationale

The rationale for this task is to assess if the source equations in the current LBB and ASME flaw evaluation procedures could overpredict the maximum loads for out-of-plane crack growth under certain service loading conditions. If current procedures are found to significantly overpredict the load modifications to existing fracture analysis methods will be made.

6.3 Task Approach

Five subtasks will be conducted in this task. Two of them are optional subtasks that would be started only with NRC approval after an interim report is completed. The subtasks are:

- | | |
|-------------|--|
| Subtask 5.1 | Assess effect of toughness anisotropy on pipe fracture under combined loads |
| Subtask 5.2 | Determine magnitude of toughness anisotropy and establish a screening criterion to predict out-of-plane crack growth |
| Subtask 5.3 | Prepare interim and topical reports on anisotropy and mixed-mode studies |
| Subtask 5.4 | Establish ductile crack growth resistance under mixed-mode loading (optional subtask) |
| Subtask 5.5 | Refine J-estimation scheme analyses for pipes (optional subtask). |

All the subtasks were inactive during the last reporting period and, hence, there is no progress to report.

6.4 Plans for Next Year of the Program

The material characterization and laboratory specimen tests in this task are almost complete. Analysis efforts in this task have been temporarily put on hold until efforts in Tasks 1 and 2 are complete.

7. TASK 6 CRACK OPENING AREA EVALUATIONS

7.1 Task Objective

The objective of this subtask is to make improvements in the crack-opening area predictions for circumferentially cracked pipe, with particular attention to cracks in welds. The crack opening area analyses will be incorporated into the SQUIRT code.

7.2 Task Rationale

From past efforts in the Degraded Piping Program, IPIRG, and ASME PVP Conference round robins, it has been found that the leakage area predictions are reasonably consistent for circumferential through-wall cracked (TWC) pipe in bending (with the cracks in the base metal). For the case of a crack in the center of the weld, the predictions showed more error in the intermediate to higher bending load levels. For the case of a crack in the base metal, but with the pipe in combined bending and tension, the error in the results was significantly greater. If the crack had been in a weld under combined loading, the scatter probably would have increased even more. The accuracy of the solutions for a crack in a weld and for cracked pipe under combined loading needs verification and improvement for LBB analyses.

7.3 Task Approach

The six specific subtasks in this task are:

- Subtask 6.1 Create combined loading improvements
- Subtask 6.2 Implement short TWC crack-opening improvements
- Subtask 6.3 Improve weld crack evaluations
- Subtask 6.4 Modify the SQUIRT Code
- Subtask 6.5 Prepare a topical report on crack-opening-area improvements
- Subtask 6.6 Leak-rate quantification.

Work was conducted only in Subtask 6.6 during this reporting period. The other subtasks were inactive and will not be discussed here.

7.3.1 Subtask 6.6 Leak-Rate Quantification

This is a subtask that was created during the course of this program. Its objective, rationale, and approach are given below.

7.3.1.1 Objective

The objective of this effort is to perform analyses to support changes to the NRC's current Regulatory Guide 1.45, "Reactor Coolant Pressure Boundary Leakage Detection Systems."

7.3.1.2 Rationale

Regulatory Guide 1.45, "Reactor Coolant Pressure Boundary Leakage Detection Systems" was published in May 1973, and its revision is being considered. The Nuclear Regulatory Commission (NRC) currently wants to update this procedure, taking into account the current leak-detection instrumentation capabilities, experience from the accuracy of leak-detection systems in the past, and current analysis methods to assess the significance of the detectable leakage relative to the structural integrity of the plant. Of the different potential sources of leakage that challenge the structural integrity of the pressure boundary in containment, circumferential cracks in piping have been of much greater significance than any other source. Cracks in steam generator tubing were excluded because there are other leakage detection requirements for them. Furthermore, few axial cracks occur in piping, but numerous cases of circumferential cracks have been reported. Consequently, the analysis in this study keyed on circumferential cracks in pipe to evaluate potential changes in NRC Regulatory Guide 1.45.

7.3.1.3 Approach

The analyses to be performed shall build on other work being done in Task 6. The specific work to be performed shall include the following activities.

- | | |
|----------------|---|
| Activity 6.6.1 | Develop the technical background information for verification of analyses |
| Activity 6.6.2 | Develop/Modify SQUIRT4 and SQUIRT5 Codes |
| Activity 6.6.3 | Evaluate the proposed changes in leak detection requirements in terms of the potential impact on LBB analyses |
| Activity 6.6.4 | Evaluate the proposed changes on leak rate for "non-LBB" piping systems |
| Activity 6.6.5 | Coordinate with NRC-RES and NRC-NRR staff |
| Activity 6.6.6 | Prepare a NUREG topical report |

Detailed approaches for the above activities are described in the second semiannual report (Ref. 7.1) and will not be repeated here. Also, additional work to modify SQUIRT4 to enable calculating crack sizes for given leak rates has been undertaken in Activity 6.6.2.

7.3.1.4 Progress

Progress to be reported is limited to several efforts under Activities 6.6.2 through 6.6.6. The details of these efforts are described below.

Activity 6.6.2 Develop SQUIRT4 and SQUIRT5 Codes

The effort in this activity involves modifications of the original SQUIRT code (Ref. 7.2) that was developed in conjunction with the IPIRG-1 program (Ref. 7.3). The new versions perform iterative calculations to obtain a crack size for a given load and allowable leak rate for a piping system. They are given the acronyms SQUIRT4 and SQUIRT5.

The SQUIRT4 program performs iterative calculations between the fracture mechanics code NRCPIPE and the thermo-hydraulic code SQUIRT. It is limited to one analysis, i.e., for a given load and allowable leak rate, it calculates a crack size for one set of crack morphology variables.

The SQUIRT4 program was modified to automatically handle more than one set of crack morphology parameters required for probabilistic analyses. Also, additional interface routines were developed to use the output of the NRCPIPE module (crack length and crack-opening displacement) to update the COD-dependent crack morphology parameters before performing SQUIRT calculations. This was done to ensure that the input parameters to SQUIRT were reasonable and did not violate the modeling assumptions of the thermo-hydraulic equations built into the code. This modified version was given the acronym SQUIRT5.

Activity 6.6.3 Evaluate the proposed changes in leak detection requirements in terms of the potential impact on LBB analyses

The effort in this activity involves stochastic fracture evaluations of circumferentially cracked pipes for leak-rate detection applications. It was accomplished in three distinct stages. First, a state-of-the-art review was conducted to evaluate the adequacy of current deterministic models for thermo-hydraulic and elastic-plastic fracture analyses. Second, a new probabilistic model was developed for structural reliability analysis of cracked piping systems under combined bending and tension. It also involved statistical characterization of various input variables such as crack morphology parameters, material properties of pipe, and crack location. Third, the proposed models from previous stages were applied for computing conditional probability of failure for various nuclear piping systems in Boiling Water Reactor (BWR) and Pressurized Water Reactor (PWR) plants. Results from this study can be used as a technical basis for potential future changes to the leak-rate detection criterion.

In our probabilistic analysis, the computer code PRAISE (Ref. 7.4) was not used to calculate the failure probabilities. Instead, we used the PSQUIRT code, which contains improved leak rate analysis using Monte Carlo method together with the PROLBB Code which contains the improved fracture mechanics analysis using FORM/SORM probabilistic analyses. The FORM/SORM probabilistic methods are much faster than Monte Carlo simulation and were essential to completing the large number of probabilistic analyses within the time frame of this project.

Review of Deterministic Models

A state-of-the-art review was conducted to evaluate the adequacy of current deterministic models. It included: (1) thermal-hydraulic models for estimation of leak rates, (2) crack-opening models for determination of crack geometry (flow area), and (3) elastic-plastic fracture mechanics models for prediction of maximum load-carrying capacity of a piping system. The results predicted from the above deterministic models were compared with experimental data obtained from past research programs, such as the Degraded Piping Program (Ref. 7.5), International Piping Integrity Research Group (IPIRG) (Ref. 7.3), and others (Ref. 7.6). These comparisons provided a basis for choosing appropriate deterministic models for needed developments in the probabilistic models. Details of this review are available in Reference 7.6. Only a brief summary of the results is presented here.

Thermal-Hydraulic Model The review of existing thermal-hydraulic models indicated that the Henry-Fauske model (Ref. 7.2) provides the best representation of fluid flow through tight cracks in a pipe. This model allows for nonequilibrium vapor generation rates as the fluid flows through the crack. The rate at which vapor is formed approaches the equilibrium value using an exponential relaxation coefficient that can be calculated from experiments. The Henry-Fauske model was chosen in this study to model the two-phase critical flow of water through cracks. Figure 7.1 compares the thermal-hydraulic predictions by the Henry-Fauske model with the data of Collier et al. (Ref. 7.7) for flow through a crack in a pipe. This model was the basis of the PICEP code (Ref. 7.8) developed by EPRI and later the SQUIRT code (Ref. 7.2) developed at Battelle in the IPIRG-1 program (Ref. 7.2). Figure 7.1 provides a plot of calculation error versus measured flow rate, where the calculation error is 100 times the quotient of the predicted minus the measured flow rate and the measured flow rate. Good agreement is obtained between the model and the experiments.

Crack Opening Model The review of the area of crack opening models indicated that the GE/EPRI estimation method (Ref. 7.9), combined with the assumptions of an elliptical crack-opening profile, provides accurate estimates of crack geometry in pipe. The estimation method involves empirical f_2 - and h_2 -functions, which are tabulated in Reference 7.9 for various geometric and material properties of pipe. Figure 7.2 shows the results of the crack-opening displacement (COD) for Experiment 4111-1 conducted in Reference 7.5. The experiment was performed on 114-mm (4.5-inch) diameter SA-333, Grade 6, carbon steel TWC pipe, which is subject to four-point bending. The solid line in this figure represents the measured COD as a function of applied load up to the load at crack initiation. It is seen that the linear regression fit of the stress-strain data over the whole strain range leads to the best estimate of COD. Note that in practical applications, the crack opening is linear elastic under normal operating stresses.

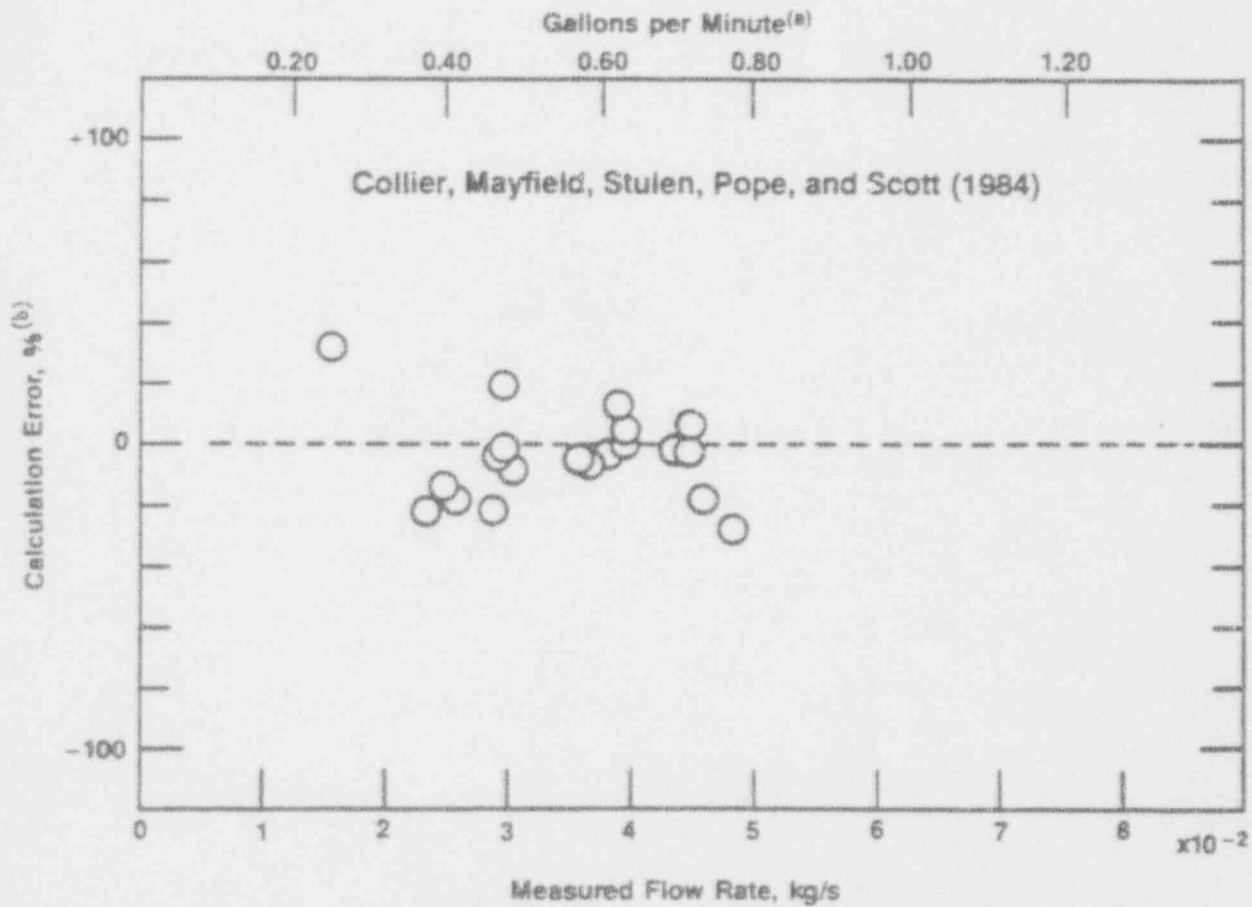


Figure 7.1 Comparison of SQUIRT thermal-hydraulic model predictions with the experimental data of Collier et al. (Reference 7.7) for cracks with a COD of $108 \mu\text{m}$

(a) Gallons per minute for water at 1 atm and 20 C

(b) Calculation error, % = (predicted minus measured flow rate divided by measured flow rate) times 100

T-6004-F2.11

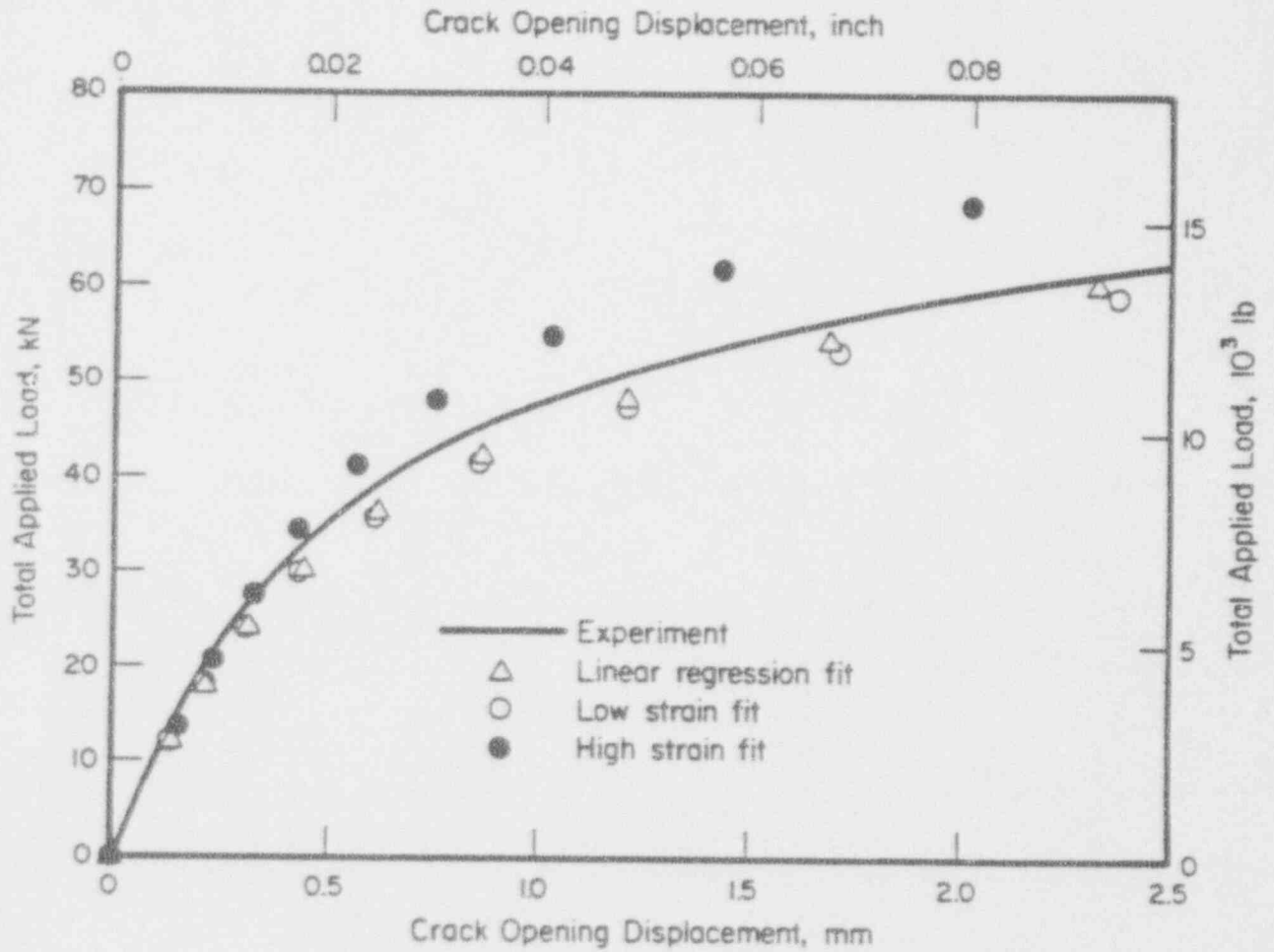


Figure 7.2 Crack-opening displacement in Experiment 4111-1 up to load at crack initiation

T-6005-F2.14

Elastic-Plastic Fracture Model In applications of nonlinear fracture mechanics, particularly for nuclear power plants, the J-tearing theory is a very prominent concept for calculating the maximum load-carrying capacity of a pipe. It is based on the fact that fracture instability can occur after some amount of stable crack growth in tough and ductile materials with an attendant higher applied load level at fracture. Figure 7.3 shows the plots of applied load versus load-line displacement of a 6-inch-diameter (nominal) stainless steel pipe with 37 percent circumferential TWC flaw, which is subject to four-point bending and tension due to internal pressure of 17.24 MPa (2,500 psi) at 288 C (500 F). The plots are obtained from several estimation methods such as LBB.ENG2, GE/EPRI, Paris/Tada, LBB.NRC (Refs. 7.3, 7.5, and 7.6) and laboratory data from the Degraded Piping Program Experiment 4131-3 (Ref. 7.5). These plots show that the LBB.ENG2 method gives reasonable predictions of load and displacement when compared with the test data. In this study, the LBB.ENG2 method was selected because of its computational efficiency and it was found to be slightly conservative yet reasonably accurate when compared with experimental data.

Development of Probabilistic Models

Statistical Characterization Statistical characterization was necessary for the material properties, crack morphology variables that affect the leak-rate calculations, and the crack location.

In conducting statistical characterizations of material properties, various analytic idealizations were considered. For example, it was assumed that the constitutive law characterizing a material's stress-strain response can be represented by the Ramberg-Osgood model. Also, the J-resistance from the C(T) specimen was deemed to be adequately characterized by a power-law equation. In this way, the material property can be defined by a finite-dimensional vector $Y = \{\sigma_y, \sigma_u, \alpha, n, J_{Ic}, C, m\}$, where σ_y is the yield stress, σ_u is the ultimate stress, α and n are Ramberg-Osgood parameters, J_{Ic} is the J-resistance at crack initiation, and C and m are power-law parameters of the J-resistance curve. Samples of raw data obtained from NRC's PIFRAC database (Ref. 7.10), the Degraded Piping Program (Ref. 7.5), IPIRG Program (Ref. 7.3), and others (Ref. 7.6) were used to generate independent samples of the random vector Y . Following standard statistical analysis, the mean and covariance of Y were estimated. Details of these results obtained for typical nuclear piping materials such as stainless steel (TP304), carbon steel (A106B), and cast stainless steel (CF8M), are available in Reference 7.6.

The key crack morphology variables, which were considered in leak-rate analyses, are surface roughness, number of turns in the leakage path, and entrance loss coefficients. However, examination of service cracks also shows that cracks frequently do not grow radially through the pipe thickness. Hence, a fourth parameter "actual crack path/thickness" representing deviation from straightness was also considered here. It has been ignored in the past. In Reference 7.6, a survey was conducted to evaluate statistical properties of these variables. An additional aspect considered was the effect of the crack opening on the surface roughness, number of turns, and straightness of flow path, details of which are also given in Reference 7.6. The sample

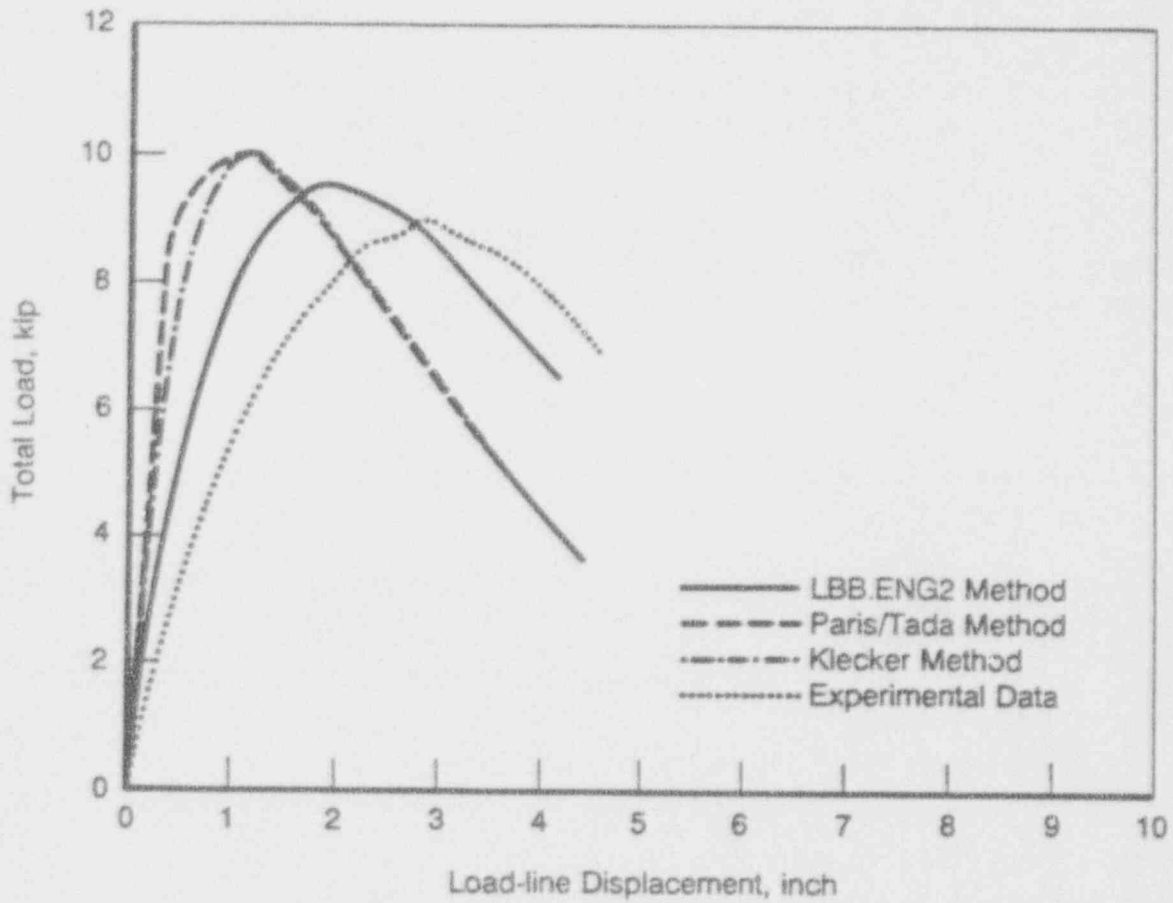


Figure 7.3 Comparisons of load-displacement of through-wall-cracked pipe under combined bending and tension (Experiment 4131-3)

T-6004-F2.21

values reported in the same reference were used to determine their means and standard deviations for corrosion fatigue, thermal fatigue, and intergranular stress-corrosion cracking (IGSCC) mechanisms.

Cracks in nuclear power plants can occur in various locations in piping systems, such as the base metal, weld metal, fusion line, and heat-affected zone. In this study, the crack location was modeled as a discrete random variable. The probabilistic characteristics of this variable can be obtained from some limited information available in the literature (Ref. 7.6). The statistics showed that the probability of cracks appearing in base and weld metals is approximately 2/3 and 1/3, respectively, for both corrosion fatigue and IGSCC cracking mechanisms (Ref. 7.6).

Probabilistic LBB Methodology

The probabilistic LBB methodology can be developed based on the general guidelines proposed in Reference 7.11. The steps of the evaluation are very similar to the steps of the deterministic LBB methodology (Ref. 7.12). These are summarized below.

- Specify a piping system to be evaluated.
- Identify the pipe material and determine its statistical properties and probability distribution.
- Identify the crack morphology variables used in leak-rate analyses and determine their statistical properties and probability distribution.
- Postulate a probability distribution function for a through-wall crack in a pipe. The size of the flaw should be large enough so that detection of leakage is ensured using the installed leak-detection equipment when the pipe is subjected to normal operating loads.
- Using the above crack size, perform structural reliability analyses based on elastic-plastic fracture mechanics to determine the maximum bending moment (M_{max}) the pipe can carry. Figure 7.4 shows a typical circumferential TWC pipe under combined bending and tension.
- Determine the maximum applied moment (M_{N+SSE}) from normal plus SSE stresses.
- For performance evaluation, compute the conditional probability of failure (P_F) where $P_F = \text{Pr}[M_{max} < M_{N+SSE}]$, i.e., the conditional probability of failure when (1) the pipe is leaking with a LBB detectable flaw size and (2) an earthquake occurs with $N+SSE$ stresses resulting in an applied bending moment equal to M_{N+SSE} .

Structural Reliability Analysis

Structural reliability analysis requires a mathematical model that relates various input random parameters for a specific performance criterion of interest. For example, consider the TWC pipe with flaw size $2a$ under combined stresses due to

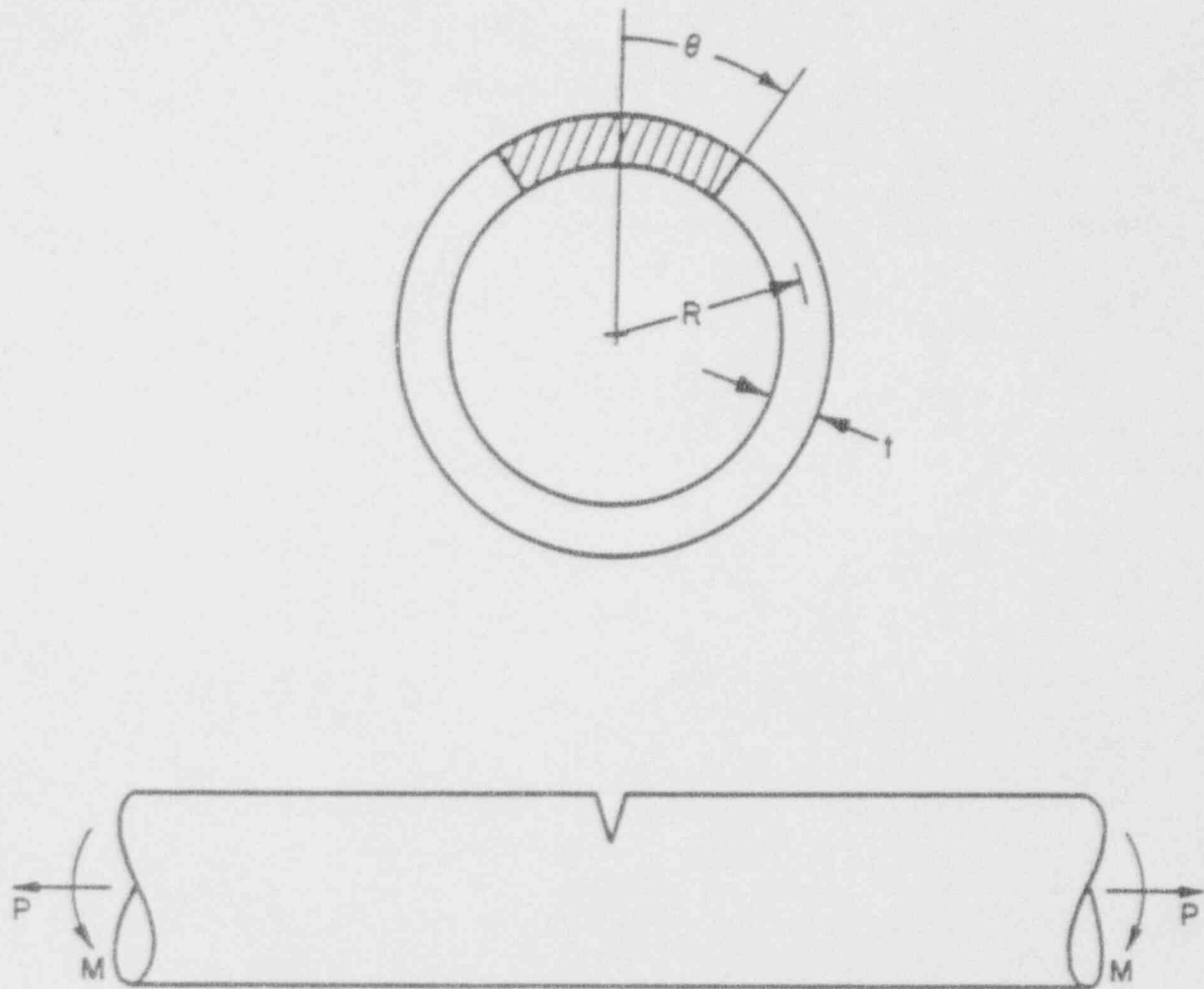


Figure 7.4 Through-wall-cracked pipe under combined bending and tension

T-6004-F2.4

tension and bending (Figure 7.4). Let M_{\max} denote the maximum moment-carrying capacity of the pipe with the constant applied tension P (due to constant internal pressure p). M_{\max} can be obtained from the solution of two nonlinear equations based on J -tearing theory (Ref. 7.6). In general, the solution of M_{\max} can be represented by

$$M_{\max} = \frac{1}{\rho} f(\sigma_y, \sigma_u, \alpha, n, J_{Ic}, C, m, 2a) \quad (7-1)$$

where f is a generic (implicit) function of various input variables (only the random components are shown in the functional dependence of M_{\max}) and ρ is a random correction factor modeling uncertainty of the predictive J -estimation formula. From the Degraded Piping Program, it was found that the mean and coefficient of variation of ρ are 0.92 and 0.13, respectively. In this study, it will be assumed that ρ follows Gaussian probability distribution with the above statistical properties.

Consider a failure criterion

$$M_{\max} < M_{N+SSE} \quad (7-2)$$

which is based on the exceedance of the applied load (M_{N+SSE}) beyond the moment-carrying capacity (M_{\max}) of the pipe. M_{N+SSE} can be estimated from the knowledge of actual $N+SSE$ stresses in nuclear power plants or from the Service Levels B, C, or D stress limits defined in Reference 7.13. This fail-safe condition can be conveniently expressed in the traditional form

$$\begin{aligned} g(\mathbf{X}) &< 0 \quad (\text{failure}) \\ g(\mathbf{X}) &= 0 \quad (\text{limit state}) \\ g(\mathbf{X}) &> 0 \quad (\text{survival}) \end{aligned} \quad (7-3)$$

where the performance function

$$\begin{aligned} g(\mathbf{X}) &= M_{\max} - M_{N+SSE} \\ &= \frac{1}{\rho} f(\sigma_y, \sigma_u, \alpha, n, J_{Ic}, C, m, 2a) - M_{N+SSE} \end{aligned} \quad (7-4)$$

in which $\mathbf{X} = \{Y, 2a, \rho\} = \{\sigma_y, \sigma_u, \alpha, n, J_{Ic}, C, m, 2a, \rho\}$ is an augmented vector of input random parameters characterizing uncertainty in all load and system parameters. Note that the performance function $g(\mathbf{X})$ itself is random, because it depends on an input random vector \mathbf{X} . Let \mathbf{x} be the sample space of random vector \mathbf{X} . In the \mathbf{x} space, the equation $g(\mathbf{x}) = 0$, also known as the limit state, separates the domain D of \mathbf{X} into the safe set $S = \{\mathbf{x}: g(\mathbf{x}) > 0\}$ and failure set $F = \{\mathbf{x}: g(\mathbf{x}) < 0\}$. P_F is defined as the probability that the failure event represented by Inequality 7-2 is true, i.e.,

$$P_F = \Pr [g(\mathbf{X}) < 0] = \int_{g(\mathbf{x}) < 0} f_{\mathbf{X}}(\mathbf{x}) \, d\mathbf{x} \quad (7-5)$$

where $f_{\mathbf{X}}(\mathbf{x})$ is the joint probability density of random vector \mathbf{X} , which is assumed to be known. It was assumed that \mathbf{Y} follows a correlated lognormal distribution with its mean and covariance properties obtained from previous statistical analyses of test data. In general, the multi-dimensional integral in Equation 7-5 cannot be determined analytically. As an alternative, numerical integration can be performed; however, it becomes impractical and the computational effort becomes prohibitive when the dimension becomes greater than two. In this case, we have nine dimensions. Note that P_F is defined here as a conditional probability of failure. The principal conditions are that (1) the pipe is leaking at a specified leak rate and (2) an earthquake occurs with induced stresses that gives rise to the applied bending moment M_{N+SSE} . The corresponding reliability (P_S) is the complement to the failure probability, i.e., $P_S = 1 - P_F$.

Methods of Reliability Analysis

First- and Second-Order Reliability Methods (FORM/SORM) First- and Second-Order Reliability Methods (FORM/SORM) are methods of structural reliability theory based on linear (first-order) and quadratic (second-order) approximations of the limit state surface $g(\mathbf{x}) = 0$ tangent to the closest point (design point) of the surface to the origin of the space. The determination of this point involves nonlinear constrained optimization and is performed in the standard Gaussian image of the original space.

The algorithms implementing these reliability methods involve several steps. They will be described here briefly assuming a generic N -dimensional random vector \mathbf{X} . First, the space of uncertain parameters \mathbf{x} is transformed into a new N -dimensional space \mathbf{u} consisting of independent standard Gaussian variables. The original limit state $g(\mathbf{x}) = 0$ then becomes mapped into the new limit state $g_U(\mathbf{u}) = 0$ in the \mathbf{u} space. Second, the point on the limit state $g_U(\mathbf{u}) = 0$ having the shortest distance to the origin of the \mathbf{u} space is determined by using an appropriate nonlinear optimization algorithm. This point is referred to as the design point or β -point, and has a distance β_{HL} to the origin of the \mathbf{u} space. Third, the limit state $g_U(\mathbf{u}) = 0$ is approximated by a surface tangent to it at the design point. Let such limit states be $g_L(\mathbf{u}) = 0$ and $g_Q(\mathbf{u}) = 0$, which correspond to two approximating surfaces: a hyperplane (linear or first-order) and a hyperparaboloid (quadratic or second-order), respectively. The probability of failure P_F [Equation 7-5] is thus approximated by $\Pr[g_L(\mathbf{u}) < 0]$ in FORM and $\Pr[g_Q(\mathbf{u}) < 0]$ in SORM. These first-order and second-order estimates $P_{F,1}$ and $P_{F,2}$ are given by (Refs. 7.6, 7.14, 7.15, 7.16)

$$P_{F,1} = \Phi(-\beta_{HL}) \quad (7-6)$$

and

$$P_{F,2} = \Phi(-\beta_{HL}) \prod_{i=1}^{N-1} (1 - \kappa_i \beta_{HL})^{-\frac{1}{2}} \quad (7-7)$$

where

$$\Phi(u) = \frac{1}{\sqrt{2\pi}} \int_{-\infty}^u \exp\left[-\frac{1}{2} \xi^2\right] d\xi \quad (7-8)$$

is the cumulative distribution function of a standard Gaussian (normal) random variable, and κ_i 's are the principal curvatures of the limit-state surface at the design point. Further details for the derivations of Equations 7-6 and 7-7 can be obtained from Reference 7.6.

Monte Carlo Simulation (MCS). Consider a generic N-dimensional random vector \mathbf{X} which characterizes uncertainty in all load and system parameters with the known joint distribution function $F_{\mathbf{X}}(\mathbf{x})$. Suppose $\mathbf{x}^{(1)}, \mathbf{x}^{(2)}, \dots, \mathbf{x}^{(L)}$ are L realizations of input random vector \mathbf{X} which can be generated independently. Methods of generating samples of \mathbf{X} are available in Reference 7.6. Let $g^{(1)}, g^{(2)}, \dots, g^{(L)}$ be the output samples of $g(\mathbf{X})$ corresponding to input $\mathbf{x}^{(1)}, \mathbf{x}^{(2)}, \dots, \mathbf{x}^{(L)}$ that can be obtained by conducting repeated deterministic evaluation of the performance function in Equation 7-4. Define L_f as the number of trials (analyses) which are associated with negative values of the performance function. Then, the estimate $P_{F,MCS}$ of the probability of failure by simulation is given by

$$P_{F,MCS} = \frac{L_f}{L} \quad (7-9)$$

which approaches the exact failure probability P_F when L approaches infinity. When L is finite, a statistical estimate on the probability estimator may be needed. In general, the required sample size is at least $10/\text{Min}(P_F, P_S)$, where $\text{Min}(P_F, P_S)$ is the minimum of P_F and P_S , for a 30 percent coefficient of variation of the estimator.

Experience with FORM/SORM and MCS. Practical experience with FORM/SORM algorithms indicates that their estimates usually provide satisfactory reliability measures. The SORM reliability is more accurate and may differ from FORM reliability when the design conditions are highly nonlinear. Besides, the SORM reliability has the property of approaching exact reliability P_S when P_S approaches 1 asymptotically. When the reliability is large (small probability of failure), FORM/SORM are extremely efficient compared with simulation methods regarding the requirement of a Central Processing Unit (CPU). The CPU time for FORM is approximately linear in N (N = number of basic input variables) and the additional CPU time for SORM grows approximately with N^2 . However, SORM based on the diagonal of the matrix of second-order derivatives at the β point (in u space) has CPU time linear in N. Obviously, the absolute CPU time depends on the CPU time required to evaluate the performance function $g(\mathbf{x})$. The CPU time may be invariant with the actual

reliability level if the calculation of $g(x)$ does not depend on different combinations of input variables. This has a bearing in that when P_S approaches 1, the computational effort by FORM/SORM may remain relatively unchanged and hence it becomes a much faster method when compared with simulations.

Direct Monte Carlo Simulation is a very general method and is based on the repeated deterministic evaluation of the $g(x)$ function due to random sampling of the input random vector X according to their joint distribution function. This method can be applied to any type of problem without requiring any continuity in the random variables or the limit state function. For a sample size L approaching infinity, the estimated reliability converges to the exact result. For a finite sample size, uncertainty estimates on the results may need to be evaluated. As a rule of thumb, the CPU time grows linearly with N and $1/\text{Min}(P_F, P_S)$ for a given coefficient of variation on the estimator. The absolute value of the CPU time depends on the time necessary to evaluate the $g(x)$ function. When P_S approaches 1 or P_F approaches 0, the Monte Carlo simulation may be inefficient and expensive and, hence, may become computationally prohibitive.

The Computer Codes PSQUIRT and PROLBB

Code PSQUIRT. In this study, a new computer code titled PSQUIRT was developed to estimate the probability density, $f_{2a}(x)$ of the LBB detectable flaw size, $2a$. It is based on straight Monte Carlo Simulation. PSQUIRT, which stands for Probabilistic Seepage Quantification of Upsets In Reactor Tubes, is essentially a combination of two separate programs titled SCRAMP (Simulation of CRACK Morphology Parameters) and SQUIRT5 (Seepage Quantification of Upsets In Reactor Tubes). SCRAMP generates independent samples of various crack morphology parameters, which are then fed into the modified version of SQUIRT (SQUIRT5) to yield corresponding realizations of $2a$. Each sample generation of $2a$ is associated with one deterministic SQUIRT analysis for a given sample of input crack morphology variables. A standard statistical analysis of these replicated samples of $2a$ provides an estimate for its probability density function.

Code PROLBB. A computer program titled PROLBB, which is the acronym for PROBABILISTIC Leak-Before-Break, was developed to evaluate the failure probability of flawed nuclear piping subject to combined stresses due to tension and bending. Various failure criteria based on the exceedance of (1) net-section collapse load, (2) crack initiation load, and (3) maximum load can be used to obtain the corresponding probability of failure. In this study, the calculation of conditional probability of failure was based on the maximum load as described earlier (see Equations 7-1 to 7-5).

PROLBB is based on: (1) First-Order Reliability Method (FORM), (2) Second-Order Reliability Method (SORM), (3) Importance Sampling, and (4) Monte Carlo Simulation (MCS). Monte Carlo simulations provide a means for evaluating the adequacy of analytical probability computation methods.

Applications to BWR and PWR Piping

The probabilistic model developed in this study was applied to pipe geometries and materials typically used in 12 nuclear piping systems (6 in BWR's and 6 in PWR's) for calculating the conditional probability of failure. Pipe sizes with large, intermediate, and small diameters typically used in reactor containment were selected. Two pipes of each size were considered with austenitic and ferritic materials. The piping systems included side riser, main steam, recirculation branch line, feedwater, bypass line, and reactor water clean-up line, main coolant, surge line, spray line, and steam generator blowdown line. Several cracking mechanisms such as corrosion fatigue and IGSCC were also considered. In all cases, simple circumferential through-wall-cracked (TWC) pipes were analyzed. Both deterministic and probabilistic considerations were given for handling crack location characteristics. Table 7.1 shows the characteristics of BWR and PWR piping systems for probabilistic pipe fracture evaluations conducted in this study.

Estimation of Applied Stresses. For the various piping systems being evaluated, the normal operation (N) stresses are needed to determine the crack size for a given leak rate, and the normal plus safe shutdown earthquake (N+SSE) stresses are needed to evaluate the stability of the cracked pipe.

Normal Operating Stresses. The actual normal operating stresses and their probabilities occurring for all plants in the U.S. are difficult to quantify. To simplify this effort, it is assumed that the ASME Section III Code stress level limits apply, even though actual stresses may be lower. For the normal operating stresses, the Class 1 piping, Service Level A limits were used, which is $1.5S_m$ by Equation (9) of Article NB-3652 in the ASME Boiler and Pressure Vessel Code (Ref. 7.13) and is given by

$$B_1 \frac{pD_o}{2t} + B_2 \frac{D_o}{2I} M \leq 1.5S_m \quad (7-10)$$

where for a circumferential crack evaluation, $B_1 = 0.5$, $B_2 = 1.0$, p = internal pressure, t = pipe wall thickness, $I = 0.0491(D_o^4 - D_i^4)$, D_o = outside diameter, D_i = inside diameter, M = applied moment, S_m = material design stress intensity from ASME Section III, Appendix I (Ref. 7.13).

Actual normal operating stresses, however, may be considerably less than this maximum limit. Hence, various stress intensities that are 50 and 100 percent of the Service Level A limits were used. The lower the Service Level A stresses, the more conservative is the LBB detectable flaw size.

Table 7.1 Through-wall-cracked BWR and PWR piping systems for probabilistic fracture evaluations

Cases	Piping System	Nominal Dia. (inches)	Thickness, mm (inches)	Base Metal	Weld ^(a) Metal	Assumed ^(b) Cracking Mechanism
BWR-1	Side Riser	28	35.8 (1.41)	TP304	SS SAW	IGSCC
BWR-2	Main Steam	28	35.8 (1.41)	A516 Gr70	CS SAW	Corrosion Fatigue
BWR-3	Recirculation Branch	18	23.9 (0.94)	TP304	SS SAW	IGSCC
BWR-4	Feedwater	18	39.4 (1.55)	A106B	CS SAW	Corrosion Fatigue
BWR-5	Bypass Line	4	8.51 (0.34)	TP304	SS SAW	IGSCC
BWR-6	Reactor Water Clean-up	4	8.51 (0.34)	A106B	CS SAW	Corrosion Fatigue
PWR-1	Main Coolant	32	76.2 (3.00)	CF8M	SS SAW	Fatigue
PWR-2	Main Coolant	32	76.2 (3.00)	A516 Gr70	CS SAW	Corrosion Fatigue
PWR-3	Surge Line	14	35.8 (1.41)	CF8M	SS SAW	Fatigue
PWR-4	Feedwater	14	35.8 (1.41)	A106B	CS SAW	Corrosion Fatigue
PWR-5	Spray Line	4	13.5 (0.53)	TP304	SS SAW	IGSCC
PWR-6	Steam Generator Blowdown	4	13.5 (0.53)	A106B	CS SAW	Corrosion Fatigue

(a) SS = stainless steel, CS = carbon steel, SAW = submerged arc weld.

(b) IGSCC = Intergranular stress-corrosion cracking.

Normal Plus Safe-Shutdown Earthquake Stresses. One of the most difficult aspects of this analysis was the selection of normal plus safe-shutdown earthquake stresses. Obviously for application to a generic document, such as the NRC Regulatory Guide 1.45, there are large number of piping systems and plant locations. It was beyond the scope of this effort to analyze all plants and piping systems. Figure 7.5 shows the comparisons of various actual N+SSE stresses obtained by performing explicit dynamic analysis of piping configurations subject to seismic ground acceleration and limit stresses from several service levels. The actual stresses were obtained from References 7.17 - 7.21 and private communications with the NRC personnel. Following statistical analyses, several histograms of these actual stresses were developed. The histograms shown in Figure 7.5 clearly indicate that they may be significantly lower than Service Level B, C, or D stress limits. Thus, actual normal plus SSE stresses may be below these service level stress limits, but these possible combinations will not be investigated here.

Based on results shown in Figure 7.5 for N+SSE stresses, the maximum stress limit in Service Level B was used. By ASME Section III - Article NB-3656, this maximum stress limit is the lower of either $1.8S_m$ or $1.5S_y$ (S_y is the code-specified yield stress) when using Equation (9) in Article NB-3652. One complication to the fracture analysis is that these stress values are elastically calculated. The actual bending stresses may be much lower due to the plastic action, which is anticipated during seismic loading of piping. Hence, there is an inherent margin in the use of the elastic stresses to determine the bending moment in the pipe system of interest. Thus, some plasticity corrections may be necessary for the Service Level B stresses. Figure 7.6 shows the correction factor as a function of elastically calculated Service Level-B stresses. It is based on the assumptions that (1) no correction is required for elastically calculated stresses smaller than yield stress σ_y , (2) a correction factor of $\pi/4$ is applied (based on the equivalence of net-section-collapse loads) for elastically calculated stresses larger than the flow stress, σ_f , where the flow stress is defined as the average of yield and ultimate stresses, and (3) a linear variation is adequate for the range of stresses between these two limits. There are alternative means for defining the plasticity correction factor which may be available in the literature. They were not explored here.

Probabilistic Characteristics of Leakage Size Flaw. The computer code PSQUIRT was used to determine the probability density function of the LBB detectable flaw size, $2a$. Figure 7.7 shows the histogram of $2a$ from PSQUIRT generated by simulating 1000 samples. It was obtained for the piping system BWR-1 with 1 gpm leak rate and 100 percent of Service Level A stresses under normal operating conditions. It is observed that the above histogram fits the lognormal probability density function also shown in Figure 7.7. Results obtained by varying leak rates, normal operating stresses, and piping systems, which are not shown here, also indicated that the density of LBB detectable flaw sizes can be approximated well by this lognormal probability. At least two parameters, such as mean and coefficient of variation, are needed to define a lognormal probability density function. Reference 7.6 has the values of these parameters for various piping systems considered in this study. For each piping system, they are further broken down for various combinations of normal operating stresses and leak rates.

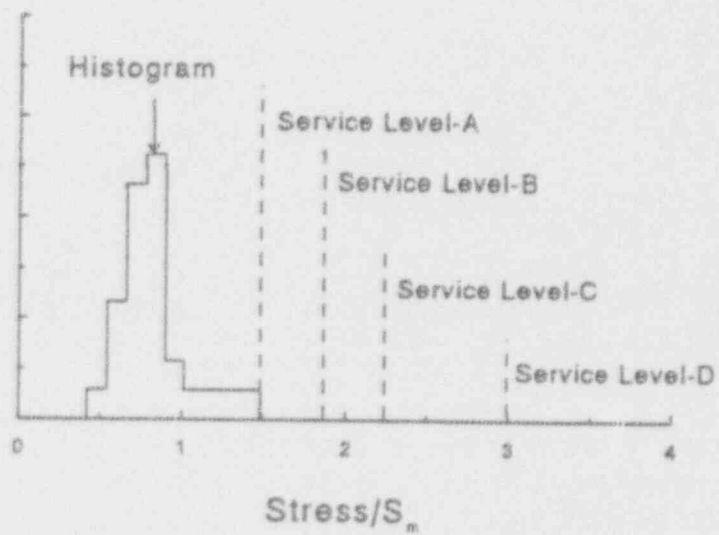
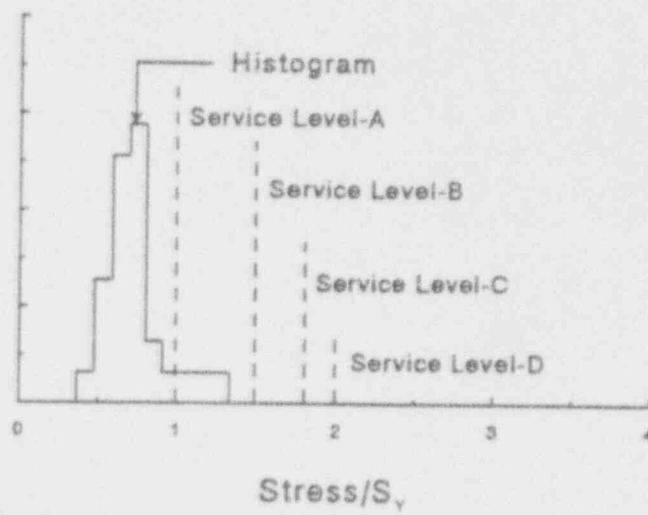


Figure 7.5 Comparisons of actual N+SSE stresses with various service limits

T-6004-F.5.1

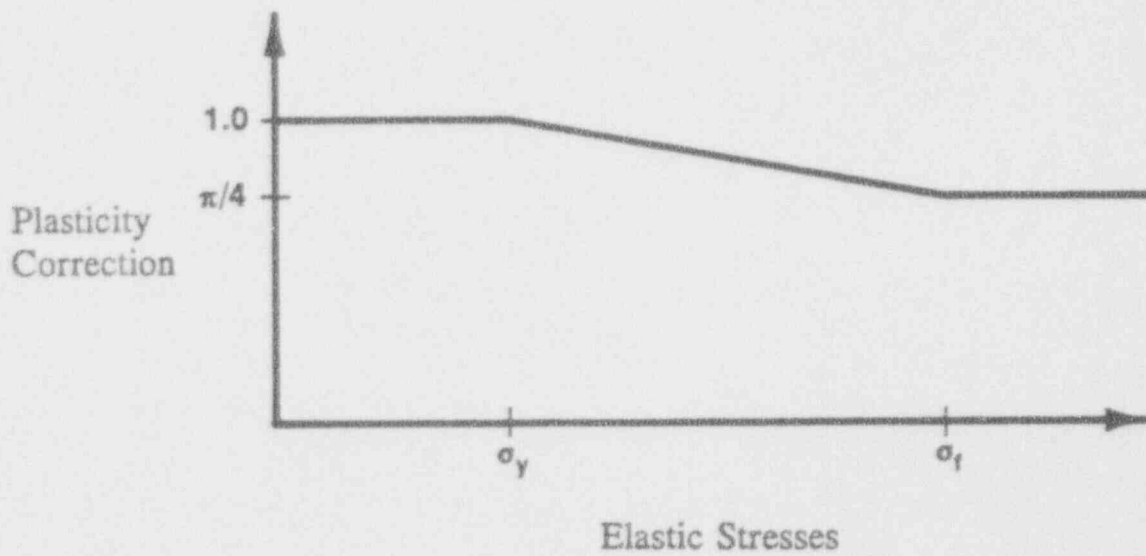


Figure 7.6 Plasticity correction for elastically calculated stresses

T-6004-F5.2

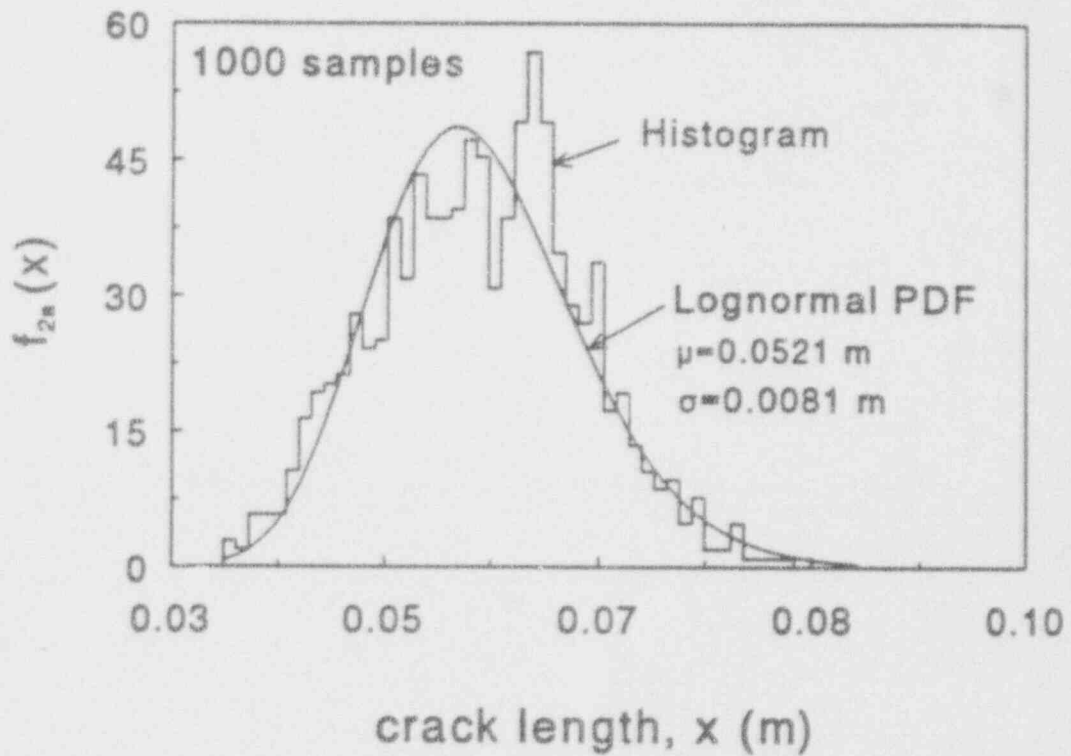


Figure 7.7 Histogram of LBB detectable flaw size for BWR-1 (1 gpm leak rate and 100 percent of Service Level-A limit)

T-6004-F5.3

Conditional Probability of Failure. In order to evaluate structural integrity, the conditional probability of failure (P_F) was computed by the code PROLBB for the nuclear piping considered in this study (see Table 7.1). Figure 7.8 shows the plots of conditional failure probability (P_F) versus leak rate obtained by several methods (FORM, SORM, and MCS) for various percentages of Service Level A stresses. They were calculated for a large-diameter BWR-1 pipe (side riser) with a crack in the base metal. Several interesting features can be observed in this figure. First it indicates that as the leak rate increases, the failure probability increases because of a larger initial crack size for a given normal operating stress (percentage of Service Level A limit). Second, for a given leak rate, the probability of failure also increases because of the larger initial flaw size due to a smaller percentage of Service Level A stresses. Third, the probability estimates obtained by the FORM and SORM methods provide accurate estimates when compared with those obtained by MCS. All of the above failure probabilities, including the estimates by MCS, were obtained using the program PROLBB. All of the conditional failure probabilities reported here were obtained using the second and a reliability method (SORM) in PROLBB.

Figure 7.9 exhibits the relative effort and computational expenses required to determine the above solutions by analytical (FORM/SORM) and simulation (MCS) methods. They were measured in terms of Central Processing Units (CPU) by executing computer codes (developed in-house) for each of these methods on a 486-33MHz Personal Computer. The plots in this figure show how the ratio of CPU time for MCS and FORM/SORM vary with the range of probability estimates made in this study. It was found that the above ratio can vary between 3 to more than 10^9 depending on the probability level being estimated. Clearly, the FORM/SORM algorithms are more efficient than MCS particularly when the failure probabilities are in the lower range.

Results for BWR. Figures 7.10 and 7.11 show the variation of conditional failure probability of two TWC pipes BWR-1 and BWR-2 for various leak rates and normal operating stresses. The above probabilities were calculated separately when the crack was assumed to be located either in the base metal or in the weld metal. Due to a significant reduction in the toughness properties of the weld metal compared to the base metal of stainless steel (TP304) pipes, the conditional probability of failure for cracks in the weld metal showed much larger values than those obtained for cracks in the base metal. These can be observed from the BWR-1 pipe, which is made of austenitic material (see Figure 7.10).

For the ferritic pipes, the failure probabilities were found to be smaller for cracks in weld metal than those for cracks in base metal due to slightly larger toughness of weld metal. These can be observed from the BWR-2 pipe which is made of ferritic material (see Figure 7.11). Similar results were also obtained for the rest of the BWR piping, the details of which are available in Reference 7.6.

As mentioned previously, the failure probabilities were obtained separately for a deterministic location of cracks in base or weld metals. However, when a random crack location is considered, with the probability being 2/3 for cracks in the base metal and 1/3 for cracks in the weld metal or fusion line, the weighted combination (the probabilities are the weights) of the failure probabilities given in the above figures can be easily obtained. The conditional failure probability calculated as a function of leak rates for random crack location is provided in Figures 7.12 - 7.17 for the six TWC BWR pipe systems considered in this study.

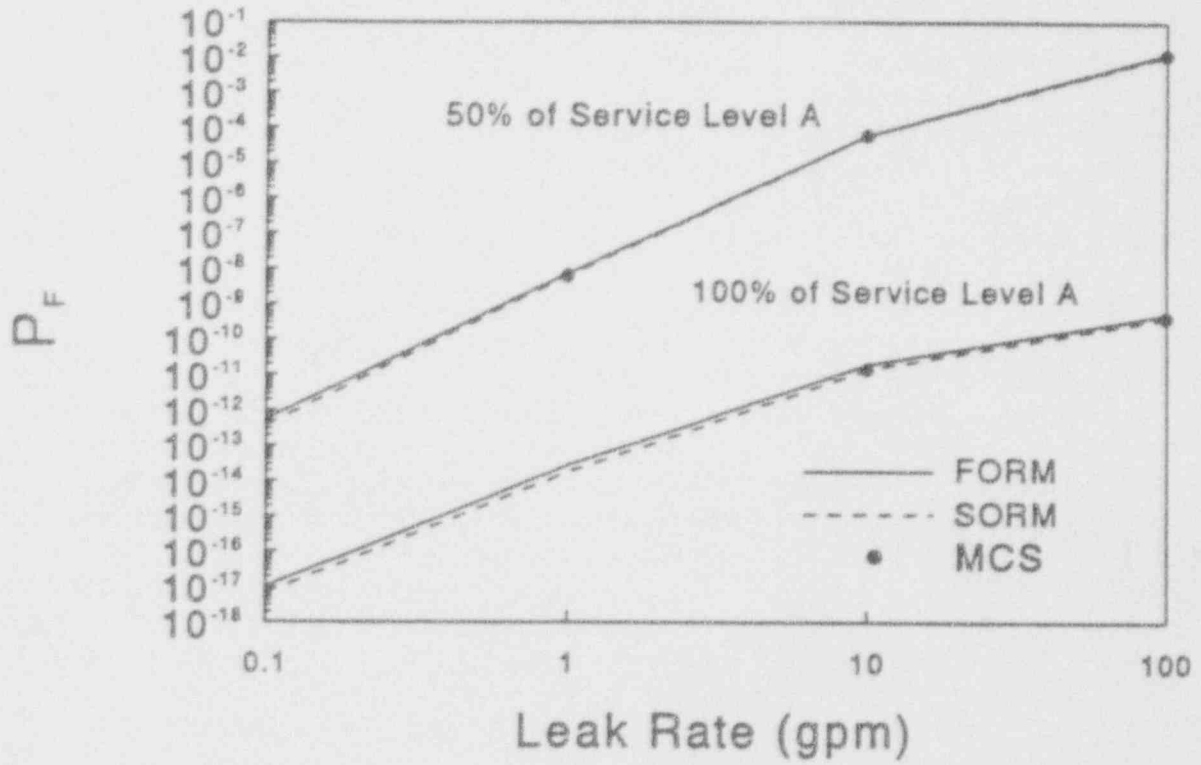


Figure 7.8 Conditional probability of failure by various methods (BWR-1)

T-6004-F5.4

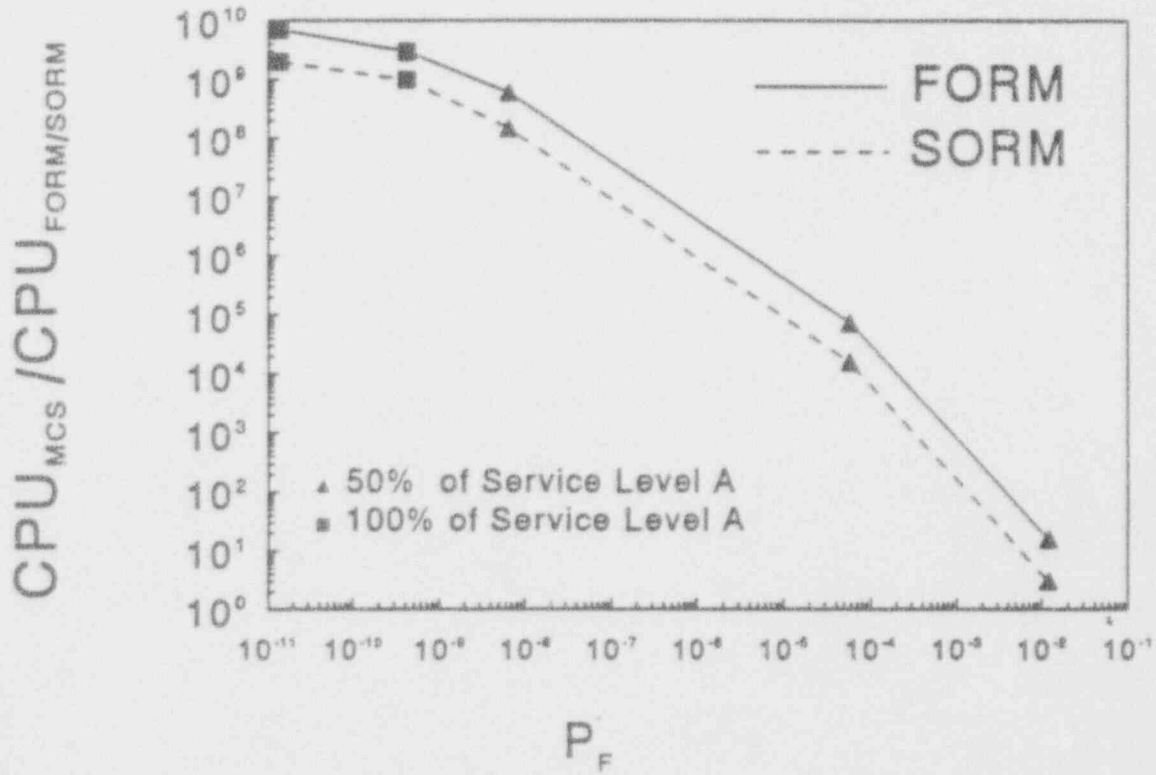


Figure 7.9 Computational efficiency of FORM/SORM (BWR-1)

T-6004-F5.5

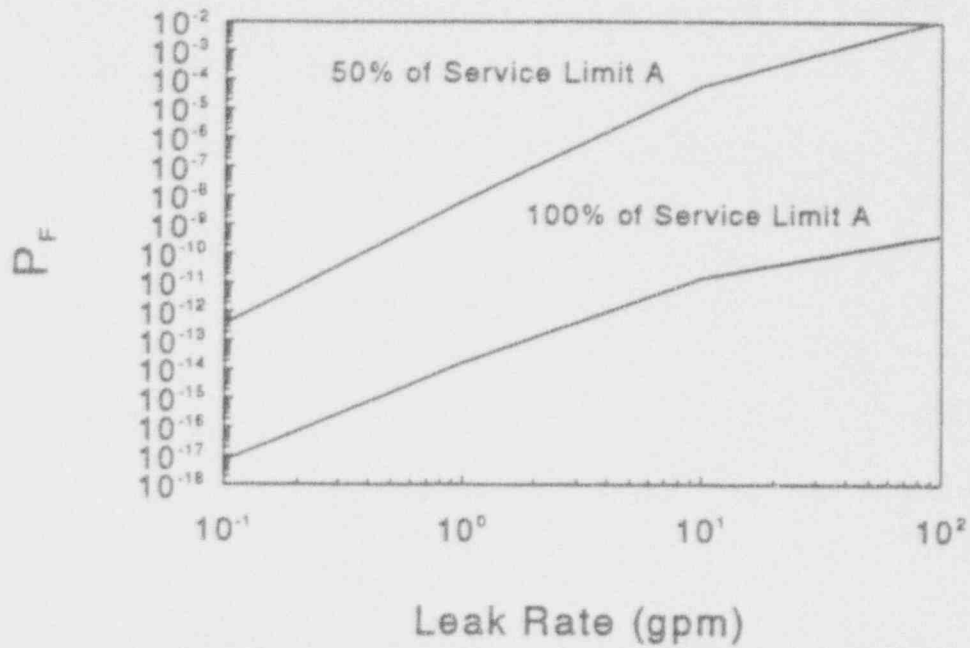


Figure 7.10(a) Conditional failure probability by SORM for BWR-1 (base metal)

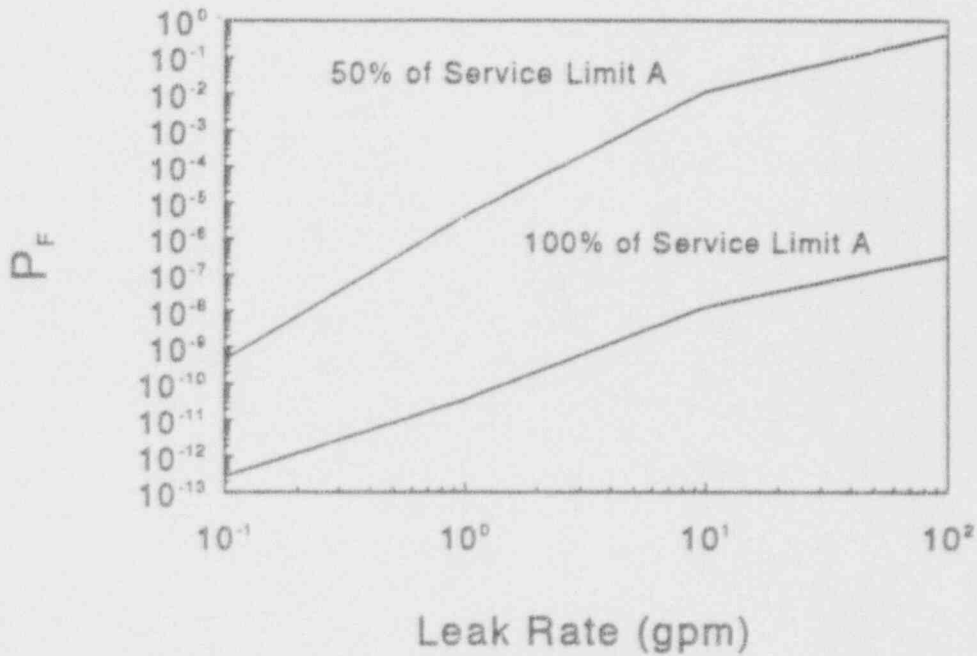


Figure 7.10(b) Conditional failure probability by SORM for BWR-1 (weld metal)

T-6004-F5.6(a)(b)

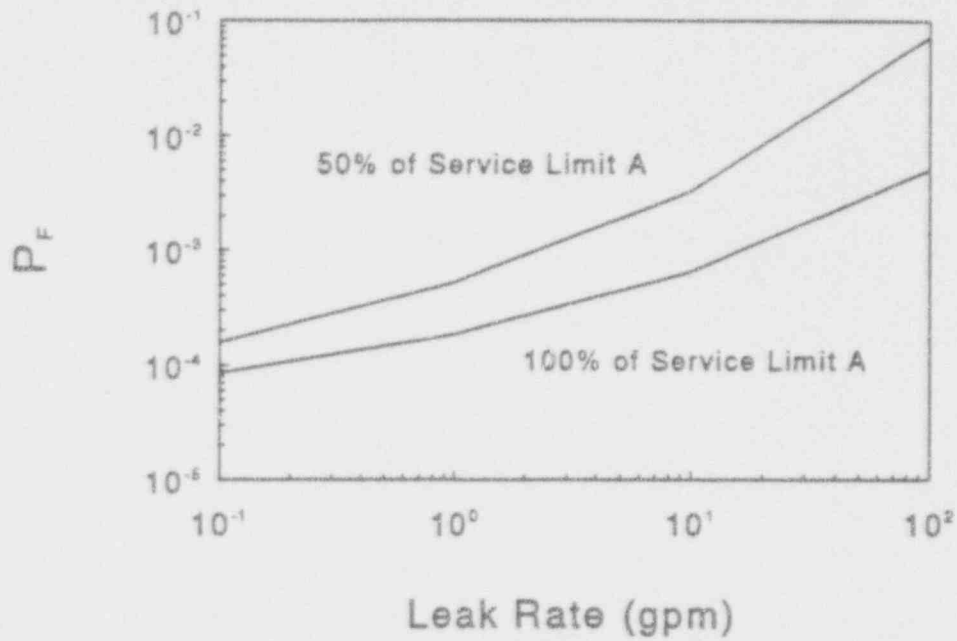


Figure 7.11(a) Conditional failure probability by SORM for BWR-2 (base metal)

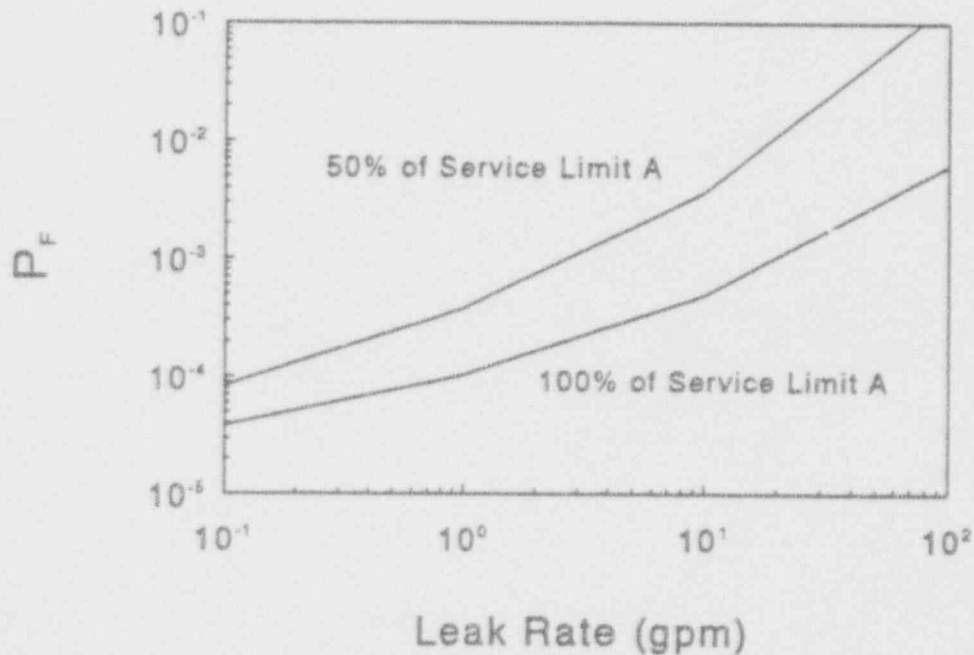


Figure 7.11(b) Conditional failure probability by SORM for BWR-2 (weld metal)

T-6004-F5.7(a)(b)

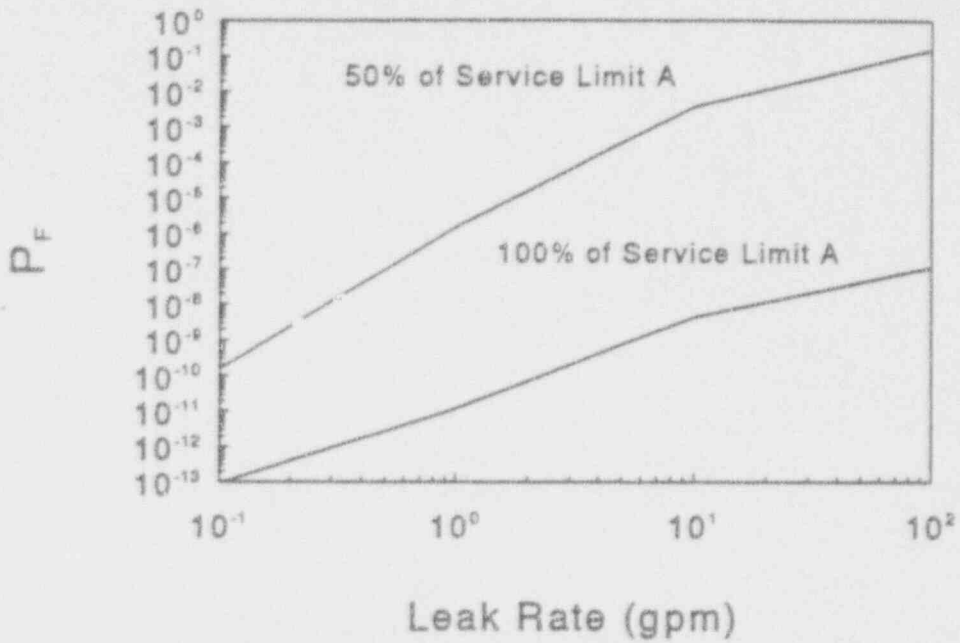


Figure 7.12 Conditional failure probability by SORM for BWR-1 (random crack location)

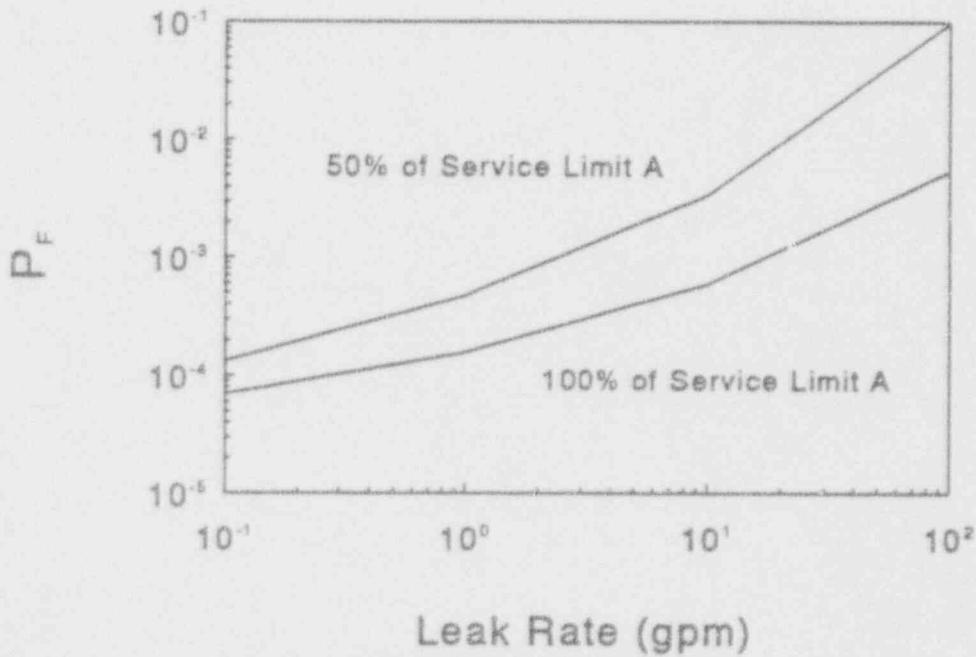


Figure 7.13 Conditional failure probability by SORM for BWR-2 (random crack location)

T-6004-F5.16/5.17

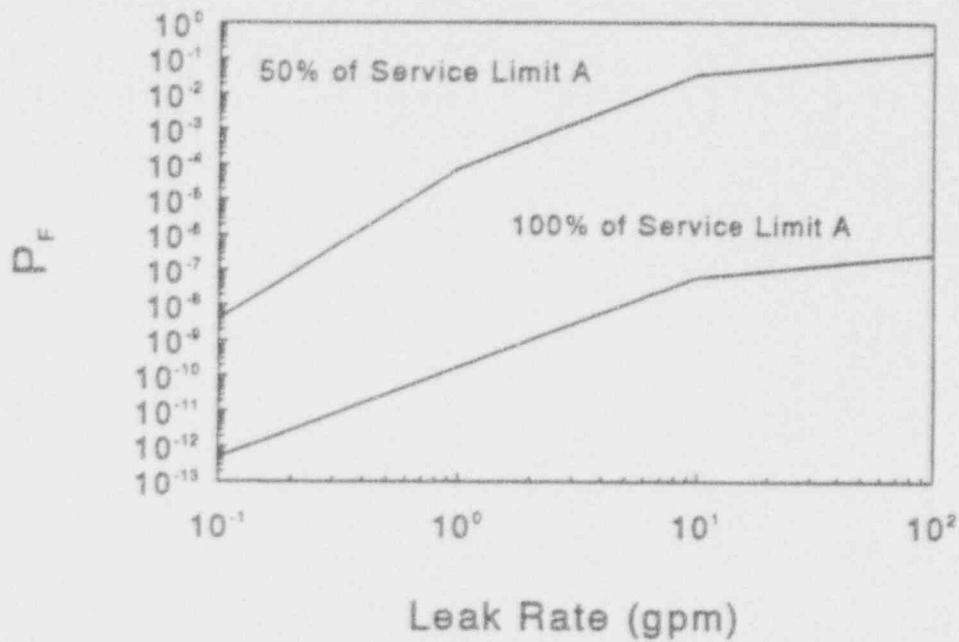


Figure 7.14 Conditional failure probability by SORM for BWR-3 (random crack location)

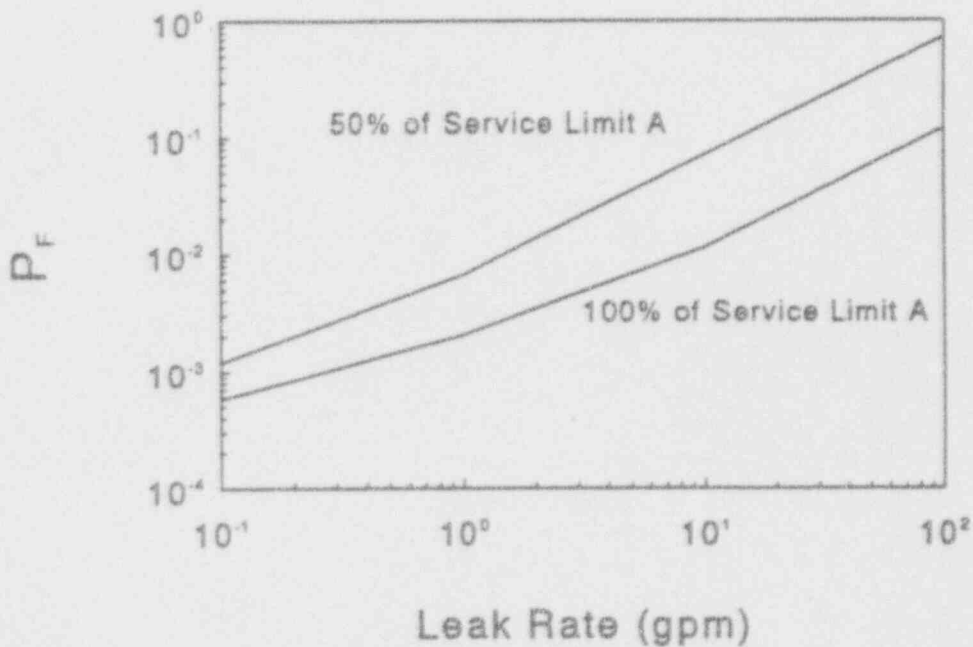


Figure 7.15 Conditional failure probability by SORM for BWR-4 (random crack location)

T-6004-F5.18/5.19

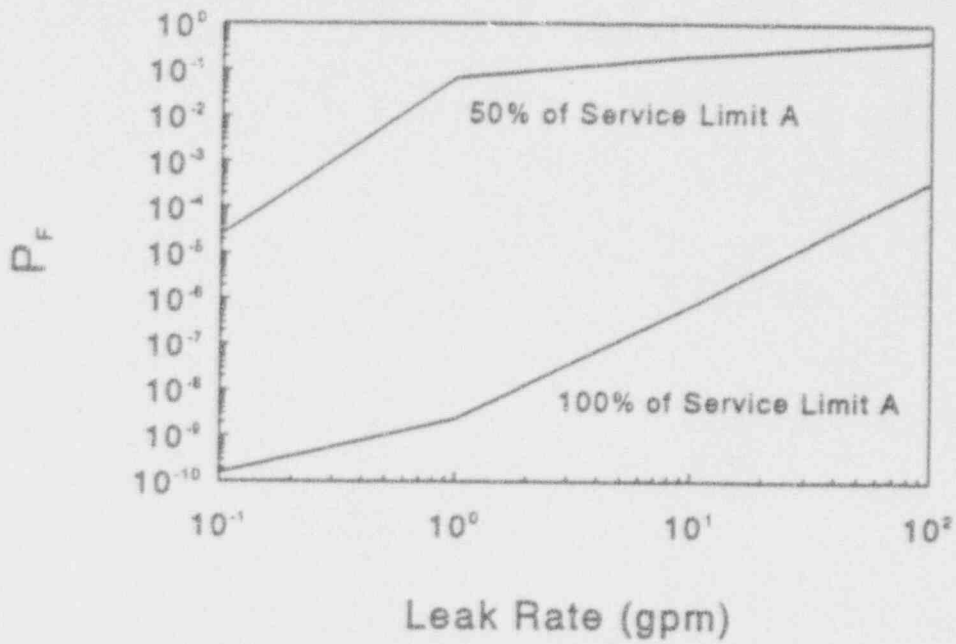


Figure 7.16 Conditional failure probability by SORM for BWR-5 (random crack location)

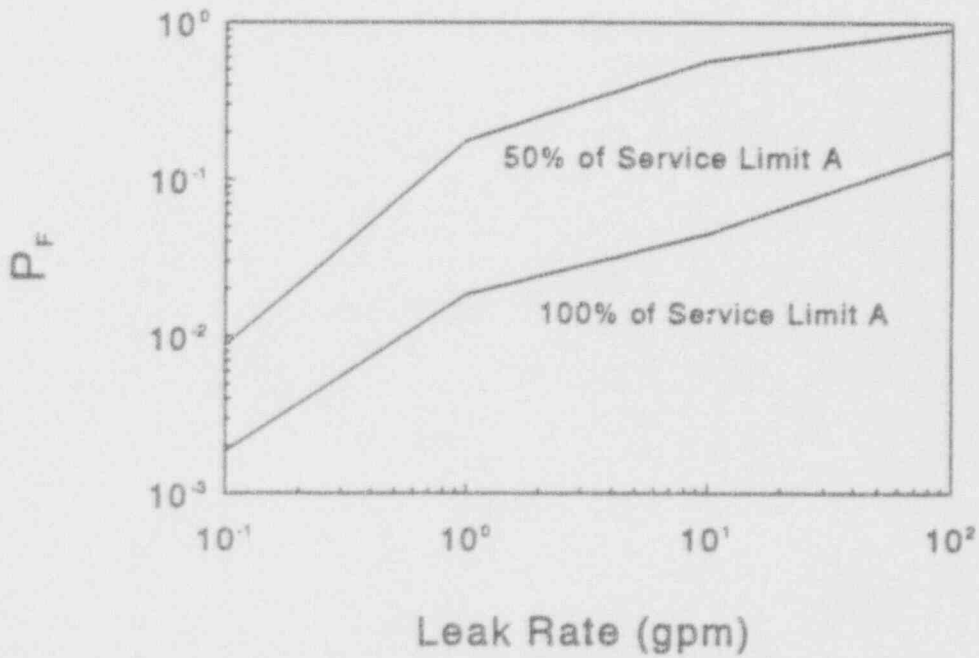


Figure 7.17 Conditional failure probability by SORM for BWR-6 (random crack location)

T-6004-F5.20/5.21

Comparisons between the failure probabilities indicate that the austenitic pipes are more reliable than the ferritic pipes.

Figure 7.18 shows several plots of conditional probability of failure (random crack location) for a given leak rate of 1 gpm as a function of diameter of BWR pipes with LBB detectable crack size obtained for both 100 and 50 percent of Service Level-A stresses. They indicate that the conditional failure probability decreases with an increase in pipe diameter for both austenitic and ferritic materials. Similar results were also obtained by Harris et al. (Ref. 7.17) and Wilson (Ref. 7.22). Also, comparisons between the failure probabilities of austenitic and ferritic pipes indicate that the austenitic pipes are more reliable than ferritic pipes, particularly for large-diameter pipes.

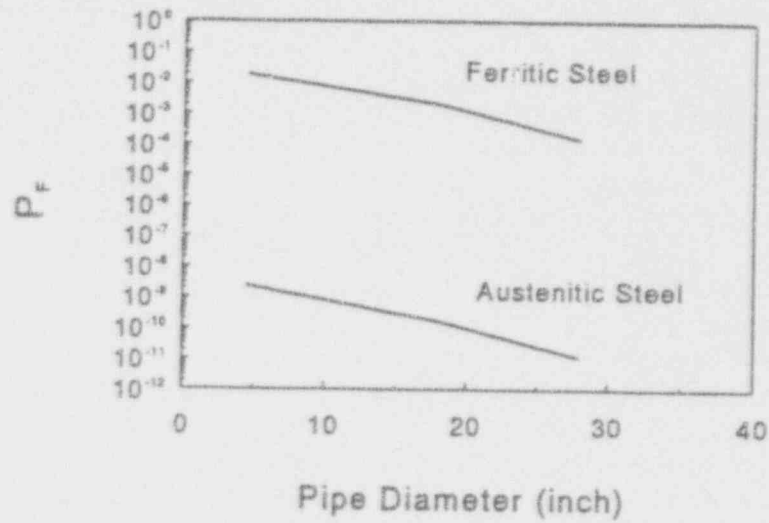
Results for PWR. Figures 7.19 and 7.20 show the variation of conditional failure probability of two PWR pipes, PWR-1 and PWR-2, which were obtained for various leak rates and normal operating stresses. As before, the probabilities were calculated separately when the crack was located either in the base metal and or in the weld metal. Due to a reduction in the toughness properties of the weld metal compared to the base metal of stainless and cast stainless steel (CF8M and TP304) pipes, the conditional probability of failure for cracks in the weld metal showed larger values than those obtained for cracks in the base metal. These can be observed from the PWR-1 pipe, which is made of austenitic material (see Figure 7.19).

For the ferritic pipes, the failure probabilities were found to be smaller for cracks in the weld metal than those for cracks in the base metal due to a higher toughness of the weld metal. These were observed for the PWR-2 pipe, which is made of ferritic material (see Figure 7.20).

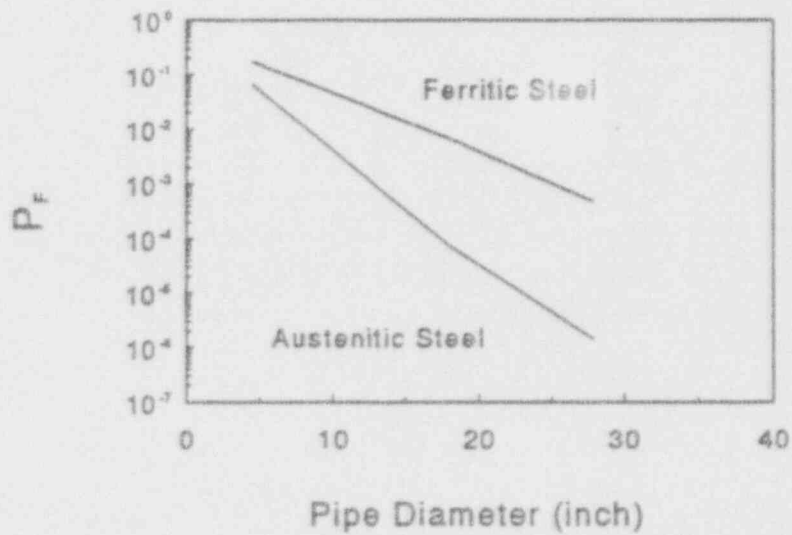
As before, when a random crack location is considered with the probability being 2/3 for cracks to be found in the base metal and 1/3 for cracks to be found in the weld metal or fusion line, the weighted average of the failure probabilities given in the above figures was obtained. The conditional failure probability calculated as a function of leak rates for random crack location is provided in Figure 7.21 - 7.26 for the six PWR pipes considered in this study. Comparisons between the failure probabilities indicate that the austenitic pipes are more reliable than the ferritic pipes. Similar conclusions were also made from the BWR pipe system analysis.

Figure 7.27 shows several plots of conditional probability of failure (random crack location) for a given leak rate of 1 gpm as a function of diameter of PWR pipes with LBB detectable flaw size obtained for both 100 and 50 percent of Service Level-A stresses. They also indicate that the conditional failure probability decreases with increase in pipe diameter for both austenitic and ferritic materials. Also, comparisons between the failure probabilities of austenitic and ferritic pipes indicate that the austenitic pipes are more reliable than ferritic pipes. Similar results were also obtained for the BWR pipes.

Potential Applications of Results. When the actual normal operating stresses and the leak-rate equipment detection capabilities are known, Figures 7.12 - 7.17 and Figures 7.21 - 7.26 can be used to calculate the conditional probability of a double-ended guillotine break for the piping systems considered in this study.



(a) 100 percent of Service Level A



(b) 50 percent of Service Level A

Figure 7.18 Conditional failure probability as a function of diameter in BWR pipes

T-6004-F5.26

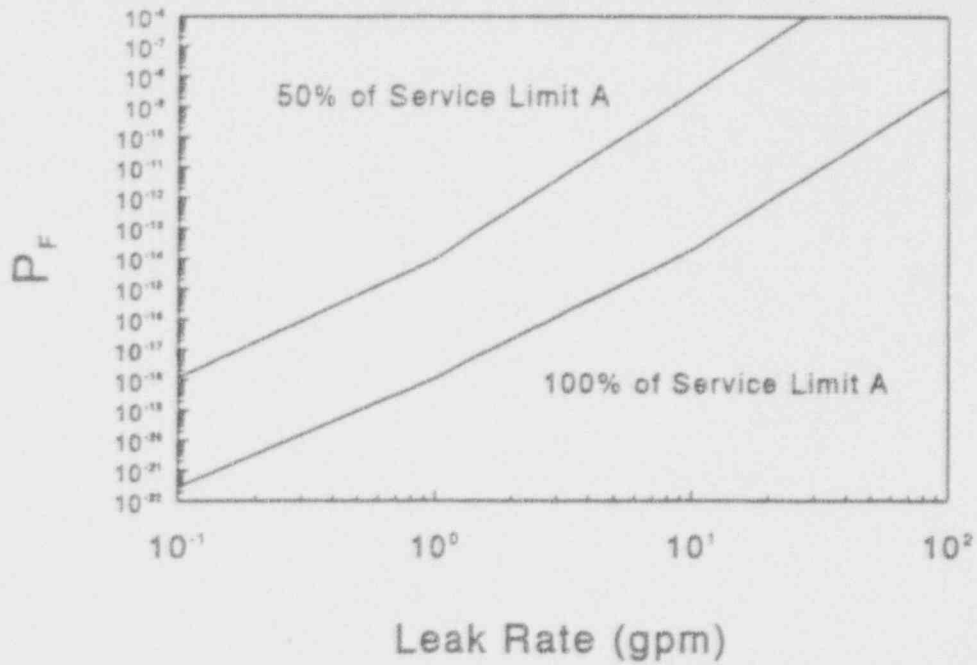


Figure 7.19(a) Conditional failure probability by SORM for PWR-1 (base metal)

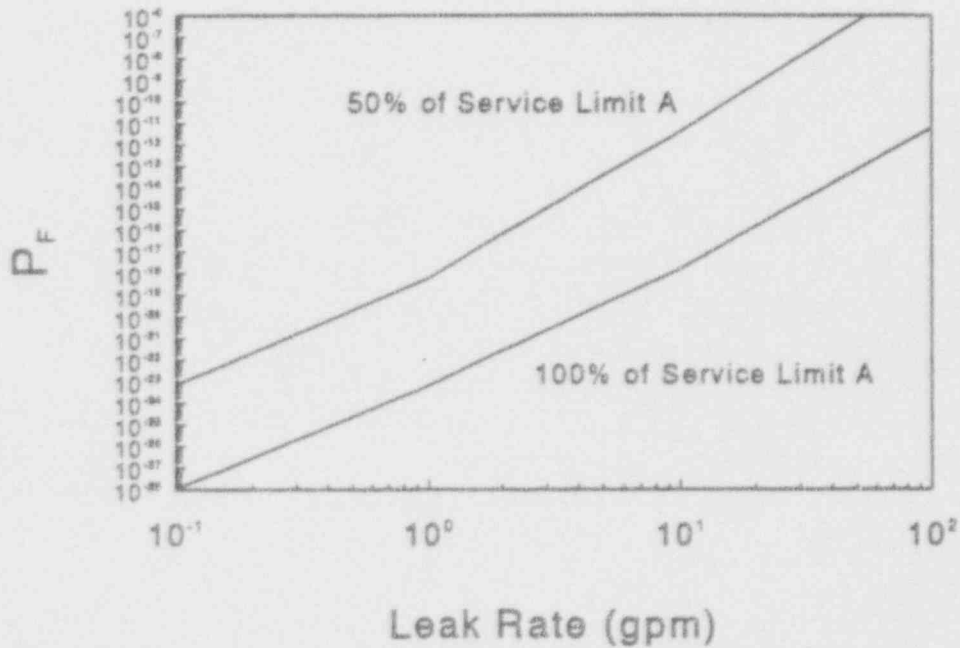


Figure 7.19(b) Conditional failure probability by SORM for PWR-1 (weld metal)

T-6004-F5.28(a)(b)

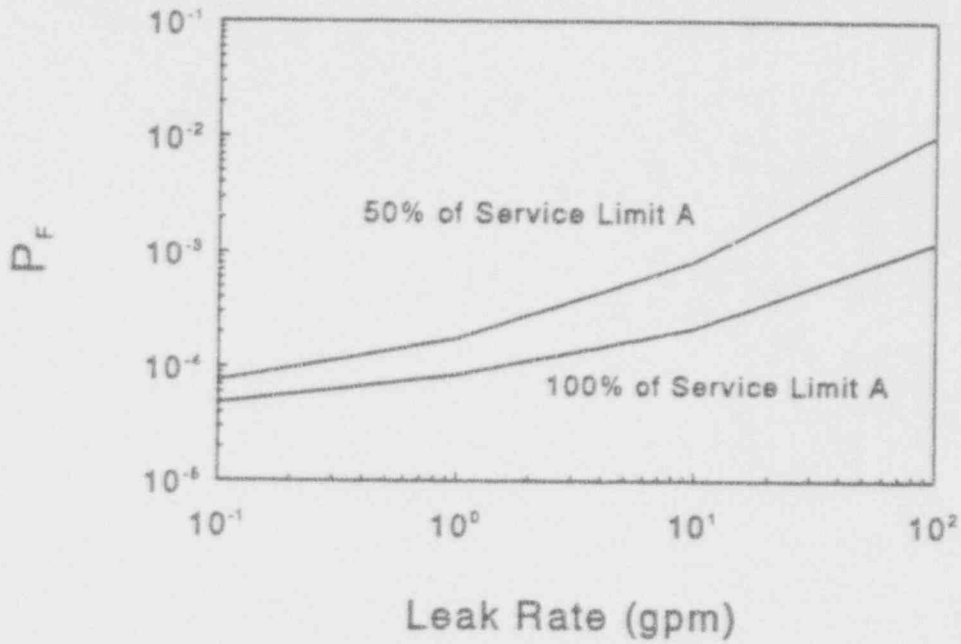


Figure 7.20(a) Conditional failure probability by SORM for PWR-2 (base metal)

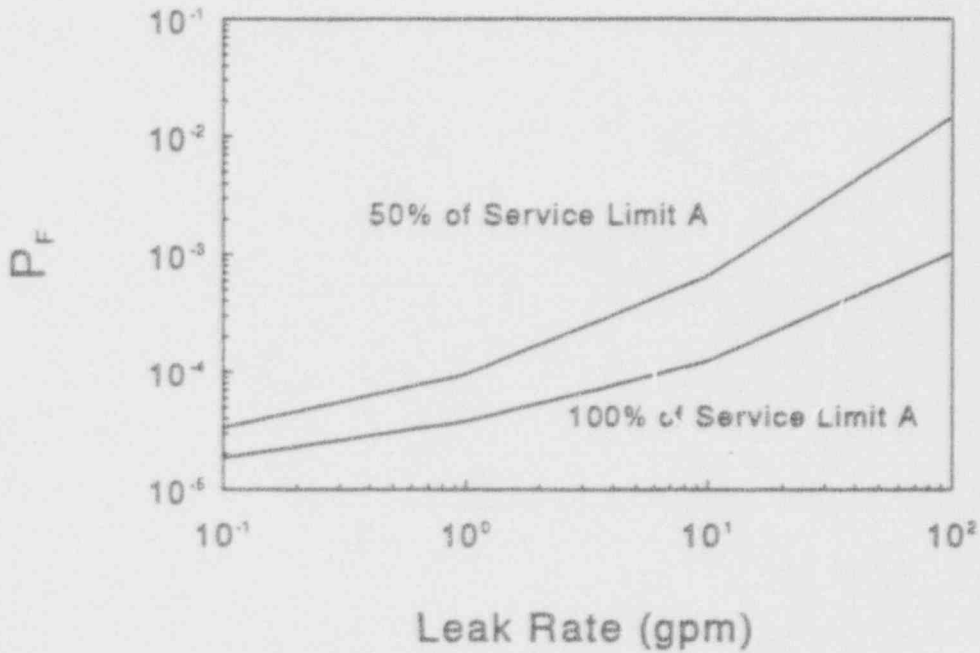


Figure 7.20(b) Conditional failure probability by SORM for PWR-2 (weld metal)

T-6004-F5.29(a)(b)

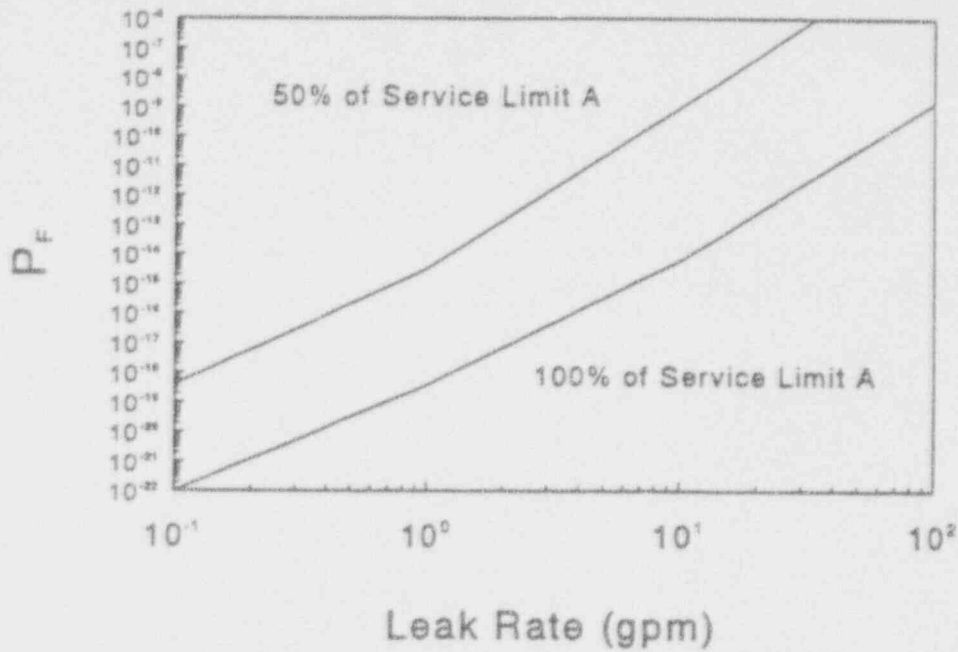


Figure 7.21 Conditional failure probability by SORM for PWR-1 (random crack location)

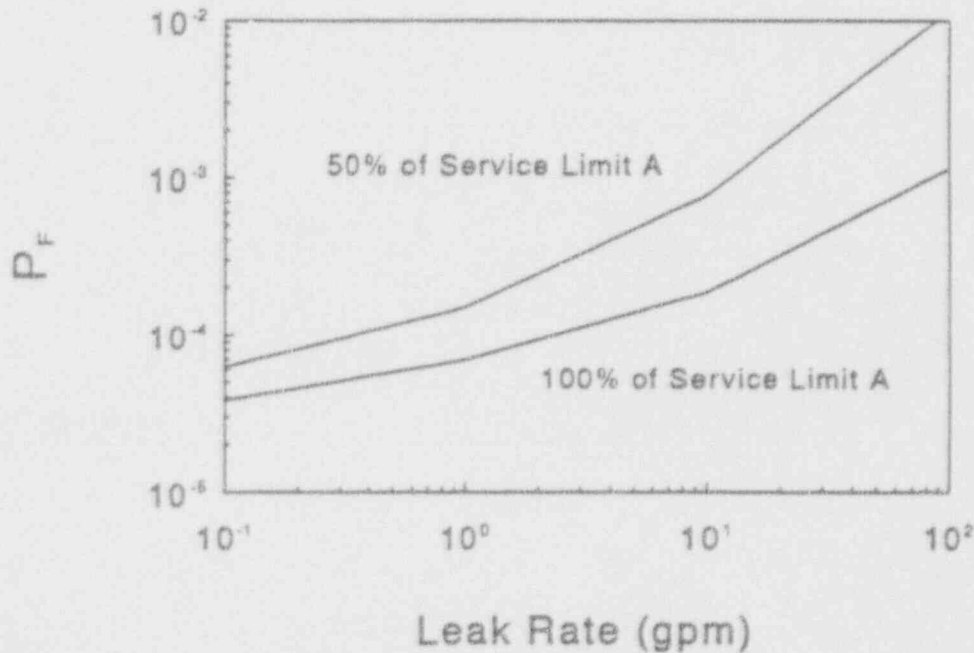


Figure 7.22 Conditional failure probability by SORM for PWR-2 (random crack location)

T-6004-F5.34/5.35

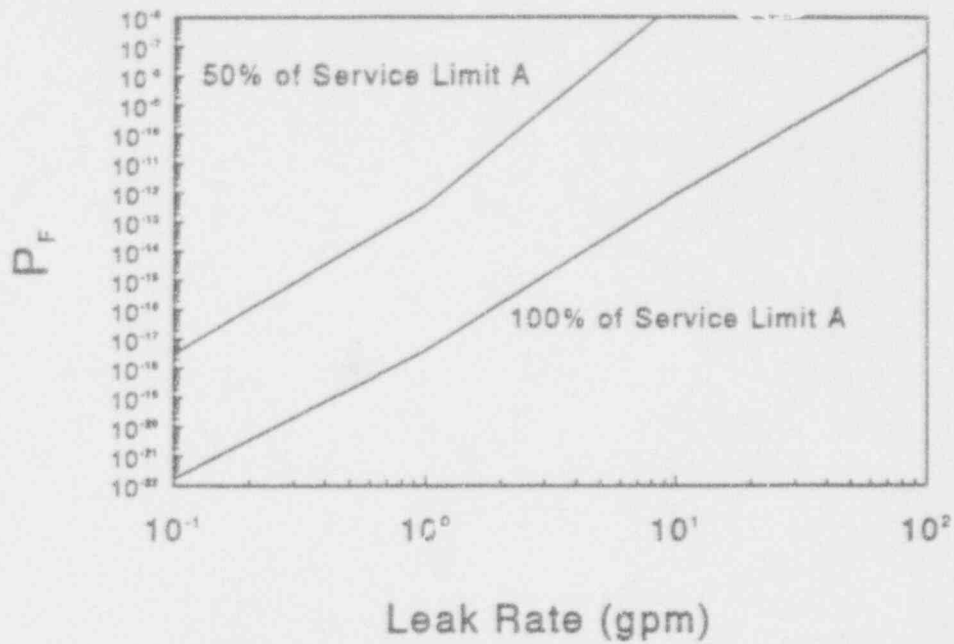


Figure 7.23 Conditional failure probability by SORM for PWR-3 (random crack location)

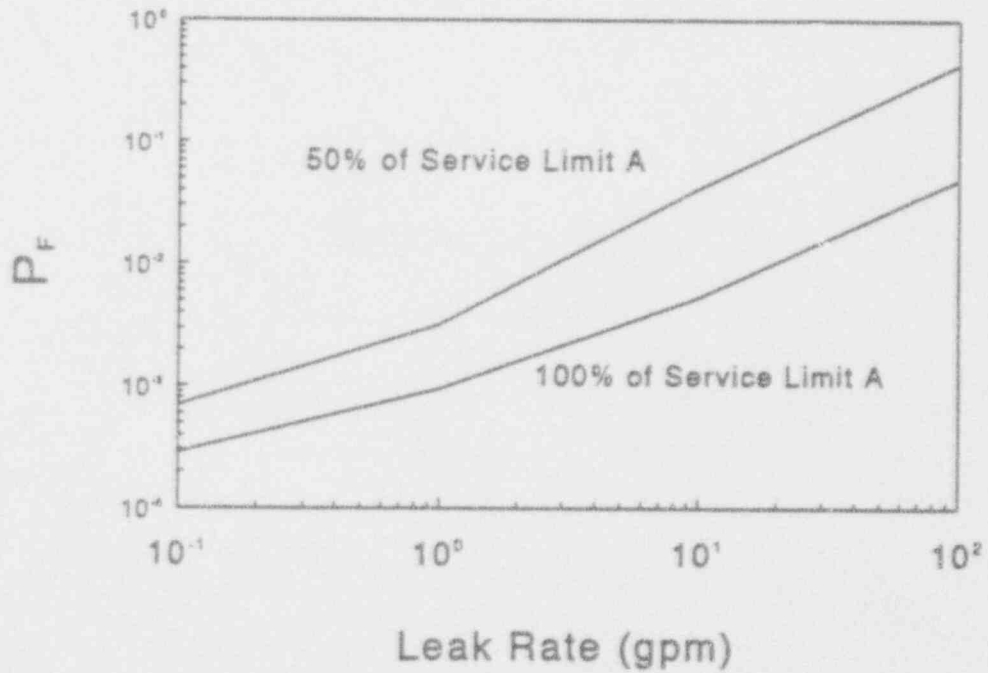


Figure 7.24 Conditional failure probability by SORM for PWR-4 (random crack location)

T-6004-F5.35/5.37

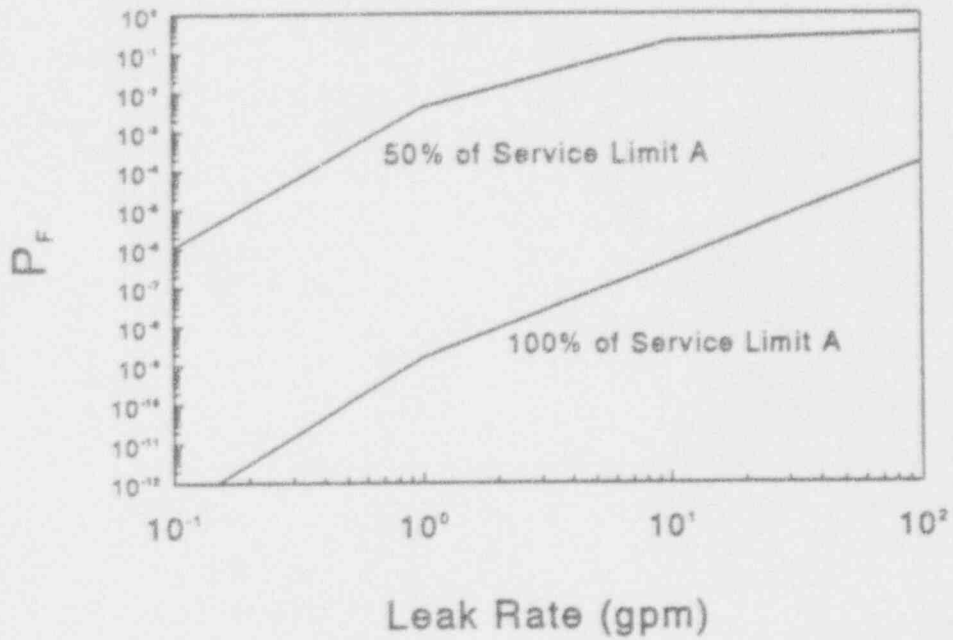


Figure 7.25 Conditional failure probability by SORM for PWR-5 (random crack location)

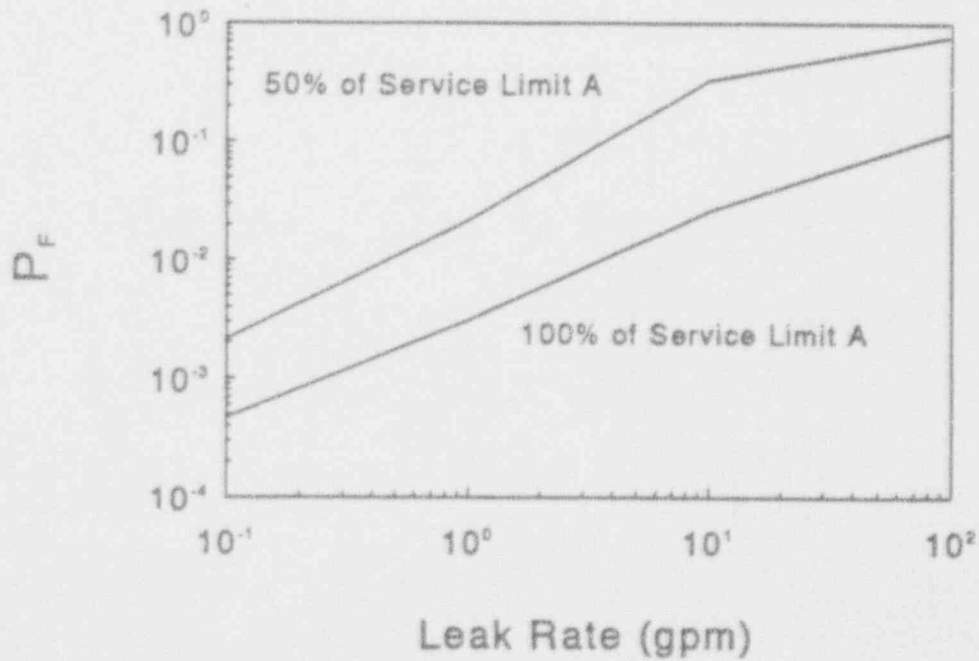
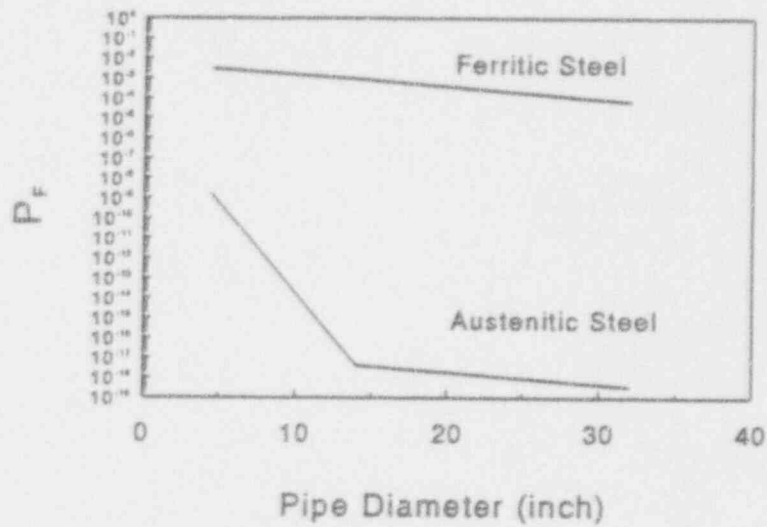
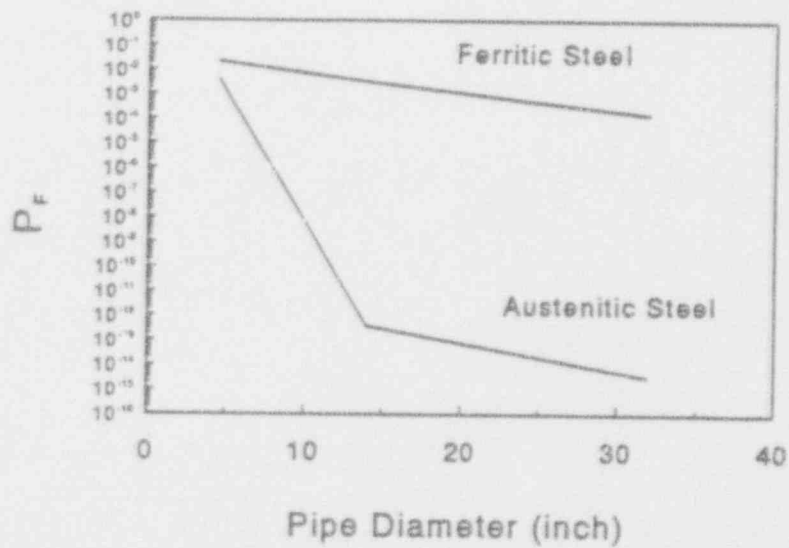


Figure 7.26 Conditional failure probability by SORM for PWR-6 (random crack location)

T-6004-F5.38/5.39



(a) 100 percent of Service Level A



(b) 50 percent of Service Level A

Figure 7.27 Conditional failure probability as a function of diameter in PWR pipes

T-6004-F5.40

An inverse problem is to determine the required leak-rate detection capability for an acceptable (target) value of conditional probability of failure. For example, a frequently used value of 10^{-6} /year could be used to determine the leak-rate requirements. If the plant life is 40 years, this will amount to an acceptable failure probability of 4×10^{-5} per plant lifetime. Using this value, the required leak rates for BWR-1 pipe from Figure 7.12 are about 3 gpm and greater than 100 gpm when the normal operating stresses are 50 and 100 percent of Service Level A stress limit, respectively.

In our analysis, it was assumed that the N+SSE stress at Service Level-B occurred with absolute certainty (i.e., a probability of 1). Considerable time was spent assessing if a more realistic probability of the N+SSE stresses could be used in a generic sense. To do so would involve the following considerations: (1) determination of the frequency of earthquakes occurring at a specific site, (2) determination of the probability distribution of the magnitude of an earthquake, (3) comparisons of the frequency of occurrence relative to the time from leakage to plant shutdown, and (4) assessment for all U.S. plants by either accounting for plant-to-plant variability or using the worst-case plant. These were not considered in this study, but if known, the probability of the seismic event occurring could be simply multiplied by our conditional failure probability to get a probability in more absolute terms.

Assessment of Current Margins for Leak Rates

Current deterministic methods for incorporating conservatism in LBB methodology is based on several safety margins. For example, safety margins of 2, $\sqrt{2}$, and 10 are being proposed on the LBB detectable flaw size, N+SSE stresses, and leak-rate detection, respectively. These margins were established using engineering judgment, but do not provide any explicit correlation with the failure probability of piping systems. In this study, the adequacy of the current margin of 10 used for leak rates is evaluated by explicitly considering the statistical variability of crack morphology variables.

Consider the stainless steel pipe in the case of BWR-1 with IGSCC under normal operating stresses. Using the program PSQUIRT, the crack morphology variables were randomly generated according to their probability distribution functions, and the corresponding leak rates were calculated under a given normal operating stress. Figure 7.28(a) shows the histogram of the random leak rate obtained from 1000 analyses when the normal operating stress is 50 percent of the Service Level-A limit. The mean and standard deviation of the leak rate are estimated to be 1.21 gpm and 0.41 gpm, respectively. Thus, when a safety margin of 10 is used, it appears that the leak rate with the above margin is 27 times the standard deviation away from the mean value. Hence, the safety margin of 10 is deemed to be more than adequate to account for crack morphology variability. Figure 7.28(b) shows the histogram of leak rate from 1000 samples when the normal operating stress is 100 percent of the Service Level-A limit. Also, in this case, the safety margin of 10 is found to be more than necessary. Similar histograms were also generated for another carbon steel pipe, BWR-2, with the cracking mechanism governed by corrosion fatigue. The histograms shown in the Figures 7.29(a) and 7.29(b) correspond to the normal operating stress being 50 percent and 100 percent of Service Level-A limit. They also support the previous conclusions made regarding the adequacy of the current margin for leak rate.

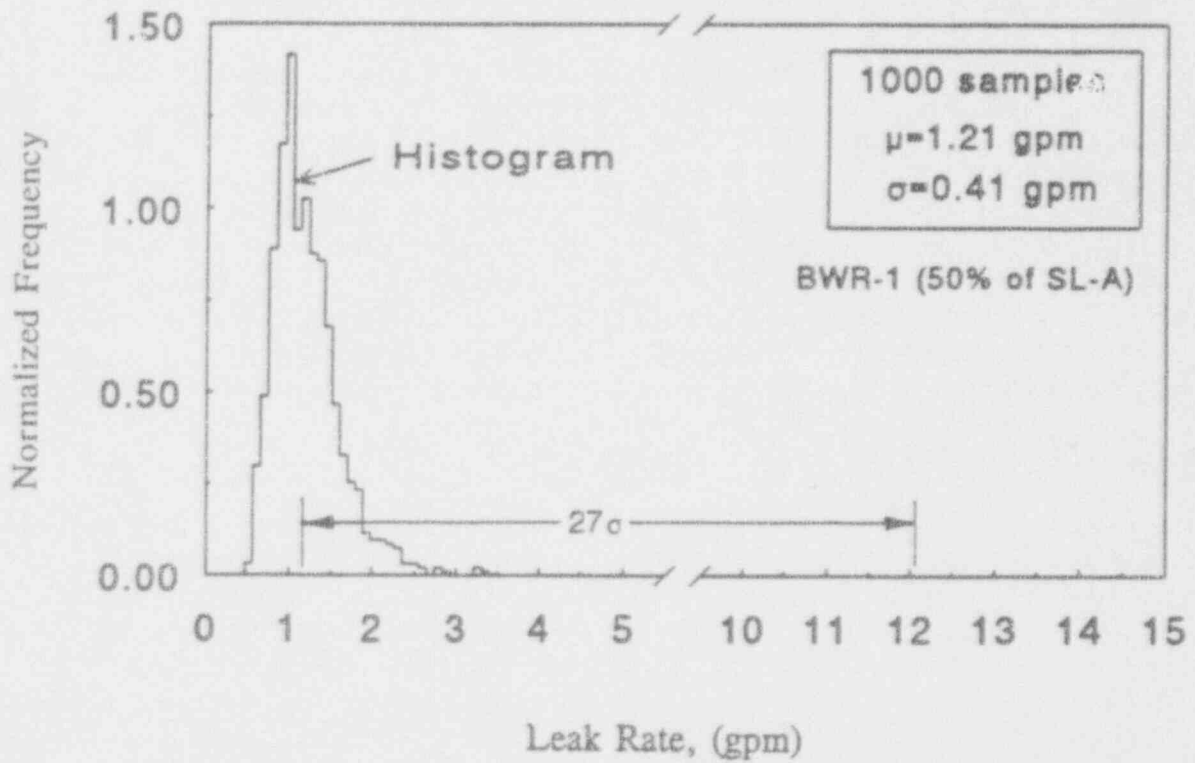


Figure 7.28(a) Histogram of leak rate under 50 percent of Service Level-A limit for BWR-1

T-6004-F5.41

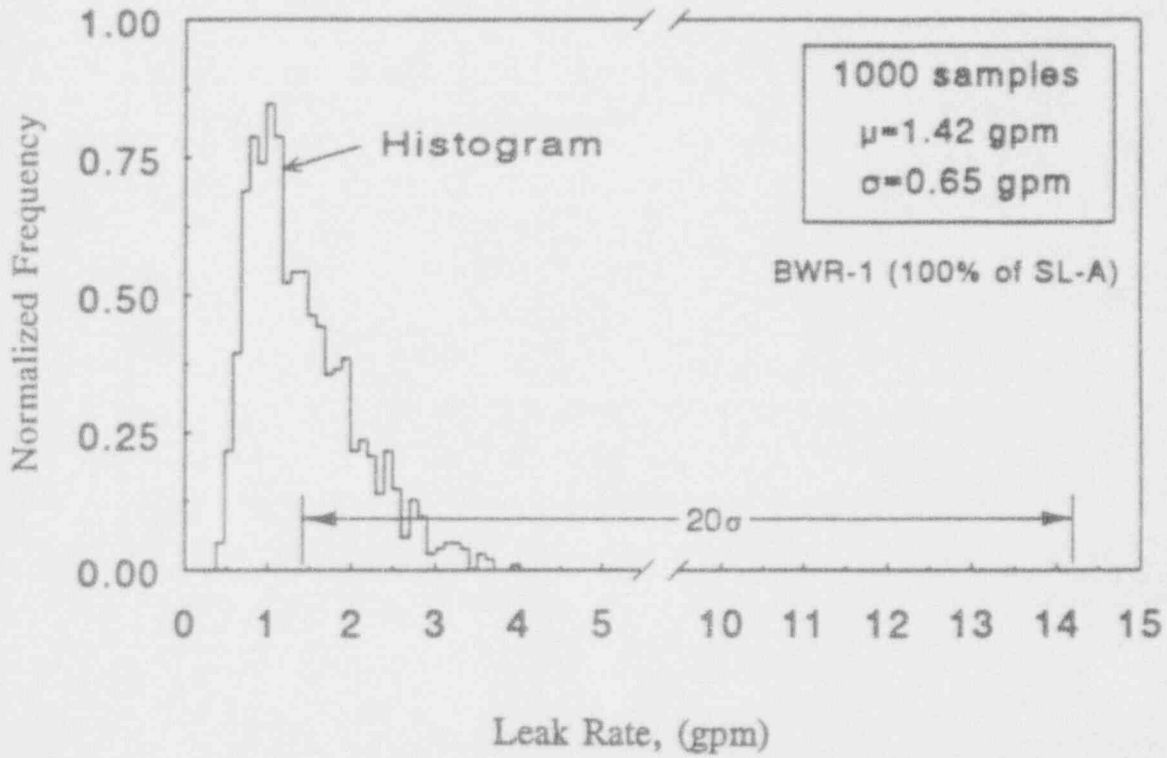


Figure 7.28(b) Histogram of leak rate under 100 percent of Service Level-A limit for BWR-1

T-6004-F5.42

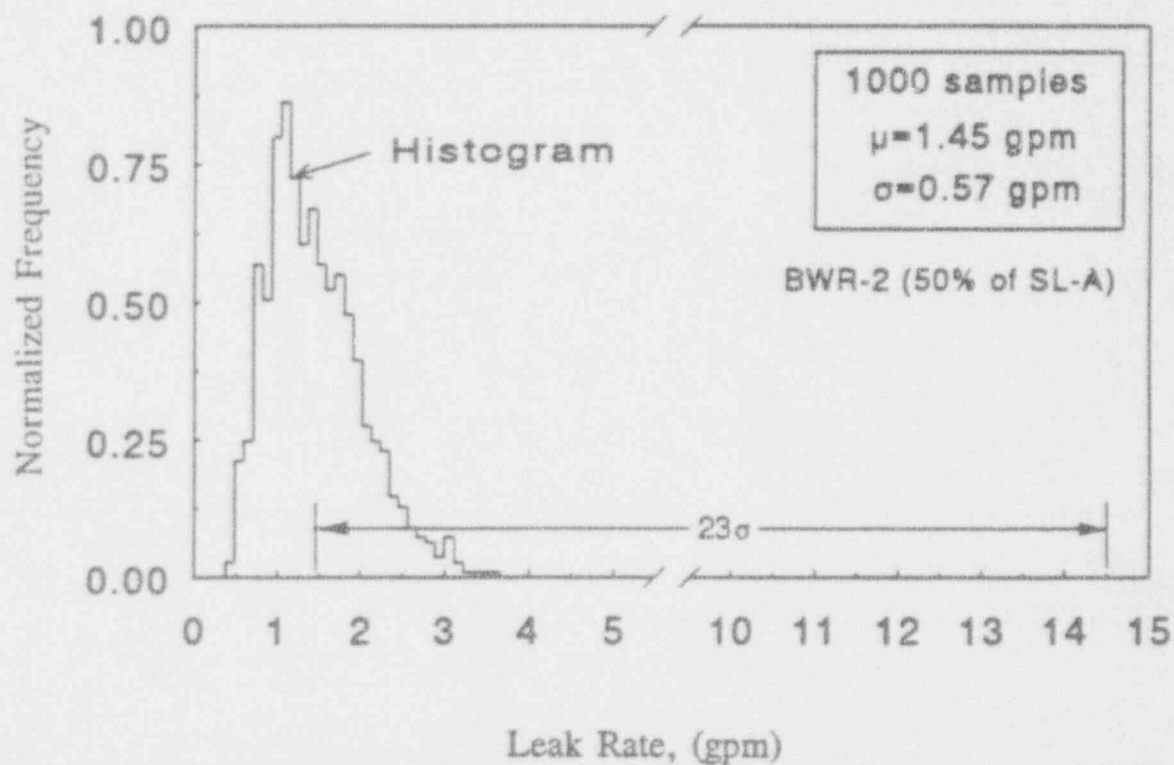


Figure 7.29(a) Histogram of leak rate under 50 percent of Service Level-A limit for BWR-2

T-6004-F5.43

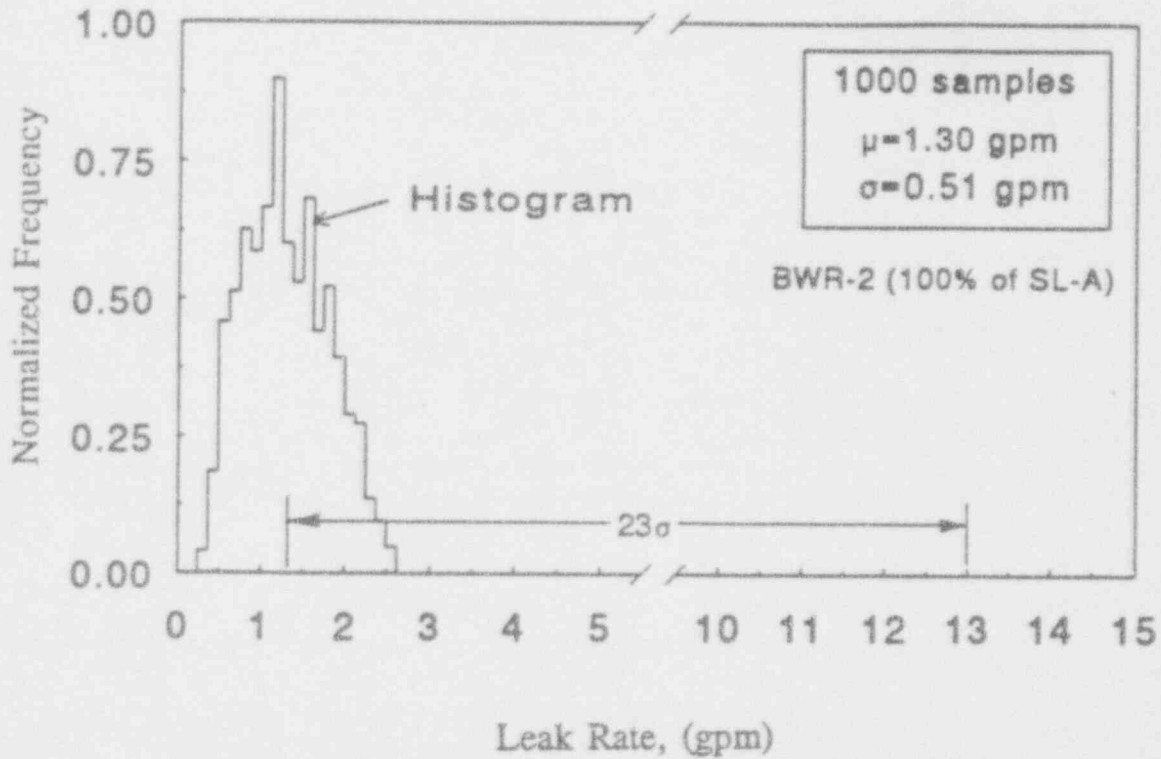


Figure 7.29(b) Histogram of leak rate under 100 percent of Service Level-A limit for BWR-2

T-6004-F5.44

In examining these histograms, it appears that a margin of approximately 2.5 may be assumed to be sufficient to account for the variability of crack morphology parameters. This means that a factor of up to 4 remains to account for the variability in leak detection equipment, actual stresses, and other variables if the total margin of 10 is to remain fixed.

Activity 6.6.4 Evaluate the proposed changes on leak rate for "non-LBB" piping systems

The effort in this activity involves stochastic fracture evaluations of "non-LBB" approved pipes for leak-rate detection applications. Calculations were performed considering several complex-cracked pipes. The complex crack is a long circumferential surface crack that penetrates the thickness of the pipe for a short length. This is more likely to occur for IGSCC cracking mechanisms. Both large and intermediate diameter pipes, each associated with two different depths of surface crack, were considered. Table 7.2 shows the characteristics of four complex-cracked pipes for probabilistic pipe fracture evaluations conducted in this study.

The conditional failure probability calculated as a function of leak rates for random crack location are provided in Figures 7.30 - 7.33 for the four BWR pipes considered in this study. The reliability of complex-cracked pipes were lower than that for through-wall-cracked pipes. For a given depth of surface crack, the conditional failure probability of piping systems was found to decrease with increasing values of pipe diameter. Similar observations were also made regarding TWC pipes.

Figure 7.34 shows several plots of conditional probability of failure (random crack location) for a given leak rate of 1 gpm as a function of d/t of the complex-cracked BWR pipes with LBB detectable crack size obtained for both 100 and 50 percent of Service Level-A stresses. The conditional probability of failure was found to increase with increasing values of the depth of surface crack. In fact, if the depth of the surface crack is large enough, then failure could occur even under normal operating loads.

Activity 6.6.6 NUREG Report

During this fiscal year, considerable amounts of effort also were spent on preparing a topical report for the leak rate quantification subtask. The report is titled "Probabilistic Pipe Fracture Evaluations for Leak-Rate Detection Applications," NUREG/CR-6004, by S. Rahman, N. Ghadiali, D. Paul, and G. Wilkowski. The report will be finalized in the next year of the program.

7.4 Plans for Next Year of the Program

The plans for efforts in the next 12 months are summarized below.

Table 7.2. Complex-cracked BWR piping systems for probabilistic fracture evaluations

Cases	Piping ^(a) System	Nominal Dia. (inches)	Thickness, mm (inches)	Base Metal	Weld ^(b) Metal	Assumed ^(c) Cracking Mechanism
BWR-7	Side Riser (d/t=0.25)	28	35.8 (1.41)	TP304	SS SAW	IGSCC
BWR-8	Main Steam (d/t=0.50)	28	35.8 (1.41)	TP304	SS SAW	IGSCC
BWR-9	Side Riser (d/t=0.25)	18	23.9 (0.94)	TP304	SS SAW	IGSCC
BWR-10	Main Steam (d/t=0.50)	18	23.9 (0.94)	TP304	SS SAW	IGSCC

(a) d/t = depth of surface crack/thickness for complex crack

(b) SS = stainless steel, SAW = submerged arc weld

(c) IGSCC = Intergranular stress-corrosion cracking

7.4.1 Subtask 6.1 Create Combined Loading Improvements

Of the three activities in this subtask, Activities 6.1.1 and 6.1.3 have been completed. The remaining Activity 6.1.2 (Account for Pressure on the Crack Face) will be started in the next year of the program.

7.4.2 Subtask 6.2 Implement Short TWC Crack-Opening Improvements

There are two activities in this subtask. No work was scheduled for this coming year. They will be started in the next year of the program.

7.4.3 Subtask 6.3 Improve Weld Crack Evaluations

There are two activities in this subtask. Activity 6.3.1 was completed. Activity 6.3.2 (Comparisons with Recent DP³II and Task 1 Data) has started and will continue as data become available. It will be completed in the next year of the program.

7.4.4 Subtask 6.4 Modify SQUIRT Code

This subtask was not scheduled to start in this fiscal year. Work will begin in the next year of the program.

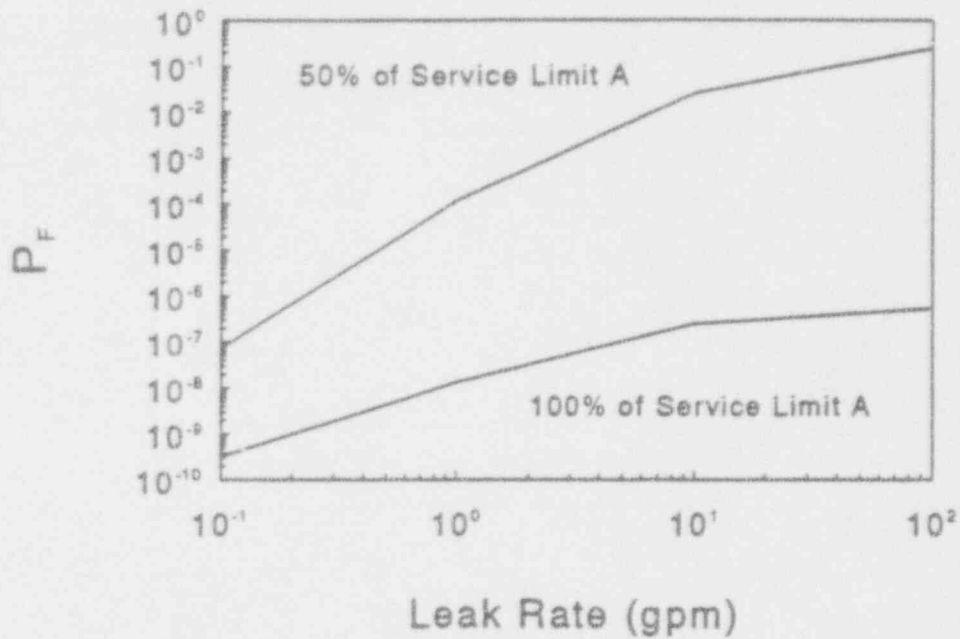


Figure 7.30 Conditional failure probability by SORM for BWR-7 (random crack location)

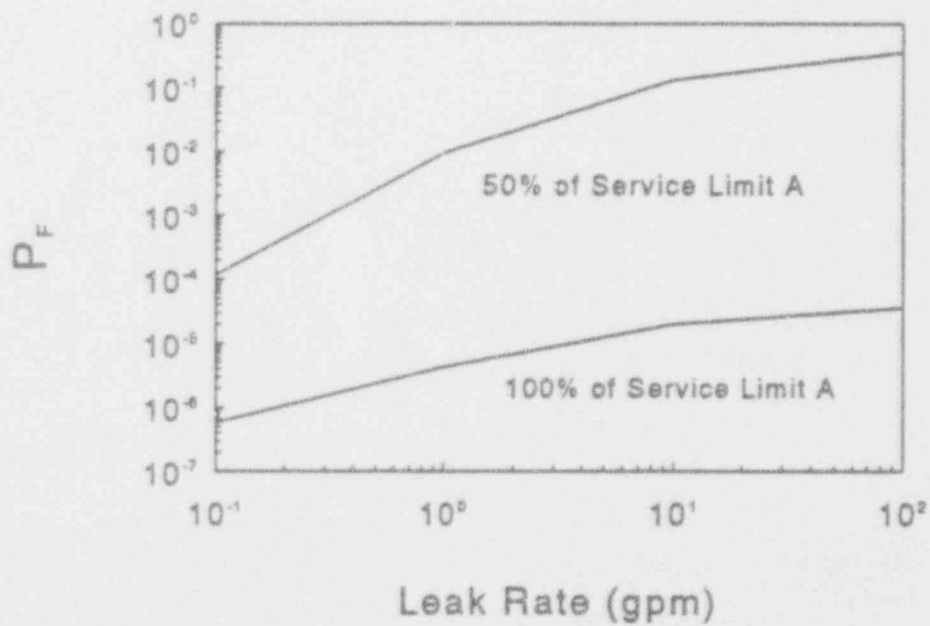


Figure 7.31 Conditional failure probability by SORM for BWR-8 (random crack location)

T-6004-F5.22/5.23

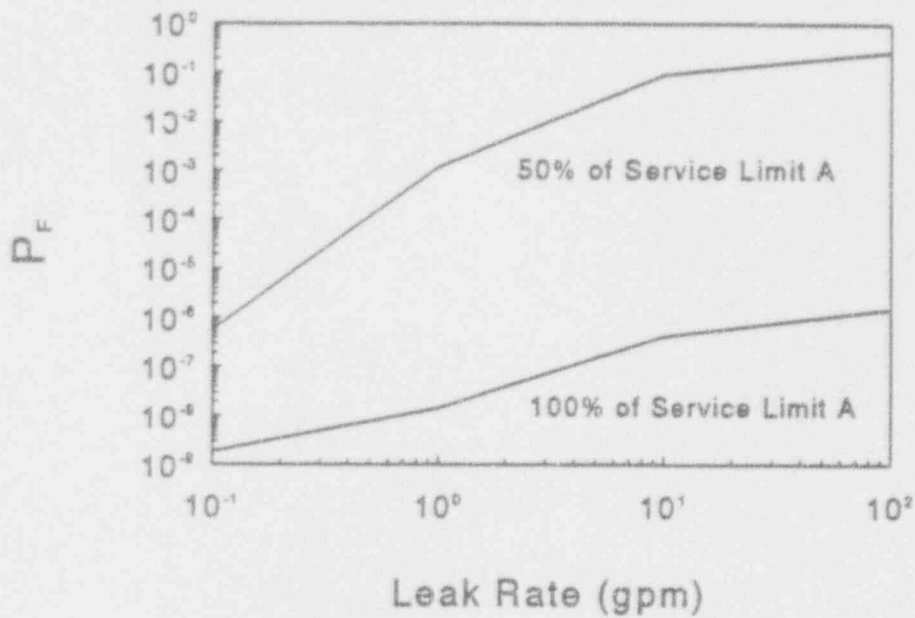


Figure 7.32 Conditional failure probability by SORM for BWR-9 (random crack location)

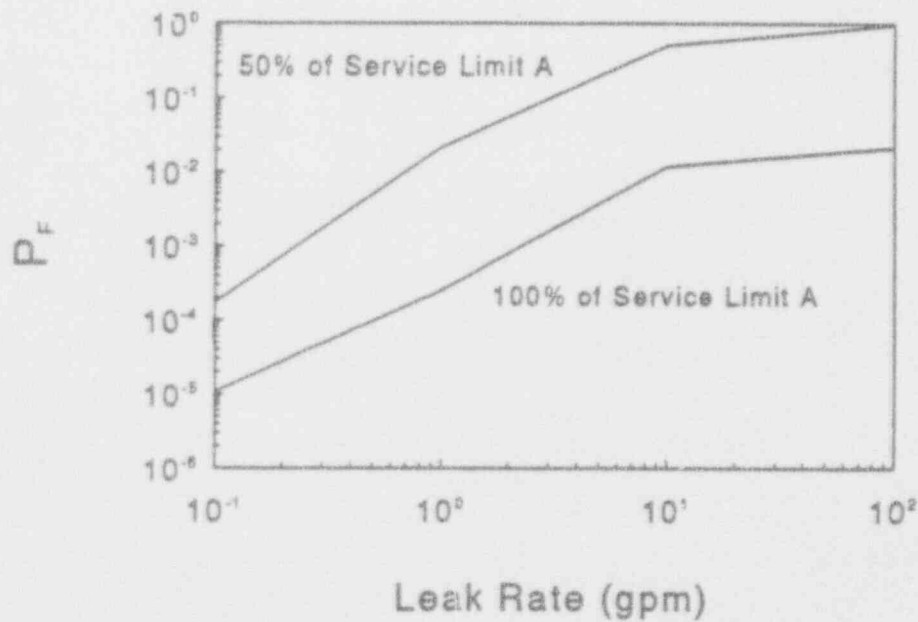
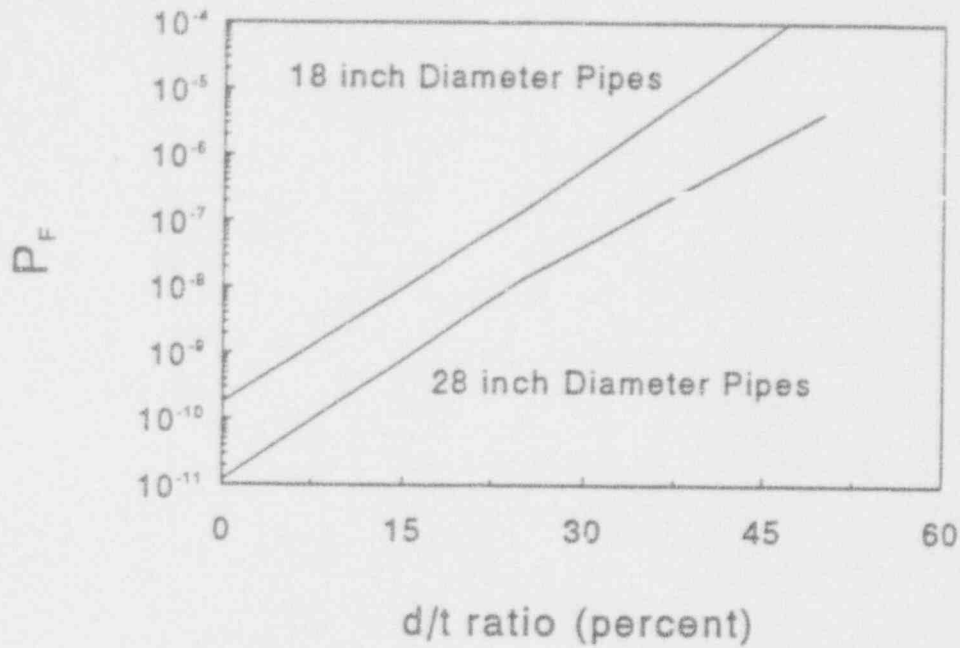
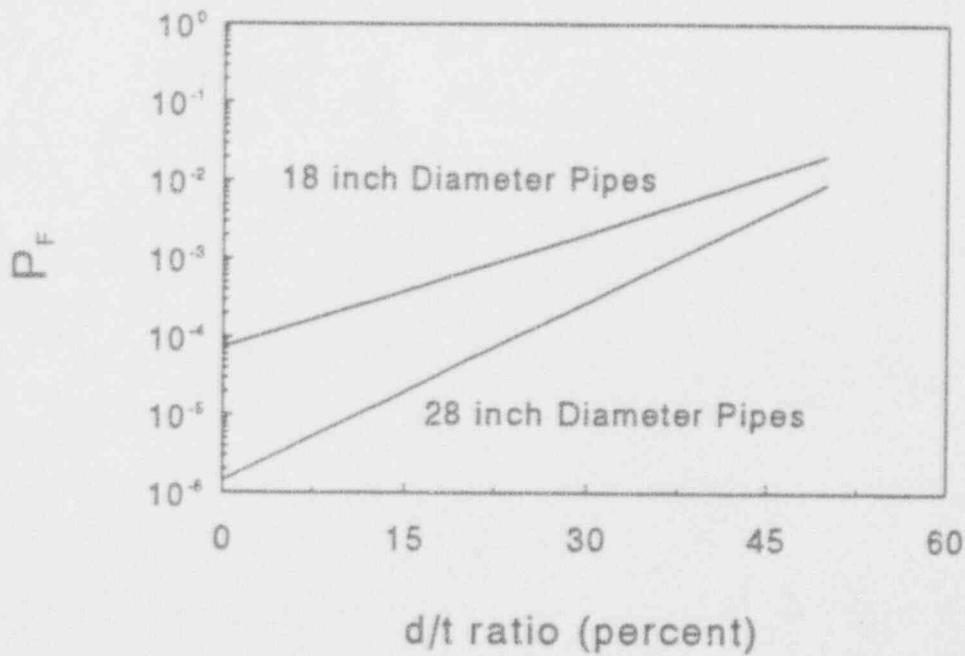


Figure 7.33 Conditional failure probability by SORM for BWR-10 (random crack location)

T-6004-F5.24/5.25



(a) 100 percent of Service Level A



(b) 50 percent of Service Level A

Figure 7.34 Conditional failure probability as a function of d/t in complex-cracked BWR pipes

T-6004-F5.27

7.4.5 Subtask 6.5 Prepare Topical Report on Crack-Opening-Area Improvements

This subtask was not scheduled to start in this year. Work will begin in the next year of the program.

7.4.6 Subtask 6.6 Leak Rate Quantification

There are six activities in this subtask. The current status and future plans for these activities are given below.

- Activity 6.6.1 Items 1 and 2 of Activity 6.6.1 have been completed. Item 3 under this activity will be completed in the next year of the program.
- Activity 6.6.2 This activity has been completed. No additional work is scheduled for the next year of the program.
- Activity 6.6.3 This activity has been completed. However, some additional work will be performed if required by NRC-RES and NRC-NRR. The tasks will be completed in the next year of the program.
- Activity 6.6.4 This activity has also been completed. However, some additional work will be performed if required by NRC-RES and NRC-NRR. The tasks will be completed in the next year of the program.
- Activity 6.6.5 Coordination with NRC-RES and NRC-NRR will be continued for their guidance on performing additional calculations made in the Activities 6.6.3 and 6.6.4.
- Activity 6.6.6 During this year, copies of the draft topical report on subtask 6.6 were sent to NRC-RES and NRC-NRR. On receiving their review comments, the report will be finalized in the next year of the program.

7.5 References

- 7.1 Wilkowski, G. M., and others, "Short Cracks in Piping and Piping Welds," Second semiannual report by Battelle, NUREG/CR-4599, Vol. 1, No. 2, April 1992.
- 7.2 Paul, D. D., and others, "Evaluation and Refinement of Leak-Rate Estimation Models," NUREG/CR-5128, April 1991.

- 7.3 Schmidt, R. A., Wilkowski, G. M., and Mayfield, M. E., "The International Piping Integrity Research Group (IPIRG) Program - An Overview," SMiRT-11, Paper G12/1, August 1991.
- 7.4 Harris, D. O., Dedhia, D. D., and Lu, S. C., "Theoretical and User's Manual for PC-PRAISE, A Probabilistic Fracture Mechanics Computer Code for Piping Reliability Analysis," NUREG/CR-5864, February 1992.
- 7.5 Wilkowski, G. M. and others, Degraded Piping Program-Phase II, NUREG/CR-4082, Final and Semiannual Reports, 1985-1989.
- 7.6 Rahman, S., Ghadiali, N., Paul, D., and Wilkowski, G., "Probabilistic Pipe Fracture Evaluations for Leak-Rate Detection Applications," NUREG/CR-6004, September 1993.
- 7.7 Collier, R. P., Stulen, F. B., Mayfield, M. E., Pape, D. B., and Scott, P. M., "Two-Phase Flow Through Intergranular Stress Corrosion Cracks and Resulting Acoustic Emission," EPRI Report No. NP-3540-LD, 1984.
- 7.8 Norris, D. and others, "PICEP: Pipe Crack Evaluation Program," Electric Power Research Institute Report, NP-3596-SR, 1984.
- 7.9 Kumar, V., German, M. D., and Shih, C. F., "An Engineering Approach to Elastic-Plastic Fracture Analysis," Electric Power Research Institute Report, NP-1931, 1981.
- 7.10 Hiser, A. L., and Callahan, G. M., "A User's Guide to the NRC's Piping Fracture Mechanics Database (PIFRAC)," NUREG/CR-4894, May 1987.
- 7.11 "Report to the U.S. Nuclear Regulatory Commission Piping Review Committee," Prepared by the Pipe Break Task Group, NUREG/CR-1061, Vol. 3., November 1984.
- 7.12 Solicitations for public comment on "Standard Review Plan 3.6.3 LEAK-BEFORE-BREAK PROCEDURES," Federal Register, Vol. 52, No. 167, Friday, August 28, 1987, Notices, pp. 32626 to 32633.
- 7.13 1992 Edition ASME Boiler & Pressure Vessel Code - Section III, Article NB-3642. Published by American Society of Mechanical Engineers, 345 East 47th Street, New York, N.Y. 10017, July 1, 1992.
- 7.14 Fiessler, B., Neumann, H. J., and Rackwitz, R. "Quadratic Limit States in Structural Reliability," Journal of Engineering Mechanics, ASCE, 105 (EM4), pp. 661-676. (1979).
- 7.15 Rackwitz, R. and Fiessler, B., "Structural Reliability under Combined Random Load Sequences," Computer and Structures, Vol. 9, pp. 484-494, 1978.
- 7.16 Madsen, H. O., Krenk, S., and Lind, N. C., Methods of Structural Safety, Prentice-Hall, Inc., Englewood Cliffs, New Jersey, 1986.

- 7.17 Harris, D. O., Lim, E. Y., and Dedhia, D. D., "Probability of Pipe Fracture in the Primary Coolant Loop of a PWR Plant," NUREG/CR-2189, Vol. 5, August 1981.
- 7.18 Mehta, H. S., Patel, N. T., and Ranganath, S., "Application of the Leak-Before-Break Approach to BWR Piping," EPRI report NP-4991, December 1986.
- 7.19 Maxham, W. D., and Yoon, K. K., "Application of Leak-Before-Break Approach to PWR Piping Designed by Babcock and Wilcox," EPRI report NP-4972, January 1987.
- 7.20 Swamy, S. A., and Others, "Application of the Leak-Before-Break Approach to Westinghouse PWR Piping," EPRI report NP-4971, December 1986.
- 7.21 Ayres, D. J., LaRussa, J. J., Ganta, B. R., and Austin, S. C., "Application of Leak-Before-Break Analysis to PWR Piping Design by Combustion Engineering," NP-5010, Final Report, February 1987.
- 7.22 Wilson, S. A., "Estimating the Relative Probability of Pipe Severance by Fault Cause," General Electric Company Report GEAP-20615, Boiling Water Reactor Systems Department, San Jose, California, September 1974.

8. TASK 7 NRCPIPE IMPROVEMENTS

8.1 Task Objective

The main objective of this task is to incorporate the analysis improvements from Subtasks 1.4 and 2.4 into the NRCPIPE code. A secondary objective is to make the NRCPIPE code more efficient and also to restructure the code to allow for ease of implementation of the activities described below.

8.2 Task Rationale

In the Degraded Piping Program, the computer code NRCPIPE was developed for circumferential through-wall-cracked pipe fracture analyses. A VAX version of the code also contained the circumferential internal surface-wall-cracked pipe algorithms. The PC version was made specifically for the through-wall-cracked analyses. Numerous J-estimation schemes were developed or modified. The improvements developed in the current program need to be incorporated into this code to take advantage of technology developments as well as to facilitate comparisons with the experimental results.

8.3 Task Approach

To accomplish the objectives of this task, four subtasks are to be undertaken:

- Subtask 7.1 Improve the efficiency of the current version of NRCPIPE
- Subtask 7.2 Incorporate TWC improvements in NRCPIPE
- Subtask 7.3 Make surface-crack PC version of NRCPIPE
- Subtask 7.4 Provide new user's manual.

The approach for each of these subtasks and progress made is discussed below.

8.3.1 Subtask 7.1 Improve Efficiency of Current Version of NRCPIPE

The current version of the NRCPIPE code is Version 1.4e. During this reporting period only minor changes were made to the code.

8.3.2 Subtask 7.2 Incorporate TWC Improvements in NRCPIPE

There are four activities in this subtask. These are:

- Activity 7.2.1 Incorporate F -, V_3 , and h_4 -function improvements
- Activity 7.2.2 Incorporate ovalization for short cracks
- Activity 7.2.3 Incorporate bending and tension improvements
- Activity 7.2.4 Incorporate improved analyses for weld and fusion line cracks.

There were no efforts in the above activities in this subtask during this reporting period.

8.3.3 Subtask 7.3 Make Surface Crack Version of NRCPIPE

There are six activities in this subtask. These are:

- Activity 7.3.1 Make circumferentially surface-cracked pipe PC code of NRCPIPE
- Activity 7.3.2 Incorporate ASME Section XI criteria in NRCPIPE (SC version)
- Activity 7.3.3 Add J_e to SC.TNP and SC.TKP
- Activity 7.3.4 Add ovalization
- Activity 7.3.5 Incorporate new LBB.ENG surface-cracked pipe solution
- Activity 7.3.6 Add pressure and bending solutions
- Activity 7.3.7 Add surface-cracked pipe weld criteria.

Progress

In Activity 7.3.1 a PC-based version of NRCPIPE (internal surface crack version) was developed from the VAX source code. This program was developed along the same lines as the TWC version discussed above and uses the SC.TNP and SC.TKP algorithms developed previously for the case of pure bending. The acronym for this program is NRCPIPES. Version 1.0 of this code was delivered to NRC for review.

In Activity 7.3.6 improved algorithms for the case of combined pressure and bending loads developed in Subtask 2.4 were reviewed and evaluated for implementing into NRCPIPES. These algorithms will be implemented when some validations with finite-element analysis are completed (new additional tasks).

8.3.4 Subtask 7.4 Provide New User's Manual

A User's Manual for the NRCPIPES code for analyzing surface cracks in pipes was delivered to the NRC.

8.4 Plans for Next Year of the Program

Efforts scheduled for the next year are discussed below.

8.4.1 Subtask 7.1 Improve Efficiency of Current Version

Efficiency improvements to the existing NRCPIPE code continue on an ongoing basis. A revised version of this code will be delivered to the NRC.

8.4.2 Subtask 7.2 Incorporate TWC Improvements in NRCPIPE

The GE/EPRI functions will be implemented into NRCPIPE in Activity 7.2.1. Efforts will also involve incorporating bending and tension improvements. The development and implementation of the weld and fusion line cracks algorithm will also be performed.

8.4.3 Subtask 7.3 Make Surface Crack Version of NRCPIPE

Quality assurance calculations will be made for Version 1.0 of the PC code NRCPIPES. Verification and implementation of a combined bending and pressure algorithm will continue in the next reporting period.

8.4.4 Subtask 7.4 Provide New User's Manual

The user's manual for both the NRCPIPE code and the NRCPIPES code will be updated.

9. TASK 8 ADDITIONAL EFFORTS

9.1 Task Objective

The objective of this task is to undertake analyses or experiments needed to clarify issues that develop during the course of this program. To date, five subtasks have been initiated.

9.2 Task Rationale

The five subtasks involving additional efforts are:

- Subtask 8.1 Validity Limits on J-R Curve Determination
- Subtask 8.2 Stainless Steel SAW Fusion-Line Toughness
- Subtask 8.3 Update PIFRAC Data Files
- Subtask 8.4 Develop Data Base for Circumferential Pipe Fracture Experiments
- Subtask 8.5 Data File Conversion from HP to IBM Format

Subtasks 8.2, 8.3, 8.4, and 8.5 were included as part of a recent modification to this program. Although efforts in these subtasks were not initiated, the objectives, rationale, approach, and deliverables for these efforts are discussed below.

9.2.1 Subtask 8.1 Validity Limits on J-R Curve Determination

9.2.1.1 Objective

The objective of this subtask is to carry out a theoretical and computational study of the limits of validity of J-R curve data from bend-type specimens under contained and fully yielded conditions. The results of the study should make it possible to validate if J_D or J_M resistance curves can be used. This work is being performed under a subcontract to Professor F. Shih at Brown University.

9.2.1.2 Rationale

The results will have direct bearing on the problem of determining J-R curves from small-bend-type specimens where it is desired to obtain valid data to characterize large amounts of crack growth for pipe and pressure vessel applications.

9.2.1.3 Approach

Through extensive and systematic numerical analyses of crack growth under small-scale yielding conditions, as well as for finite crack geometries, the parameters which characterize the validity limits for the determination of J-R curves will be identified. The effect of crack tip constraint on the crack growth behavior also will be examined in detail. A critical assessment of the several definitions of J that are used in the analysis of crack growth will be made.

9.2.1.4 Progress

We have studied several publications on the J_M parameter and have completed an in-depth evaluation of the theoretical underpinnings of J_M . A short report on the theoretical basis of the J_M parameter is being prepared.

We have implemented a predictive model, which incorporates a local fracture criterion characterizing the fracture process well within the plastic zone, into our finite element code. The model involves a traction-separation law specified on the prospective crack plane to characterize the fracture process (Refs. 9.1 — 9.4). The model partitions the work that goes into plastic dissipation from that which is absorbed by the local fracture processes required to separate the crack faces. The solid is specified by its elastic properties and plastic properties (tensile yield stress and strain hardening exponent). Crack initiation and subsequent growth are calculated in terms of the parameters characterizing the separation law and the elastic-plastic properties of the solid.

9.2.2 Subtask 8.2 Stainless Steel SAW Fusion-Line Toughness

9.2.2.1 Objective

The objective of this effort is to determine the fracture toughness associated with a crack growing along the fusion line in an austenitic stainless steel submerged-arc weldment.

9.2.2.2 Rationale

During the conduct of Pipe Experiment 1.2.3.16 (surface crack test of a stainless steel submerged-arc weld, SAW) and previous pipe tests in the Degraded Piping Program with cracks centered in stainless steel welds, the cracks have tended in many cases to propagate from the center of the weld to the fusion line of the weld. This indicates that the fusion line may often be the least fracture resistant, whereas previously the flux weld metal has been thought to be the lowest toughness crack location. If the findings confirm the indications described above, then flaw assessment criteria should be based on the fusion-line toughness rather than on the weld-metal toughness. That result could affect the IWB-3640 flaw evaluation criterion and possibly LBB analyses for wrought and cast stainless steel pipes.

9.2.2.3 Approach

A two-phase effort will be undertaken to accomplish this item. The first phase involves conducting basic verification of methodology experiments on a base metal, using compact specimens having either a straight (conventional) or a slant notch—the objective being to see if the J-R curve is the same for the two different orientations. If these results are acceptable, then the second phase will be initiated with NRC's approval. This second phase involves testing of: (a) conventionally notched specimens from specially prepared welds having one fusion line perpendicular to the plate surfaces, and (b) slant notch specimens from typical single-arc welds. Other than a Charpy test, the slant-notch C(T) specimen is typical of the only type of specimen that could be tested for archival single-vee weldments for development of data in the future.

Phase 1. In this phase, four C(T) specimens will be tested. Two will have the L-C orientation and two will have a slant orientation with a slant notch, but the crack plane will be the same as the L-C oriented specimen (see Figure 9.1). A 76-mm (3-inch) thick TP304 stainless-steel safe end from the cold-leg pipe we have at Battelle will be used for these tests. Since the crack is in the same plane, the toughness of the two specimen orientations should be similar.

Phase 2. Two different weldments will be subjected to testing. One, already available, is a submerged-arc girth weld in a 16-inch-diameter by 25-mm (1-inch) thick wall TP304 stainless steel pipe. Standard J-R curve data for a crack in the center of the weld metal in that weldment were determined previously. The second weldment will be prepared in 25-mm (1-inch) thick TP304 or TP316 stainless steel plate, using the submerged-arc weld procedure given in NUREG/CR-4878. That weldment will have a cross-section profile similar to that shown in Figure 9.2, here referred to as a slant-vee weld.

The purpose of preparing such a profile is to have one of the fusion lines perpendicular to the plate surfaces to facilitate the machining of compact specimens and Charpy specimens having the notch located at the fusion line. We also considered a K-weld preparation, but such a weld prep has the higher heat input root passes in the middle of the thickness. This causes the fusion line to bulge out-of-plane there, which is undesirable (see Figure 9.3). The slant-vee root passes are near one surface, and out-of-plane bulging of the fusion line could be machined away. Note that the slant-vee weld preparation is a standard weld preparation (see Table 9.1, which is reproduced from the AWS Welding Handbook — Volume 2).

One of the difficulties in fusion line toughness testing is the origination of the crack. Standard testing requires the crack to be perpendicular to the specimen surface. For standard single-vee welds from pipes, it is not possible to make standard C(T) specimens with fusion line crack orientations because of the angle of the fusion line to the pipe or plate surface. Hence, we will make a slant-vee weld so the fusion line will be properly oriented for standard specimens. However, it may be desired also to test archival welds for plant specific applications. Here only a standard single-vee weld may exist. Hence, we will test slant notch C(T) specimens. Such specimens have a combined Mode I and Mode III component loading. Past Battelle work showed that the combined J_{Ic} and J_{IIIc} was equal to standard J_{Ic} results for the different materials (see Figure 9.4). If successful for fusion lines, the slant-notch specimen could be used for LBB requirements to assess the lowest toughness region of the material as required by NRC's S.R.P. 3.6.3.

The following tests will be performed.

- a. Ten J-R curve tests at 288 C (550 F), with five each from the two weld fusion lines (one fusion line perpendicular to the plate thickness, see Figure 9.2, and the other along a typical 37-degree single-vee weld bevel). In each specimen, the notch will lie along the fusion line, as is illustrated in Figures 9.5 and 9.6. Note that Figure 9.6 shows a slant-notch compact specimen in which the notch lies along the 37-degree weld bevel.
- b. Six Charpy V-notch impact tests in the slant-vee weld (Figure 9.2), three at room temperature and three at 288 C (550 F) and three at room temperature with the notch along the fusion line, which is perpendicular to the plate surfaces.

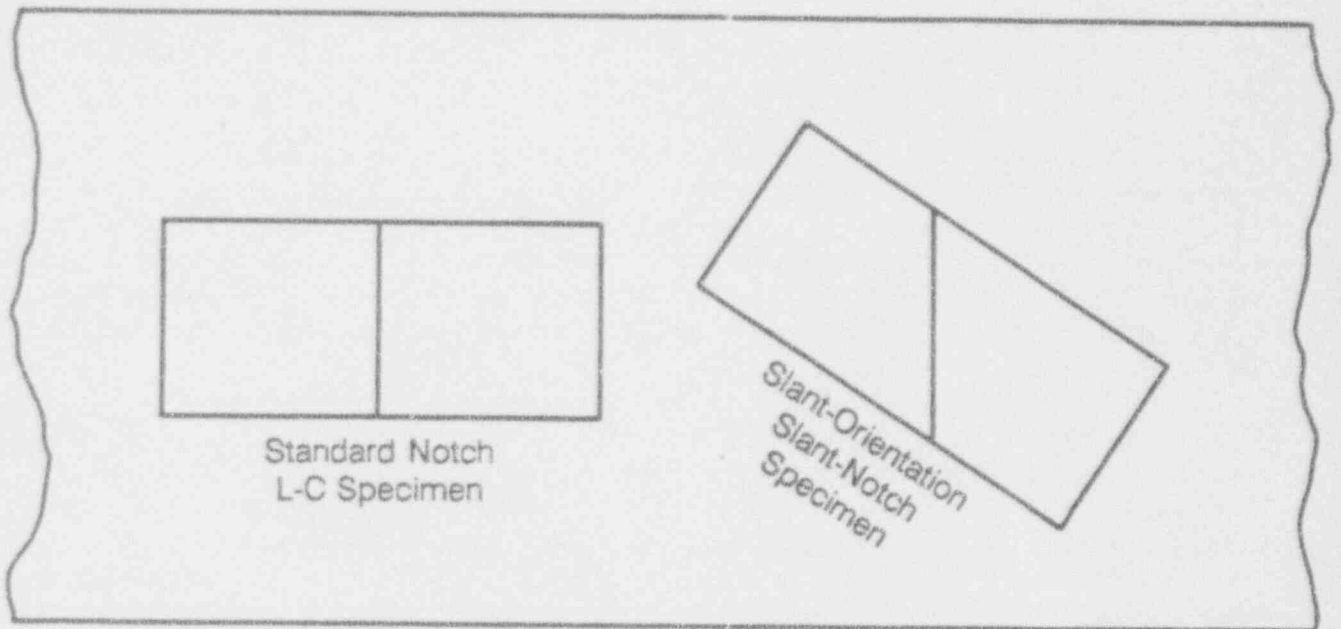


Figure 9.1 Schematic of straight and slant-notch oriented C(T) specimens

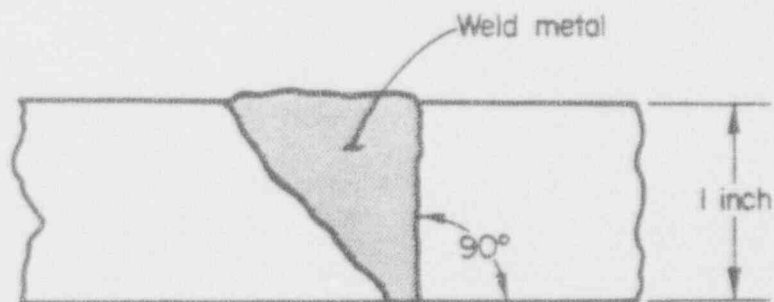
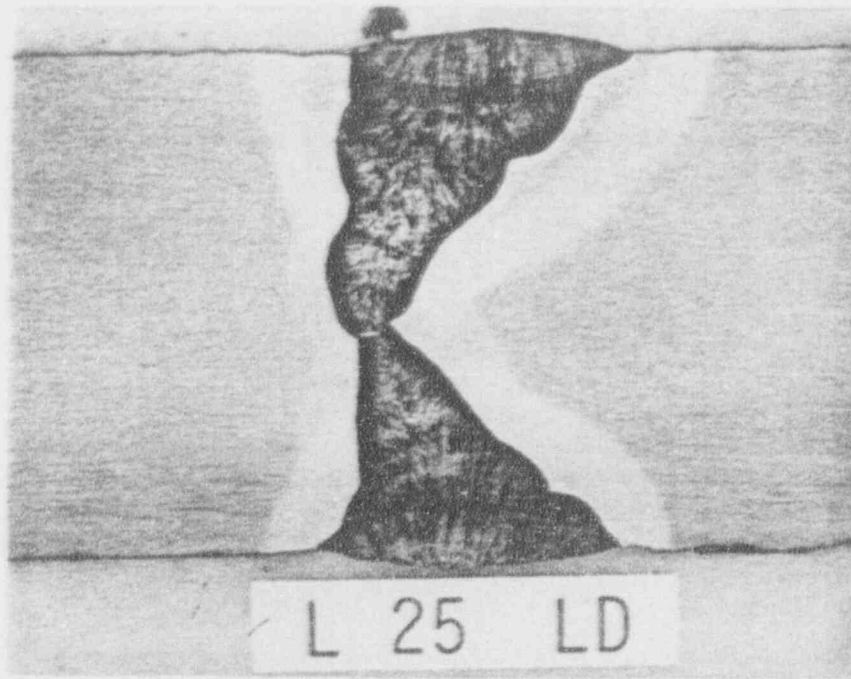
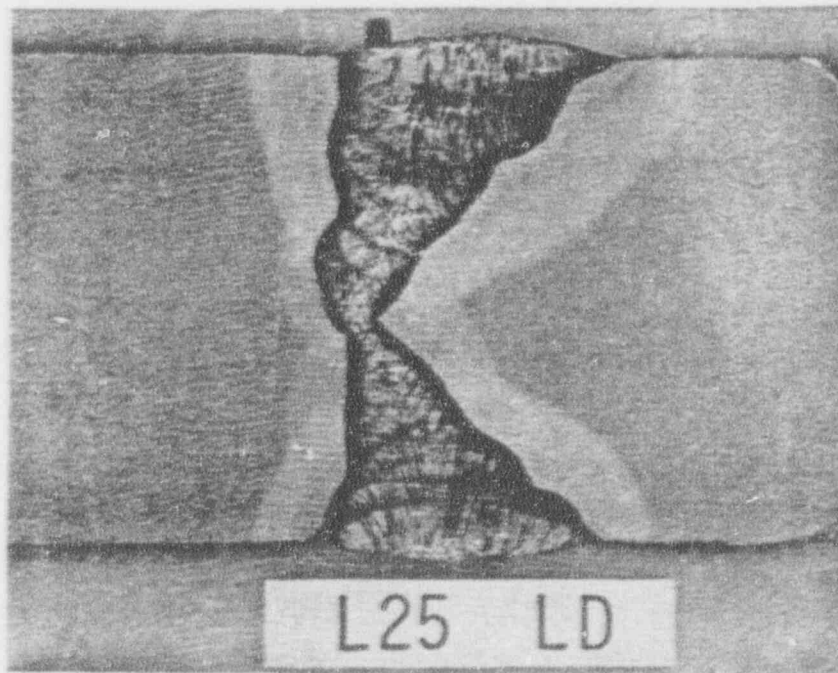


Figure 9.2 Schematic illustration of slant-vee weld



2.5X

(a) Horizontal weld prepared using heat input of approximately 3.54 kJ/mm

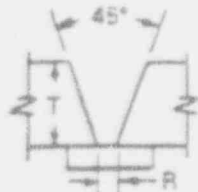
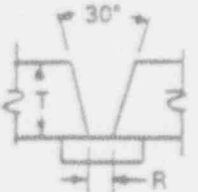
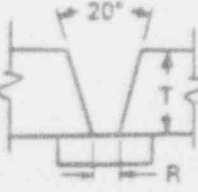
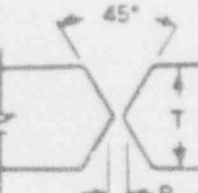
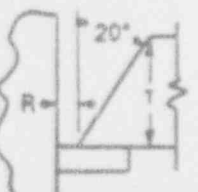


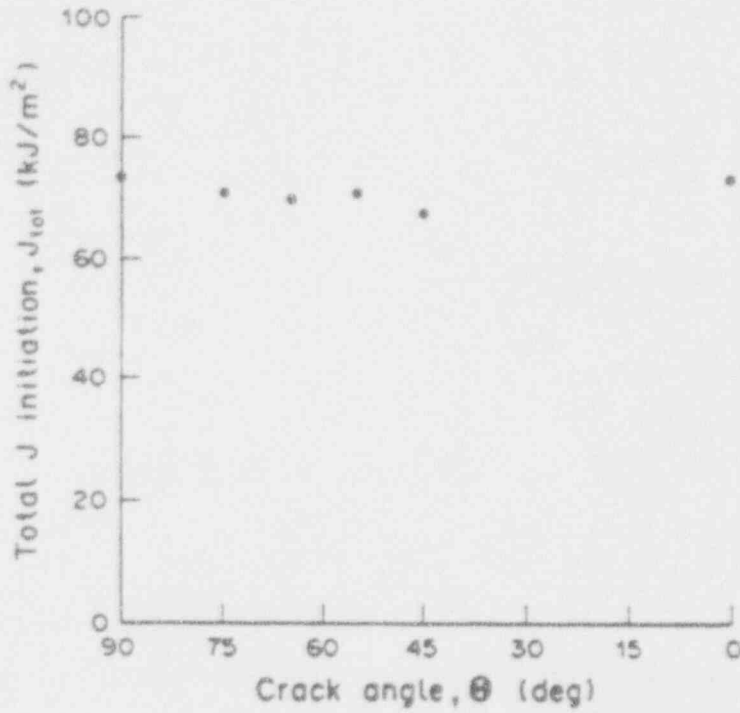
2.5X

(b) 25 mils below surface of (a)

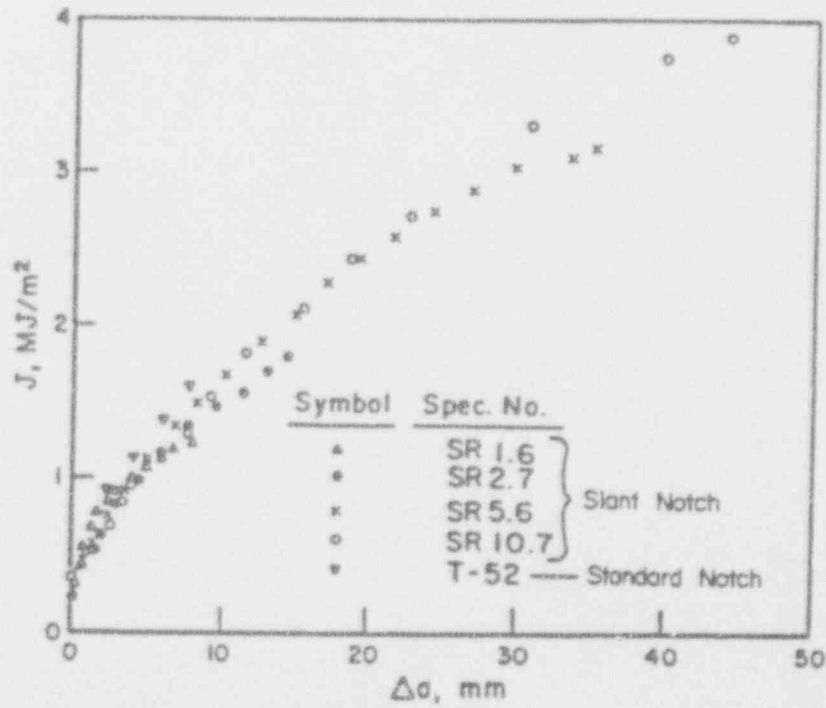
Figure 9.3 Examples of K-weld preparation with out-of-plane bulging of the fusion line at the root passes

Table 9.1 Typical self-shielded flux-cored arc-welding procedures for stainless steels using stainless steel electrodes (from AWS *Welding Handbook* - Volume 2)

Joint design	Weld size, T		Root opening, R		Total passes	Electrode diameter		Welding power		Production rate		Electrode extension	
	mm	in.	mm	in.		mm	in.	A	V	m/h	ft/h	mm	in.
	Flat position groove welds												
	6	1/4	3	1/8	1	2.38	3/32	300	27.5	18	60	25	1
10	3/8	3	1/8	2	2.38	3/32	300	27.5	10	33	25	1	
	13	1/2	5	3/16	2	2.38	3/32	300	27.5	8	27	25	1
	19	3/4	5	3/16	4	2.38	3/32	300	27.5	2	7	25	1
	22	7/8	10	3/8	6	2.38	3/32	300	27.5	2	7	25	1
	32	1-1/4	10	3/8	8	2.38	3/32	300	27.5	2	5	25-32	1 to 1-1/4
	13	1/2	3	1/8	2	2.38	3/32	300	27.5	9	30	25	1
	76	3	3	1/8	25	2.38	3/32	300	27.5	0.5	1.5	25-32	1 to 1-1/4
	10	3/8	10	3/8	3	2.38	3/32	300	27.5	6	20	25	1
	32	1-1/4	10	3/8	8	2.38	3/32	300	27.5	2	5	25-32	1 to 1-1/4



(a) Results from Ref. (1) on 1090 carbon steel with different angles of slant notches



(b) Results from Ref. (2) on A533 GrB steel with 45-degree and standard perpendicular notches

Figure 9.4 Comparison of slant-notch and standard-notch orientation effect on toughness of base metals

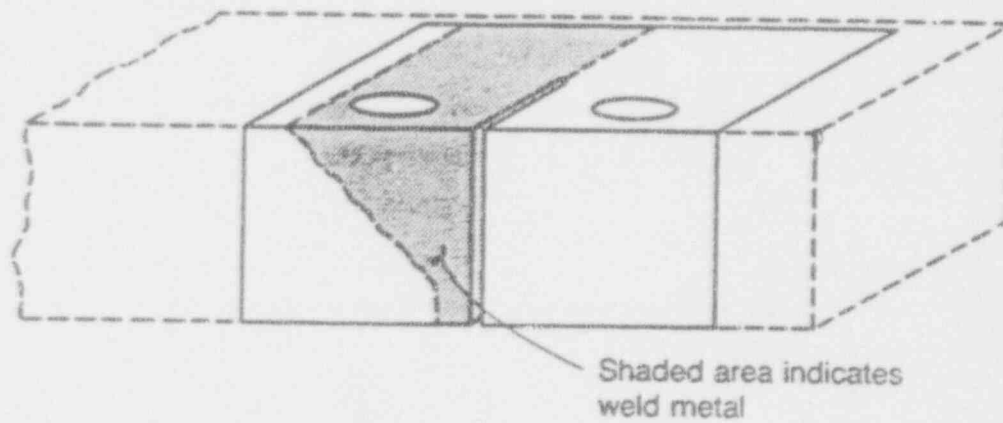


Figure 9.5 Schematic illustration of fusion-line C(T) specimen machined from a slant-vee weld

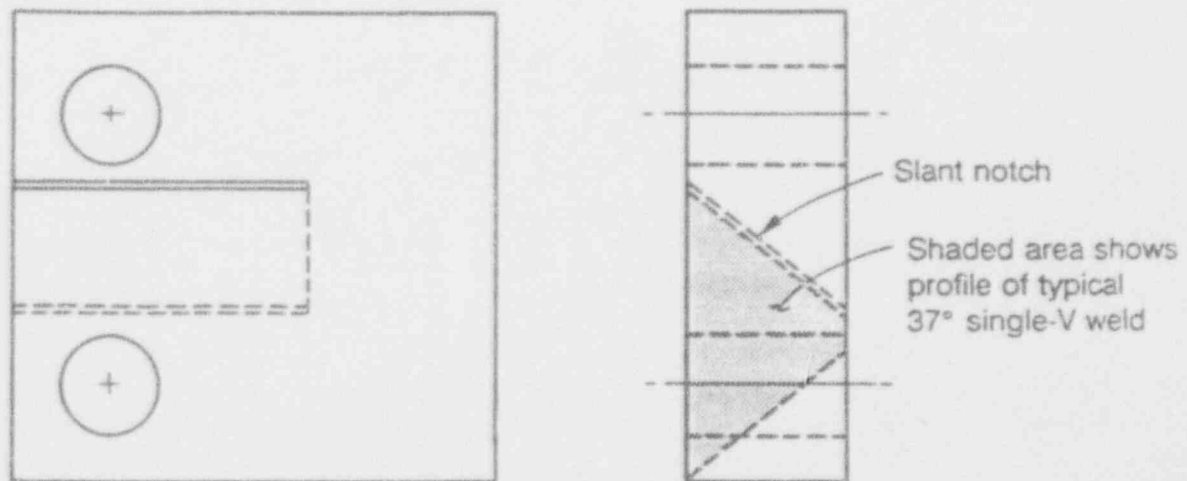


Figure 9.6 Schematic illustration of slant-notch C(T) specimen

- c. Six Charpy V-notch impact tests with slanted specimen orientations in the single-vee weld (Figure 9.6) so the notch is in line with the fusion line, three at room temperature and three at 288 C (550 F) with the notch on the fusion line.
- d. Chemical analysis of the welds.

9.2.2.4 Deliverables

Data will be recorded digitally and reduced to a format identical to that used in the past on Degraded Piping Program data record book entries and will be available for input into the NRC PIFRAC data base. The results will also be presented in monthly, semiannual, and final reports as appropriate. The results will be included in the topical report in Subtask 2.5.

9.2.3 Subtask 8.3 Update PIFRAC Data Files

9.2.3.1 Objective

The objective of this effort is to update the PIFRAC data base to include data from NRC-sponsored programs and industry-funded programs to the extent that these data are readily available.

9.2.3.2 Rationale

PIFRAC, a computerized data base for material properties of nuclear grade piping materials, which was developed under other NRC funding, was last updated in 1989. Since that time, considerable additional data have been developed from NRC-sponsored programs at Battelle and from a number of industry-funded programs. The NRC desires that the PIFRAC data base be updated to include the data from the NRC-sponsored programs and the industry-funded programs.

9.2.3.3 Approach

Battelle will update the PIFRAC data base to include data from this program, from the IPIRG program (NRC-04-86-106), and any data from the Degraded Piping Program Phase II (NRC-04-84-103) that were not included in the 1989 update. Additionally, data from the Aging of Cast Stainless Steel program at Argonne National Laboratory (FIN A2243) will be obtained from Argonne and included in this update. Finally, any data known to Battelle, developed in industry-sponsored research programs and in which those data have been or will be supplied to Battelle in a format compatible with PIFRAC, will be included in this update. This includes data from the following programs:

- EPRI/Westinghouse (RP-1238-2)
- EPRI/GE stainless steel weld data (Project T303-3)
- EPRI/B&W carbon steel weld data (EPRI NP-6264)
- Ontario Hydro carbon steel pipe data.

This effort specifically excludes literature searches or other surveys to identify such data. The effort will be limited to data from programs currently known to Battelle or the NRC where digital data exist.

9.2.3.4 Deliverables

The deliverables from this effort will be computer disks with the updated PIFRAC data files.

9.2.4 Subtask 8.4 Develop Data base for Circumferential Pipe Fracture Experiments

9.2.4.1 Objectives

The objective of this task is to expand the data base of circumferentially cracked pipe fracture experiments.

9.2.4.2 Rationale

In addition to Battelle, a number of other organizations worldwide have conducted, and are conducting, pipe fracture experiments on circumferentially cracked pipe. To date there is no single reference, or data base, which lists the test conditions and results for these experiments. Such a data base would be useful to those individuals assessing the validity of analytical or code approaches in that the appropriate experiments necessary for confirming the approach would be readily identified. Also such a data base would be helpful in eliminating any redundancy in efforts between organizations.

9.2.4.3 Approach

As part of our ASME Section XI Code Committee efforts we have developed a data base of circumferentially cracked pipe fracture experiments. This data base, in its current form, includes the test conditions, experimental results, and applicable material property data from

- the Degraded Piping Program - Phase II (Ref. 9.5),
- the IPIRG-1 Program (Ref. 9.6),
- the Short Cracks in Piping and Piping Welds Program (Ref. 9.7),
- two David Taylor Research Center (DTRC) programs on A106 Grade B pipe (Ref. 9.8) and welded Type 304 stainless steel pipe (Ref. 9.9), and
- two Battelle programs conducted for EPRI on small-diameter stainless steel pipe (Ref. 9.10,9.11).

Currently the data base has entries for over 140 circumferentially cracked-pipe fracture experiments. As part of this task we will expand the data base to include the data from a number of other organizations/programs. Table 9.2 is a comprehensive list of programs for which we will include data. Some of the data represented in Table 9.2 already exists in referenced journals while some of the data will need to be obtained from the appropriate organization. Table 9.3 is a list of the test parameters (i.e., test conditions, experimental results, and material property data) that will be

Table 9.2 List of programs for which circumferential pipe fracture data will be included

Sponsoring Agency	Laboratory	Program or Report Number	Scope of Experiment
USNRC	Battelle	Degraded Piping	TWC, SC, CC; P&B, P, B; 4"-4-1/2" diameter, QS
USNRC	Battelle	IPIRG-1	TWC and SC; B, P&B; 6", 16", 30" diameter
USNRC	Battelle	Short Cracks	Large diameter, short cracks, TWC and SC
AEC	Battelle	BMI-1908	Carbon steel, pressure tests, SC
EPRI	Battelle	NP-192	Small diameter, stainless steel, TWC
EPRI	Battelle	NP-2347	RT, stainless steel, TW and SC
AGA-NG18	Battelle	Battelle Files	CS, TWC, line pipe pressure
AGA-WSC	Battelle	Battelle Report	Girth weld defects
AGA-WSC	Battelle	Battelle Report	Repair grooves
Offshore Program	Battelle	Battelle Files	4" diameter, bending, carbon steel base metal
EPRI	GE	NP-2472	4" diameter, axial tension, RT
AEC	GE	GEAP-10023	Small diameter, A106, RT
USNRC	DTRC	NUREG/CR-3740	8" A106B
USNRC	DTRC	NUREG/CR-4538	Stainless TIG
USNRC	DTRC	Unpublished	4" Stainless Base
USNRC	DTRC	Unpublished	Carbon steel MIG
STA	JAERI	NED Paper	Stainless steel, 6" and 16" diameter, TWC, SC
STA	JAERI	JAERI Reports	Carbon steel, 6" and 16" diameter, TWC, SC
ENE	CISE	LBB - Tokyo	Carbon steel, small diameter, TWC
ENEA	CISE	NED paper	Stainless steel, small diameter, TWC
Westinghouse Owner's Group	Westinghouse	ASME PVP-95	Cast stainless steel, small diameter, TWC
CEGB	CEGB	Technical paper	Thin wall, carbon steel tests
KWU	KWU	Technical paper	Carbon steel bend tests
MITI	NUPEC	NED paper	Stainless steel pipe in tension
MITI	NUPEC	NED paper	Carbon steel pipe, pressure and bend
STA	NRC DP	ASME PVP-150	Pipe system tests
BMFT	MPA	Phase I	Pressure to burst, LWR, large diameter
BMFT	MPA	Phase II	Pressure and bend
Hitachi	Hitachi	NED paper	Stainless steel pipe in tension

Table 9.3 List of test parameters, results, and material property data included in database

Test Parameters
Data Record Book Number
Experiment Number
Pipe Material Identification Number
Pipe Material
Outside Diameter
Schedule
Wall Thickness
Inner Span for Four-point Bending Experiments
Outer Span for Four-point Bending Experiments
Test Pressure
Crack Length
Crack Depth
Experimental Results
Load at Crack Initiation
Maximum Load
Moment at Crack Initiation
Maximum Moment
Material Property Data
Yield Strength
Ultimate Strength
Percent Elongation
Reduction in Area
Ramberg-Osgood Coefficients
J-value at Crack Initiation
dJ_D/da (initial slope of J-R curve)
Extrapolated J_D -R Curve Constants
Upper Shelf Charpy Energy
Room Temperature Charpy Energy
Room Temperature Shear Area Percent

included in the data base for each of the experiments. As part of this effort we envision the size of the data base will expand from approximately 140 experiments to over 400 experiments.

9.2.4.4 Deliverables

The deliverable for this task will be a computer data base of pipe fracture experiments with over 400 experiments. The data base will include experiments from various organizations worldwide. The data base will be in a Lotus 1-2-3 spreadsheet format.

9.2.4.5 Progress

Development of this data base was initiated as part of our involvement in ASME Section XI activities (Task 9). Since this work now falls under Subtask 8.4 we shall report the progress below.

Circumferentially Cracked Pipe Data Base (QS-CIRC.WK1) A data base of past circumferentially cracked pipe fracture experiments has been developed. The data base, in its current form, includes the test conditions (pipe diameters, wall thicknesses, test temperatures, pressures, flaw sizes, etc.), experimental results (loads and moments at crack initiation and maximum load), and applicable material property data (tensile, fracture toughness, and Charpy impact data) for over 140 pipe fracture experiments. The data included to date come from the Degraded Piping Program (Ref. 9.5), the IPIRG program (Ref. 9.6), the Short Cracks in Piping and Piping Welds Program (Ref. 9.7), two David Taylor Research Center (DTRC) programs on A106 Grade B pipe (Ref. 9.8) and welded Type 304 stainless steel pipe (Ref. 9.9), and two Battelle programs conducted for EPRI on small-diameter stainless steel pipe (Refs. 9.10 and 9.11).

In the future the size of the data base will expand such that it includes entries for over 400 pipe fracture experiments from over 20 pipe fracture experimental programs. In this reporting period this data base has been presented to the Pipe Flaw Evaluation Task Group of Section XI. (Version 1.0 of the data base with its 140 entries was passed out at a recent Section XI meeting.) Researchers at DTRC have reviewed the entries in the data base pertaining to the pipe experiments conducted at David Taylor Research Center to check the quality of the data inputs. All errors in the data noted by DTRC have been corrected in the data base. Also several IPIRG-1 members have agreed to contribute data for inclusion into the data base from programs conducted at their respective organizations. To date Battelle has received data for approximately 95 pipe fracture experiments from ENEA in Italy. Those data are currently being reviewed for inclusion in the data base.

One of the early uses of the data base has been helping the ASME Section XI Pipe Flaw Evaluation Task Group develop an appropriate definition of flow stress for use in the Code. As part of this effort, Battelle used the Plastic-Zone Screening Criterion (Ref. 9.11) to establish which of the circumferentially cracked pipe experiments in the current data base (QS-CIRC.WK1 Version 1.0) should be analyzed using limit-load analyses. The Task Group is using these limit-load experiments in their assessment of how to define flow stress, i.e., some multiple of the design stress (S_m) or some function of the code specified yield strength (S_y) and ultimate strength (S_u) values. This is a continuing effort for that task group.

9.2.5 Subtask 8.5 Data File Conversion from HP to IBM Format

9.2.5.1 Objective

The objective of this task is to convert all of the Degraded Piping Program data files that existed in HP9845 format to Lotus 1-2-3 format for IBM PC DOS compatible computers.

9.2.5.2 Rationale

The data acquisition system used in the Degraded Piping Program, Phase II (Ref. 9.12) was a Hewlett Packard (HP) HP3497A system controlled by an HP85 computer. After the experiment, the raw data were manipulated with software developed specifically for an individual experiment or a series of experiments and written in Basic on an HP9845 computer. With the advent of the personal computer (PC) and commercially available software such as LOTUS 1-2-3, this technology is now obsolete. The old HP data files and floppy disks in their present format are incompatible with PCs and commercially available software packages. However, even though the file format technology is obsolete, the data from these experiments are still of great value. The data are still frequently used in the verification of new pipe fracture analyses. Consequently, there is a need to convert these data into a universally used format; i.e., IBM PC format using Lotus 1-2-3 software.

9.2.5.3 Approach

As part of this effort Battelle will convert the experimental data files for 59 Degraded Piping Program - Phase II pipe fracture experiments from HP to IBM PC compatible format.

9.2.5.4 Deliverables

The deliverables for this task will be IBM compatible computerized data files for the pipe fracture experiments conducted as part of the Degraded Piping Program - Phase II (Ref. 9.12). These will be sent to NRC with the corresponding pipe test and data record book identification.

9.3 Plans for Next Year of the Program

The efforts described below will be undertaken during the next year.

9.3.1 Subtask 8.1 Validity Limits on J-R Curve Determination

Needleman (Refs. 9.1, 9.2), Varias, et al. (Ref. 9.13) and Tvergaard and Hutchinson (Ref. 9.4) have used the traction-separation law model to obtain crack growth resistance curves under small-scale yielding. In their analyses, the crack driving force is given solely by K_I so that the effect of geometry on crack growth resistance could not be explored. In the first phase of this study, the traction-separation law model in conjunction with modified boundary layer formulation (MBL) was employed in which the remote tractions are given by the first two terms of the small-displacement-

gradient linear elastic solution (Ref. 9.14). Therefore, the driving force is specified by both K_I and the T-stress. Studies by Hancock and coworkers (Refs. 9.15, 9.16) and O'Dowd and Shih (Refs. 9.17, 9.18) have shown that the T-stress provides a convenient means to investigate and parameterize specimen geometry effects on near-tip fields under well-contained yielding. The combined MBL and traction-separation law model provides an approach to systematically investigate specimen geometry effects on crack growth resistance under conditions of contained yielding.

In the second phase, finite-width tension and bend geometries containing shallow and long flaws will be investigated. As many overall characterizing quantities as possible will be calculated, including J_D and J_M as defined by loading-point quantities and by the line integral definition of J_D and its range of path-independence. An essential part of the study will be an evaluation of geometry effects on J_D and J_M crack growth resistance curves and comparison with resistance curves generated by MBL analyses. These comparisons will permit the range of validity of the J_M parameter for the crack geometries of interest to be identified.

9.3.2 Subtask 8.2 Stainless Steel SAW Fusion-Line Toughness

It is expected that the Phase 1 tests will be completed and if the results are satisfactory and approval is received from the NRC, the Phase 2 tests will also be initiated and completed during the next year.

9.3.3 Subtask 8.3 Update PIFRAC Data Files

During the next year, data from various sources will be implemented in the PIFRAC data base.

9.3.4 Subtask 8.4 Develop Data Base for Circumferential Pipe Fracture Experiments

During the next year, the data represented in Table 9.2 which already exists in referenced journals will be input into the circumferentially cracked pipe fracture data base. There may be specific test parameters, results, or material data needed for the data base which are not included in these referenced journals. If so, the appropriate organization will be contacted for the needed additional information. Also the appropriate organizations for the programs listed in Table 9.2 for which the data do not currently exist in referenced journals will be contacted.

9.3.5 Subtask 8.5 Data File Conversion from HP to IBM Format

During the next year, the process of converting the old HP9845 files to IBM compatible files will be initiated.

9.4 References

- 9.1 Needleman, A., "A Continuum Model for Void Nucleation by Inclusion Debonding," J. Appl. Mech., Vol. 54, p. 525, 1987.

- 9.2 Needleman, A., "An Analysis of Tensile Decohesion Along an Interface," J. Mech. Phys. Solids, Vol. 38, p. 289, 1990.
- 9.3 Varias, A. G., O'Dowd, N. P., Asaro, R. J., and Shih, C. F., "Failure of Bimaterial Interfaces," Mater. Sci. Engrg., Vol. A126, p. 65-93 1990.
- 9.4 Tvergaard, V. and Hutchinson, J. W., "The Relation Between Crack Growth Resistance and Fracture Process Parameters in Elastic-Plastic Solids," J. Mech. Phys. Solids, Vol. 40, pp. 1377, (1992).
- 9.5 Kanninen, M. F., and others, "Development of Plastic Fracture Methodology," Battelle report to EPRI, NP-1734, see Appendix C and D, March 1981.
- 9.6 Schmidt, R. A., Wilkowski, G. M., and Mayfield, M. E., "The International Piping Integrity Research Group (IPIRG) Program - An Overview," SMIRT-11, Paper G12/1, August 1991.
- 9.7 Wilkowski, G. M., and others, "Short Cracks in Piping and Piping Welds," Second Semiannual Report by Battelle, NUREG/CR-4599, Vol. 1, No. 1, August 1991.
- 9.8 Vassilaros, M. G., Hays, R. A., Gudas, J. P., and Joyce, J. A., "J-Integral Testing Instability Analysis for 8-Inch Diameter ASTM A106 Steel Pipe," U.S. David W. Taylor Naval Ship Research and Development Laboratory, NUREG/CR-2347, April 1984.
- 9.9 Hays, R. A., Vassilaros, M. G., and Gudas, J. P., "Fracture Analysis of Welded Type 304 Stainless Steel Pipe," Prepared by David Taylor Naval Ship R&D Center (DTNSRDC) for NRC, NUREG/CR-4538 Vol. 1, May 1986.
- 9.10 Kanninen, M. F., and others, "Instability Predictions for Circumferentially Cracked Type 304 Stainless Steel Pipes Under Dynamic Loading," EPRI Report, NP-2347, April 1982.
- 9.11 Kanninen, M. F., and others, "Mechanical Fracture Predictions for Sensitized Stainless Steel Piping with Circumferential Cracks," Final Report, EPRI NP-192, September 1976.
- 9.12 Wilkowski, G. M., and others, "Degraded Piping Program, Phase II," Final Report, NUREG/CR-4082, Vol. 8, March 1989.
- 9.13 Varias, A. G. and Shih, C. F., "Quasi-static Crack Advance Under a Range of Constraints - Steady-State Fields Based on a Characteristic Length", J. Mech. Phys. Solids, Vol. 41, pp. 835-861, 1993.
- 9.14 Williams, M. L., "On the Stress Distribution at the Base of a Stationary Crack," J. Appl. Mech., Vol. 24, p. 111, 1957.
- 9.15 Berégon, C. and Hancock, J. W., "Two Parameter Characterization of Elastic-Plastic Crack Tip Fields," J. Appl. Mech., Vol. 58, p. 104, 1991.

- 9.16 Du, Z-Z. and Hancock, J. W., "The Effect of Non-Singular Stresses on Crack Tip Constraint," J. Mech. Phys. Solids, Vol. 39, pp 555, (1991).
- 9.17 O'Dowd, N. P. and Shih, C. F., "Family of Crack-Tip Fields Characterized by a Triaxiality Parameter: Part I Structure of Fields," J. Mech. Phys. Solids, Vol. 39, p. 989, 1991.
- 9.18 O'Dowd, N. P. and Shih, C. F., "Family of Crack-Tip Fields Characterized by a Triaxiality Parameter: Part II Fracture Applications," J. Mech. Phys. Solids, Vol. 40, p. 939, 1992.

10. TASK 9 INTERPROGRAM COOPERATION AND PROGRAM MANAGEMENT

10.1 Task Objective

The objectives of this task are to develop and maintain national and international cooperation through sharing data and analysis procedures and to maintain program administration.

10.2 Task Rationale

One of the most important elements of this program is the transfer of the technology developments into ASME Section XI flaw evaluation procedures and LBB analysis procedures for the NRC. The results of this program will be presented to the ASME Section XI Pipe Flaw Evaluation Task Group. This will help implement the results into U.S. Codes and Standards. Additionally if appropriate, results will be presented to the ASTM E8 (formerly E24) fracture committee. Finally, there is the incorporation of ongoing efforts from programs conducted elsewhere in the world that enhance the efforts from this program.

10.3 Task Approach

There are seven subtasks. These are:

- Subtask 9.1 Technical Exchange and Information Meetings
- Subtask 9.2 Internal Program Coordination
- Subtask 9.3 Reports
- Subtask 9.4 Review Meetings
- Subtask 9.5 Travel
- Subtask 9.6 Quality Assurance and Control
- Subtask 9.7 Task Management

Only technical progress in Subtask 9.1 is discussed in semiannual reports.

10.3.1 Subtask 9.1 Technical Exchange and Information Meetings

10.3.1.1 Objective

The objective of this subtask is to enhance the program's technical efforts by developing a forum to exchange technical information both nationally and internationally. Specifically, this involves coordinating technical information with any aspects that may be helpful to ASME code or NRC criteria.

10.3.1.2 Rationale

The timely exchange of technical developments offers the opportunity for peer review and acceptance of the results of this program, and enhances implementation of the results into regulatory or code criteria.

10.3.1.3 Approach

There are four activities within this subtask:

Activity 9.1.1	ASME Section XI meetings
Activity 9.1.2	ASTM meetings
Activity 9.1.3	Other technical meeting coordination
Activity 9.1.4	Coordination with Japanese Elastic-Plastic Fracture in Inhomogeneous Materials program.

Only progress in Activities 9.1.1 and 9.1.4 is reported here.

10.3.1.4 Progress

Activity 9.1.1 ASME Section XI Meetings

Battelle has conducted a number of activities as part of its involvement with the Pipe Flaw Evaluation Task Group of the Section XI Committee for the ASME Pressure Vessel and Piping Code. These activities are discussed below.

Elastic Plastic Fracture Mechanics (EPFM) Criterion for Axial Cracks An axial crack EPFM analysis using a Charpy energy approach was prepared and presented to the ASME Section XI Pipe Flaw Evaluation Group. The analysis method uses the semi-empirical axially cracked failure assessment equations developed by Maxey (Ref. 10.1) to establish the allowable flaw depths for flawed piping meeting the EPFM criteria incorporated in Appendix H. The allowable flaw depths for a given end of evaluation period flaw length, l_f , for normal operating (including upset and test) or emergency and faulted conditions are determined using the following formula.

$$\sigma_h = \frac{2 \sigma_f \arccos[e^{-F_1}]}{\pi(SF) M_1} \quad (10.1)$$

where

M_1	=	$[(\frac{t}{a}) - (\frac{1}{M_2})]/[(\frac{t}{a}) - 1]$
a	=	flaw depth, inch
t	=	wall thickness, inch
σ_h	=	hoop stress, ksi
σ_f	=	flow stress, $2.4 S_m$, ksi
F_1	=	$12 E \pi CVP/[A_c 4000 \ell_f (2.4 S_m)^2]$
CVP	=	Charpy upper-shelf energy, i.e., energy at 100 percent shear area, ft-lb
A_c	=	area of Charpy specimen, in ²
M_2	=	$[1 + (1.614 R_m t) \ell^2]^{1/2}$
SF	=	safety factor
	=	3.0 for normal operating (including upset and test) conditions
	=	1.5 for emergency and faulted conditions
E	=	elastic modulus, ksi
ℓ	=	total axial crack length, inch
R_m	=	mean radius, inch.

The limit of applicability of this equation is for $0.75 \geq a/t$ and $\ell < \ell_{crit}$.

The value of ℓ_{crit} is determined by the conditions for the stability of through-wall flaws and is used in place of ℓ in M_2 when using Equation (10.2)

$$\sigma_h = \frac{2}{\pi} \frac{\sigma_f}{M_2} \arccos[e^{-F_1}] \quad (10.2)$$

If Charpy upper-shelf energy (100 percent shear area) data, CVP, are not available, there are two options. The first option is to use the Charpy energy data from the mill that is typically at room temperature or some other lower temperature. The second option is to estimate the upper-shelf energy from available Charpy data using the following expression (Ref. 10.2).

$$CVP = (CVN \cdot 100)/(SA + 25) \quad (10.3)$$

where

CVP	=	Charpy V-notch upper-shelf energy
CVN	=	Charpy V-notch energy at any temperature
SA	=	Shear area percent at the same temperature as the CVN energy.

At this time, the final technical revision for implementing this Charpy energy axial crack EPFM criterion has been presented to the committee. All changes to Appendix H were considered and the next time Appendix H is revised, this criterion will be voted on.

Analysis Spreadsheet for IPIRG Pipe System Experiments In our dealings with the Pipe Flaw Evaluation Task Group, Battelle has developed an analysis spreadsheet for the five cracked pipe

system experiments conducted as part of the IPIRG-1 program (Ref. 10.3). This spreadsheet includes the test conditions (pipe dimensions, flaw dimensions, etc.), experimental results (experimental stresses, elastically calculated stresses, and ratios of experimental to calculated stresses), and the material property data (tensile and fracture toughness data) for each of the cracked-pipe system experiments. For the experimental and elastically calculated stresses, the total stress is broken down into the various stress components (e.g., membrane, inertial, seismic anchor motion stresses, and thermal expansion stresses). This was done to assess the effect that the various stress components have on the calculated fracture ratio, i.e., the ratio of the elastically calculated stresses from the ANSYS finite-element analysis to the Code allowable stresses. The Pipe Flaw Evaluation Task Group is analyzing the stainless steel base metal pipe system experiment in detail in order to make a critical assessment of the ASME pipe flaw evaluation procedures. From Figure 10.1, it can be seen that if one includes the stress contribution due to the seismic anchor motions, then the calculated fracture ratio increases 20 to 35 percent. Similarly, if one includes the thermal expansion stress contribution in the analysis of the stainless steel base metal experiments, then the calculated fracture ratio increases approximately 10 to 15 percent.

Assessment of Limit-Load Analysis in DPFAD Approach The final activity Battelle undertook as part of its Section XI involvement was to make an assessment of the limit-load analysis that is used in the DPFAD approach for axial surface cracks in Appendix J of Section XI. This formulation is also used in the low upper-shelf reactor pressure vessel criteria. The local limit-load analysis, which was developed by Chell (Ref. 10.4), is given by the equation below.

$$p_o(\text{CHELL}) = [2\sigma_o t / (R_i \sqrt{3})] (1 - d/t) / (1 + d/R_i) \quad (10.4)$$

where

- p_o = failure pressure
- σ_o = flow stress
- t = thickness
- R_i = inside radius
- d = surface crack depth.

This equation is for an infinitely long flaw. For a semi-elliptical flaw, the depth of the crack, d , is replaced by a^* where,

$$\begin{aligned} a^* &= d \{1 - [1 + \ell^2 / (2t^2)]^{-0.5}\} / \{1 - (d/t)[1 + \ell^2 / (2t^2)]^{-0.5}\} \\ \ell &= \text{the total axial flaw length.} \end{aligned} \quad (10.5)$$

The assessment Battelle undertook for the Pipe Flaw Evaluation Task Group involved a comparison of the predicted failure pressures using the Chell local limit-load solution to the Maxey limit-load solution for axial surface cracks. Maxey's limit-load solution is incorporated into the limit-load analyses of ASME Section XI Articles IWB-3640 and IWB-3650. Maxey's solution (Ref. 10.1) is given below.

or

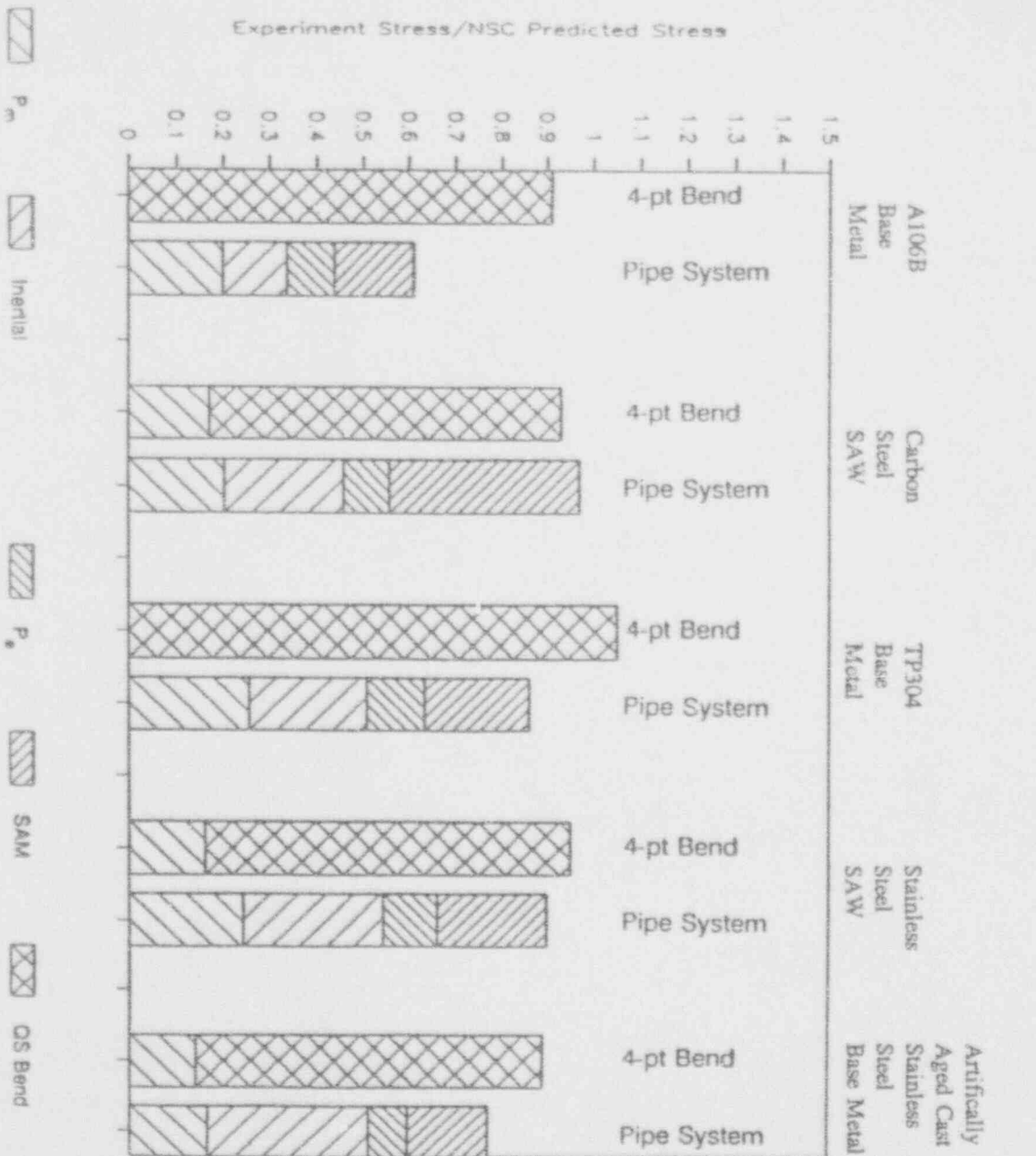


Figure 10.1 Comparison of quasi-static pipe test loads at failure to IPIRG-1 pipe system test failure loads on identical pipes with same crack size

$$\sigma_h = \sigma_o[(1 - d/t)/(1 - d/(tM_T))] = p_o D_m / (2t) \quad (10.6)$$

or

$$p_o(\text{Maxey}) = (2t\sigma_o/D_m)[(1 - d/t)/(1 - d/(tM_T))] \quad (10.7)$$

where:

- D_m = mean pipe diameter
- M_T = Folias through-wall-crack bulging factor
- = $\{1 + [1.61/(4Rt_m)]t^2\}^{0.5}$.

Figures 10.2 to 10.4 show the ratio of the Maxey limit-load predicted failure pressure to the Chell local limit load predicted failure pressure for R_i/t values of 10, 15, and 20. Here it can be seen that the Maxey values are much higher than the Chell predicted failure pressures except for shallow flaws. The effect of R_i/t is relatively small.

The next comparison was to choose surface-cracked pipe fracture experiments where limit-load failure occurred and compare the experimental data with the Maxey and Chell local limit-load predictions. This is done in Figure 10.5. Figures 10.2 to 10.4 indicate the range of crack lengths over which the experimental failure pressures were evaluated. This range of crack lengths happen to be the most sensitive range for discriminating the two analyses. (No shallow flaw data exist.) The failure pressures using Maxey predictions were found to be conservative by 1 to approximately 60 percent. The Chell local limit-load analysis predictions were conservative by 30 to 230 percent. This evaluation shows that the Maxey solution is slightly conservative, yet it was a much better predictor of the failure pressures than the Chell local limit-load solution. It also shows that both analyses tend to become more conservative as the surface-crack depth-to-thickness ratio increases.

Activity 9.1.4 Coordination with Japanese Elastic-Plastic Fracture in Inhomogeneous Materials Program

Objective

In this section, the effects of residual stresses on the near-tip fields for cracks in Type 304 stainless steel weldment are presented. This effort complements work being done in the Japanese Elastic-Plastic Fracture in Inhomogeneous Materials Program, Ref. 10.5. The objective is to numerically assess the effect of residual stresses on fracture of an inhomogeneous structure like a pipe girth weld. In this analysis, thermal residual stresses induced by multi-pass butt welding processes are obtained by a classical thermoelastic-plastic finite-element analysis under plane strain conditions. A crack is introduced, and the path independence of the computed J-integral is to be evaluated. This work is being conducted at the University of Michigan by Dr. Jwo Pan and his associate Dr. M. Kim with the

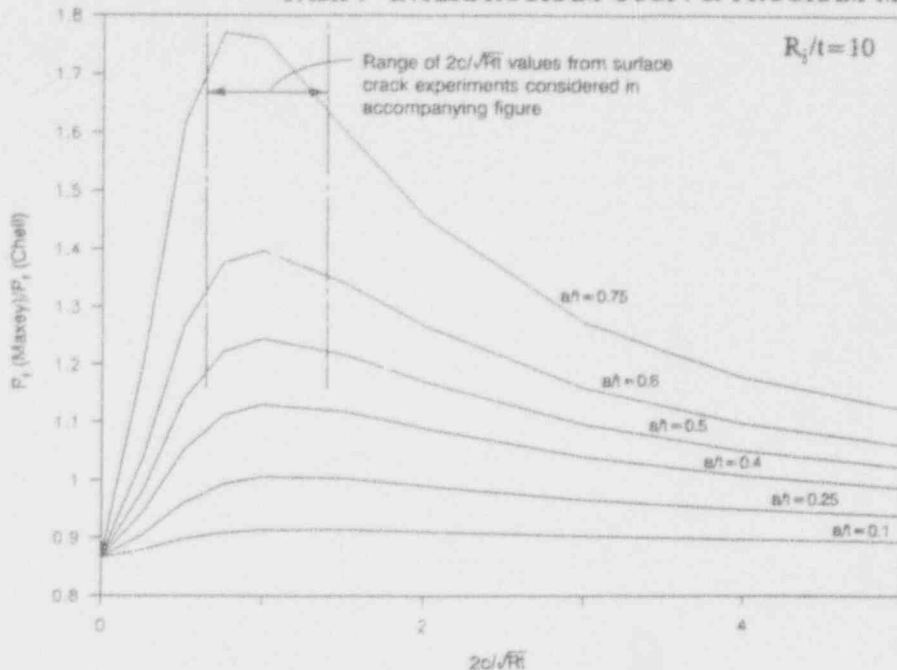


Figure 10.2 Comparison of Maxey with Chell local limit-load axial surface-cracked pipe failure pressures for $R_1/t = 10$

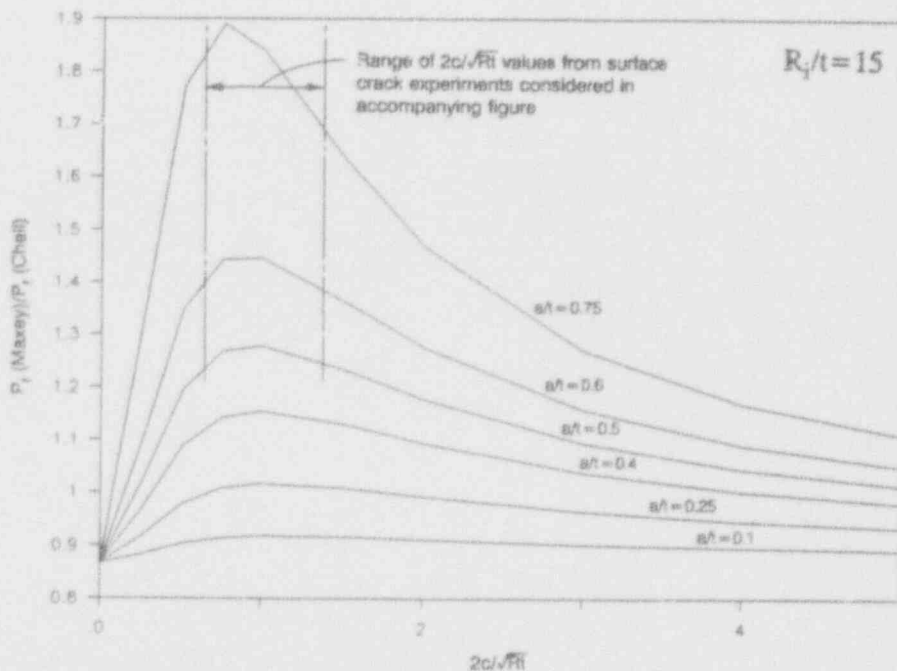


Figure 10.3 Comparison of Maxey with Chell local limit-load axial surface-cracked pipe failure pressures for $R_1/t = 15$

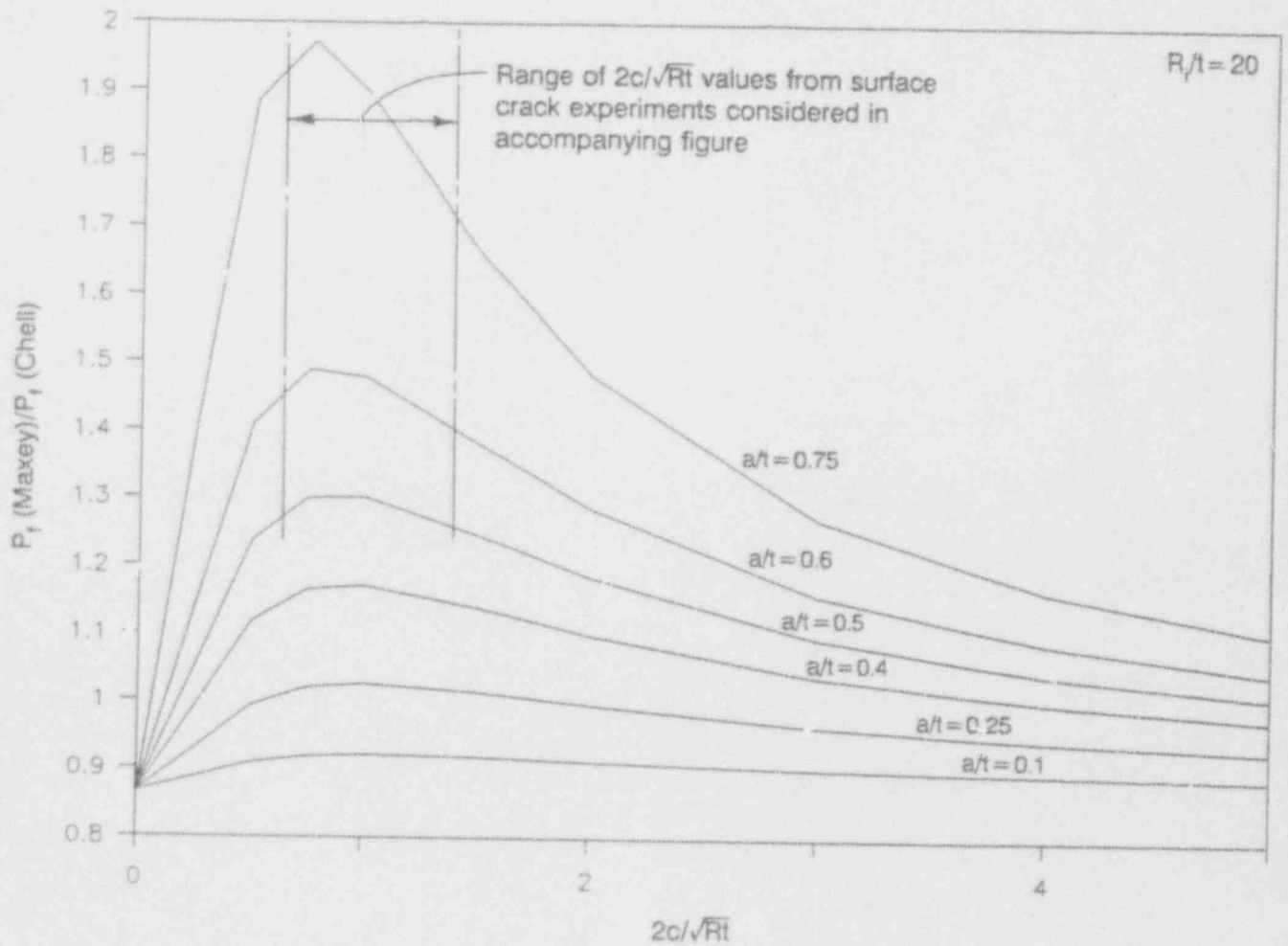


Figure 10.4 Comparison of Maxey with Cheli local limit-load axial surface-cracked pipe failure pressures for $R_i/t = 20$

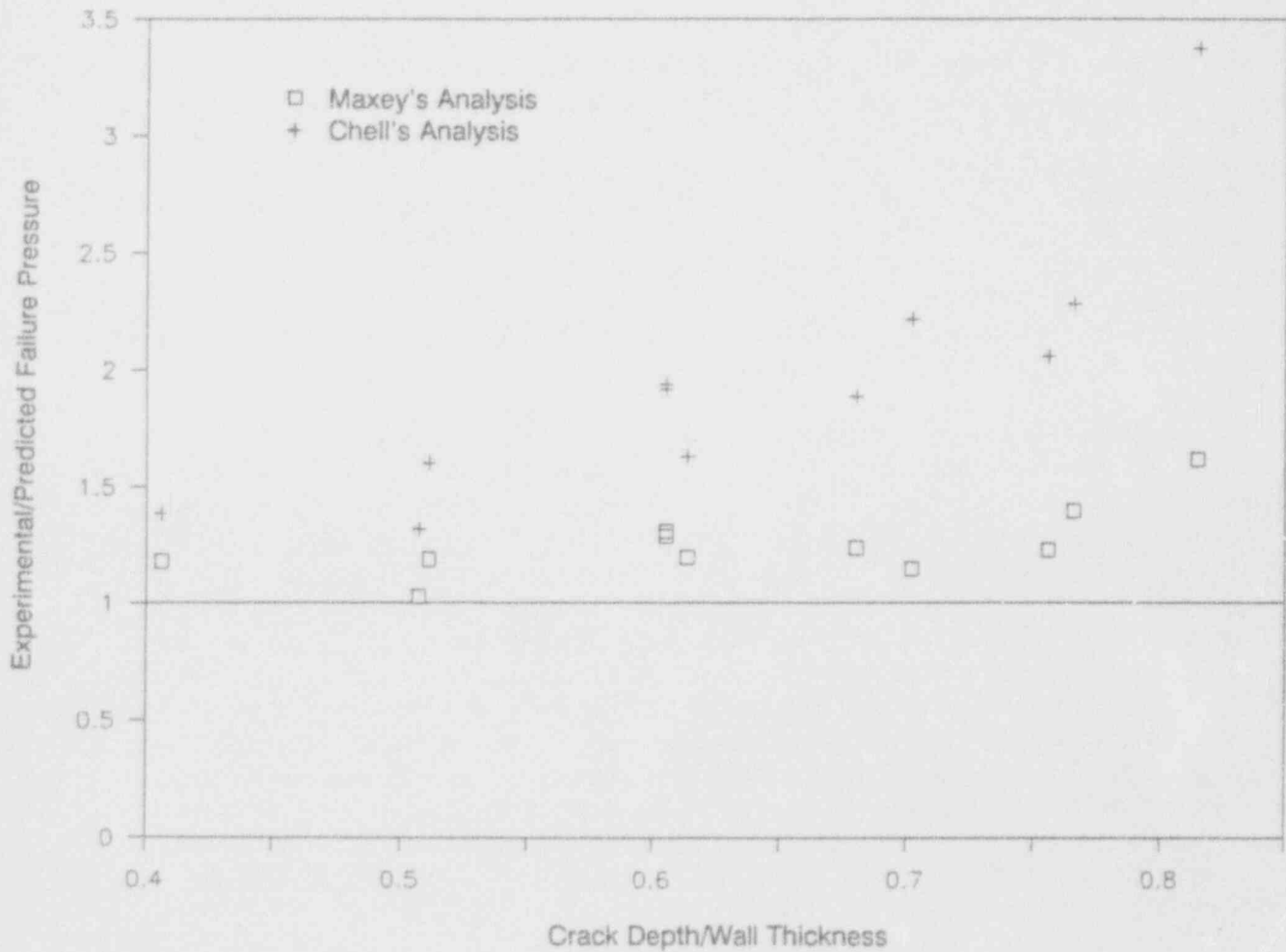


Figure 10.5 Comparison of Maxey and Chell local limit-load predicted failure pressures with experimental data from Battelle (flow stress = $(\sigma_y + \sigma_u)/2$ in both analyses)

assistance of Battelle staff. As such, the crack-tip opening angle (CTOA) is adopted to characterize the crack-tip fields for low values of J . The CTOA is larger than that without the tensile residual stresses when the remote tensile stress is less than 80 percent of the tensile yield stress at room temperature.

Introduction

During welding processes, high localized regions of base metal adjacent to the weld are heated above the melting point and mixed with molten filler materials. These welding zones, generally referred to as the heat-affected zone (HAZ), are critical for the strength and the life expectancy of welded structures, because the residual stresses and metallurgical changes induced by the welding process as well as weld defects can lead to cracking in service. Tensile residual stresses developed in or around the welds during the welding process play a dominant role in the cracking of the welded structure. This is especially true for the crack nucleation process. However, these tensile residual stresses can be mitigated effectively by using special welding techniques. Thus, a thorough understanding of the effects of weld-induced residual stresses on the near-tip fields of a crack near or in the weld is important for the safety analysis of welded structures.

Much research has been carried out to understand the residual stress distributions induced by the welding processes, but little work has been done to study the effect of the residual stresses on the near-tip fields of a crack in welded structures experimentally as well as analytically. Friedman (Ref. 10.6) studied the butt weld of plates by using finite-element methods under plane strain conditions. The incremental thermoelastic-plastic theory was used within the context of the small strain approach. The computational results showed that the longitudinal stress (i.e., longitudinal is in the weld length direction) was dominant due to the plane strain constraint. The highest longitudinal residual stress, which exceeds the room temperature yield stress, was observed in the weldment and HAZ. Anderson (Ref. 10.7) used the classical thermoplastic-elastic theory in a finite-element analysis of a butt welded plate under generalized plane strain conditions. Temperature-dependent material properties were used to incorporate the effect of the martensitic phase transformation due to temperature and stress changes. The computational results of the *temperature distribution* showed very good agreement with the experimental results at the bottom and the top of the plate, but the computed *residual stresses* showed higher values than the experimentally inferred residual stresses at the bottom and the top of the plate. This discrepancy is not significant, but the source of the error may be the assumption of generalized plane strain, which may not be valid for the finite welding speed and the finite plate size. The largest longitudinal and transverse stresses were found in the weld metal and HAZ, according to both the computational and experimental results.

Argyris et al. (Ref. 10.8) analyzed the butt welding of rectangular steel plates with a double-V groove under quasi-stationary plane strain conditions. They used a thermoelastic-viscoplastic finite-element method with consideration of the rate dependency due to the thermal transient behavior, and also studied the effect of different thermoelastic models. They obtained similar computational results from these thermoelastic models. The experimental results agreed well with the thermoelastic-viscoplastic computational results, which showed the highest residual stresses in the HAZ. Argyris et al. (Ref. 10.8) showed that the thermo-mechanical coupling in the heat-conduction equation is insignificant for the welding problems.

Papazoglou and Masubuchi (Ref. 10.9) performed a finite-element analysis of multipass gas-metal arc welding (GMAW) of HY-130 plates under plane strain conditions. The thermo-mechanical problem was assumed to be uncoupled with the thermal and mechanical parts being treated separately. By using the history of microstructure formation during the cooling stage of each point in the HAZ and weldment, the average thermal expansion coefficient for each phase (austenite, bainite, and martensite) and the transformation strain for each separate phase change (martensite to austenite, austenite to bainite, and austenite to martensite) was used to account for the phase transformation effect on the residual stresses. The temperature distributions from the computation results were in good agreement with those of the experimental results. They computed the residual strains and stresses only for the first welding pass due to the high computational cost. However, the strain and stress distributions of the computational results at the top of the plate agreed well with those of the experimental results.

Tekriwal and Mazumder (Ref. 10.10) obtained the residual stress and strain distributions of butt-welded plates by using a three-dimensional model. An incremental thermoelastic-plastic finite-element analysis was adopted in their study. The computational results showed that the transverse stress is the dominant residual stress, which is different from what we observed in the two-dimensional analyses (shown later) based on plane strain assumptions. The computed residual strains were compared with the experimentally measured results, which showed the same trend. It should be mentioned that the model they chose for their study was not large enough (5.8 mm x 25.4 mm x 127.0 mm).

Brust and Rybicki (Ref. 10.11) examined the effectiveness of the backlay welding process to reduce the tensile residual stress, which causes cracking of the HAZ of a weld pipe. Later, Brust and Kanninen (Ref. 10.12) investigated the effectiveness of the backlay and heat-sink welding procedures for BWR piping to reduce the tensile residual stresses induced by welding. Kanninen, et al. (Ref. 10.13) have developed a thermoplastic finite-element method to study crack growth in the presence of weld-induced residual stresses. They assumed the location of the cracks in the HAZ of a welded pipe and studied stress-corrosion cracking (SCC) in a girth-welded pipe, fatigue crack growth under cyclic loading in a butt-welded plate, and dynamic crack propagation under impact loading in a butt-welded plate. They assumed symmetry of the welded plate along the center line. This is equivalent to assuming the existence of two identical cracks in the HAZ on each side of the weld. Nakagaki et al. (Ref. 10.14) have performed an experimental and analytical study of ductile crack growth in a high-toughness austenitic stainless steel weld. However, the residual stresses were not considered in their analytical study.

Harrison et al. (Ref. 10.15) introduced the crack-opening displacement (COD) design curve to measure the toughness of welded structures. The COD, which takes into consideration the effects of residual stresses and geometric stress concentrations, can be widely applied to welded structures. Green and Knott (Ref. 10.16) showed in their experiment that the constant increase in COD per increment of crack growth is an indication of a constant crack-tip-opening angle (CTOA) for a fibrous crack. This implies that the CTOA required for the growth of a crack is constant. This is consistent with the theoretical hypothesis that the opening angle of a growing fibrous crack is constant. Green and Knott (Ref. 10.16) used a definition of the CTOA as an average value of the crack-opening angle based on the COD at the original crack tip position. Work by de Koning (Ref. 10.17) also showed the same result in experiments on 2024-T3 aluminum using finite-element analysis. He observed that soon after the initiation of crack growth, CTOA, which reflects the actual slope of the crack face at

the crack tip, is constant and nearly independent of the element size applied in the crack tip region. The measured CTOA was in good agreement with the computational result. Finally, de Koning (Ref. 10.17) concluded that a crack starts to grow when the CTOA exceeds a certain critical value. Kanninen et al. (Ref. 10.18) also showed that the CTOA is constant for limited amounts of crack growth. In contrast, the crack-opening angle (COA) based on the original crack tip varies monotonically with stable crack extension. They compared actual measurements and computed results, which showed a good agreement.

In this section, a finite-element analysis of the effect of the weld-induced residual stresses on the near-tip fields of cracks was performed under plane strain conditions. The location of the crack was assumed, and introduced after the residual stresses were calculated. Two different weld groove geometries were examined for two plates of different thickness. The computational results showed that the effect of the groove geometry to the J-integral was not significant. For the purpose of comparison, we performed a parallel analysis that does not include thermal residual stresses. The computations were performed based on the thermoelastic-plastic finite-element analysis program that was developed at Battelle.

Calculations Procedure

A welded plate with a crack subject to residual stress and remote loading is considered here. Figure 10.6 shows the coordinate system and the geometry of the welded plate. Here, the welding torch moves along the T direction. As the weld torch approaches and passes the modeled cross section, the temperature history for each material point in the model cross section is produced. Since the plate is assumed to be long and the weld torch moves fast enough, a plane strain condition is assumed in the T direction. Then the welding process can be simplified to a two-dimensional problem. Due to the symmetry, only the shaded area shown in the figure is considered and discretized to finite elements. A crack was placed at the symmetry plane by releasing coupled nodal points after the residual stresses were calculated. It should be noted that no crack was introduced during the welding process. Although in general practice V-groove geometries are exclusively used, in this study two different groove geometries, straight groove and V-groove, were examined for the two plates of different thickness. The thickness of one plate is 8.64 mm (0.34 inch) and the thickness of the other is 33 mm (1.3 inches). A finite-element model of a half plate is shown in Figures 10.7(a) and 10.8(a). The V-groove structures are shown in Figures 10.7(b) and 10.8(b). The straight groove geometry and path definitions are shown in Figures 10.7(c) and 10.8(c). Figure 10.7(d) shows an actual weld sequence for an 8.64-mm (0.34-inch) thick plate. Comparing Figures 10.7(d) and 10.7(b), one can see the weld pass assumption and centerline symmetry assumption made here. Note that due to the latter, the crack is considered to be at the weld centerline here only. The nodal point at the right lower corner was fixed in the R-direction only, to allow the plate to bend freely. The gravity effect of the plate was neglected. The material used in the calculation is Type 304 stainless steel for both the base metal and weldment, for convenience. The temperature-dependent material properties for the stainless steel are used as shown in Figure 10.9 (Ref. 10.19). Phase changes are not included in the analyses, because their effect is minimal for Type 304 stainless steel.

Temperature Solution. First, the residual stresses due to the welding process were computed by using an incremental thermoelastic-plastic finite-element analysis. In order to find the residual

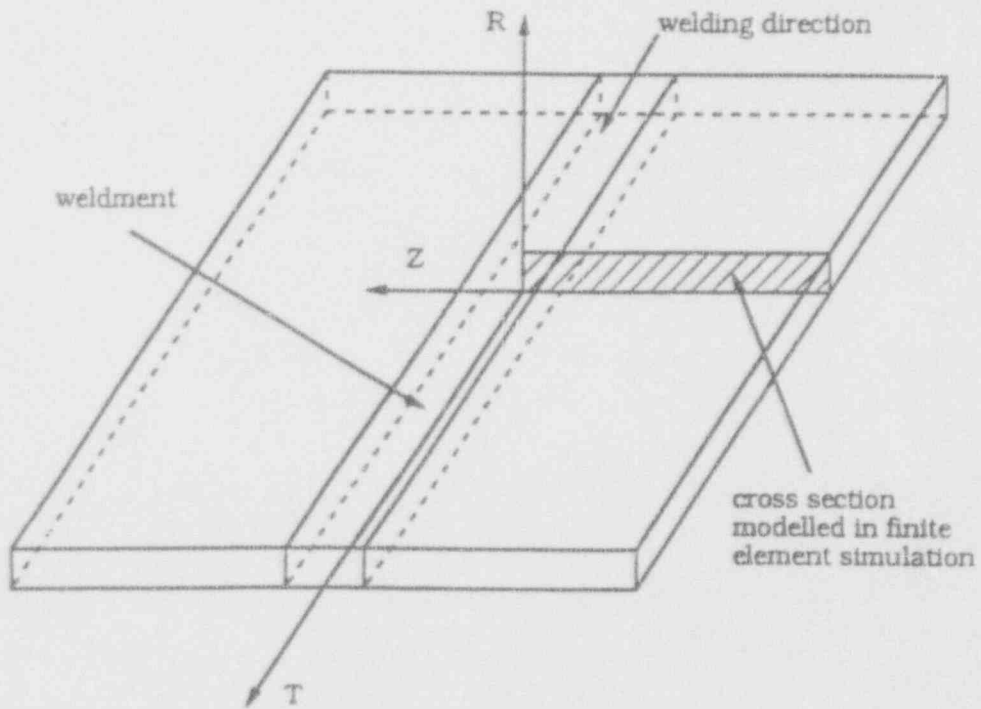
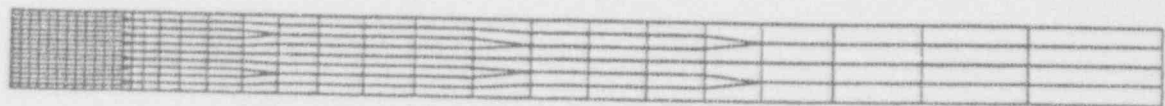
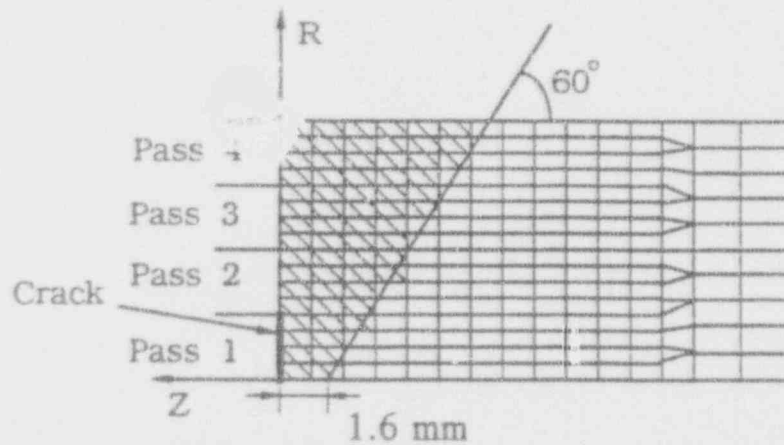


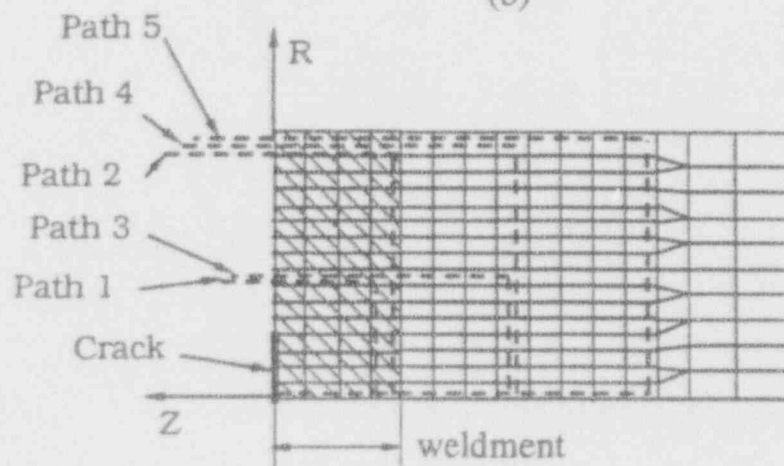
Figure 10.6 A schematic plot of the geometry of the welded plate and the coordinate system for modeling the welding process



(a)



(b)



(c)

Figure 10.7 (a) Finite-element mesh for 8.64-mm (0.34-inch) thick plate and 127-mm (5-inch) width plate for straight and V-groove geometry, (b) the welding passes with the V-groove geometry, (c) J-integral paths and the straight groove geometry, and (d) actual weld sequence of an 8.64-mm (0.34-inch) thick plate

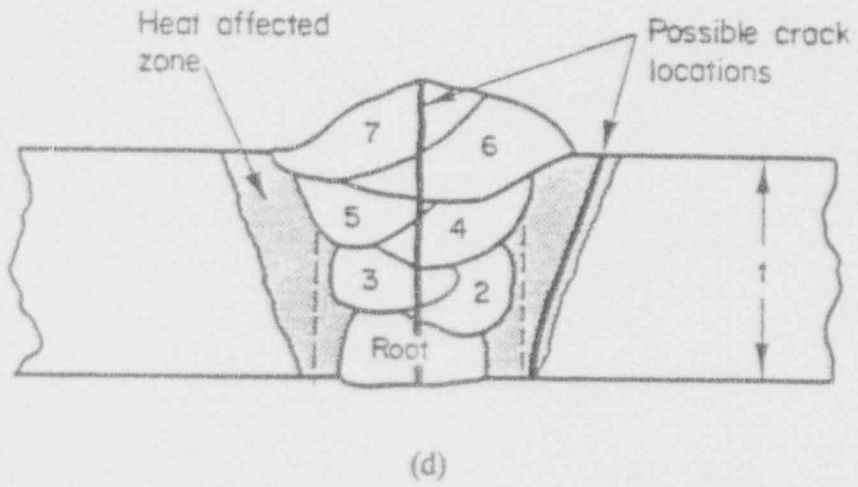


Figure 10.7 (Concluded)

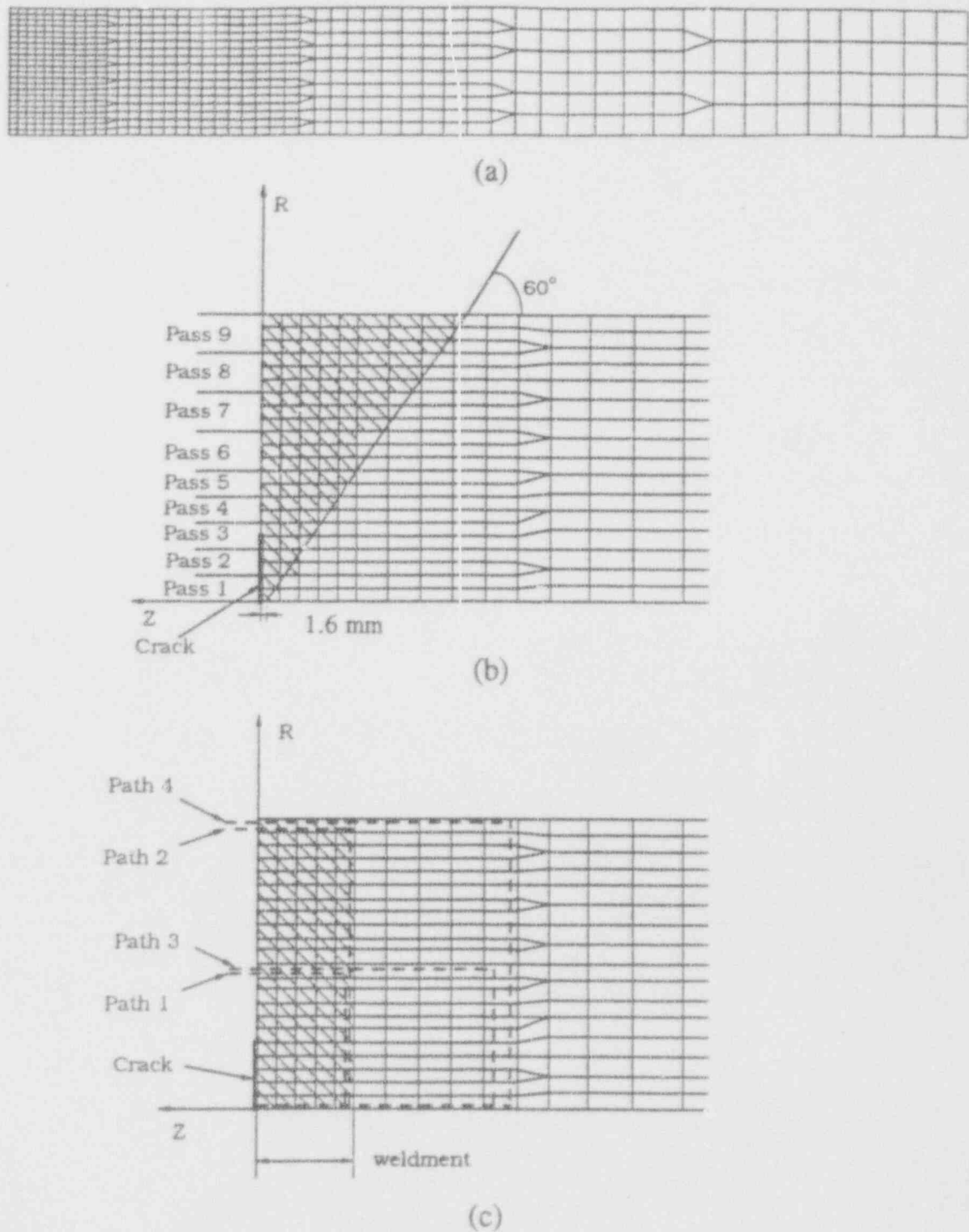
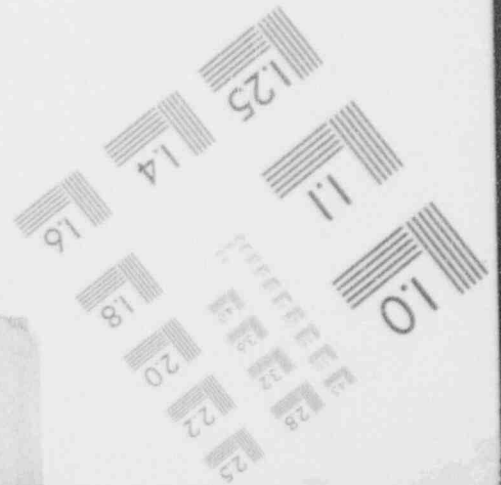
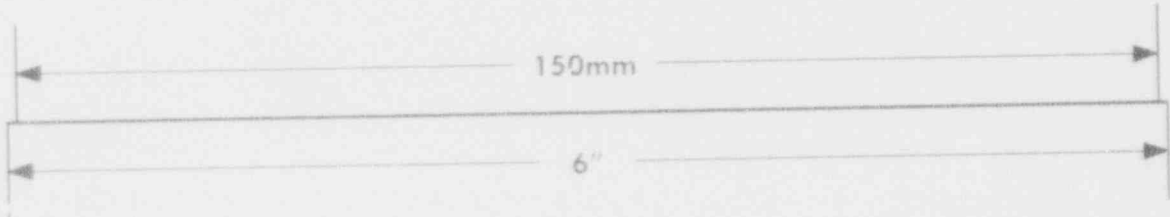
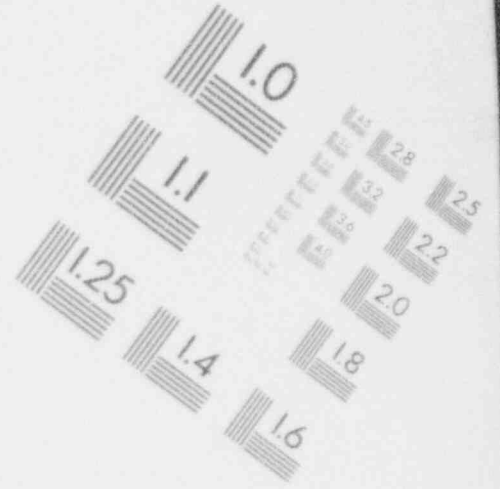
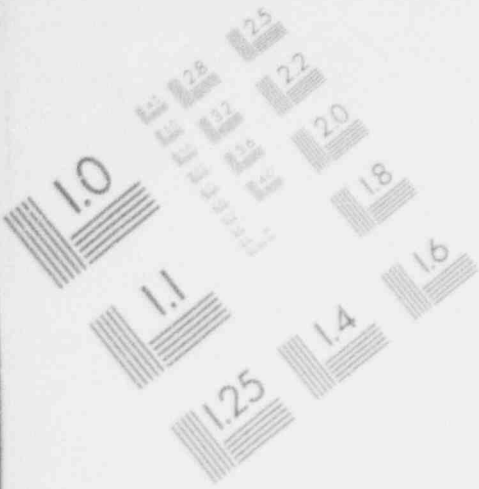


Figure 10.8 (a) Finite-element mesh for 33-mm (1.3-inch) thick plate and 254-mm (10-inch) wide plate for straight and V-groove geometry, (b) the welding passes with V-groove geometry, and (c) J-integral paths and the straight groove geometry

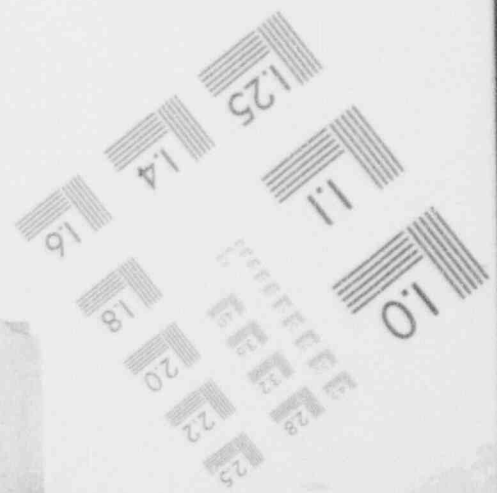
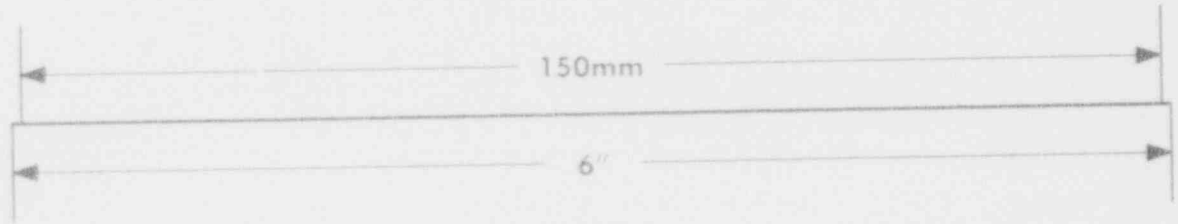
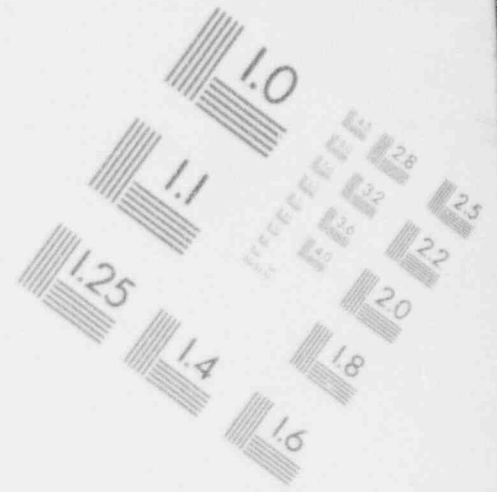
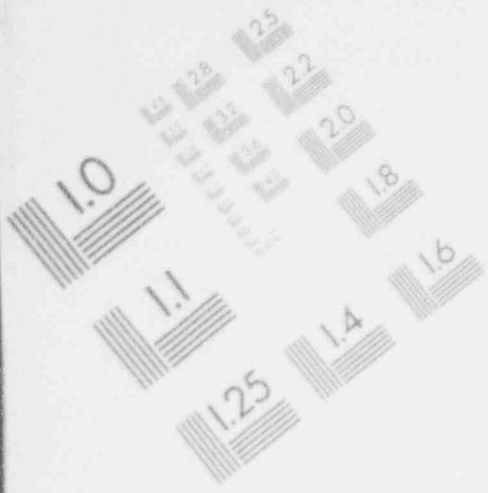
1

IMAGE EVALUATION TEST TARGET (MT-3)



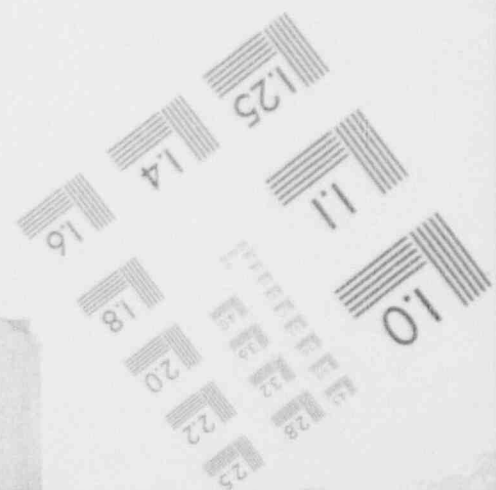
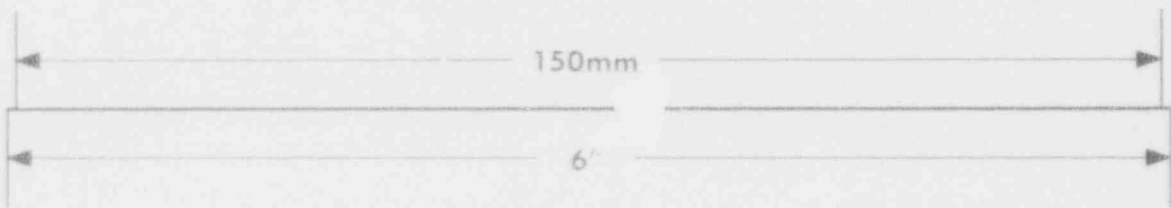
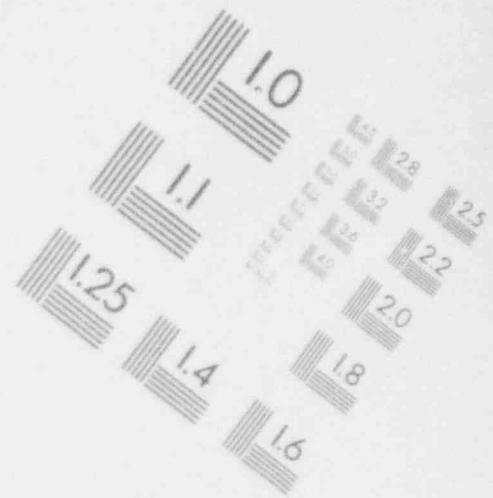
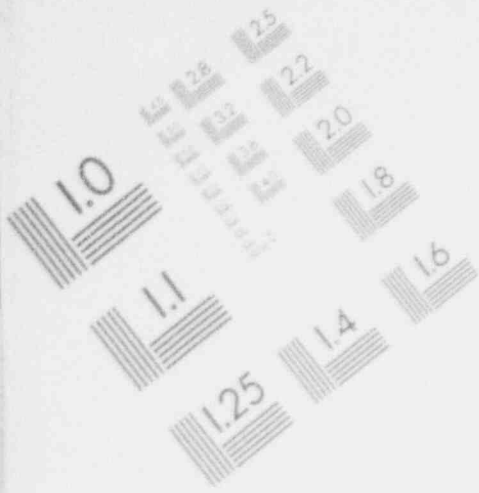
1

IMAGE EVALUATION TEST TARGET (MT-3)



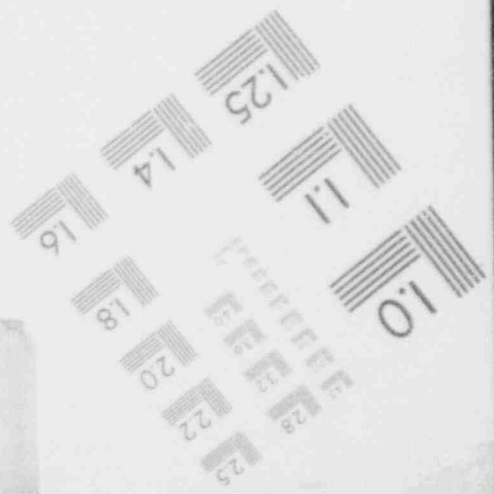
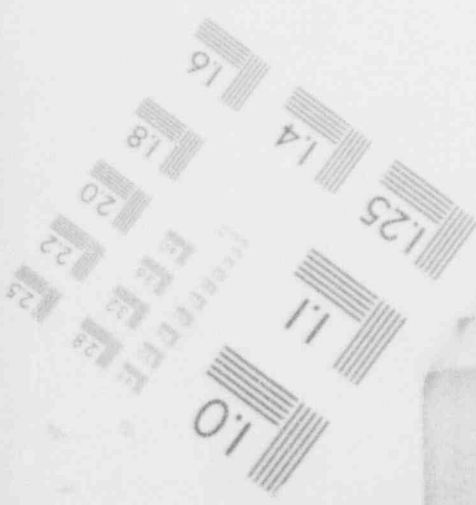
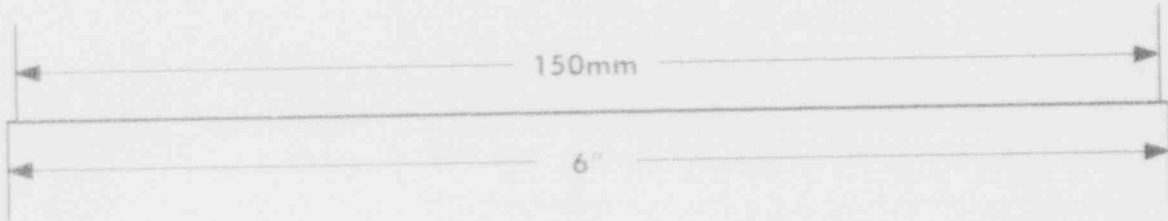
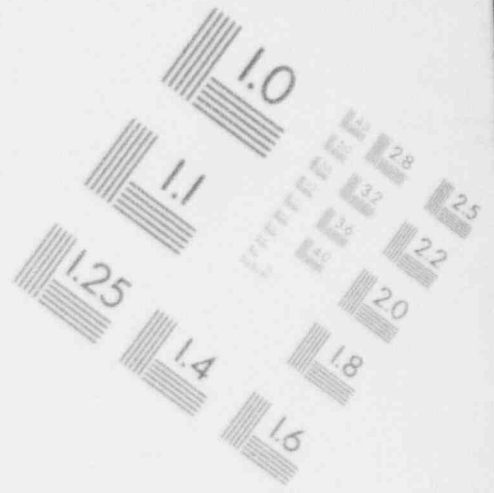
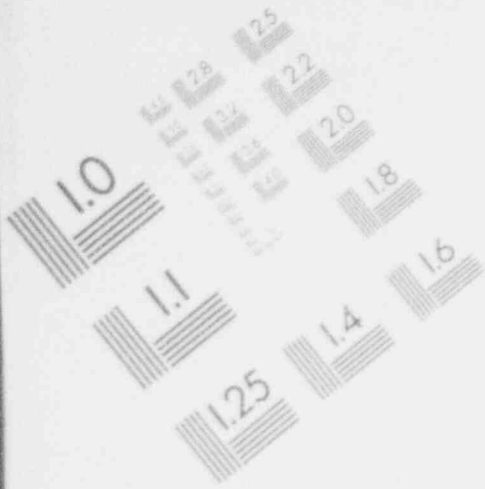
1

IMAGE EVALUATION TEST TARGET (MT-3)



1

IMAGE EVALUATION TEST TARGET (MT-3)



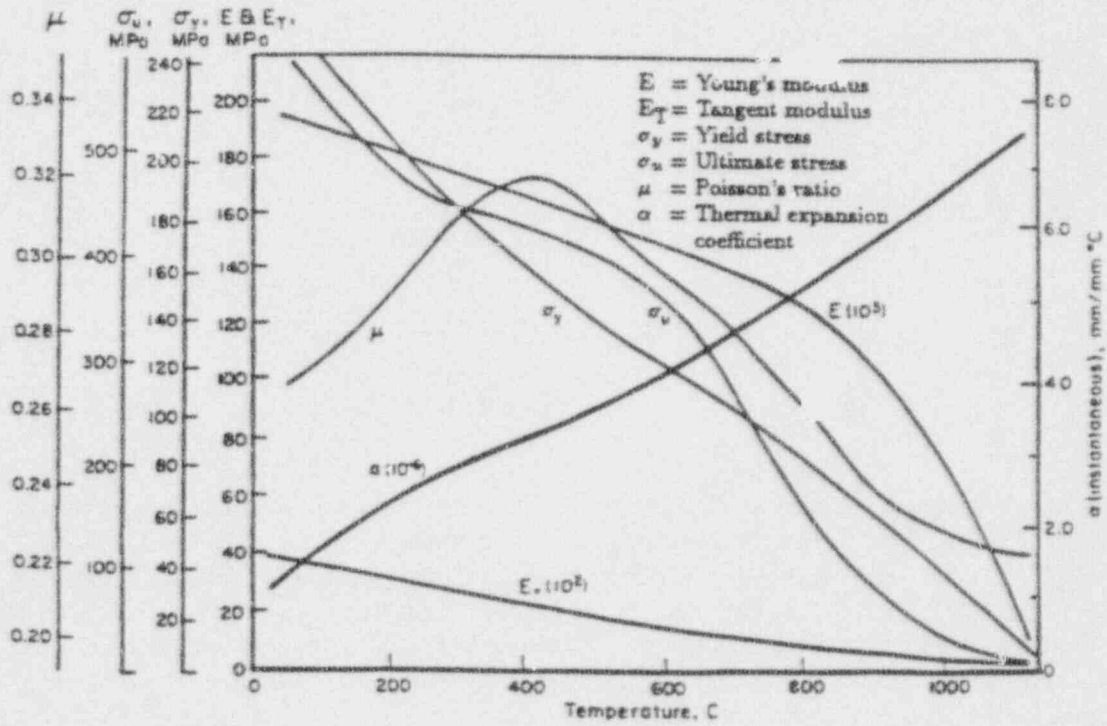


Figure 10.9 Temperature-dependent material properties for 304 stainless steel
 (From Ref. 10.19)

stresses, the temperature distribution due to the welding process was calculated based on a steady-state solution of a point heat source moving in an infinite solid at a constant velocity. The equation was given by Rosenthal (Ref. 10.20) as

$$T_w(r_h, \xi) = T_o + \frac{q}{4\pi k r_h} \exp [(-\xi + r_h)V/2a_h] \quad (10.8)$$

where

T_w	=	Temperature of weldment
T_o	=	Ambient temperature
q	=	Rate of heat input
k	=	Thermal conductivity
V	=	Heat source velocity
ξ	=	Distance from heat source along a line parallel to the direction of its movement, $\xi = T - Vt$, t represents time
r_h	=	Distance from heat source $(r_h = \sqrt{\xi^2 + Z^2 + T^2})$
c_h	=	Heat capacity
a_h	=	k/c_h

The parameters of the welding process for the computations of temperature distributions are given in Table 10.1 (Ref. 10.19). When a weldment is deposited, the temperature of the weldment is given as 1,260 C (2,300 F), which is close to the melting point of 1,427 C (2,600 F) for Type 304 stainless steel. The thermal history of the deposited weldment was simulated by using finite numbers of heating and cooling phases. For the 8.64-mm (0.34-inch) thick plate, heating of the base metal due to the weldment is divided into seven phases until the base metal reaches the highest temperature. The base metal and the weldment will cool down until the next weldment is deposited. This cooling process is divided into seven phases as well. The base metal and weldment were cooled to 65 C (150 F) between each welding pass. After the final welding pass, the base metal and the weldment were cooled to room temperature, 21 C (70F). For the 33-mm (1.3-inch) thick plate, there are nine welding passes. Each pass has six heating and six cooling phases to model the thermal history. Rybicki and Stonesifer (Ref. 10.21) used Equation (10.8) to obtain the temperature distributions due to multi-pass welds in piping systems. Their calculated temperature distributions were in good agreement with the experimentally measured temperature distributions. Reference 10.27 shows similarly accurate predictions between model predictions and thermocouple data.

Stress Analysis. These computed temperature distribution histories were used as input to an incremental elastic-plastic finite-element analysis to determine the stress and formation state of the weldment and the base metal as the weldment is deposited. The final residual stress states are what exist at the completion of all of the welding passes. Because there are a number of passes in this welding process, it is handled automatically in the computational process. The method used in the program is that the not yet deposited weldment is given a negligible stiffness until it becomes active.

Table 10.1 Welding parameters used in computations

Thickness, mm (inches)	Weld Pass	Welding Speed, mm/min (in./min)	Heat Input, W/mm	Final Temperature, C(F)	Heat Conductivity, Btu/mm sec., C	Heat Capacity, Btu/mm, C
8.64 (0.34)	1	81.3 (3.2)	65.04	21.0 (70)	0.000026	0.003104
	2	66.0 (2.6)	49.92	65.6 (150)	0.000026	0.003104
	3	180.3 (7.1)	61.93	65.6 (150)	0.000026	0.003104
	4	180.3 (7.1)	43.31	21.0 (70)	0.000026	0.003104
33.0 (1.30)	1	45.7 (1.8)	29.76	21.0 (70)	0.000021	0.002835
	2	141.7 (5.58)	86.02	65.6 (150)	0.000021	0.002835
	3	141.7 (5.58)	86.02	65.6 (150)	0.000021	0.002835
	4	141.7 (5.58)	86.02	65.6 (150)	0.000021	0.002835
	5	141.7 (5.58)	86.02	65.6 (150)	0.000021	0.002835
	6	155.4 (6.12)	103.98	65.6 (150)	0.000021	0.002835
	7	155.4 (6.12)	103.98	65.6 (150)	0.000021	0.002835
	8	155.4 (6.12)	103.98	65.6 (150)	0.000021	0.002835
	9	155.4 (6.12)	103.98	21.0 (70)	0.000021	0.002835

Dawes (Ref. 10.22) suggested that a crack be introduced at the weld center line to measure the weld metal fracture toughness, because the weld center line coincides with both the weakest planes of the coarse columnar solidification structures and the greatest concentrations of the weak grain boundary segregates. In service, though, many cracks develop in the weld. Such cracks are not considered here and will be reported on later. During the residual stress computation, the nodal points along the symmetry line were given very high stiffness in the Z direction to constrain the displacement in the Z direction. After the completion of the residual stress computation, the prepositioned crack along the symmetry line was introduced by completely releasing this high stiffness over 10 increments for each nodal point. The nodal points were sequentially released, starting from the bottom surface of the plate until the crack tip reached a quarter of the plate thickness. One can assume that the crack is introduced slowly due to SCC or a fatigue mechanism. Finally, with a remote tensile load being applied to achieve Mode I crack-tip fields, the values of the J-integral (Ref. 10.23) were calculated as

$$J = \int_{\Gamma} \left[W n_1 - t_i \frac{\partial u_i}{\partial x_1} \right] ds \quad (10.9)$$

Here, Γ represents a contour starting from the lower crack face extending counterclockwise around the crack tip to a point on the upper face, W is the strain energy density, t_i are the components of

the traction, u_i are the components of the displacement vector, and n_1 is the component in the x_1 direction of the outward unit normal vector to the contour Γ . Several paths are selected in the computations of the J-integral as shown in Figures 10.7(c) and 10.8(c) for both the straight groove and V-groove geometry. The definition of the CTOA used in these computations is

$$\text{CTOA} = 2 \tan^{-1} \left[\frac{\delta_e}{h_e} \right] \quad (10.10)$$

where δ_e is the displacement at the nodal point right behind a crack tip, and h_e is the size of the element in the crack-line direction right behind the crack tip.

Computational Results

Figure 10.10 shows the residual stress distributions for the equivalent stress $\sigma_e = (3\hat{\sigma}_{ij}\hat{\sigma}_{ij}/2)^{1/2}$ (where $\hat{\sigma}_{ij}$ are the deviatoric stresses), the three in-plane stress components σ_R , σ_Z , σ_{RZ} , and the out-of-plane stress components σ_T along the symmetry line ($Z = 0$) in the thickness direction of the 9.64-mm (0.380-inch) thick plate. The σ_Z distribution showed the same trend as that indicated in References 10.24, and that of the three-dimensional finite-element computations of Ramamurti et al. (Ref. 10.25). Ueda et al. (Ref. 10.26) computed the three-dimensional residual stress distributions in a thick plate caused by welding. They sliced the welded specimen in the thickness and welding direction to measure the inherent residual strains. The distribution of the strains was used as an input to their finite-element analysis to find the residual stress distributions.

In Figure 10.10, we noticed that the stress levels of the three in-plane stresses are significantly lower than that of the out-of-plane normal stress, σ_T , which is the largest and has a magnitude from 200 MPa (29 ksi) to 275 MPa (40 ksi) through the thickness^(a). The fact that the out-of-plane deformation is constrained due to the plain strain assumption attributes to elevate the level of the out-of-plane stress component σ_T . The transverse stress, σ_Z , is tensile and about 124 MPa (18 ksi) at the bottom of the plate for the straight groove case and about 150 MPa (21.75 ksi) for the V-groove case. The tensile stresses will contribute to increase the propensity for crack nucleation and for crack growth after the crack is introduced.

Figure 10.11 shows the same trend of the residual stress distributions along the symmetry line in the weld of the 33-mm (1.30 inch) thick plate. Note that the shear stress at this symmetry plane is zero, as it must be. In this figure, σ_Z , which is considered to play an important role in cracking of a plate, becomes very large at the bottom of the plate; it is about 300 MPa (43.5 ksi) in the straight groove case and 375 MPa (54.4 ksi) in the V-groove case. Note that the yield stress at room temperature for

(a) Note that shear stress, σ_{RZ} , should be zero because it is evaluated at a symmetry plane. Figure 10.10, therefore, gives an indication of the computational accuracy. Also, of course, σ_R is small and is zero at the top and bottom free surface of the plate.

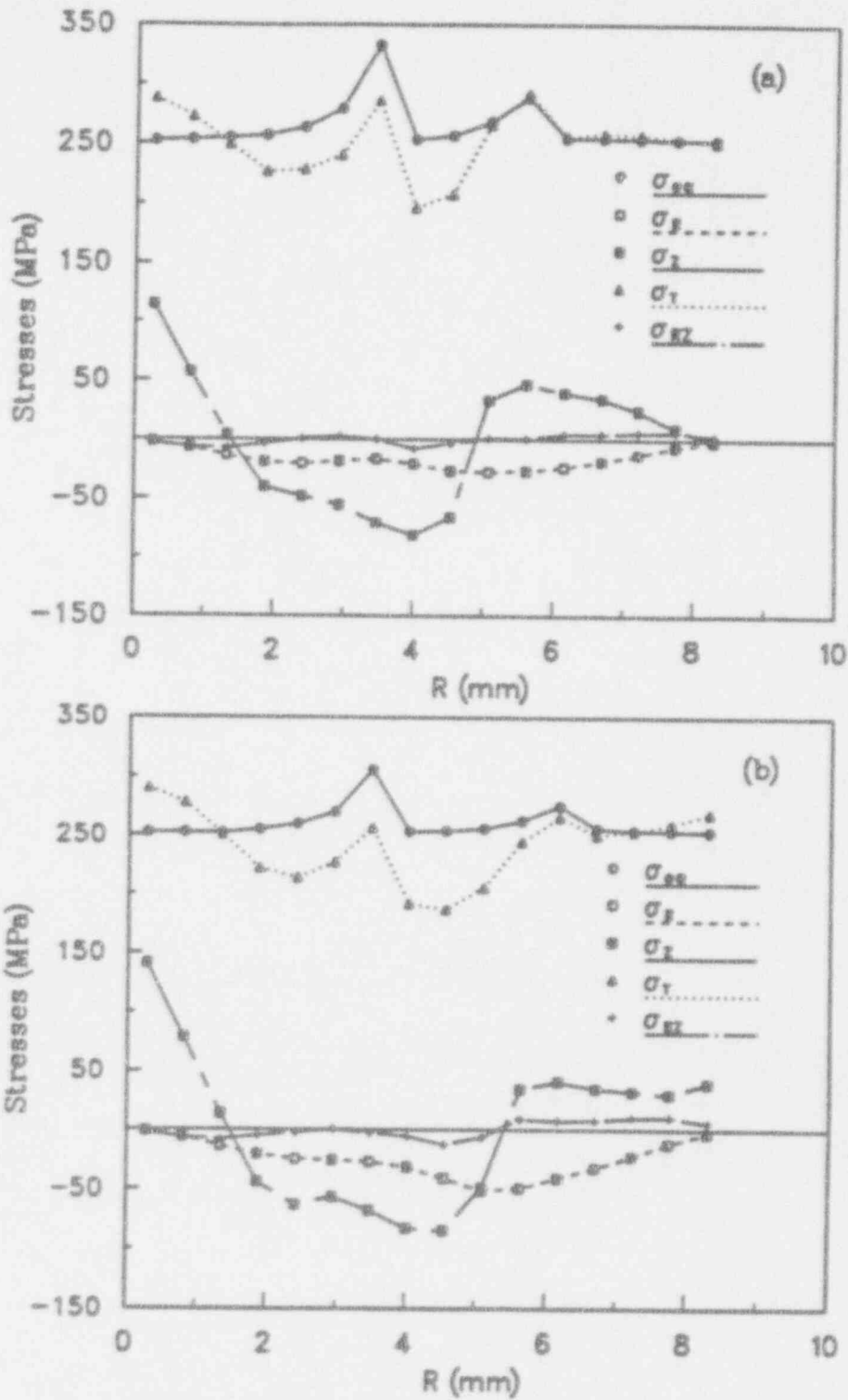


Figure 10.10 Residual stress distributions along the crack line for 8.6-mm (0.34-inch) thick plate, (a) straight groove, (b) V-groove

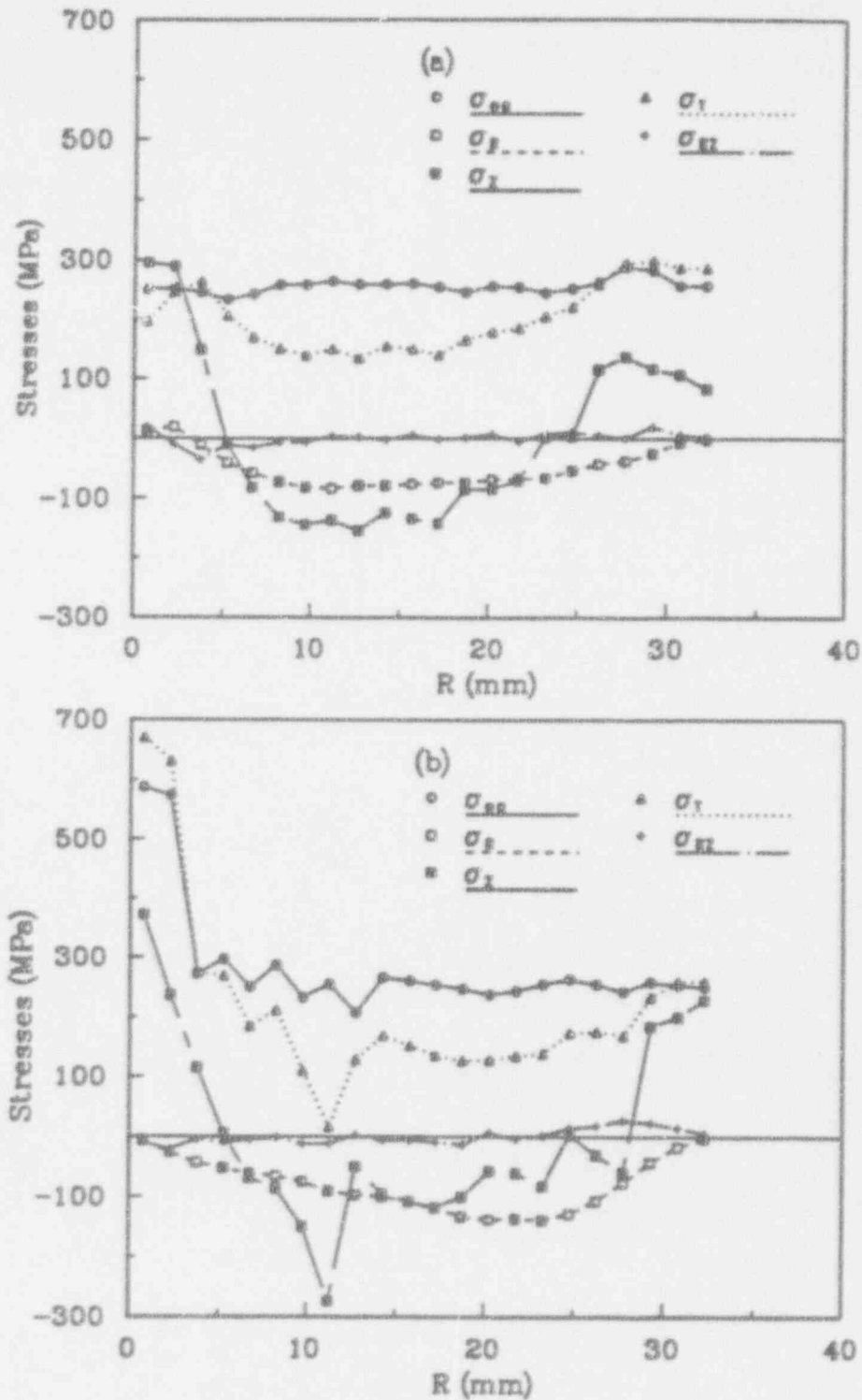


Figure 10.11 Residual stress distributions along the crack line for 33-mm (1.3-inch) thick plate, (a) straight groove, (b) V-groove

the 304 stainless steel is set at 240 MPa (34.8 ksi) in these computations. The reason for this higher residual stresses for the thick plate is that more welding passes and molten weldment were applied to the 33-mm (1.3 inch) thick plate than the 8.6-mm (0.34-inch) thick plate. The welding process starts from the bottom of the plate and piles up the weldment to the top of the plate. For each welding pass, the bottom of the plate experiences a cycle of heating and cooling. Since the plates are constrained such that bending is allowed, the tensile residual stress, therefore, builds up at the bottom of the weldment. Due to the high values of the residual stress, σ_T , a crack may grow from the bottom of the plate along the symmetry plane for the thick plate. Note that the σ_T stresses are quite large here. A crack would actually want to grow in the 'T' direction because of this. However, due to the two-dimensional nature of our analysis, and because σ_T stresses are probably overpredicted compared to a real welded plate due to the over constraint introduced by plane strain assumptions, we can only consider the crack to occur due to σ_z stresses here.

The residual stress σ_z distribution in the weldment and HAZ is shown in Figures 10.12(a), 10.12(b), 10.12(c), and 10.12(d) for the 8.64-mm (0.34-inch) and 33-mm (1.3-inch) thick plates with the straight groove and V-groove. From these figures, we can see that the highest stress (σ_z) is located at the bottom of the plate along the symmetry line, although heat-affected-zone stresses are high also.

The residual stresses in the middle part of the plate were initially compressive; but as a crack is introduced into this section, the stress, especially σ_z , becomes tensile. Figure 10.13(a) shows the opening stress σ_z for the 33-mm (1.3-inch) thick plate with the straight weld groove geometry before and after 10 nodal points were released. The release of 10 nodal points corresponds to a crack length (a) to plate thickness (t) ratio $a/t = 0.25$, or $a = 8.25$ mm (0.325-inch) for the 33-mm (1.3-inch) thick plate. This same crack-growth ratio was used for the 8.64-mm (0.34-inch) thick plate case. Figure 10.13(b) shows the same results for the V-groove. In these figures, the finite elements used in the computation are twice as small as those shown in Figure 10.8. The size of the finite elements near the crack tip is not small enough to show the singularity of the stress and its amplitude right ahead of the crack tip. Note that after a crack is introduced, σ_z continues to be tensile at the tip of the crack.

Figures 10.14(a) and 10.14(b) show the values of the J-integrals for both the 8.64-mm (0.34-inch) and 33-mm (1.3-inch) thick plate under remote tensile load without considering the residual stresses. Both figures show the path independence of the J-integral very well. The J-integral (Ref. 10.23) shown in Equation (10.9) is based on the deformation theory of plasticity and is valid if nearly proportional loading occurs everywhere except in a small neighborhood of the crack tip. If proportional loading occurs everywhere, the value of the J-integral of the incremental theory of plasticity coincides with that based on the deformation theory of plasticity. However, when the residual stresses induced by multi-pass welding processes were considered, combined with the non-proportionality introduced when a crack is introduced, the results of the computations showed that the J-integral is not path independent. This can be seen in Figures 10.15 and 10.16.

Figures 10.15(a) and 10.15(b) show the values of the J-integral for different contours of 8.64-mm-thick plate with the straight groove and single V groove geometry, respectively. In these figures, we can clearly see the path dependency of the J-integral. In Figure 10.15(a), the values of the J-integral

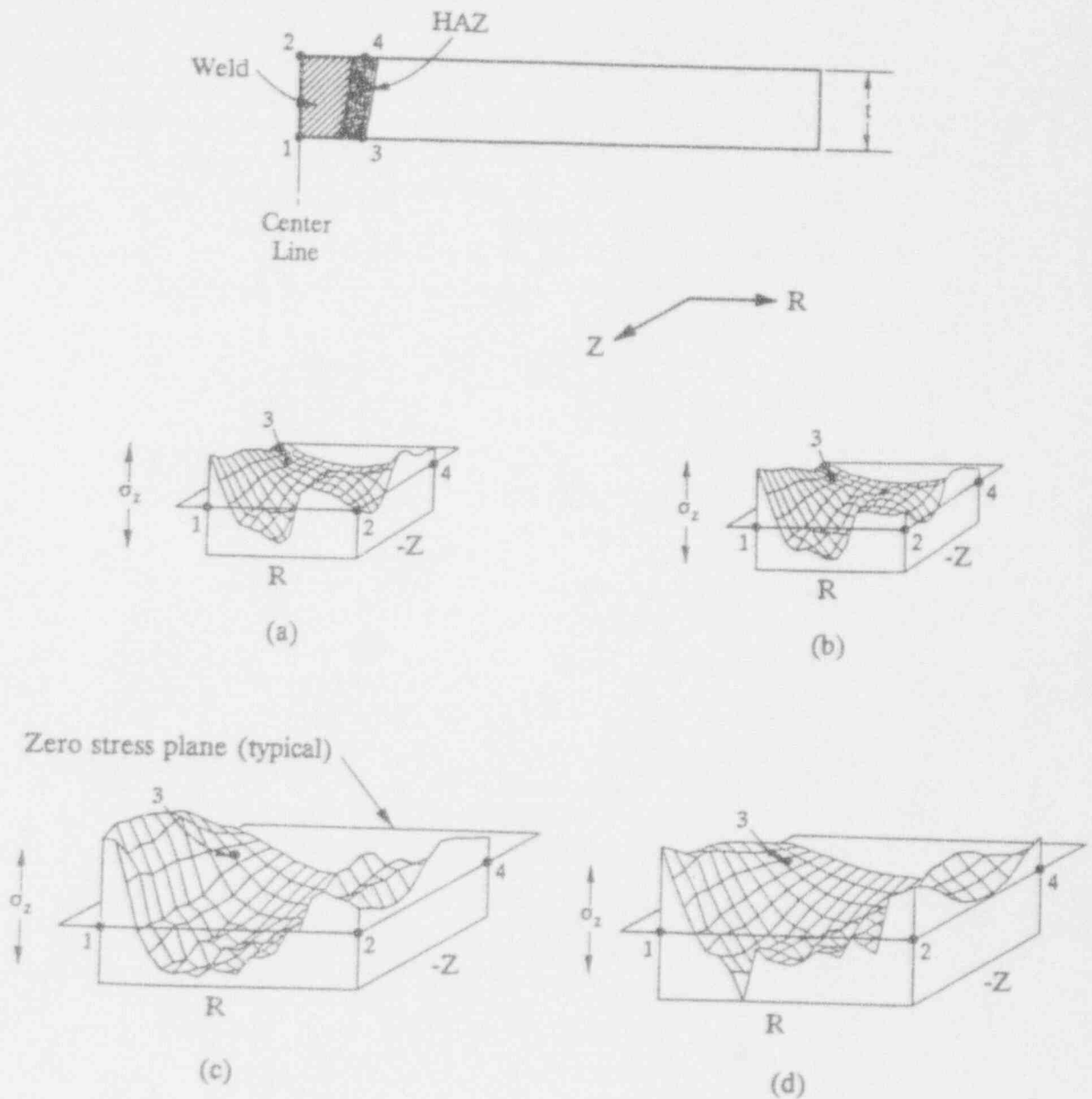


Figure 10.12 Residual σ_z stress distributions in weldment and HAZ for 8.6-mm (0.34-inch) thick plate with (a) straight groove, (b) single-V groove for 33-mm (1.3-inch) thick plate with (c) straight groove (d) V-groove. See Figure 10.6 for coordinate definitions and see Figures 10.5 and 10.6 to observe magnitudes for the plane $Z = 0$.

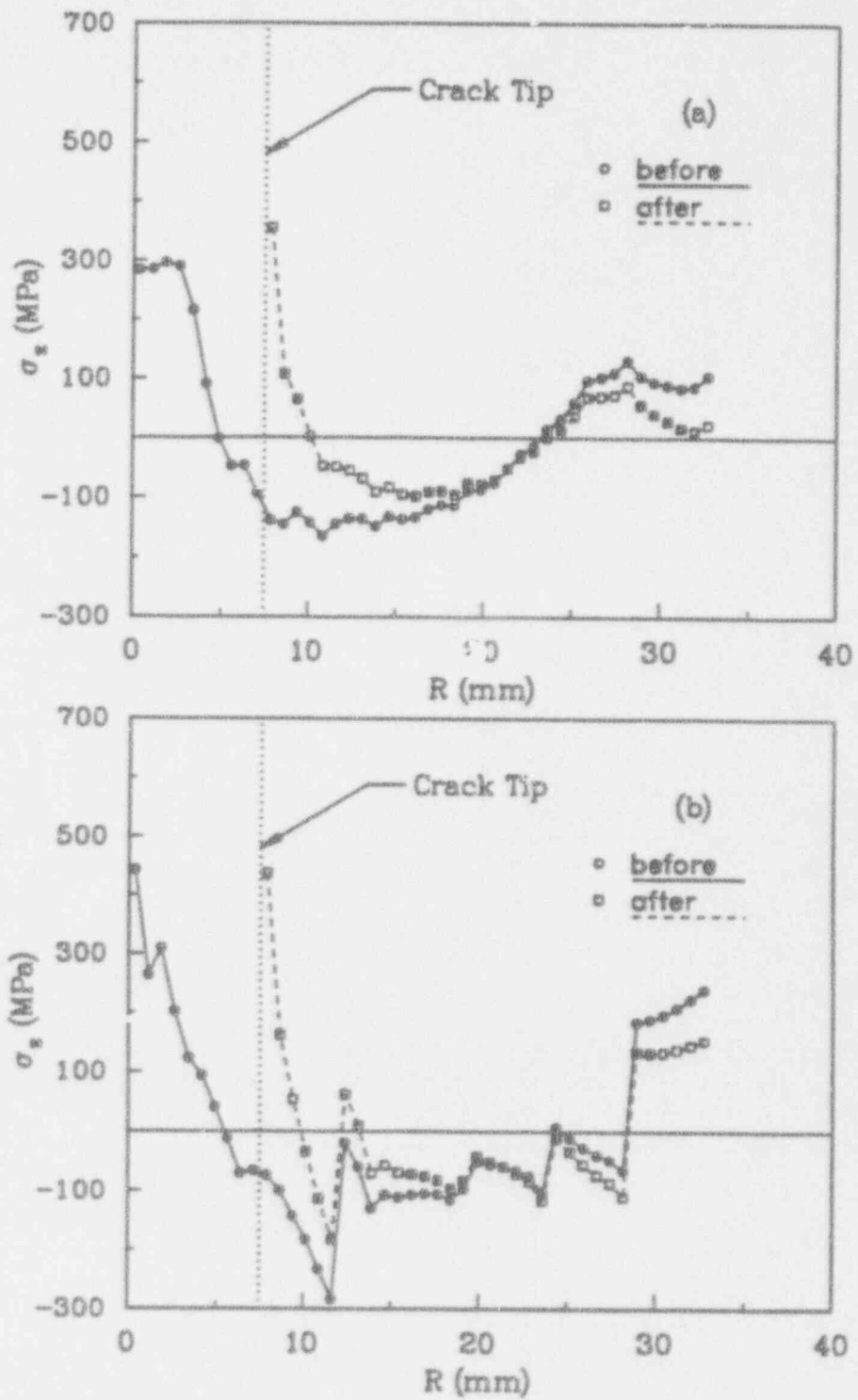


Figure 10.13 σ_x distributions along the crack line before and after releasing 10 nodal points for the refined mesh of 33-mm (1.3-inch) thick plate, (a) straight groove, (b) single-V groove

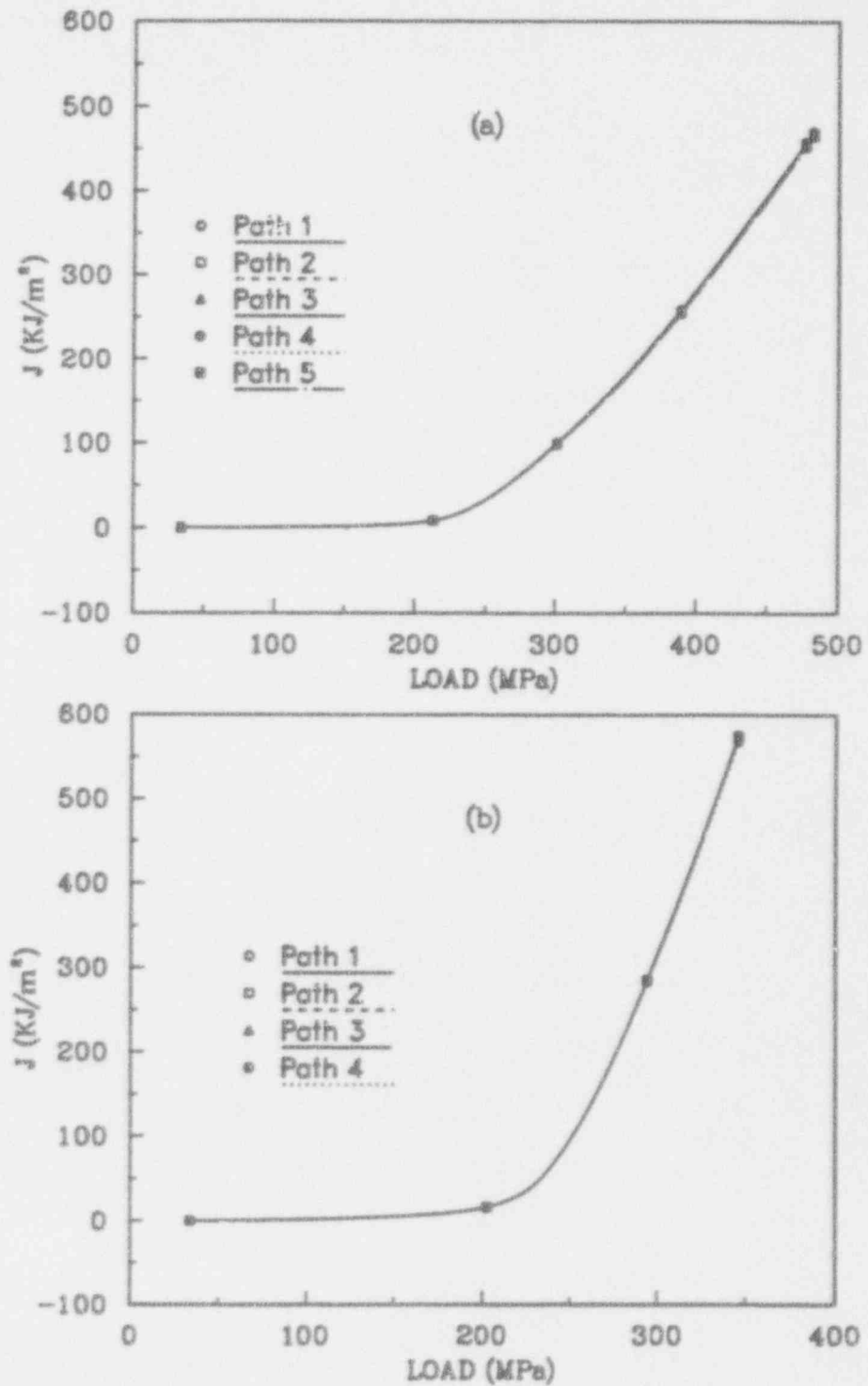


Figure 10.14 J-integral versus applied load (without thermal residual stresses),
 (a) 8.64-mm (0.34-inch) thick plate, (b) 33-mm (1.3-inch) thick plate

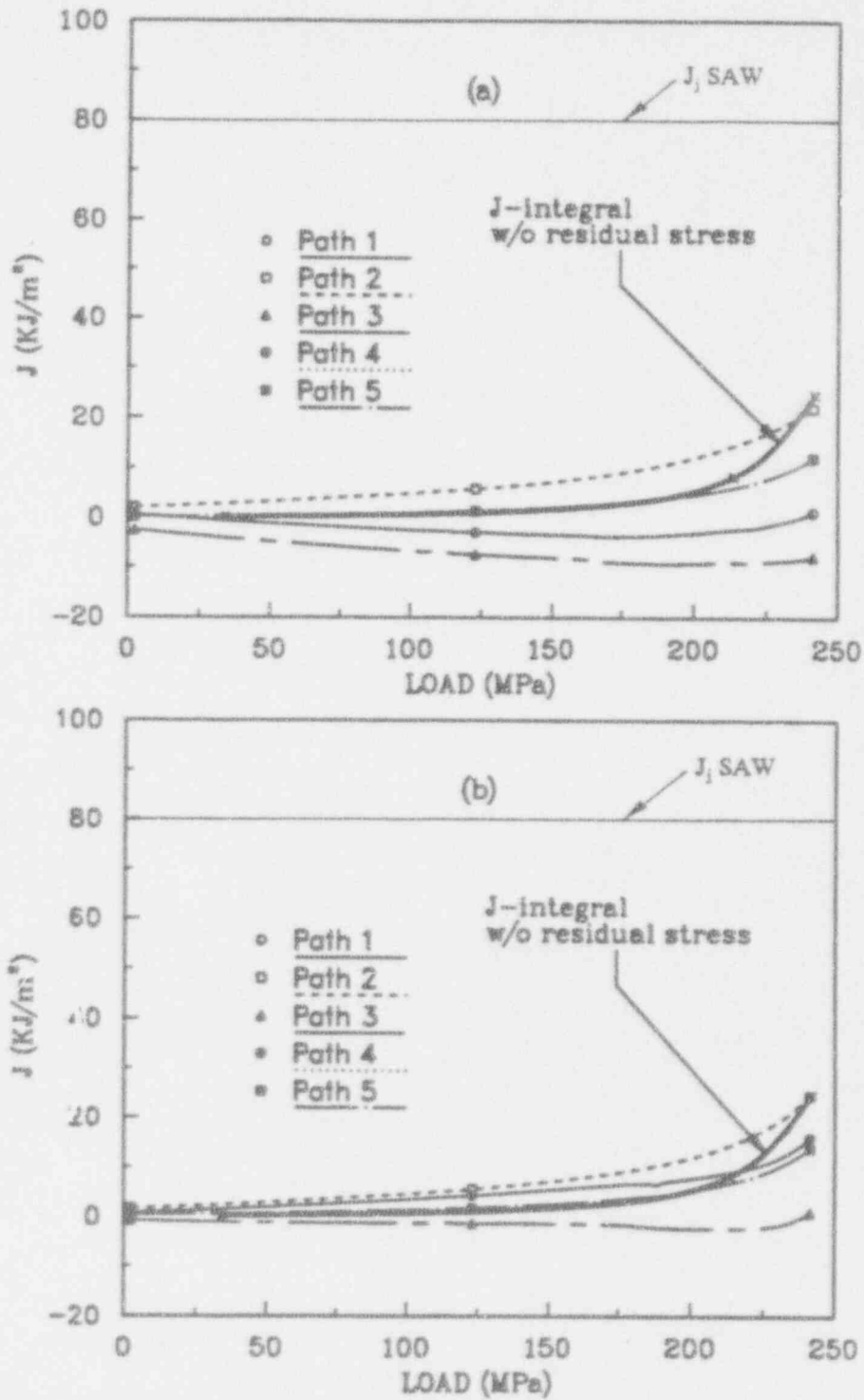


Figure 10.15 J-integral values for different contours for 8.64-mm (0.34-inch) thick plate with the thermal residual stresses, (a) straight groove, (b) single-V groove

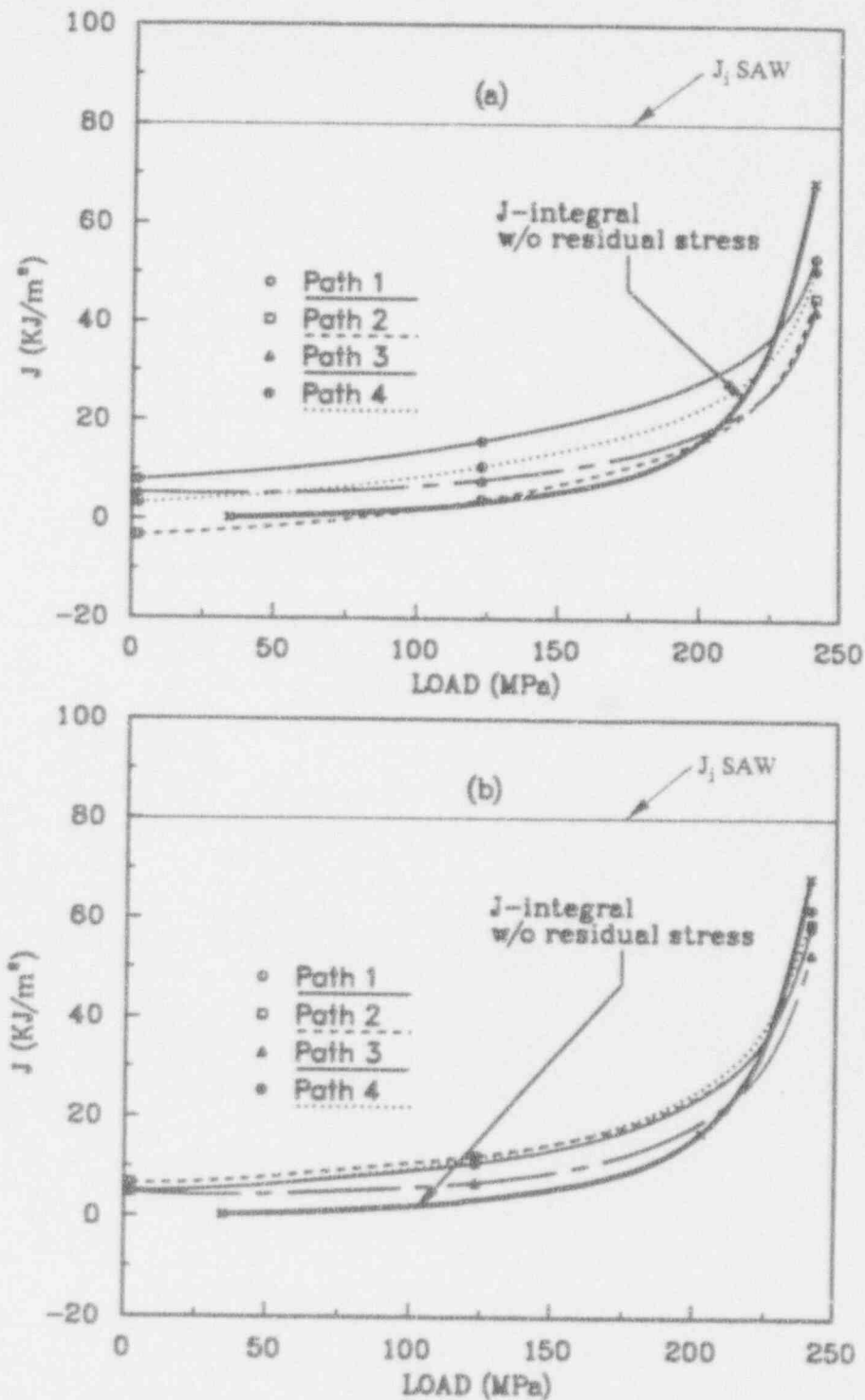


Figure 10.16 J-integral values for different contours for 33-mm (1.3-inch) thick plate with the thermal stresses, (a) straight groove, (b) single-V groove

of Path 4 and Path 5, which encompass the HAZ as well as the welding part, are very close throughout the whole loading. The same characteristic can be seen in Figure 10.15(b). Path 1 and Path 3 in Figure 10.15(a), which cover the lower half of the plate, show negative values of the J-integral up to the load level of 227 MPa. Figure 10.16(a) shows the values of the J-integral for different contours of the 33-mm (1.3-inch) thick plate with straight weld groove geometry. The differences between the values of the J-integral of different paths are not large compared with the computational results of the 8.6-mm (0.34-inch) thick plate. However, the difference in the values of the J-integral is still large enough so that the path independence of the J-integral cannot be confirmed. The values of the J-integral of Path 2 in Figure 10.16(a) remain negative until the applied tensile load reaches 76 MPa (11 ksi). Figure 10.16(b) shows the values of the J-integral for the 33-mm (1.3-inch) thick plate with the single-V groove geometry. In this case, the values of the J-integral of Path 1 and Path 4 are close up to the load level of 275 MPa (40 ksi). But the other two paths give quite different values of the J-integral from those of Path 1 and Path 4. The J-integral does not show path independence for this case either. When the same computation was done to the refined mesh of the 33-mm (1.3-inch) thick plate, the residual stresses showed a good agreement with that of the coarse mesh. However, the J-integral was still not path independent.

The results of the J-calculations up to large loads are shown in Figures 10.17 and 10.18 for the 8.64 and 33-mm (1.3-inch) thick plate analyses, respectively. The room temperature yield stress for Type 304 stainless steel is 240 MPa (34.8 ksi). Hence, the maximum applied gross stress of 340 MPa (49.3 ksi) for the 8.6-mm (0.34-inch) thick plate represents 1.42 times the yield stress, while the applied stress for the 33-mm (1.33-inch) thick plate of 475 MPa (68.9 ksi) represents almost twice the room temperature yield stress. For the thick plate (Figure 10.18), J becomes nearly path independent for both the straight and single-V groove geometries. For the thin plate (Figure 10.17), J remains path dependent even at high loads; however, the percentage of difference between the paths continually decreases with increasing load. The percentage difference between the different J-paths is hundreds of percent at low loads (Figures 10.15 and 10.16) and less than 10 percent at high loads (Figures 10.17 and 10.18). In effect, the importance of the non-proportionality introduced by the weld-induced residual stresses and crack growth is "washed out" at large loads. At large loads, the additional plastic strains caused by the load begin to dominate those caused by the residual stresses, and J again becomes a valid parameter.

Material Property Considerations

The initiation value of J (J_i) depends on the welding process used. For a tungsten inert gas (TIG) weld, $J_i \cong 500 \text{ kJ/m}^2$ (2855 in-lb/in²), while for a shielded metal-arc weld (SMAW),

$J_i \cong 80 \text{ kJ/m}^2$ ^(a) (457 in-lb/in²). Both types of welds are typically found in nuclear plants. The welding parameters listed in Table 10.1 are typical of those used for a SMAW weld. Let us now consider these fracture properties in relation to Figures 10.15 to 10.18.

(a) In reality, the statistical distribution of J_i for a TIG weld may vary between 263 and 2,100 kJ/m² (1,502 kJ/m² and 11,991 lb/in²), while for a SAW, the variation is between 52 and 140 kJ/m² (297 and 799 in-lb/in²). The values of 500 and 80 kJ/m² (1,502 and 11,991 in-lb/in²) are considered as typical average values.

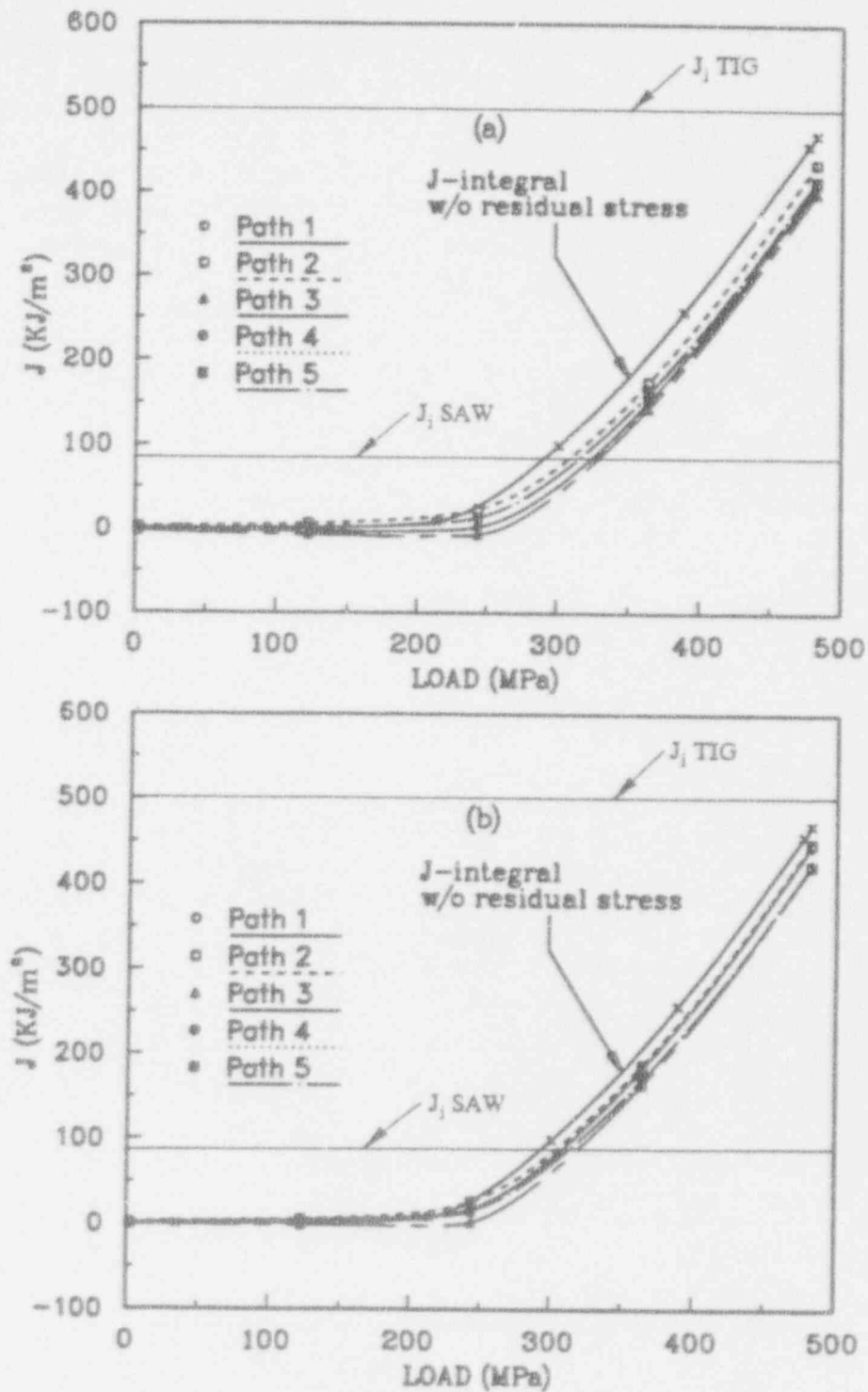


Figure 10.17 J-integral values for different contours for 8.6-mm (0.34-inch) thick plate with the thermal residual stresses, (a) straight groove, (b) V-groove

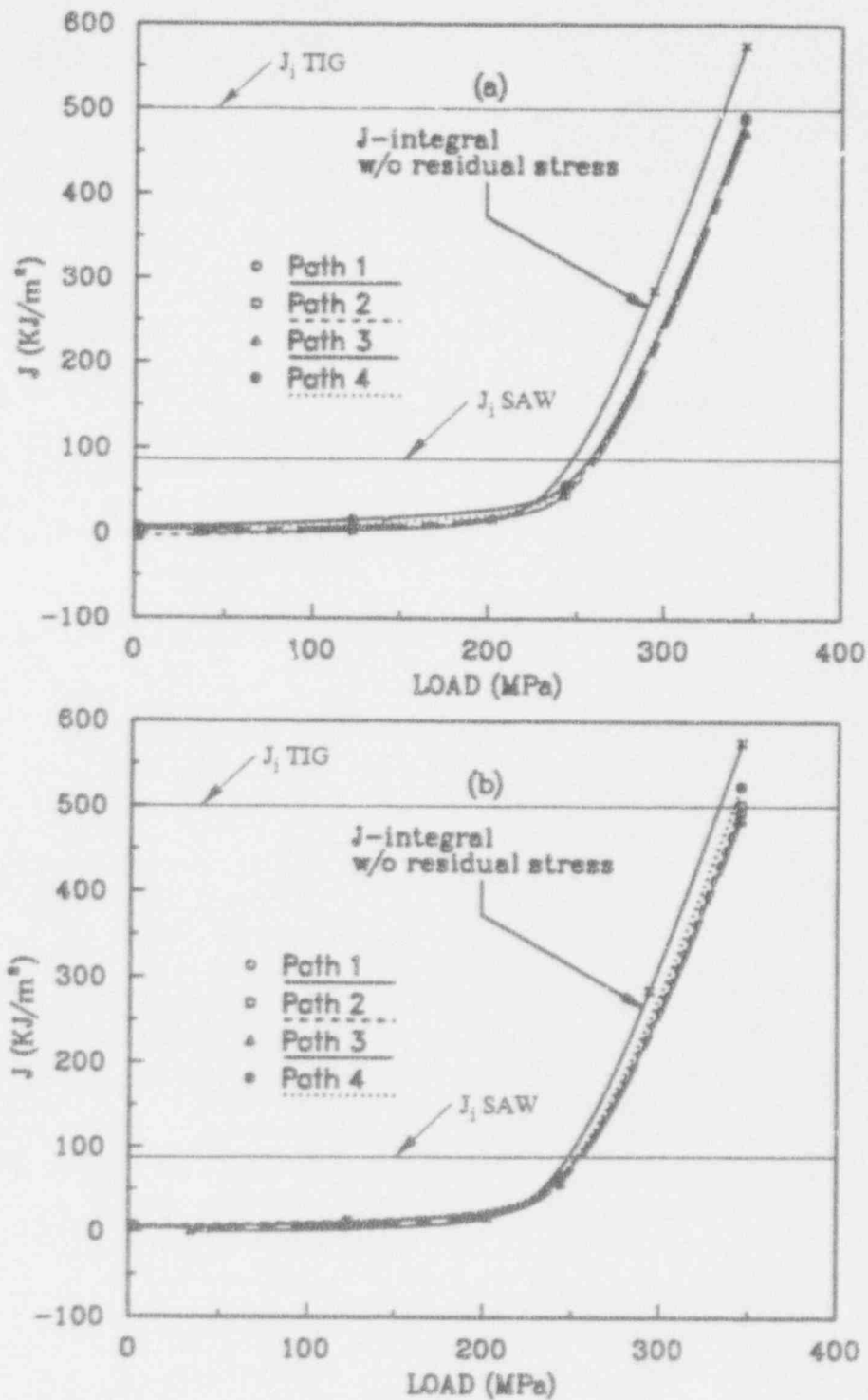


Figure 10.18 J-integral values for different contours for 33-mm (1.3-inch) thick plate with the thermal residual stresses, (a) straight groove, (b) single-V groove

For a TIG weld, it is clear that the large value of J_i at crack initiation essentially renders the effect of residual stresses on the crack growth process negligible. In Figures 10.17 and 10.18, by the time the driving force values of J reach the TIG J_i value, J is nearly path independent. Hence, J may be used as a characterizing parameter. Note also from Figures 10.17 and 10.18 that the value of J for the case without residual stress is higher than corresponding values with residual stress. This implies that for a TIG weld

- (1) The residual stresses actually improve the fracture resistance
- (2) Neglecting residual stresses will lead to a conservative prediction.

For the SAW case, the results depend on the plate thickness. For a thin plate (8.64 mm [0.34-inch], Figures 10.15 and 10.17), J is still path dependent at $J_i = 80 \text{ kJ/m}^2$ (457 in-lb/in²). Hence, J may not accurately characterize crack-tip events. However, it is also seen that neglecting residuals stress effects will lead to conservative predictions because J without residual stresses is higher than J with residual stresses at the initiation value of J_i . However, for the thicker plate (Figures 10.16 and 10.18), J is nearly path independent at J_i .

Hence, for monotonic loading to failure, the following conclusions may be drawn regarding the effect of residual stresses on J .

- For a TIG weld, J may be used with confidence to predict weld fracture for any thickness plate. Moreover, estimating J without considering residual stress effects will lead to conservative predictions.
- For a SAW weld, the validity of J to characterize fractures is plate thickness dependent; the thicker the plate, the more appropriate J is. However, in all cases, estimating J by neglecting residual stresses will lead to conservative predictions.

While the effects of residual stresses may be neglected when predicting monotonic load fracture in Type 304 stainless steel plate, the same conclusion cannot be drawn regarding the prediction of SCC or fatigue crack growth. The room temperature yield stress of this material is about 240 MPa (34.8 ksi). Therefore, in service loads of the type that would influence SCC or fatigue are expected to be less than one half this value or $\sigma_{\text{service}} < 120 \text{ MPa}$ (17.4 ksi). From Figures 10.15 and 10.16, it is clear that, at these load levels, J is markedly path dependent and certainly cannot characterize crack-tip events. Moreover, J -predictions neglecting residual stresses are, in general, lower than the corresponding values including residual stresses. Hence, using J (or equivalently K) as an SCC or fatigue growth law is inappropriate if residual stress effects are not considered, as nonconservative results would occur. For this reason, the crack tip opening angle parameter was subsequently examined.

Figure 10.19 shows the CTOA computed at various levels of applied tensile load for the 8.64-mm (0.34-inch) thick plate. In this figure, the CTOA is compared with the CTOA computed without the residual stresses. In Figure 10.19(a), the CTOA with the residual stresses shows higher values than those without the residual stresses until the applied tensile load reaches 193 MPa (28 ksi) or 80 percent of the yield stress. When the applied tensile load is larger than 193 MPa (28 ksi), the near-

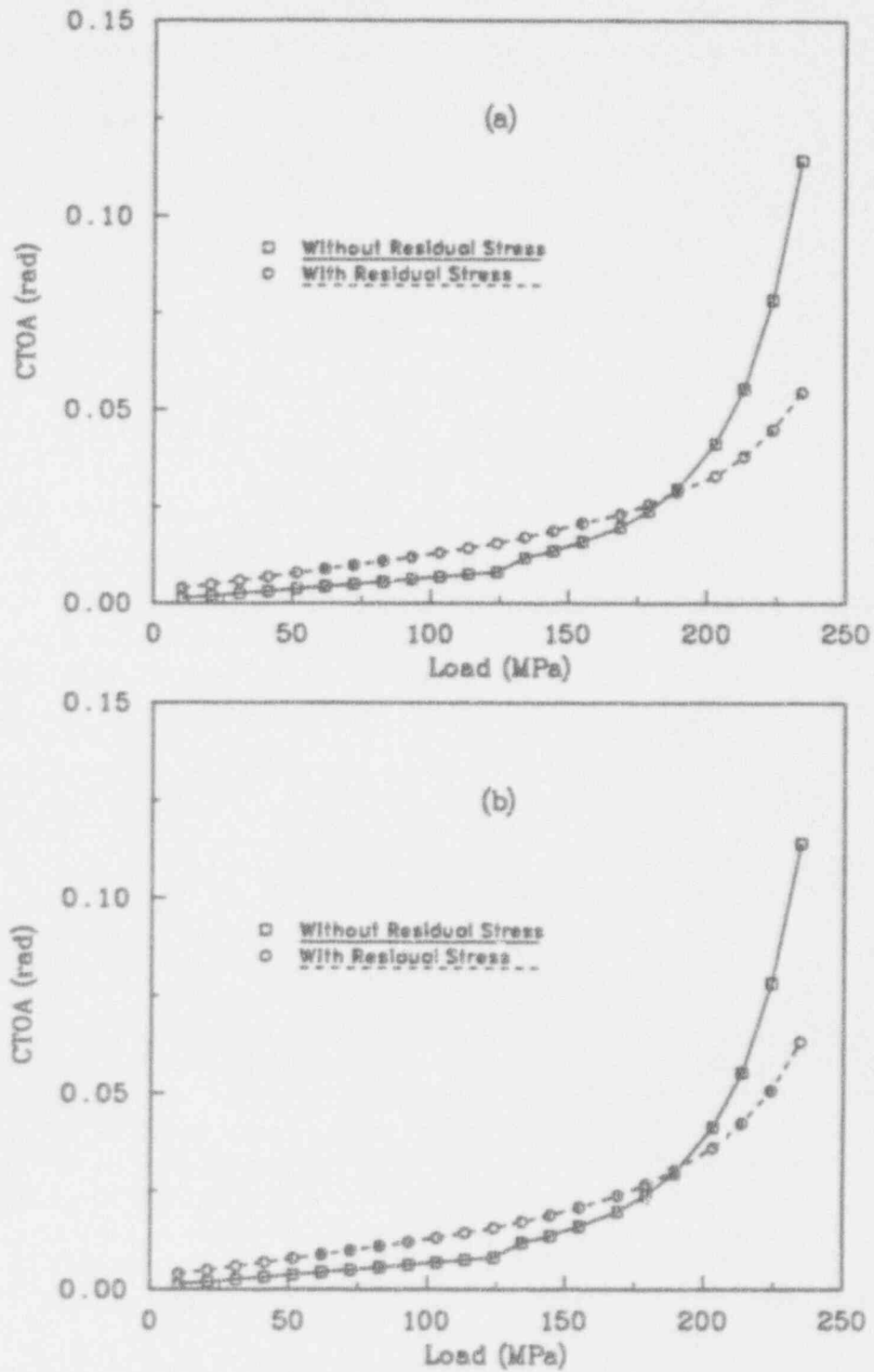


Figure 10.19 CTOA versus applied load for 8.64-mm (0.34-inch) thick plate
 (a) straight groove, (b) single-V groove

tip material with the residual stresses behaves stiffer. The CTOA for the 8.6-mm-thick plate with the single-V groove geometry shown in Figure 10.19(b) has the same characteristics as that of the straight groove geometry. For the 33-mm (1.3-inch) thick plate, the remote tensile load level at which the plate with the residual stresses becomes stiffer than that without the residual stresses is about 207 MPa (30 ksi) (or about 86 percent of the yield stress), for both the straight and V-groove geometry. This is shown in Figures 10.20(a) and 10.20(b). From Figures 10.19 and 10.20 we can see that the values of CTOA for the straight groove geometry and single-V groove geometry are very close so that the weld groove geometry does not affect the near-tip behavior significantly. However, at low applied tensile load, the near-tip material becomes more compliant than that without residual stresses. The results here show that, for service loads (σ -applied < 120 MPa (17.4 ksi)), the crack tip intensity based on CTOA is much more severe when residual stresses are included.

Discussion

Most of the actual welding processes require multi-pass welds. As each weld pass is deposited, the weld bead initially heats up the material adjacent to the molten weld. In fact, the temperature of the weldment is high enough that some of the base material also melts. At this high temperature, the hot weld and base material attempt to expand. However, this expansion is constrained by the bulk of the pipe or plate that remains near the ambient room temperature. Therefore, a region adjacent to the weld bead in the base material experiences compressive plastic deformation. This occurs in part because the yield strength of the base material adjacent to the weld is quite small at the high temperatures. Then as the weld puddle cools and begins to solidify, the opposite occurs: i.e., this same material that just experienced compressive plastic strain now undergoes tensile plastic deformation. This occurs for each weld pass.

In addition to the above-mentioned cyclic hardening, a residual stress state develops due to the welding process. For a pipe weld, tensile stresses develop on the inner pipe wall for all but very thick pipes. In a plate or a thick pressure vessel, the tensile residual stress state develops in different regions, depending on the far-field constraint conditions and other factors. For ferritic steels, some material experiences a phase change during each weld pass cycle. Therefore, an accurate assessment of the damage state of the welding zone is critical for the strength and life expectancy of welded structures because the three damage modes identified (cyclic plasticity, tensile residual stresses, and phase changes) can cause cracking of the welded structures in service. Methods such as heat sink welding and induction heating for stress improvement were developed (Ref. 10.27), which cause compressive stresses on the pipe inner wall. These techniques basically cool the pipe inner wall during the later stages of the welding process, which pulls the inner wall into compression after the weld cools. This favorable residual stress state mitigates SCC development. However, these techniques do not eliminate the cyclic plasticity on the inner wall caused by the welding process. More importantly, there are many weldments in plants that are not treated and thus have experienced all three damage modes due to the welding processes.

As the finite-element analysis has shown, the value of the CTOA is higher in the welded plate compared with the unwelded plate when the remote tensile stress is less than 193 MPa (28.0 ksi). This clearly suggests that the propensity for crack growth during operating loads via fatigue or an SCC mechanism might be higher for cracks growing in plate weld regions. Moreover, for some lower toughness ferritic plates, where J_{1c} is significantly lower, residual stresses may play an

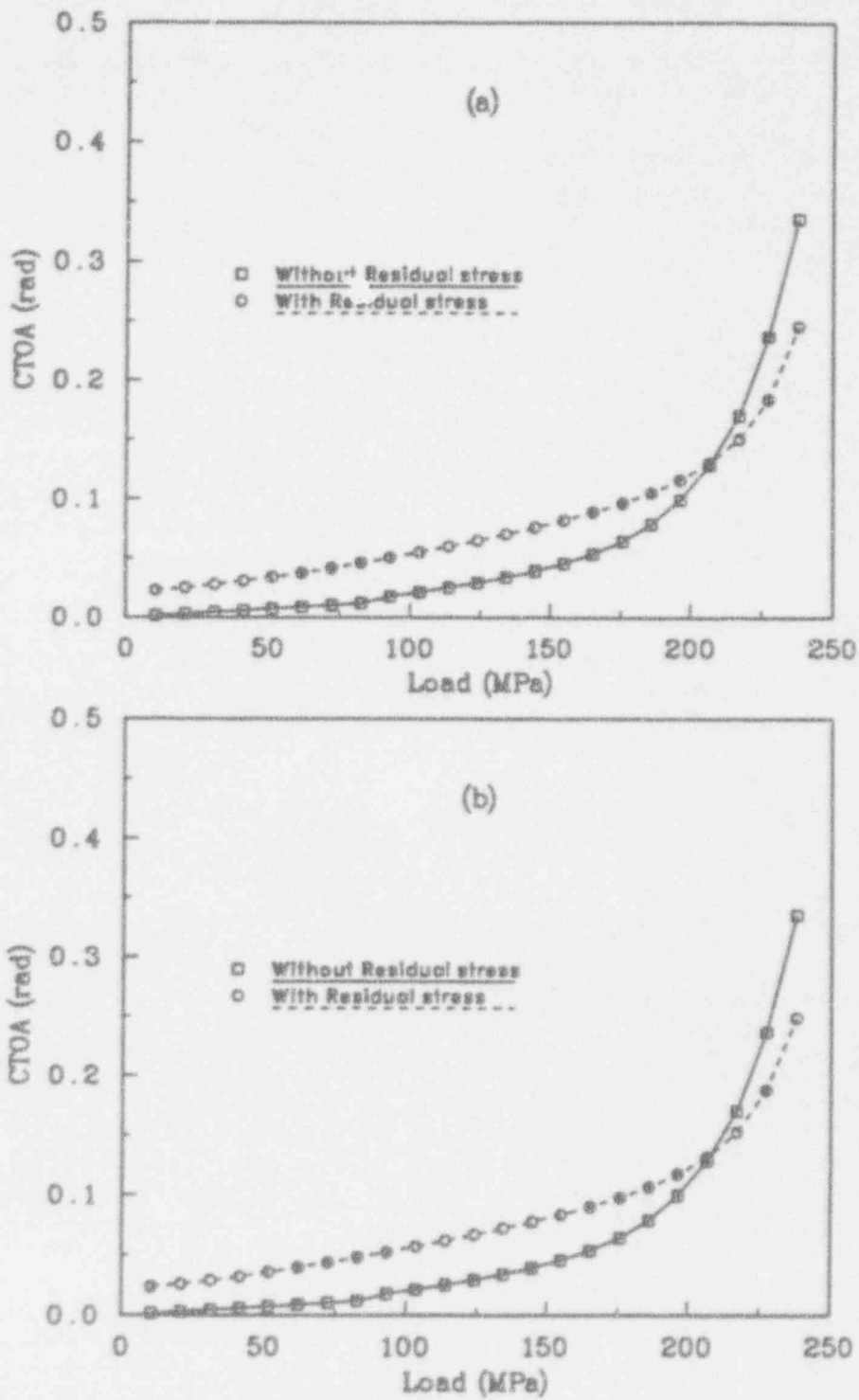


Figure 10.20 CTOA versus applied load for 33-mm (1.3-inch) thick plate
 (a) straight groove, (b) single-V groove

important role and the J-based fracture theories may not be appropriate for predicting monotonic failure loads. The effects of residual stresses on cracks in the HAZ may be different from those on cracks in the weldment. We expect that the residual stress plays a more important role for pipes than for plates because the weld bead shrinkage tends to clamp the pipe. This greatly increases the inner wall residual stress state due to the imposed bending caused by this weld clamp. Moreover, the zone of tensile residual stresses extends deep through the pipe wall due to this effect. This will be reported on in the next report.

Conclusions

For Type 304 stainless steel plate with a weld crack, we have shown that the effect of residual stresses on the crack initiation loads is small for monotonic loading to failure. For TIG welds, this is completely true, while for SAW welds, the thicker the plate, the less important the residual stresses are to the crack initiation load. Moreover, if J is estimated entirely neglecting residual stresses, conservative predictions will result. Note that these conclusions are not necessarily valid for ferritic steel welds where fracture toughness may be lower and phase changes occur.

On the other hand, residual stresses play an important role at loads typical of those seen in service. These load levels are typical of those important in SCC and fatigue crack growth predictions. J and K have little meaning in this regime, and CTOA may be a useful parameter. Further work to examine these effects would be useful.

10.4 Plans for Next Year of the Program

10.4.1 Subtask 9.1 Technical Exchange and Information Meetings

The two activities in this subtask are discussed below.

Activity 9.1.1

Efforts will continue to coordinate with the ASME Section XI Pipe Flaw Evaluation Task Group.

Activity 9.1.4

The plans for next year include looking at the effects of weld-induced residual stresses in pipe geometries. Results similar to those reported above for plates will be evaluated and reported next year.

10.5 References

- 10.1 Kiefner, J. F., Maxey, W. A., Eiber, R. J. and Duffey, A. R., "Failure Stress Levels of Flaws in Pressurized Cylinders," Progress in Flaw Growth and Fracture Toughness Testing, ASTM STP 536, 1973, pp. 461-481.
- 10.2 Wilkowski, G. M. and Scott, P. M., "A Statistically Based Circumferentially Cracked Pipe Fracture Mechanics Analysis for Design or Code Implementation," Nuclear Engineering and Design, Vol. 111, pp. 173-187, 1989.
- 10.3 Schmidt, R. A., Wilkowski, G. M., and Mayfield, M. E., "The International Piping Integrity Research Group (IPIRG) Program: An Overview," SMiRT-11, Paper G23/1, August 1991.
- 10.4 Chell, G. C., "Application of the CEGB Failure Assessment Procedure, R6, to Surface Flaws," ASTM STP 1074, 1990, pp. 525-544.
- 10.5 Yagawa, G., Century Research Corporation, Tokyo, Japan, "Study on Elastic-Plastic Mechanics in Inhomogeneous Materials and Structures III," Century Research Corporation report CRC-EPI-3 to NRC, March 1991.
- 10.6 Friedman, E., "Thermomechanical Analysis of the Welding Process Using the Finite Element Method," *ASME Journal of Pressure Vessel Technology*, Vol. 97, pp. 206-213 (1975).
- 10.7 Anderson, B. A. B., "Thermal Stresses in a Submerged-Arc Welding Joint Considering Phase Transformations," *ASME Journal of Engineering Materials and Technology*, Vol. 100, pp. 356-361 (1978).
- 10.8 Argyris, J. H., Szimmat, J., and William, K. J., "Computational Aspects of Welding Stress Analysis," *Computer Methods in Applied Mechanics and Engineering*, Vol. 33, pp. 635-666 (1982).
- 10.9 Papazoglou, V. J., and Masubuchi, K., "Numerical Analysis of Thermal Stresses During Welding Including Phase Transformation Effects," *Journal of Pressure Vessel Technology*, Vol. 104, pp. 198-202 (1982).
- 10.10 Tekriwal, P., and Mazumder, J., "Transient and Residual Thermal Stress-Stain Analysis of GMAW," *ASME Journal of Engineering Materials and Technology*, Vol. 113, pp. 336-343 (1991).
- 10.11 Brust, F. W., and Rybicki, E. F., "A Computational Model of backlay Welding for Controlling Residual Stresses in Welded Pipes," *ASME Journal of Pressure Vessel Technology*, Vol. 102, pp. 226-232 (1981).

- 10.12 Brust, F. W., and Kanninen, M. F., "Analysis of Residual Stresses in Girth Welded Type 304 Stainless Steel Pipes," *Journal of Materials for Energy Systems*, Vol. 3, pp. 56-62 (1981).
- 10.13 Kanninen, M. F., Brust, F. W., Ahmad, J., and Abou-Sayed, I. S., "The Numerical Simulation of Crack Growth in Weld-Induced residual Stress Fields," *Residual Stress and Stress Relaxation*, Editors E. Kula and V. Weiss, pp. 227-248, Plenum Publishing Corporation (1982).
- 10.14 Nakagaki, M., Marschall, C. W., and Brust, F. W., "Elastic-Plastic Fracture Mechanics Evaluations of Stainless Steel Tungsten/Inert-Gas Welds," *Nonlinear Fracture Mechanics: Volume II - Elastic-Plastic Fracture*, ASTM STP 993, J. D. Landes, A. Saxena, and J. G. Merkle, Eds., American Society for Testing and Materials, pp. 214-243 (1989).
- 10.15 Harrison, J. D., Dawes, M. G., Archer, G. L., and Kamath, M. S., "The COD Approach and Its Application to Welded Structures," *Elastic-Plastic Fracture*, ASTM STP 668, J. D. Landes, J. A. Begley, and G. A. Clarke, Eds., American Society for Testing and Materials, pp. 606-631 (1979).
- 10.16 Green, G., and Knott, J. F., "On Effects of Thickness on Ductile Crack Growth in Mild Steel," *Journal of the Mechanics and Physics of Solids*, Vol. 23, pp. 167-183 (1975).
- 10.17 de Koning, A. U., "A Contribution to the Analysis of Quasi Static Crack Growth in Sheet Materials," *Fracture 1977, Advances in Research on the Strength and Fracture of the Materials*, Proceedings of the Fourth International Conference on Fracture, Pergamon Press, New York, pp. 25-31 (1978).
- 10.18 Kanninen, M. F., Rybicki, E. F., Stonesifer, R. B., Broek, D., Rosenfield, A. R., Marshcall, C. W., and Hahn, G. T., "Elastic-Plastic Fracture Mechanics for Two-Dimensional Stable Crack Growth and Instability Problems," *Elastic-Plastic Fracture*, ASTM STP 668, J. D. Lanes, J. A. Begley, and G. A. Clarke, Eds., American Society for Testing and Materials, pp. 121-150 (1979).
- 10.19 "Effect of Weld Parameters on Residual Stresses in BWR Piping Systems," EPRI Final Report NP-1743, Electric Power Research Institute, Palo Alto, California, Prepared by Battelle Memorial Institute (1981).
- 10.20 Rosenthal, D., "Mathematical Theory of Heat Distribution During Welding and Cutting," *Welding Journal Research Supplement*, pp. 220-234 (1941).
- 10.21 Rybicki, E. F., and Stonesifer, R. B., "Computation of Residual Stresses Due to Multipass Welds in Piping Systems," *ASME/CSME Pressure Vessels and Piping Conference*, Montreal Canada (June 1978).
- 10.22 Dawes, M. G., "Contemporary Measurements of Weld Metal Fracture Toughness," *Welding Journal*, Vol. 55, pp. 1052-1057 (1976).

- 10.23 Rice, J. R., "A Path Independent Integral and the Approximate Analysis of Strain Concentration by Notches and Cracks," *ASME Journal of Applied Mechanics*, Vol. 35, pp. 379-386 (1968).
- 10.24 Ueda, Y., Fukuda, K., and Tanigawa, M., "New Measuring Methods of Three-Dimensional residual Stresses Based on Theory of Inherent Strain," *Transactions of JWRI*, Welding Research Institute of Osaka University, Osaka, Japan, Vol. 8, pp. 89-96 (1979).
- 10.25 Ueda, Y., and Nakacho, K., "Distributions of Welding Residual Stresses in Various Welded Joints of Thick Plates," *Transactions of JWRI*, Welding Research Institute of Osaka University, Osaka, Japan, Vol. 15, pp. 113-124 (1986).
- 10.26 Ramamurti, V., Suresh, S., Raghuraman, B., and Ravichandran, G., "Residual Stress Analysis in Weldments," *Engineering Fracture Mechanics*, Vol. 38, pp. 385-391 (1991).
- 10.27 "Controlling Residual Stresses by Heat Sink Welding," EPRI Final Report, EPRI NP-2159-LD, Prepared by Battelle Memorial Institute (1981).

BIBLIOGRAPHIC DATA SHEET

(See instructions on the reverse)

1. REPORT NUMBER
(Assigned by NRC. Add Vol., Supp., Rev.,
and Addendum Numbers, if any.)

NUREG/CR-4599
BMI-2173
Vol. 3, No. 1

2. TITLE AND SUBTITLE

Short Cracks in Piping and Piping Welds

Semiannual Report
April 1992 - September 1992

3. DATE REPORT PUBLISHED

MONTH YEAR
October 1993

4. FIN OR GRANT NUMBER

B5702

5. AUTHOR(S)

G. M. Wilkowski, F. Brust, R. Francini, N. Ghadiali,
T. Kilinski, P. Krishnaswamy, M. Landow, C. W. Marschall,
S. Rahman, and P. Scott

6. TYPE OF REPORT

Technical

7. PERIOD COVERED (Inclusive Dates)

8. PERFORMING ORGANIZATION - NAME AND ADDRESS (If NRC, provide Division, Office or Region, U.S. Nuclear Regulatory Commission, and mailing address; if contractor, provide name and mailing address.)

Battelle
505 King Avenue
Columbus, OH 43201

9. SPONSORING ORGANIZATION - NAME AND ADDRESS (If NRC, type "Same as above"; if contractor, provide NRC Division, Office or Region, U.S. Nuclear Regulatory Commission, and mailing address.)

Division of Engineering
Office of Nuclear Regulatory Research
U.S. Nuclear Regulatory Commission
Washington, D.C. 20555 -0001

10. SUPPLEMENTARY NOTES

11. ABSTRACT (200 words or less)

This is the fifth semiannual report of the U.S. Nuclear Regulatory Commission's Short Cracks in Piping and Piping Welds research program. This 4-year program began in March 1990. The overall objective of this program is to verify and improve fracture analyses for circumferentially cracked large-diameter nuclear piping with crack sizes typically used in leak-before-break analyses or in-service flaw evaluations. During this reporting period, the overall program and results were critically reviewed and consequently several changes to the current program were made to meet the final program objectives.

Progress during this reporting period involved: (1) for the surface-cracked pipe evaluations, the tensile and Charpy V-notch data for a carbon-manganese submerged arc weld metal were completed, and 3D finite-element (FE) analyses of uncracked stainless steel pipe experiments to resolve the discrepancies between experimental data and FE predictions were completed. (2) Significant leak-rate analyses for cracked pipe using advanced probabilistic analysis was conducted to provide a technical basis for changes to NRC Reg. Guide 1.45. (3) A new PC-based circumferential surface-cracked pipe code, NRCPIPES Version 1.0, was completed. (4) Subcontracted efforts include; numerical analysis of residual stresses on elastic-plastic fracture of cracks in welds (being conducted at the University of Michigan), and evaluation of "Validity Limits on J-R Curve Determination" (being conducted at Brown University). (5) Finally, technical efforts related to the ASME Section XI pipe flaw evaluation efforts are summarized.

12. KEY WORDS/DESCRIPTORS (List words or phrases that will assist researchers in locating the report.)

Pipe, Fracture Mechanics, Cracks, J-Integral/Tearing Modulus,
Leak Rate, Elastic-Plastic Fracture Mechanics, Nuclear Piping
Steels

13. AVAILABILITY STATEMENT

unlimited

14. SECURITY CLASSIFICATION

(This Page)

unclassified

(This Report)

unclassified

15. NUMBER OF PAGES

16. PRICE



Federal Recycling Program

UNITED STATES
NUCLEAR REGULATORY COMMISSION
WASHINGTON, D.C. 20555-0001

OFFICIAL BUSINESS
PENALTY FOR PRIVATE USE, \$300

SPECIAL FOURTH-CLASS RATE
POSTAGE AND FEES PAID
USNRC
PERMIT NO. G-67

120555139531 1 1A1RFP1P5
US NRC-CADM PUBLICATIONS SVCS
CIV FORIA & PURES
TAS-PCR-NURES
P-211
WASHINGTON DC 20555